DEMOCRITUS UNIVERSITY OF THRACE- MEDICAL PHYSICS DEPARTMENT

ΔΙΑΠΑΝΕΠΙΣΤΗΜΙΑΚΟ ΔΙΑΤΜΗΜΑΤΙΚΟ ΠΡΟΓΡΑΜΜΑ ΜΕΤΑΠΤΥΧΙΑΚΩΝ ΣΠΟΥΔΩΝ (ΔΔΠΜΣ)
«Ιατρική Φυσική- Ακτινοφυσική»

MASTER THESIS

«NUMERICAL ANALYSIS OF THE HEMODYNAMICS IN UNRUPTURED CEREBRAL ANEURYSMS: A COMPARISON BETWEEN DSA AND MRA DERIVED MODELS»

CHRISTOS GIANNIOTIS

PHYSICS BSc, UNIVERSITY OF IOANNINA

RESEARCH SUPERVISOR:

Ioannis Seimenis, Professor in Medical Physics, School of Medicine,
Democritus University of Thrace, Greece

Alexandroupolis 2019

EXAMINATION COMMITTEE

Ioannis Seimenis, Professor in Medical Physics, School of Medicine, Democritus University of Thrace, Greece

Michael Mantatzis, Assistant Professor in Radiology-Neuroradiology, Department of Radiology-Neuroradiology, University Hospital of Alexandroupolis, Democritus University of Thrace, Greece

Athanasia Kotini, Associate Professor in Medical Physics, School of Medicine, Democritus University of Thrace, Greece

Abstract

A cerebral aneurysm is a vascular disorder characterized by abnormal focal dilation of a brain artery which is considered as a serious and presumably life-threatening condition. Cerebral aneurysms affect around 2%-5% of the general population and they can rupture with an overall mortality rate of more than 50%. By exploiting appropriate Computational Fluid Dynamics tools, we can gain insight into cerebral aneurysm's behavior and characteristics, such as development, growth and rupture. These tools consist of a set of partial differential equations, the solution of which provides information on a variety of parameters. There has been extensive speculation in the literature about the factors that potentially affect the growth and rupture of brain aneurysms, leading to new aspects of treatment of this disease.

This thesis provides a review of the medical problem of brain aneurysm, as well as of the relevant treatment methods. Moreover, six cerebral aneurysms of the middle cerebral artery, depicted by Magnetic Resonance Angiography (MRA) and Digital Subtraction Angiography (DSA, were studied. Following aneurysm segmentation and modelling from both the MRA and DSA datasets, corresponding hemodynamic fields were simulated and analyzed by employing the computational fluid dynamics method. Geometric and hemodynamic parameters that are considered to be associated with the risk of aneurysm rupture were calculated. A comparison was performed between corresponding results obtained from MRA- and DSA-derived models. Finally, numerical analyses were carried out in virtual aneurysm occlusion scenarios simulating potential post- endovascular treatment situations. The conclusions of this thesis can be divided in three parts.

First, the maximum values of hemodynamic parameters like pressure, WSS and Area Averaged Wall Shear Stress revealed a difference that ranges from 5 to 57%. This can be attributed to the different geometry derived from the DSA and MRA examinations and suggests that the DSA examination is the gold standard thanks to its better spatial resolution, while MRA can be useful for follow up examinations.

Second, the virtual occlusion scenarios lead to specific hemodynamic changes, which suggest a reduced risk of rupture as is the case in regular clinical practice.

Third, the modelling and simulation process are both highly user dependent. This makes the creation of a general protocol of this process highly recommended, in order to apply Computational Fluid dynamics in daily clinical use.

Keywords: Cerebral, Aneurysm, Computational Fluid Dynamics, Simulation of Hemodynamics, Aneurysm Modelling, Aneurysm Occlusion, Aneurysm Treatment

Title and Abstract (in Greek)

«Μελέτη μη ραγέντων εγκεφαλικών ανευρυσμάτων με αριθμητική ανάλυση: Σύγκριση γεωμετρικών και αιμοδυναμικών χαρακτηριστικών μετά από μοντελοποιήσεις βασισμένες σε δεδομένα MRA και DSA**»**.

Τα εγκεφαλικά ανευρύσματα αποτελούν αγγειακή βλάβη που χαρακτηρίζεται από την τοπική διάταση ενός ενδοκράνιου αγγείου. Πρόκειται για μια σοβαρή και υπό συνθήκες θανατηφόρα νόσο που απαντάται στο 2-5% του πληθυσμού, με ποσοστό θνησιμότητας πάνω από 50%. Η χρήση λογισμικών εργαλείων αριθμητικής ανάλυσης και προσομοίωσης προσφέρει τη δυνατότητα αξιολόγησης καίριων χαρακτηριστικών αναφορικά με τη δημιουργία, αύξηση και ρήξη των εγκεφαλικών ανευρυσμάτων. Τα λογισμικά αυτά επιλύουν μια σειρά μερικών διαφορικών εξισώσεων και δίδουν τη δυνατότητα μελέτης και υπολογισμού ποικίλων παραμέτρων που σχετίζονται με την εξελικτική πορεία των ανευρυσμάτων. Συνεπώς, ανοίγουν νέους ορίζοντες τόσο σε προγνωστικό όσο και σε θεραπευτικό επίπεδο.

Αυτή η μεταπτυχιακή διατριβή παρέχει μία ανασκόπηση των εγκεφαλικών ανευρυσμάτων, καθώς και των μεθόδων θεραπείας τους. Μελετήθηκαν, επίσης, έξι μη ραγέντα εγκεφαλικά ανευρύσματα της μέσης εγκεφαλικής αρτηρίας τα οποία είχαν απεικονισθεί με μαγνητική αγγειογραφία (MRA) και Ψηφιακή Αφαιρετική Αγγειογραφία (DSA). Τα MRA και DSA απεικονιστικά δεδομένα χρησιμοποιήθηκαν ξεχωριστά για την τμηματοποίηση και μοντελοποίηση του κάθε ανευρύσματος. Στη συνέχεια, πραγματοποιήθηκε προσομοίωση και αριθμητική ανάλυση των αιμοδυναμικών πεδίων εντός των μοντελοποιημένων ανευρυσμάτων καθώς και υπολογισμός των γεωμετρικών και αιμοδυναμικών παραμέτρων που θεωρείται ότι συνδέονται με τον κίνδυνο ρήξης του ανευρύσματος. Ακολούθησε σύγκριση των αποτελεσμάτων που προήλθαν από τα βασισμένα σε MRA και DSA μοντέλα και τέλος, έγιναν προσομοιώσεις σε εικονικά σενάρια ενδοαγγειακής θρόμβωσης των ανευρυσμάτων. Η επιμέρους ανάλυση όλων των παραπάνω, οδήγησε στην τμηματοποίηση των συμπερασμάτων σε τρία βασικά σκέλη.

Πρώτον, τα αποτελέσματα της σύγκρισης των αιμοδυναμικών παραμέτρων της πίεσης, του Wall Shear Stress και του Area Averaged Wall Shear Stress αποκάλυψαν διαφορές που κυμαίνονται από 5-57%. Κάτι τέτοιο αποδίδεται στην διαφορετική γεωμετρική απεικόνιση των ανευρυσμάτων από τις δύο απεικονιστικές μεθόδους και υποδεικνύει την DSA ως την προτιμώμενη εξέταση αναφοράς χάριν της διακριτικής της ικανότητας και την MRA ως χρήσιμη σε follow-up εξετάσεις.

Δεύτερον, τα εικονικά σενάρια θεραπείας οδήγησαν σε μείωση της έκτασης των περιοχών όπου εμφανίζεται χαμηλή τιμή Wall Shear Stress, επιβεβαιώνοντας τον μειωμένο κίνδυνο ρήξης που επιτυγχάνεται έπειτα από την κλινική θεραπεία των εγκεφαλικών ανευρυσμάτων.

Τρίτον, τα βήματα τα οποία εκτελούνται καθ΄ όλη την διάρκεια της μοντελοποίησης και της προσομοίωσης εξαρτώνται σε μεγάλο βαθμό από την κρίση του εκάστοτε ερευνητή. Συνεπώς χρειάζεται ένα πρωτόκολλο με συγκεκριμένες οδηγίες

μοντελοποίησης και προσομοίωσης προκειμένου τα αποτελέσματα των αντίστοιχων λογισμικών να ξεπεράσουν τα όρια του ερευνητικού ενδιαφέροντος και να αξιοποιηθούν σταδιακά στην κλινική πράξη.

Λέξεις-κλειδιά: Ανεύρυσμα Εγκεφάλου, Λογισμικό Μοντελοποίησης και Προσομοίωσης, Αιμοδυναμικές παράμετροι, Μοντελοποίηση Ανευρύσματος, Απόφραξη ανευρύσματος, Θεραπεία Ανευρύσματος

Acknowledgements

First, I would like to thank my teacher and advisor Prof. Ioannis Seimenis for his support, guidance and immediacy. His academic knowledge and ideas where of great importance and thanks to his kind and supportive nature I was able to keep my motivation throughout this research.

Also, I would like to thank Assistant Professor Michalis Mantatzis for his aid and eagerness to help in issues that came up, with his medical experience and expertise. I also extend my thanks to Assoc. Professor A. Kotini who acted as a member of the Examination Committee.

Many thanks to Kostantinos Athanasoulis. Sharing his former know-how with me was very important for the initialization of this thesis.

Thanks to Nicolas Aristokleous for his patience whenever I needed his help with the CFD analysis.

Thanks to Irini for her phycological support throughout this thesis.

Finally, I warmly thank my family for their immense support and motivation throughout the years that I am studying.

Table of Contents

GENERAL SECTION

1. Scope of the study

Cerebral aneurysms are vascular dilations on brain vessels that affect around 1%–5% of the general population and can cause life-threatening intracranial hemorrhage when ruptured with an overall mortality rate of more than 50% [2-4]. Computational fluid dynamics (CFD) has emerged as a promising tool to study cerebral aneurysms in recent years, particularly for rupture risk assessment.

In this study Magnetic Resonance Angiography (MRA) and Digital Subtraction Angiography (DSA) were utilized for the imaging of six cerebral aneurysms. These aneurysms were modelled and hemodynamically examined using appropriate computer programs. The scope of this thesis is to study the geometric and hemodynamic differences that arise when two different techniques are applied to image the same entity, a cerebral aneurysm. Finally, gradual decreases in the aneurysm geometry are applied in order to simulate virtual treatment scenarios.

2. Cerebral Aneurysm

2.1 Introduction

Cardiovascular diseases are statistically the third primary cause of death in the western world [1] and Cerebral aneurysms is one of them. Cerebral aneurysms are weak areas in brain vessels which usually grow in a balloon shape causing the arterial wall strength to decrease to a point where it could rupture and cause a stroke. Ruptured aneurysms cause subarachnoid hemorrhage. Often the aneurysm heals over, bleeding stops, and the person survives. In more serious cases, the bleeding may cause brain damage with paralysis or coma. In the most severe cases the bleeding leads to death.

Statistics show that 50% of those people die within minutes of a massive hemorrhage. Of the 50% who survive, half will suffer delayed death. The remaining survivors, depending upon the level of hemorrhage, usually live with severe long-term deficits. Most cerebral aneurysms do not show any symptoms until they grow significantly in size or they rupture, thus the high mortality rate.

Figure 1 shows multiple aneurysms that occurred in cerebral arteries.

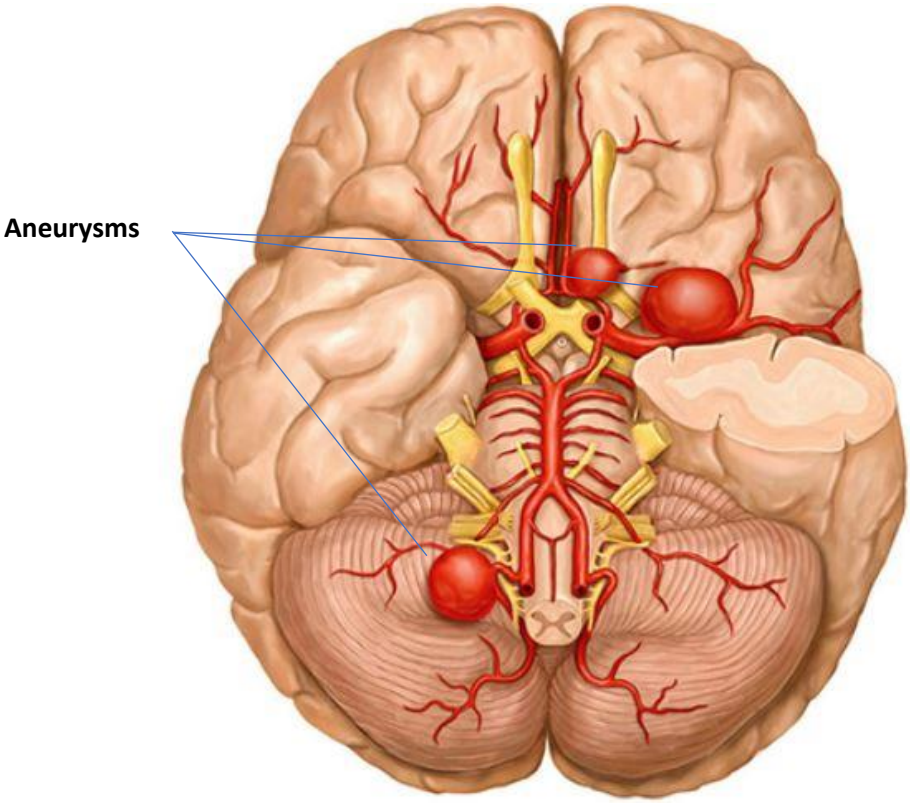

Figure 1: Cerebral aneurysms in brain vessels

2.2 Categorization

Cerebral aneurysms are characterized upon their size and shape.

Based on their shape, there are two types of cerebral aneurysms, the saccular and the fusiform ones. The saccular aneurysms are most common and in 90% of the cases are located in the anterior artery.

Saccular aneurysms consist of three parts which are the parent artery, the aneurysm's neck and the aneurysm's dome. Depending on the area of the incident, the artery may have various branches and more importantly different size. The aneurysm neck is the part where important variation of wall thickness occurs and high shear forces are applied as a result of the high blood's velocity as it enters the aneurysm dome. The thickness of the dome is considered uniform across the aneurysm however it may change depending on the aneurysm growth [2]. Figure 2 shows the common sections of a saccular aneurysm.

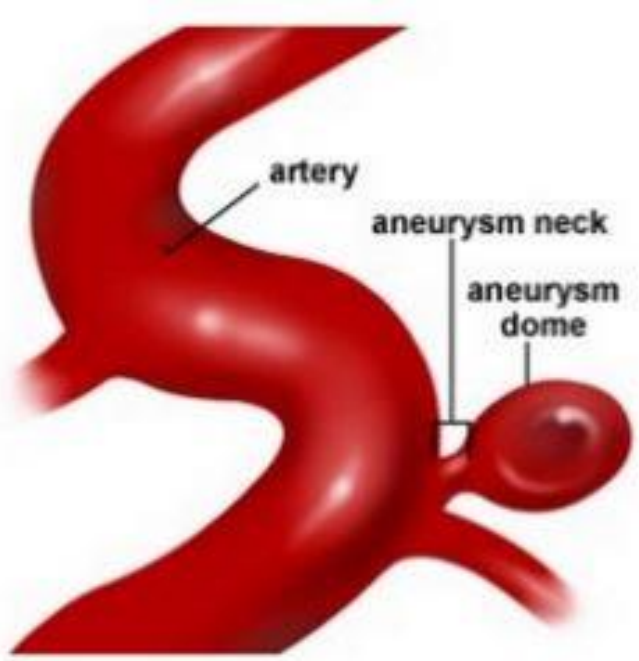

Figure 2: Sections of a Saccular aneurysm

A fusiform aneurysm is typically formed by the widening along the walls of the artery, as shown in Figure 3.

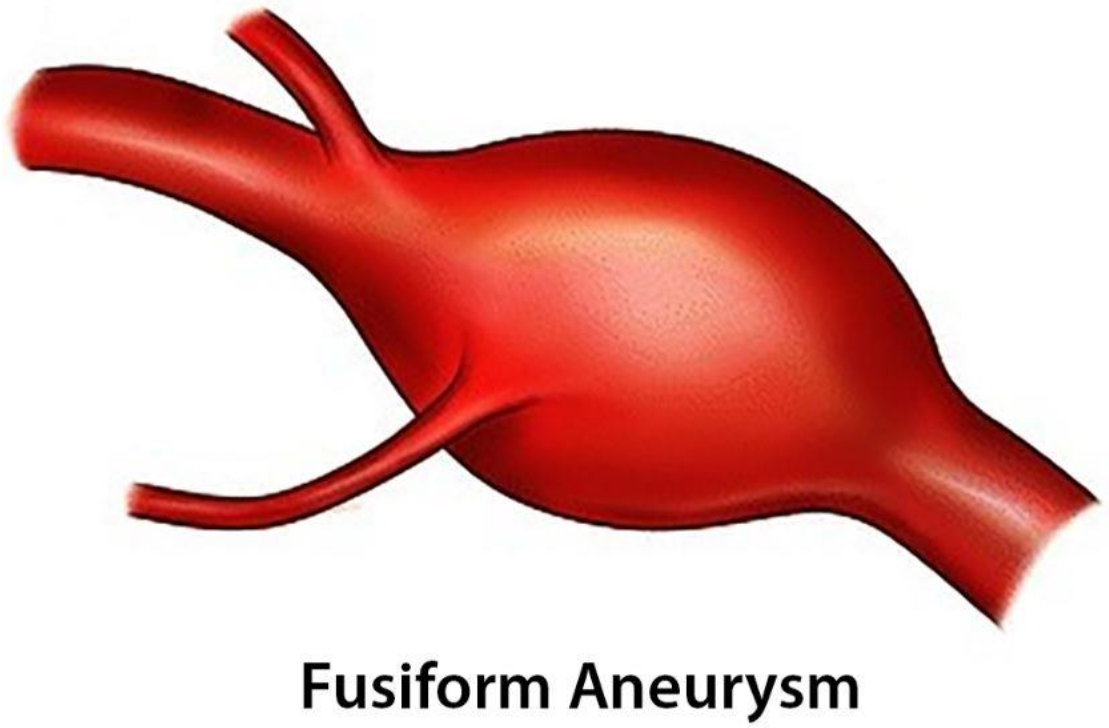

Figure 3: Fusiform aneurysm

Cerebral aneurysms are also classified according to their size, measured in millimeters (mm). The size of an aneurysm can be measured either by the angiography image of the patient or a model of the aneurysm, if available. However, because the construction of a 3D model can differentiate the dimensions of the aneurysm, it is preferable for the measurements to be made on the angiography.

Aneurysms are characterized as small for diameter less than 5mm, large for diameter 6-13 mm and giant aneurysms are greater than 13mm [3].

Other measurements which are usually obtained are the following:

- Angiographic neck width (N)
- Dome height (H)
- Dome diameter (D)
- Semi-axis height (S)

The D/H and H/S ratios are considered of great importance because they define the shape of the aneurysm.

Figure 4 shows a schematic diagram of aneurysm measurements.

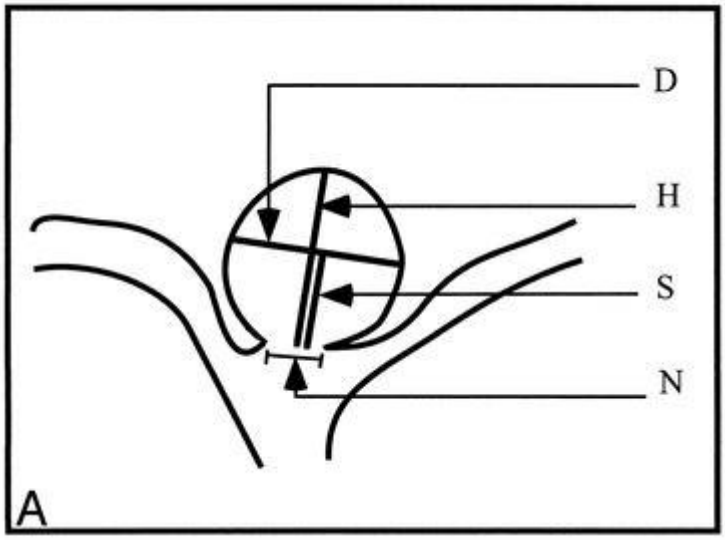

Figure 4: Schematic diagram of aneurysm measurements

The most essential ratio calculated though, is the aspect ratio (AR). The aspect ratio describes the relationship between the aneurysm height (H) and the aneurysm neck (N) and is calculated by dividing the corresponding measurements.

$$AR = H/N$$

Aspect ratio ≥1.3 and irregular shape are associated with aneurysm rupture regardless of aneurysm size and location, and independent of patient characteristics [25].

2.3 Causes and symptoms

The causes of the development of cerebral aneurysms is a controversial subject amongst researchers and has not been attributed to any particular cause yet. However, there are a number of risk factors that contribute to the formation of aneurysms [4]. These are:

- Smoking
- High blood pressure (hypertension)
- Strong family history of brain aneurysms (familial aneurysms)
- Age (over 40)
- Gender: women have an increased risk of aneurysms
- Race: people of color have an increased risk of ruptured aneurysms
- Other disorders: Ehlers-Danlos syndrome, autosomal dominant polycystic kidney disease, Marfan syndrome, and fibromuscular dysplasia
- Presence of an arteriovenous malformation (AVM)
- Congenital abnormality in the artery wall
- Drug use, particularly cocaine
- Excessive alcohol use
- Infection
- Severe head trauma

Fortunately, two of the most significant causes, cigarette smoking and high blood pressure (hypertension), can be controlled.

As mentioned above, unruptured cerebral aneurysms usually have no symptoms. This occurs because in most cases aneurysms are small. Many of them are found incidentally when tests are being done to screen other conditions or simply due to the evolution of imaging and their increased use in clinical practice.

In some cases though, unruptured aneurysms grow in size resulting into an extra press on surrounding nerves which can cause symptoms like:

- Blurred or double vision
- A drooping eyelid
- A dilated pupil
- Pain above and behind one eye
- Weakness and/or numbness

When a brain aneurysm ruptures, it causes bleeding into the compartment surrounding the brain, the subarachnoid space, causing a subarachnoid hemorrhage (SAH). This, can cause sudden symptoms, as listed below:

- Sudden and severe headache
- Nausea/vomiting
- Stiff neck
- Blurred or double vision

- Sensitivity to light
- Seizure
- Drooping eyelid
- A dilated pupil
- Pain above and behind the eye
- Loss of consciousness
- Confusion
- Weakness and/or numbness

2.4 Imaging and Diagnosis

Neuroimaging is [5] a critical element in evaluating] the size and morphologic features of an intracranial aneurysm. Each neuroimaging technique has its own strengths, weaknesses and ongoing developments. Three major imaging methods are used for medical imaging of cerebral aneurysms:

- Computed Tomography Angiography (CTA)
- Magnetic Resonance Angiography (MRA)
- Digital Subtraction Angiography (DSA)

Computed Tomography Angiography (CTA)

CTA can be used to examine blood vessels in many key areas of the body including the kidneys, pelvis, lungs and brain. Using thin-section contrast material, CT scanning and the aid of software generated images, CTA shows cerebral vessels in three-dimensional views [6,7].

In a typical CTA scan the patient lies on a narrow examination table which slides into and out of a rotating ring, called a gantry. The gantry consists of an x-ray tube and electronic x-ray detectors located opposite each other. The computer workstation that processes the imaging information is located in a separate control room.

Figure 5 shows a typical CTA configuration.

Figure 5: CTA configuration

During the procedure, multiple x-ray beam sources and sets of x-ray detectors spin around the body at high speed. The x-ray beam sources send multiple small high-energy x-ray beams through the body and the detectors capture those x-rays that come out of the brain. Then, a fast computer takes the information gathered from the scanner, produces images of the brain and processes a large volume of CT scan data to create three-dimensional images of the body.

Formerly, a contrast material has been introduced to the bloodstream, which clearly defines the blood vessels being examined by making them appear bright white.

Sensitivities of CTA range from 77% to 97% and specificities range from 87% to 100% [7]. Sensitivity for aneurysms smaller than 3 mm drops to a range of 40% to 91% [7]. The role of CTA is very limited in patients with impaired renal function, since a large bolus of contrast material is often administered.

Figure 6 shows a CT angiogram of an unruptured right internal carotid artery aneurysm.

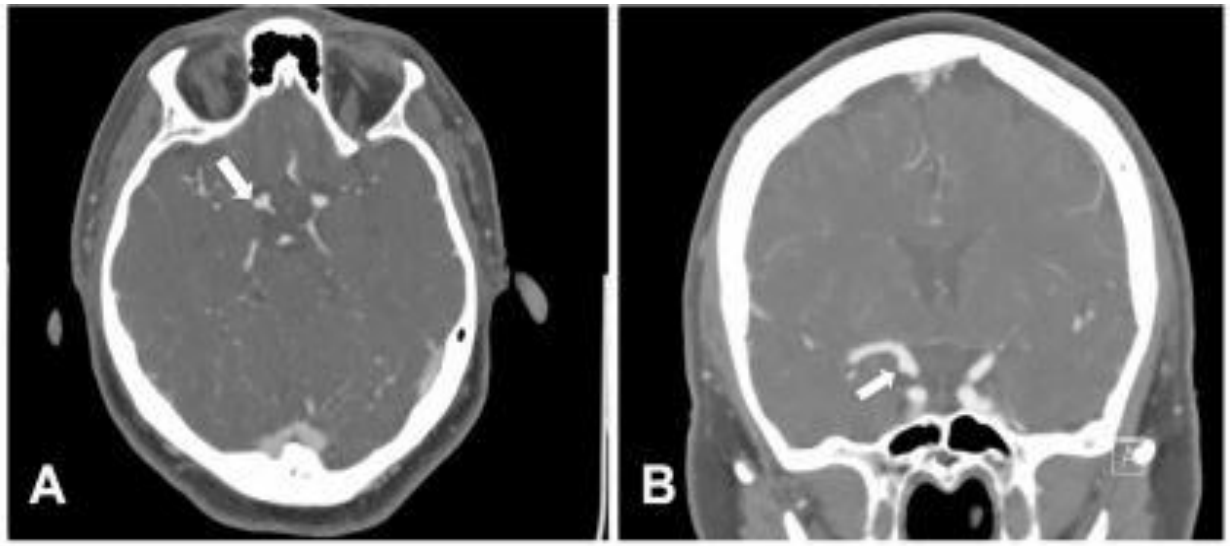

Figure 6: a) Axial CT angiogram demonstrating 3-mm blister aneurysm (arrow). b) Coronal CT angiogram reconstruction of the aneurysm (arrow)

Magnetic Resonance Angiography (MRA)

MR angiography (MRA) uses a powerful magnetic field, radio waves and a computer to image blood vessels and help identify abnormalities and diseases of the blood vessels. It may require the injection of gadolinium which is a contrast material.

A typical MRA unit consists of a large cylinder-shaped tube surrounded by a circular structure which contains the principal magnet windings plus copper coils for transmitting and receiving signals used. The patient lies on a moveable examination table that slides into the center of a magnet. There is also a computer workstation that processes the imaging information in a separate room from the scanner.

Figure 7 shows a typical MRA configuration.

Figure 7: MRA configuration

MRA uses protons, which are abundant in the human body. All protons spin creating a small magnetic charge. The strong static magnetic field generated by the circular magnet forces the protons to align with it. Then the MRA technician introduces a radiofrequency pulse utilizing the transmitting coils, which disrupts the protons from their initial state and forces them into either a 90 or 180 degree realignment with the static magnetic field. Since the radiofrequency pulse pushed the protons against their natural energy state, once this pulse is turned off, the protons realign with the magnetic field, releasing electromagnetic energy. The receiving coils are able to detect this energy and differentiate various tissues based on how quickly they release energy after the pulse is turned off. A computer then processes the signals and generates a series of images, each of which shows a thin slice of the body. The images can then be studied from different angles by the interpreting radiologist.

Among the MRA techniques available, Time-of-Flight (TOF) MRA, Phase-contrast (PC) MRA are mostly applied in the case of cerebral aneurysms.

MRA has a sensitivity of 70% to 99%, and a specificity of 100% for aneurysms 3 mm or greater in diameter; however, the sensitivity diminishes for very small aneurysms (under 3 mm in diameter) to as low as 40% [7]. MRA is more difficult to use in critically ill patients because it takes considerably more time to perform and is more expensive. On the other hand, it does not use ionizing radiation and offers the ability to obtain images without the need for administration of intravenous contrast agents.

Figure 8 shows a CT angiogram of an unruptured right internal carotid artery aneurysm.

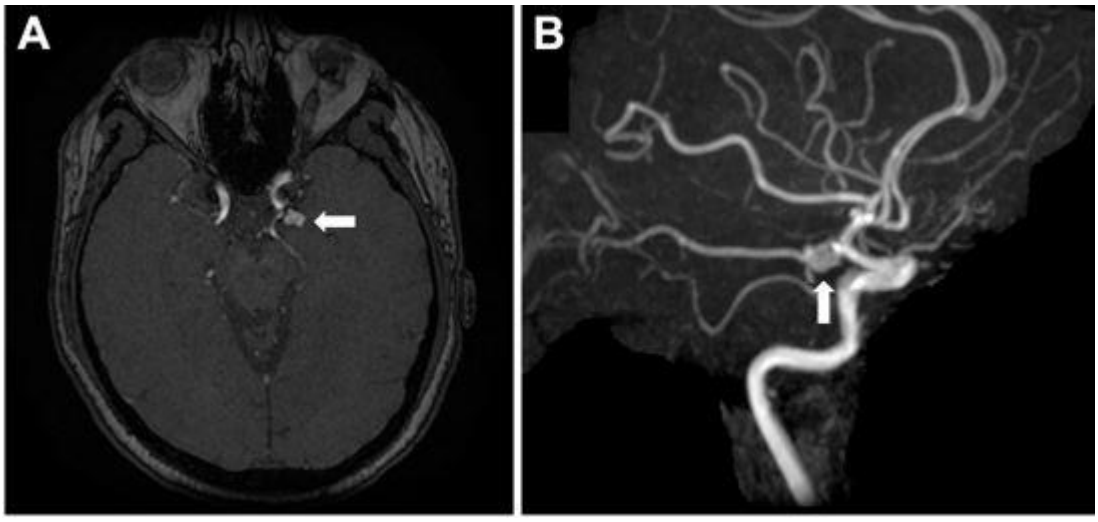

Digital Subtraction Angiography (DSA)

Figure 8: a) 3D TOF MRA demonstrating irregular 8-mm aneurysm (arrow).
b) 3D MRA reconstruction of the aneurysm (arrow)

DSA is a fluoroscopic technique that provides an image of the blood vessels in the brain to detect a problem with blood flow. The procedure involves inserting a catheter (a small, thin tube) into an artery in the leg and passing it up to the blood vessels in the brain. A contrast dye is injected through the catheter and X-ray images are taken of the blood vessels [8].

The fluoroscopy unit consists of a Biplane digital angiographic /fluoroscopy unit (c-arm) that can be rotated axially and sagittally around the floating-top table where the patient lies and a Programmable imaging system (digital) for post processing.

Figure 9 shows a typical DSA configuration.

Figure 9: Typical DSA configuration

During the DSA, the patient lies on a table then electrodes are placed on the chest to monitor heart health. A non-contrast image (image mask) of the region is taken before the injection of contrast material which shows only anatomy, as a regular x-ray image would. Afterwards, contrast images are taken while contrast material is being injected. These images show the opacified vessels superimposed on the anatomy and are stored on the computer. In succession the mask image is then subtracted from the contrast images and the resulting image shows only the filled vessels only. The

subtraction images can be viewed in real time. Figure 10 shows a carotid angiogram before and after the digital subtraction.

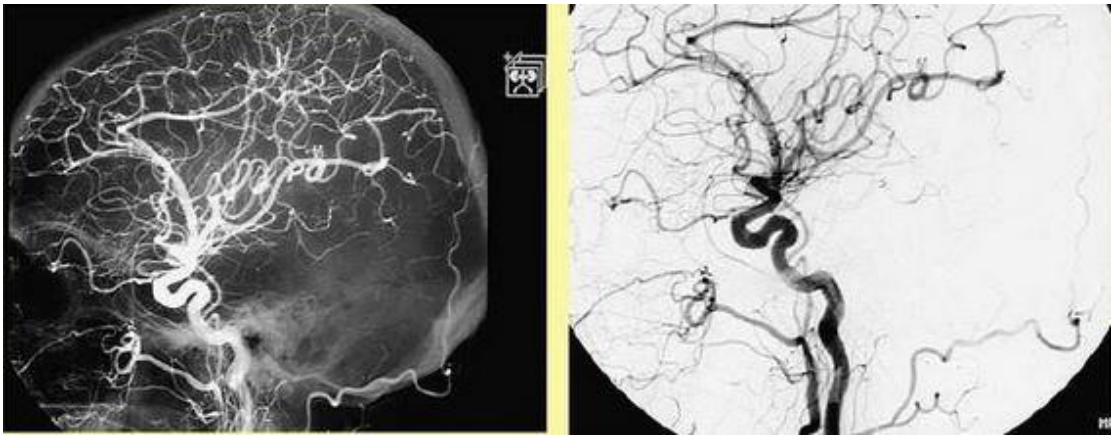

Figure 10: Left) nonsubtracted carotid angiogram, Right) Subtracted carotid angiogram

Figure 11 is a digital subtraction angiography (DSA) of an aneurysm arising from anterior communicating artery, from two different perspectives after a DSA examination.

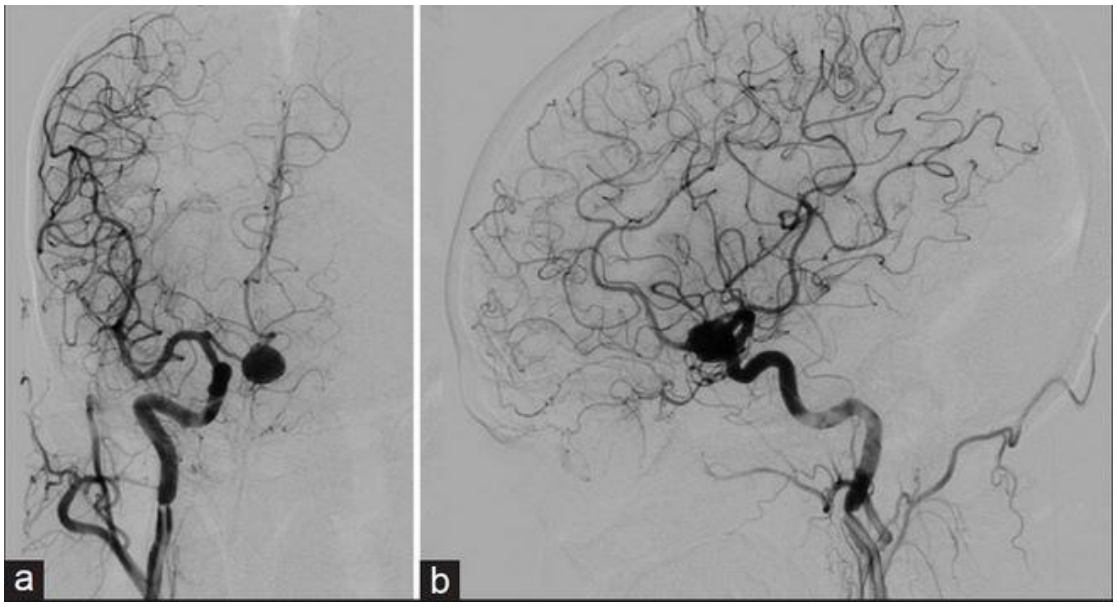

Figure 11: Cerebral aneurysm of an anterior communicating artery from two different prospectives

Similar to CTA, DSA requires the use of ionizing radiation and iodinated contrast. In addition, this procedure is invasive and requires operator expertise. DSA also has high spatial resolution to identify aneurysms compared to CTA and MRA. However, it is more expensive and invasive than either MRA or CTA. Its risks, even in the hands of

experienced operators, include neurologic complications. occurring in 1.0% to 2.5% of cases, with permanent impairment in 0.1% to 0.5% [7]. Other associated risks include femoral-artery injury (0.05% to 0.55%), groin hematoma (6.9% to 10.7%), and adverse renal effects induced by contrast material (1% to 2%) [7].

2.5 Treatment

When a patient is diagnosed with a cerebral aneurysm, it is crucial to proceed to treatment, whether it has ruptured or not. When an aneurysm has ruptured and caused subarachnoid hemorrhage, its treatment must be immediate since ruptured aneurysms have a very high risk of new bleeding. Optimum management of an unruptured intracranial aneurysm includes the comparison of the risk of aneurysmal rupture without any intervention with the risks of treatment. Other factors that should be considered are the location, size and morphology of the aneurysm along with patient factors such as age, medical history, history of subarachnoid hemorrhage and family history of subarachnoid hemorrhage. [7].

There are three management options for unruptured cerebral aneurysms: conservative management, surgical clipping and endovascular treatment.

Conservative management

For patients over the age of 60 years without a family history of subarachnoid hemorrhage and for small (<7 mm) aneurysms no interventional procedure is usually considered. Conservative management consists of routine periodic follow-up imaging with MRA or CTA on a regular basis defined by the physician, to observe any potential changes in size or shape of the aneurysm. All patients treated conservatively are counselled about potential risk factors like hypertension and smoking [9].

Surgical clipping

Surgical clipping is an invasive method of treatment. An open craniotomy is required in order to gain access to the aneurysm. The aneurysm is dissected out and a small metallic clip is placed at the neck to isolate the aneurysm from the parent blood vessel. Surgical clipping has proven to be highly effective since complete occlusion is obtained in more than 90% of the cases. [10].

Figure 12 shows a lateral view of craniotomy incision with inset of cranial aneurysm clipping.

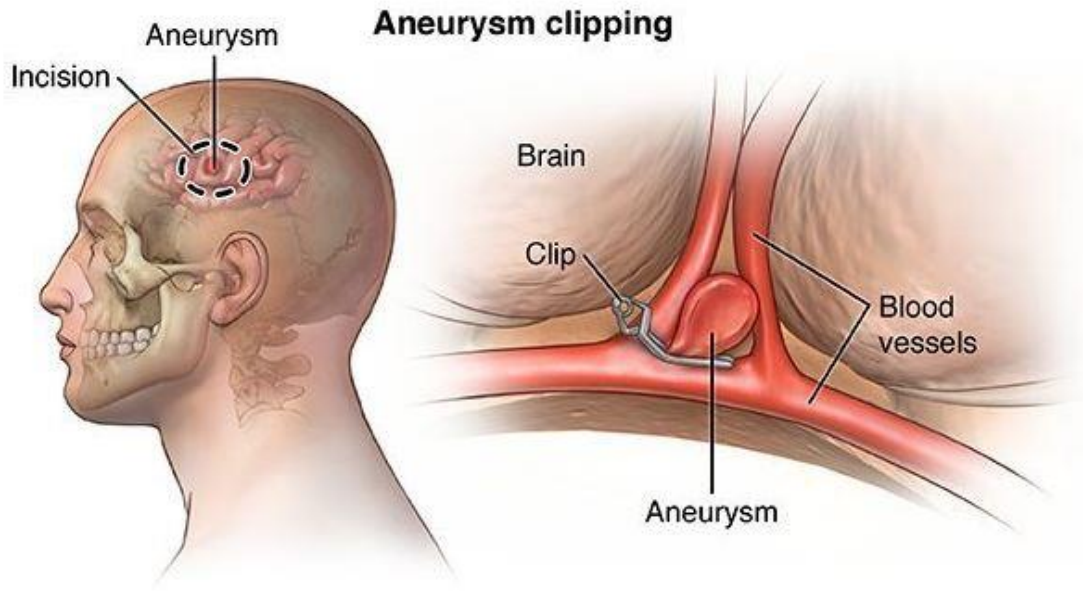

Figure 12: Lateral view of craniotomy incision with inset of cranial aneurysm clipping

Endovascular treatment

The endovascular techniques [11,12] which are utilized for aneurysm treatment are:

1. Packing the aneurysm with coils with or without complementary techniques such as balloon inflation or stent placement at the aneurysm neck
2. Use of flow diverting stents

The most common form of endovascular treatment is the deployment of coils into the aneurysm using a microcatheter. These coils initiate a local thrombosis and thus isolate the aneurysm from the parent artery. No complementary techniques are usually applied as long as the aneurysms treated have a narrow neck (<4mm) and low dome-to-neck ratio (<2). Complementary techniques such as balloon inflation or stent placement at the aneurysm neck are used in more difficult cases where a neck of width (>4mm) or dome-to-neck-ratio (>2) is observed. The purpose of these techniques is to prevent the coils from protruding through the aneurysm neck into the parent artery and reduce the risk of thromboembolic complications.

Figure 13 shows an aneurysm after the coiling procedure has been made.

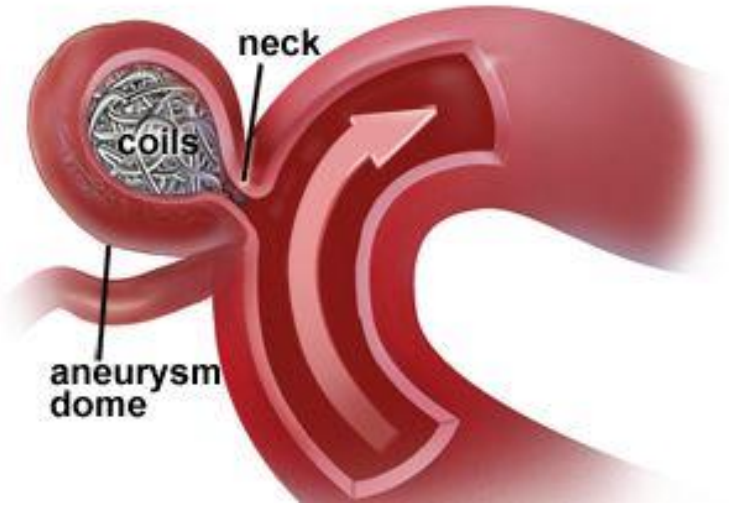

Figure 13: Aneurysm after coiling treatment

Figure 14 shows an aneurysm with coils and a stent placed.

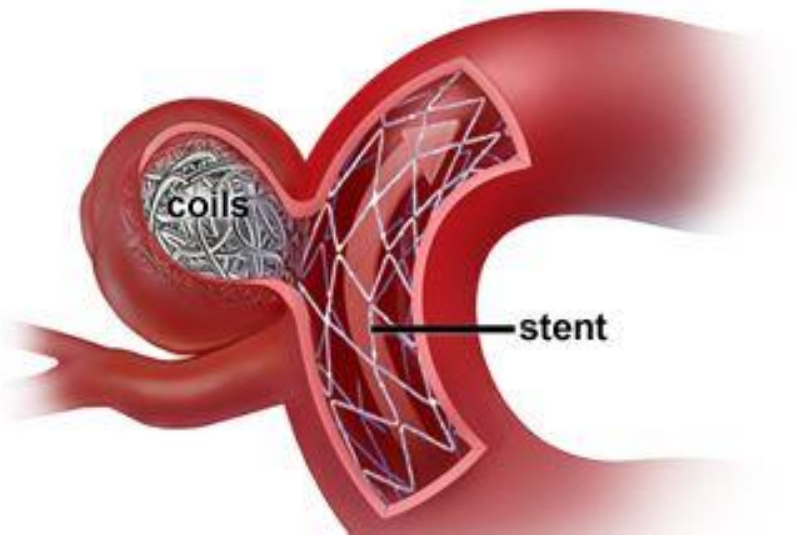

Figure 14: Aneurysm after coils and a stent have been placed

Flow diverting devices consist of tightly braided mesh which allows flow into vessel branches, but causes stagnation of blood in the sac which results in the occlusion of the aneurysm. Flow diverters are indicated for large unruptured saccular or fusiform intracranial aneurysms (>10 mm) of the anterior circulation from the petrous segment to the superior hypophyseal segment [13].

Figure 15 shows the results after a flow diverting device was been placed in the parent artery of the aneurysm.

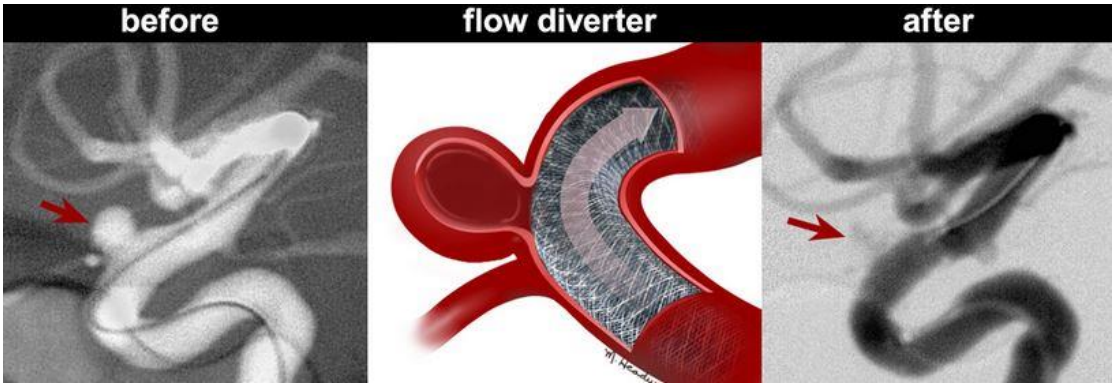

Figure 15: Results of a flow diverter placement in a cerebral aneurysm

In general, microsurgical clipping is used for young patients (<50) with small aneurysms (<10 mm) in the anterior circulation unless such a patient has significant medical comorbidities that may increase their surgical risk [7]. Moreover, clipping may be favored over coiling in some wide-necked aneurysms or aneurysms with branches arising from the neck or body. Furthermore, endovascular coiling is ideal for patients with several medical comorbidities with increased surgical risk or patients with aneurysms that have narrow necks. Aneurysms with wide necks may be coiled using stent assisted coiling or balloon angioplasty assisted coiling. Flow diverters are ideal for carotid cavernous aneurysms as well as large and giant internal carotid artery aneurysms. The optimum management of small unruptured intracranial aneurysms remains unclear.

Figure 16 shows a flow chart for the management of unruptured cerebral aneurysms.

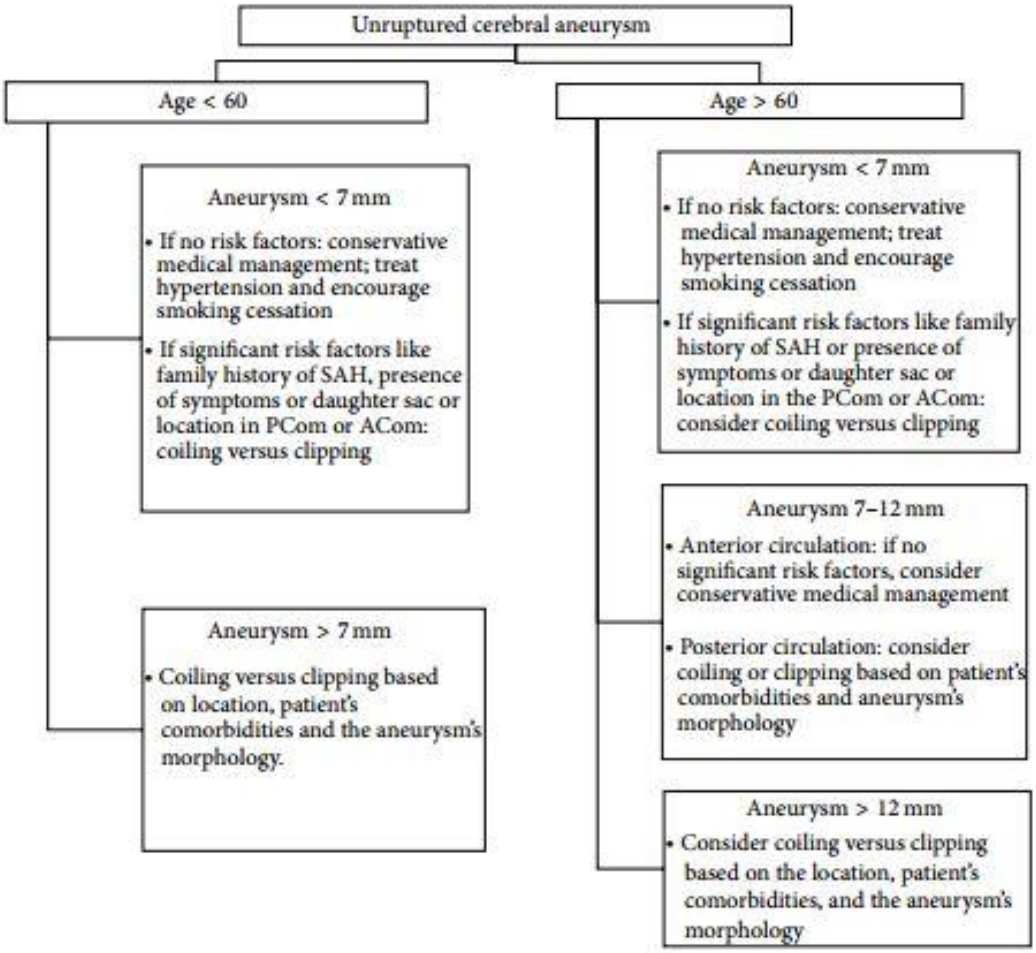

Figure 16: Flow chart for the management of unruptured cerebral aneurysms

3. Computational Fluid Dynamics

3.1 Introduction

Computational Fluid Dynamics (CFD) is a field of fluid mechanics that applies numerical analysis to data structures in order to analyze and solve problems that involve fluid flows. It provides quantitative estimations when fluids flow, often with the complication of spontaneous flow or heat, phase change (boiling, freezing, melting), mass transfer, mechanical movements (fans, pistons) or chemical reactions (rusting, combustion). [14]

A CFD analysis is performed in three stages. Preprocessing, processing and post processing.

- The preprocessing stage includes problem set up. At first the geometry and physical boundaries of the problem are defined using Computer Aided Design (CAD) software. Thereupon the fluid domain is extracted and the volume occupied by the fluid is divided into discrete cells (meshing process). The mesh can be uniform or non-uniform, structured or unstructured, consisting of a combination of hexahedral, tetrahedral, prismatic, pyramidal or polyhedral elements. Then the physical modeling is defined by choosing the appropriate equations of fluid motion and boundary conditions are applied in order to specify the fluid behavior at all bounding surfaces of the fluid domain.
- Processing involves the use of a strong computer to solve the mathematical equations that simulate the fluid flow. The required equations are already integrated in the simulation software and boundary conditions are applied to solve the problem.
- In the post-processing stage, the data generated by the CFD analysis are evaluated. Finally, the results are analyzed both numerically and graphically.

CFD is applied to a wide range of research and engineering problems in many fields of study and industries including architecture, chemical and process engineering, electronics and computer, HVAC (heat, ventilation &cooling), petroleum, train design, turbo machinery, aerospace analysis, environmental engineering and weather simulation. Its physiological applications includes cardiovascular flow in the heart, or major vessels and flows in lungs, breathing passages and cerebral aneurysms.

Figures 17-21 show applications of CFD in different research fields.

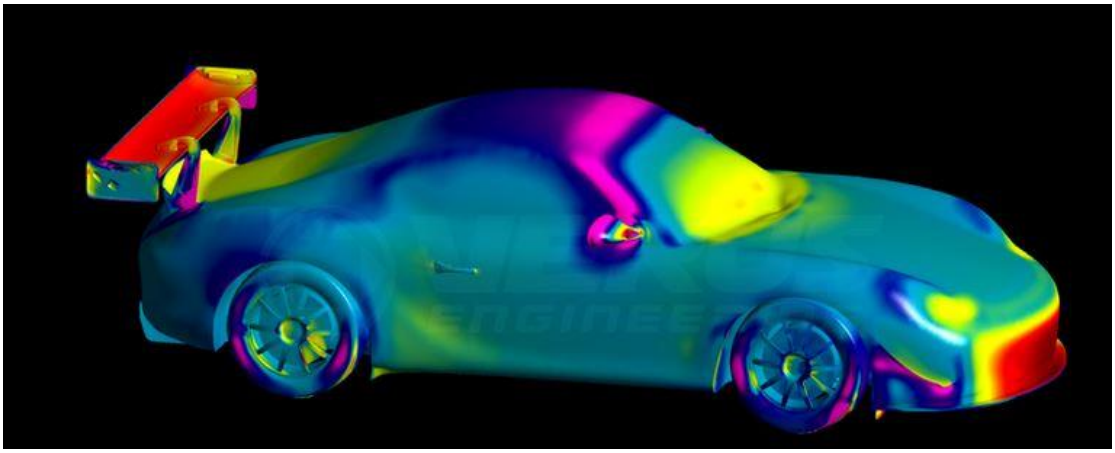

Figure 17: A simulation of aerodynamic package of a Porsche 987.2 Cayman.

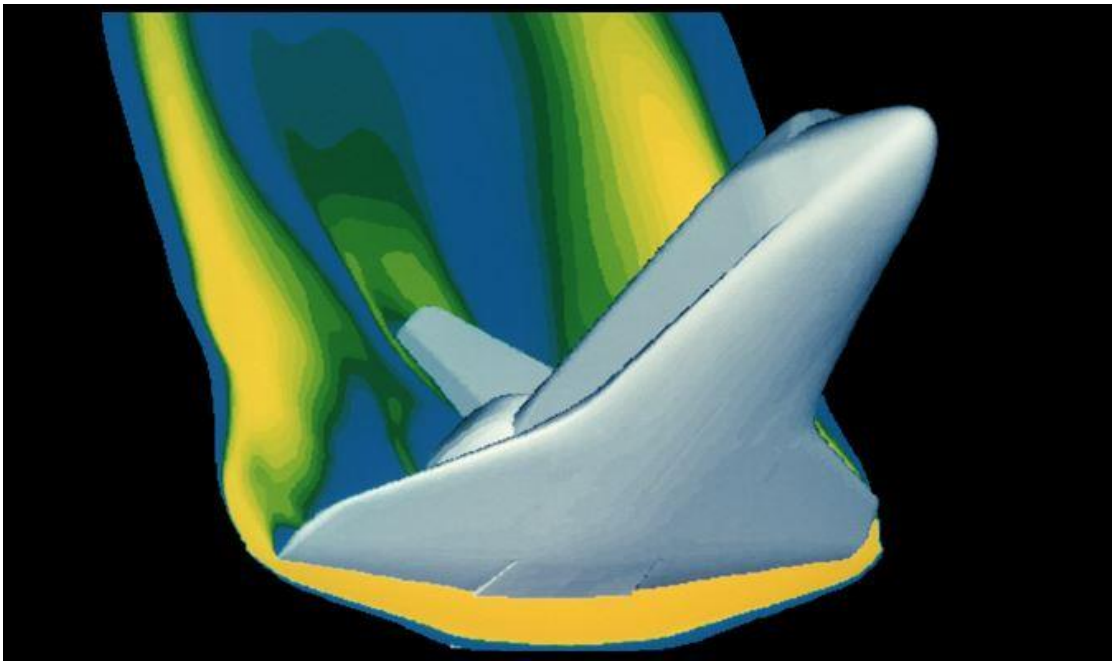

Figure 18: A computer simulation of high velocity air flow around the Space Shuttle during re-entry.

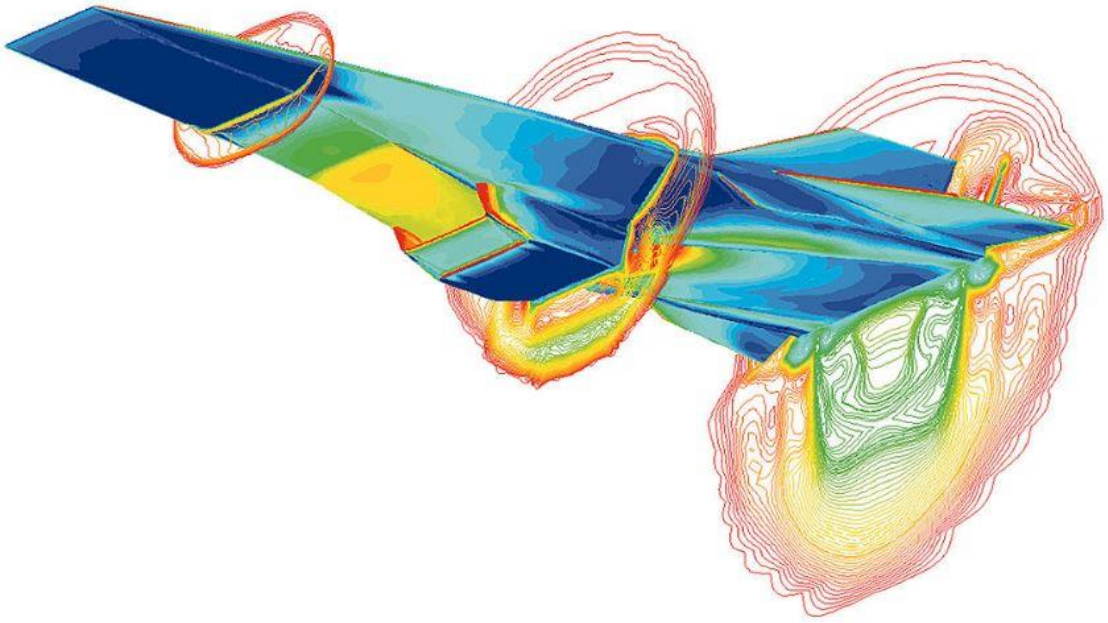

Figure 19: A simulation of the Hyper-X scramjet vehicle in operation at Mach-7

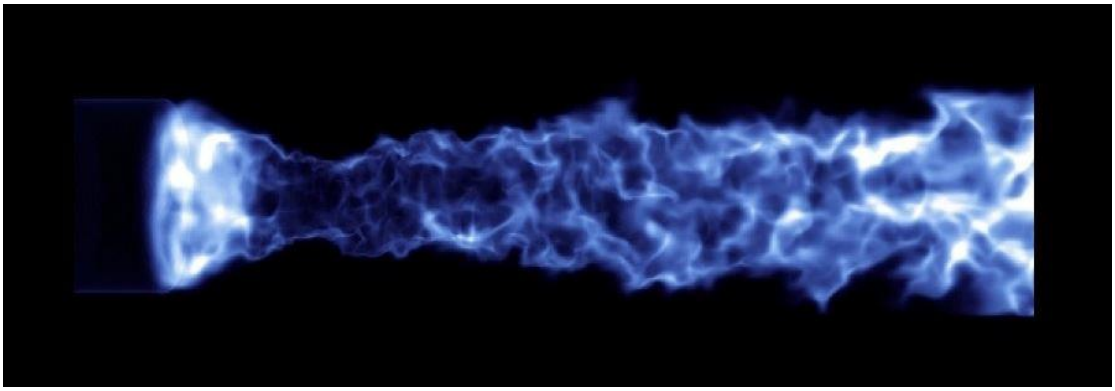

Figure 20: Volume rendering of a non-premixed swirl flame as simulated by LES.

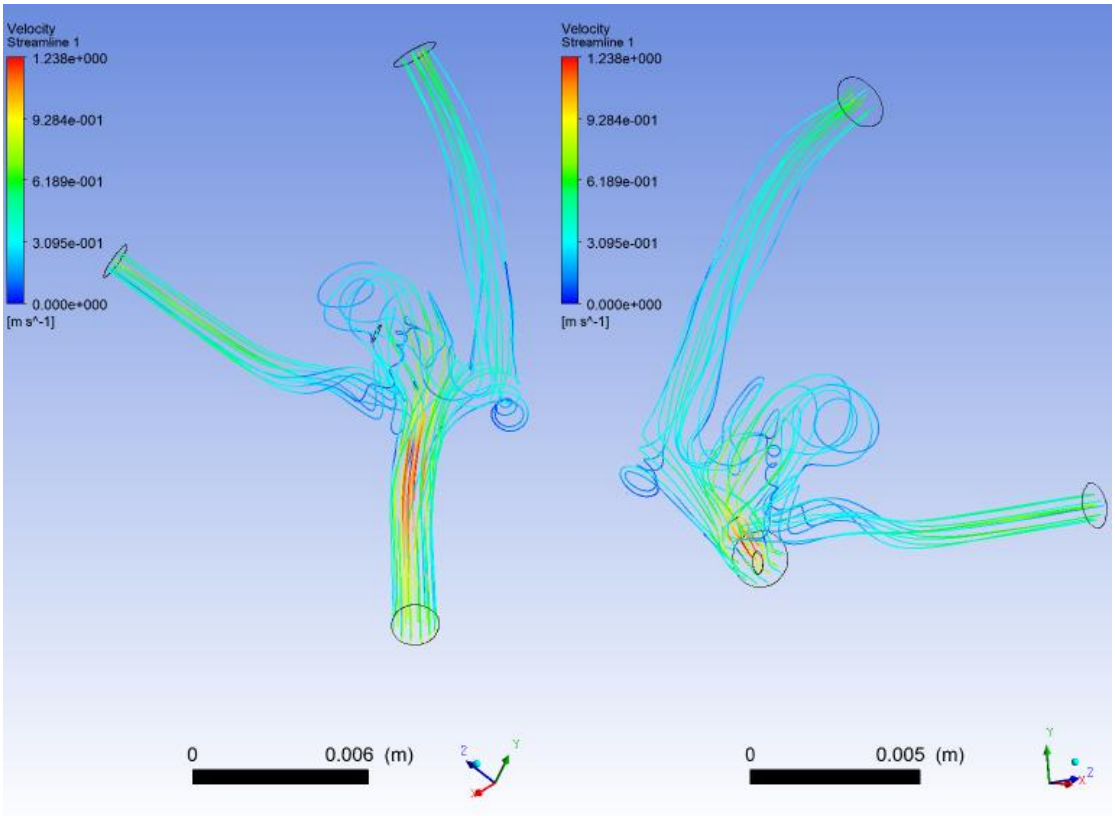

Figure 21: Simulation of blood flow in a human cerebral aneurysm

3.2 Theory

3.2.1 Fluid Properties

The two properties of fluids which determine most their type of flow and behavior, are density and viscosity.

Density, ρ, of a fluid is the ratio of its mass per unit volume. It's SI unit of measurement is one kilogram per cubic meter ($kg\ /\ m^3$).

$$p = \frac{m}{V}$$

The **viscosity**, μ, of a fluid is a measure of its resistance to deformation at a given rate. Viscosity can be conceptualized as quantifying the frictional force that arises between adjacent layers of fluid that are in relative motion. It's SI unit of measurement is one Pascal-second ($Pa \cdot s = N \cdot \frac{s}{m^2} = \frac{kg}{m/s}$).

3.2.2 Newtonian fluids

A Newtonian fluid is a fluid in which the viscous stresses arising from its flow, at every point, are linearly [15] proportional to the local strain rate—the rate of change of its deformation over time.[16,17] That is equivalent to saying those forces are proportional to the rates of change of the fluid's velocity vector as one moves away from the point in question in various directions.

Newtonian fluids are named after Isaac Newton, who first used the differential equation to postulate the relation between the shear strain rate and shear stress for such fluids. For an incompressible and isotropic Newtonian fluid, the viscous stress is related to the strain rate by the following equation:

$$\tau = \mu \frac{du}{dy}$$

Where:

- τ is the shear stress in the fluid
- μ is a scalar constant of proportionality, the shear viscosity of the fluid
- $\frac{du}{dy}$ is the derivative of the velocity component that is parallel to the direction of shear, relative to displacement in the perpendicular direction

Water, honey, air, alcohol, glycerol, and thin motor oil are all examples of Newtonian fluids over the range of shear stresses and shear rates encountered in everyday life. Single-phase fluids made up of small molecules are generally (although not exclusively) Newtonian.

Viscosity is the main property of Newtonian fluids, the value of which depends on their molecular nature and the state (pressure and temperature) in which the fluid exists.

3.2.3 Types of fluid flow

A fluid's flow can be classified in different categories depending on the criterion used to describe it. For the needs of this thesis two types of flow need to be highlighted:

In fluid dynamics**, laminar flow** (or streamline flow) occurs when a fluid flows in parallel layers, with no disruption between the layers.[18] At low velocities, the fluid tends to flow without lateral mixing, and adjacent layers slide past one another like playing cards. There are no cross-currents perpendicular to the direction of flow, nor eddies or swirls of fluids. In laminar flow, the motion of the particles of the fluid is very orderly with particles close to a solid surface moving in straight lines parallel to that surface. The velocity, pressure, and other flow properties at each point in the fluid remain constant [15]

Turbulent flow, is a type of fluid (gas or liquid) flow in which the fluid undergoes irregular fluctuations, or mixing, in contrast to laminar flow, in which the fluid moves in smooth paths or layers. In turbulent flow the speed of the fluid at a point is continuously undergoing changes in both magnitude and direction. The flow of wind and rivers is generally turbulent in this sense, even if the currents are gentle. The air or water swirls and eddies while its overall bulk moves along a specific direction.

Most kinds of fluid flow are turbulent, except for laminar flow at the leading edge of solids moving relative to fluids or extremely close to solid surfaces, such as the inside wall of a pipe, or in cases of fluids of high viscosity (relatively great sluggishness) flowing slowly through small channels. Common examples of turbulent flow are blood flow in arteries, oil transport in pipelines, lava flow, atmosphere and ocean currents, the flow through pumps and turbines, and the flow in boat wakes and around aircraft-wing tips.

A dimensionless quantity, called the **Reynolds number,** is the ratio of inertial forces to viscous forces and is a convenient parameter for predicting if a flow condition will be laminar or turbulent. It can be interpreted that when the viscous forces are dominant (slow flow, low Re) they are sufficient enough to keep all the fluid particles in line, then the flow is laminar. Even very low Re indicates viscous creeping motion, where inertia effects are negligible. When the inertial forces dominate over the viscous forces (when the fluid is flowing faster and Re is larger) then the flow is turbulent.

An increasing Reynolds number indicates an increasing turbulence of flow.

It is defined as:

$$Re = \frac{pVD}{\mu} = \frac{VD}{v}$$

where:

- **V** is the flow velocity,

- **D** is a characteristic linear dimension, (travelled length of the fluid; hydraulic diameter etc.)
- **ρ** fluid density (kg/m3),
- **μ** dynamic viscosity (Pa.s),
- **ν** kinematic viscosity (m2/s); $\nu = \mu / \rho$.

Laminar flow occurs at low Reynolds number; because the flow is steady, hence viscous force is less. For a laminar flow, the Reynolds number is less than 2100.

Turbulent flow occurs at high Reynolds number, as the flow is unsteady and velocity is high resulting in more inertial force. For a turbulent flow, the Reynolds number is greater than 4000.

In the transition flow the Reynolds number ranges from 2100 to 4000.

Figure 22 sums up the different type of flows along with the Reynolds number.

Figure 23 shows the transition of the plume of a candle's flame from laminar to

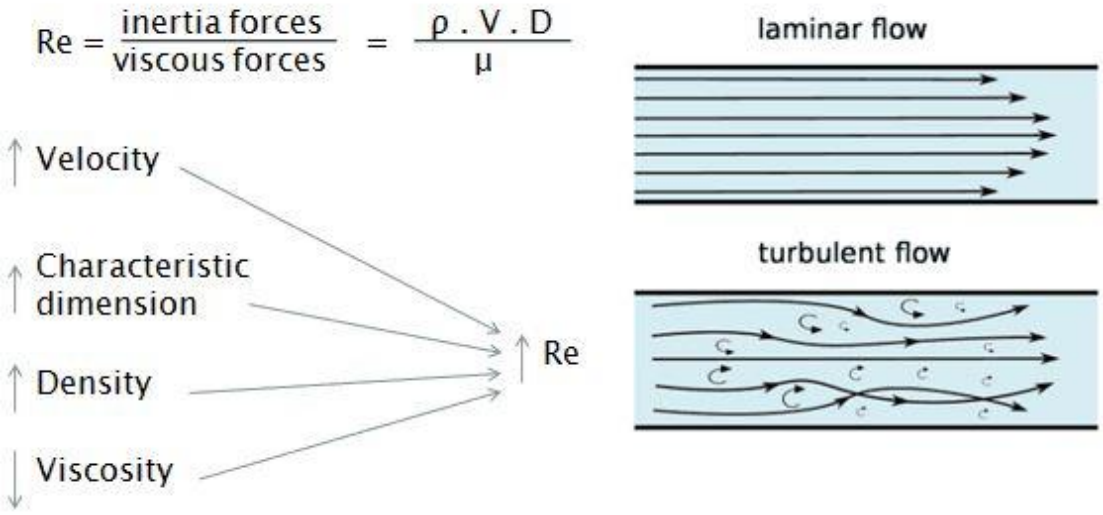

Figure 22: Reynolds number and it's association with the type of fluid flow

turbulent. The Reynolds number can be used to predict where this transition will take place.

Figure 23: Transition from laminar to turbulent flow

3.2.4 Navier-Stokes equations

In physics the Navier-Stokes equations describe the motion of viscous fluid substances. It is a system of three partial differential equations which result from the law of conservation of energy, mass and momentum. These equations result from applying Isaac Newton's second law to fluid motion, along with the assumption that stress in the fluid is the sum of a diffusing viscous term (proportional to the gradient of velocity) and a pressure term-hence describing the viscous flow.[19].

They are defined as:

$$p\frac{du_i}{dx} = pF_i - \frac{\partial p}{\partial x_i} + \frac{\partial}{\partial x_i}\{\mu\left(\varepsilon_{ij} - \frac{1}{3}\Delta\delta_{ij}\right)\}$$

The Fi coefficient includes all the forces applied to the fluid.

In the case of unchanged viscosity and incompressible flow, the equation is as follows:

$$p\frac{d\vec{u}}{dt} = p\vec{f} - \nabla p + \mu\nabla^2\vec{u}$$

The x,y,z coordinates are:

X coordinate: $p(\frac{\partial U_x}{\partial t} + U_x\frac{\partial U_x}{\partial x} + U_y\frac{\partial U_x}{\partial y} + U_z\frac{\partial U_x}{\partial z} = -\frac{\partial p}{\partial x} + pf_x + \mu(\frac{\partial^2 U_x}{\partial x^2} + \frac{\partial^2 U_x}{\partial y^2} + \frac{\partial^2 U_x}{\partial z^2})$

Y coordinate: $p(\frac{\partial U_y}{\partial t} + U_x\frac{\partial U_y}{\partial x} + U_y\frac{\partial U_y}{\partial y} + U_z\frac{\partial U_y}{\partial z} = -\frac{\partial p}{\partial y} + pf_y + \mu(\frac{\partial^2 U_y}{\partial x^2} + \frac{\partial^2 U_y}{\partial y^2} + \frac{\partial^2 U_y}{\partial z^2}$

Z coordinate: $p(\frac{\partial U_z}{\partial t} + U_x\frac{\partial U_z}{\partial x} + U_y\frac{\partial U_z}{\partial y} + U_z\frac{\partial U_z}{\partial z} = -\frac{\partial p}{\partial z} + pf_z + \mu(\frac{\partial^2 U_z}{\partial x^2} + \frac{\partial^2 U_z}{\partial y^2} + \frac{\partial^2 U_z}{\partial z^2})$

These equations are non-linear because of the transport coefficient, μ, which makes the solution quite difficult. Consequently, they can be used with a respectable precision only in certain cases, like a fluid that is characterized by a laminar flow.

Finally, the continuity equation is also essential for the equation system to be solvable, which indicates the conservation of energy, mass and momentum.

It's form is:

$$\frac{d}{dt}\int_{V(t)} Qdv + \int_{S(t)} \vec{n}Fds = \int_{V(t)} pdv$$

3.3 Computational Fluid Dynamics in Medicine

CFD is a tool that has been applied in many fields of science. Medicine and especially the endovascular system has been greatly assisted by this tool.

Cerebral aneurysms seem to be of great interest in CFD applications during the last years, since the current Medical equipment provides information regarding only the geometry of the aneurysm. Their initiation, growth and rupture is associated with hemodynamic parameters as well, making CFD an essential tool towards a better understanding of cerebral aneurysms.

4. Hemodynamic parameters of the flow

CFD is utilized to determine important hemodynamic parameters associated with aneurysm initiation, growth and rupture. The more frequently used are: blood velocity, velocity streamlines, Wall Shear Stress (WSS), Oscillatory Shear Index (OSI), Relative Residence Time (RRT), Time Averaged WSS (TAWSS) and Wall Shear Stress Gradient (WSSG).

WSS is the tangential force exerted by the viscosity of the movement of the blood wall. [20]. Shearing velocity is calculated by dividing velocity along the wall by distance from wall to the velocity measuring point. WSS is defined as the multiplication of fluid viscosity and shearing velocity of the neighboring vascular wall [21].

$$WSS = \frac{\partial u_t}{\partial y}$$

WSS is considered the most important hemodynamic parameter in the aneurysm initiation, rupture and growth. It is measured in Pa.

TAWSS is the time average of WSS magnitude.

$$TAWSS = \frac{1}{T}\int_0^T \|\tau\| dt$$

It is measured in Pa.

OSI is a dimensionless measure of how much the instantaneous WSS vector is aligned with the time-averaged WSS vector, or in other words a measure of changes in direction of shear forces on wall during cardiac cycle.

$$OSI = 0.5[1 - \frac{\left|\int_0^T \overrightarrow{WSS} dt\right|}{\int_0^T \left|\overrightarrow{WSS}\right| dt}]$$

OSI ranges from 0 to 0.5. 0 corresponds to no changes in the direction of shear forces, while 0.5 corresponds to a 180^o directional change of the WSS vector.

RRT is a parameter that defines how long the blood stays on the aneurysm wall. It is a marker of disturbed blood flow, marked by low magnitude and high oscillatory wall shear stress (WSS).

$$RRT = \frac{1}{(1 - 2 * OSI) * TAWSS}$$

It is measured in 1/Pa.

WSSG is a spatial derivative measure along the direction of the flow. It is used in unruptured cerebral aneurysms

$$WSSG = \sqrt{\left(\left|\frac{\partial \vec{\tau}_W}{\partial x}\right|\right)^2 + \left(\left|\frac{\partial \vec{\tau}_W}{\partial y}\right|\right)^2 + \left(\left|\frac{\partial \vec{\tau}_W}{\partial z}\right|\right)^2}$$

It is measured in Pa.

5. Literature Review of CFD studies on Cerebral Aneurysms

CFD is an essential part towards a better understanding of aneurysm initiation, growth and rupture. According to a recent review [20], 81 different geometric and hemodynamic parameters have been used in CFD studies regarding cerebral aneurysms. This great number of different parameters and the lack of resemblance in the sets of parameters examined among studies make the use of CFD results in clinical practice quite difficult.

Aspect ratio, aneurysm size, WSS, OSI and size ratio along with inflow angle and impingement zone are parameters worth mentioning, because they correlate most strongly with aneurysm growth and rupture [20].

5.1 Aneurysm Size, Aspect Ratio, Shape and Size Ratio

Before the processing power of computers became significant, the utility of CFD as a research tool was quite limited. Therefore, clinical decision making regarding aneurysm management of Cerebral Aneurysms was mainly based on geometric parameters.

Aneurysm size (diameter), is a useful discriminant of whether or not to treat an unruptured aneurysm. The risk of rupture increases with size, with 7 mm being a threshold [22]. Aneurysms with size >7 mm pose an increasing risk of rupture.

Aspect Ratio (aneurysm height divided my maximum neck diameter) is also correlated with aneurysm rupture. [23,24]. Aspect ratio ≥1.3 along with irregular shape are associated with aneurysm rupture independent of aneurysm size and location, and independent of patient characteristics [25]. An aneurysm is defined as being irregularly shaped when blebs, aneurysm wall protrusions, or multiple lobes are present. The presence of a daughter sac-bleb is also an indicator of aneurysm rupture [26].

Finally, another geometric parameter, Size Ratio (Ratio of aneurysm size to parent vessel diameter) has been proposed as better at predicting IA rupture risk than aneurysm size only [27, 28].

5.2 Impingement zone, Inflow jets and Inflow Angle

It has been shown that concentrated inflow jets, small impingement regions, and secondary flow patterns are indicators of aneurysm rupture [29]. These parameters may also play a major role in the initiation of side-wall aneurysm initiation [30] but it is undetermined if this role is through direct or indirect mechanisms.

Inflow angle is another parameter that incorporates the relation of the aneurysm dome to the parent vessel. Its spatial relationship has been shown to be an important determinant of flow patterns inside the aneurysm dome. An increasing inflow angle can lead to a deeper migration of the flow recirculation zone into the aneurysm, and result in higher inflow velocity and wall shear stress in both the inflow zone and dome, thus causing rupture [31]. Furthermore, aneurysms located at small parent vessels (PcoA and AcoA) and have a big inflow angle, are also very critical in determining the rupture behavior of small cerebral aneurysms [32].

Figure 24 shows wall shear stress, impingement zone and inflow jet, while figure 25 shows the aneurysm inflow angle (IA=180-a).

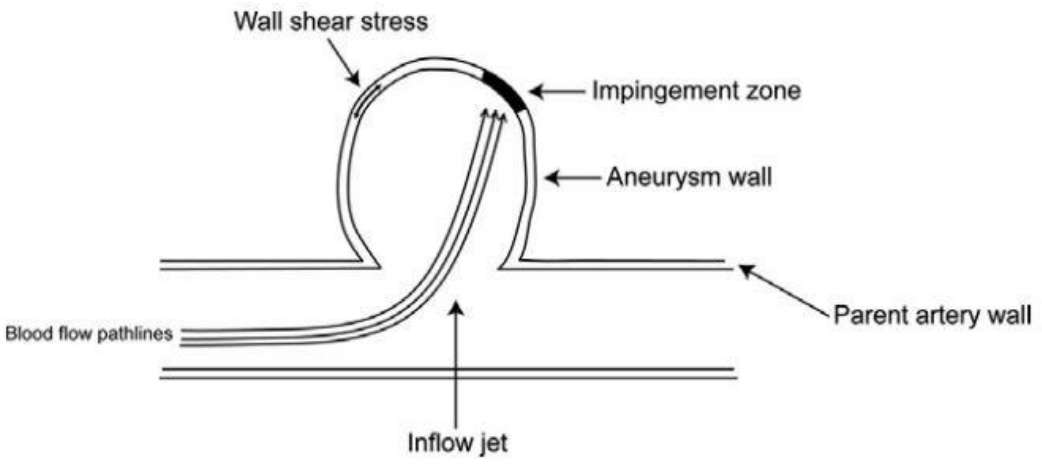

Figure 24: WSS, impingement zone and inflow jet

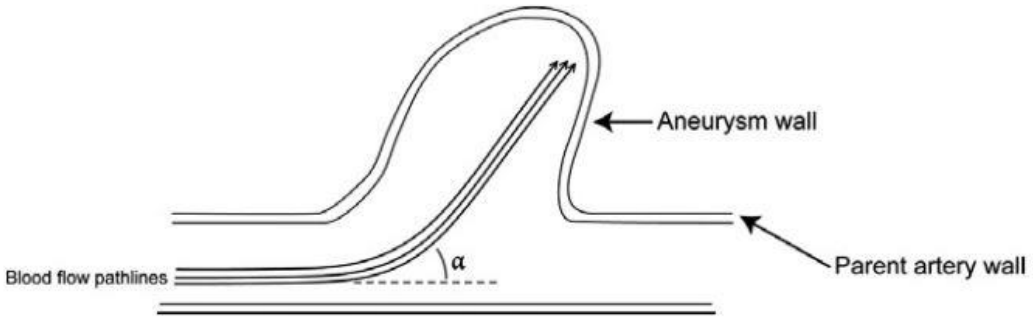

Figure 25: Aneurysm inflow angle (IA=180-a)

5.3 Treatment Results

CFD analysis after coiling has shown intra aneurysmal flow and energy flux into the dome to be significantly reduced by coiling, which also decreased the WSS and WSS gradient. Interestingly, these effects were dependent on the coil orientation, with the effectiveness order being parallel > transverse > orthogonal [33, 34]. Higher WSS were also noted at recurrent partially occluded cerebral aneurysms and the high WSS area of the residual neck coincided with the location where the aneurysm recanalization occurred [33].

Placement of a flow-diversion device causes an increase in the intra aneurysmal pressure, which can potentially cause the rupture of the aneurysm, especially giant aneurysms which usually have very weak walls. This relates both to the inherent flow diversion into the higher resistance parent artery pathway in combination with cerebral autoregulation leading to higher pressure gradients and to changes in the parent artery configuration such as reduction of a proximal parent artery stenosis [35]. Moreover, it has been suggested that flow diverter can generate stagnant aneurysmal flow and excessively low WSS, which may promote wall degradation via the inflammatory pathway.

5.4 WSS and OSI

The most highlighted and controversial parameter correlated with aneurysm growth and rupture, is WSS. Both high and low aneurysmal WSS have been separately correlated with such events [28] There is an agreement though among the research community on the role of hemodynamic forces interaction in aneurysmal formation/initiation.

Several studies have shown that aneurysms initiation is related to flow acceleration. In these areas a vascular remodeling, with different gene expression by endothelial cells occur due to high WSS and positive WSSG [36]. Through endothelial cell mechanotransduction, these hemodynamic stresses initiate biochemical cascades

when they exceed certain thresholds, leading to local production and activation of proteases (most important, matrix metalloproteinase 2 and 9) by mural cells, massive internal elastic lamina damage, and apoptosis which are responsible for media thinning and bulge formation [37]. Most interesting, inflammatory cell infiltration was not observed in early-stage intracranial aneurysm initiation, [38] and macrophage depletion did not attenuate aneurysm formation, indicating that hemodynamic initiation of intracranial aneurysms is not mediated by infiltrating inflammatory cells [39].

WSS reaches the highest peak in the very early stage of aneurysm formation and tends to decrease after this phase (with mean values of about 1.5 N/m2) [40, 41].

Figure 26 is useful to explain the two contradicting pathways of aneurysm growth and rupture/stabilization.

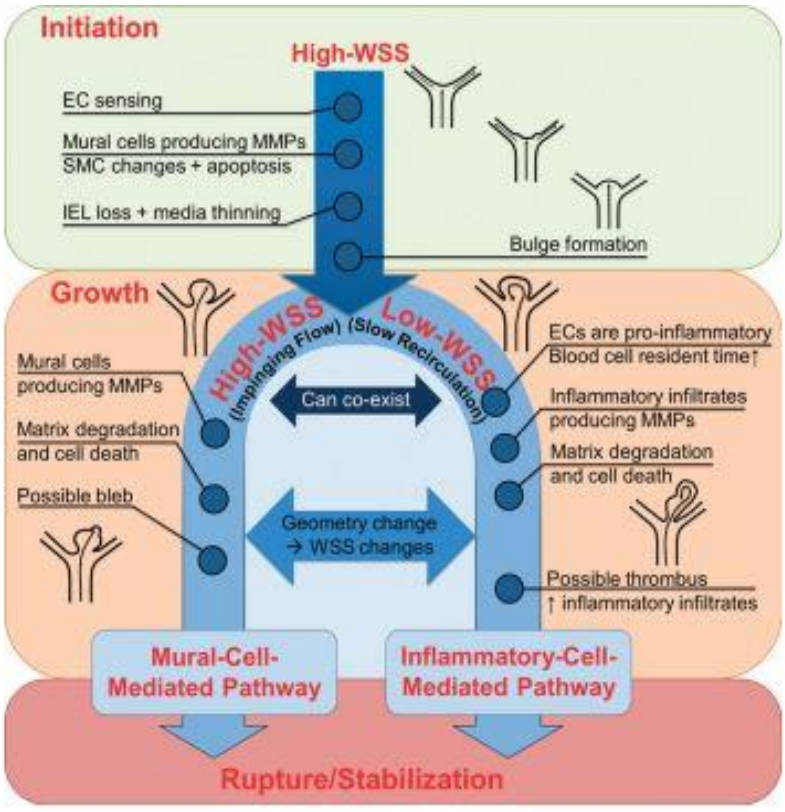

Figure 26: A unified role of high and low WSS in aneurysm initiation, growth, and rupture

After initiation, aneurysmal bulge enlargement exposes the sac to a gradually lowering WSS, leading to the biologic pathway illustrated by the right branch in Figure 26. That is, the flow environment is likely to be dominated by low and oscillating WSS after a recirculation zone has been formed in the sac especially if instability increases and/or secondary vortices form. Low and oscillatory shear stress elicits an inflammatory

response in the endothelium. Endothelial cells produce reactive oxygen species and upregulate surface adhesion molecules and cytokines in the vessel wall and increase luminal permeability [42]. A “sticky” and “leaky” endothelium, along with an increased blood residence time, provokes leukocyte transmigration into the wall during aneurysm development. These inflammatory infiltrates can massively produce matrix metalloproteinases to degrade the ECM, and consequently tipping the balance between eutrophic and degradative processes, thus driving intracranial aneurysm growth and rupture. Furthermore, such “disturbed flow” environments also promote the formation of atherosclerotic plaques which exacerbate the effects of inflammatory cells. [28].

On the other hand, impinging flow may persevere after bulge formation in some aneurysms, so that high WSS and positive WSS gradient could remain widespread in the aneurysmal sac. According to the left branch in Figure 26, mural cells are responsible for the destructive changes in the wall just as in the initiation phase and phenotype-modulated smooth muscle cells are the source of proteolytic activities.

Some authors have reported that high OSI correlates with the cause and location of atherosclerotic plaques, endothelial damage, aneurysm formation, and rupture. High OSI modulates the gene expression of endothelial cells to upregulate endothelial surface adhesion molecules, cause dysfunction of flow-induced NO, increase endothelial permeability, and thereby promote the rupture process [43, 44].

6. Scope of the study

The scope of this thesis is to study the hemodynamic differences that may arise, when two different techniques are applied to image the same geometry, a cerebral aneurysm. Furthermore, gradual decreases in the aneurysm geometry are applied in order to simulate virtual treatment scenarios.

SPECIFIC SECTION

7. Methods and Materials

The aim of this section is to analyze the CFD Workflow followed in this study. The stages of segmentation, meshing and simulation are thoroughly explained.

7.1 Study Group

Six patients were the basis of this study. Each of them was found with one cerebral aneurysm which was imaged both with DSA and MRA.

7.2 Medical Imaging Techniques

Time of flight (TOF) was the technique applied at all the MRA examinations with a resolution of 0.3mmx0.3mmx0.8mm. The image files are acquired in DICOM (digital imaging and communications in medicine) format. The MRA machine used is Philips Multiva 1.5T.

The DSA examination was performed with a Philips Allura Clarity bi-plane system. The result of this examination which is exported in WRL format, is a three dimensional object compared to the image files derived from the MRA.

7.3 Overview of the modeling and simulation procedure

Figure 27 is a schematic overview of a general CFD workflow.

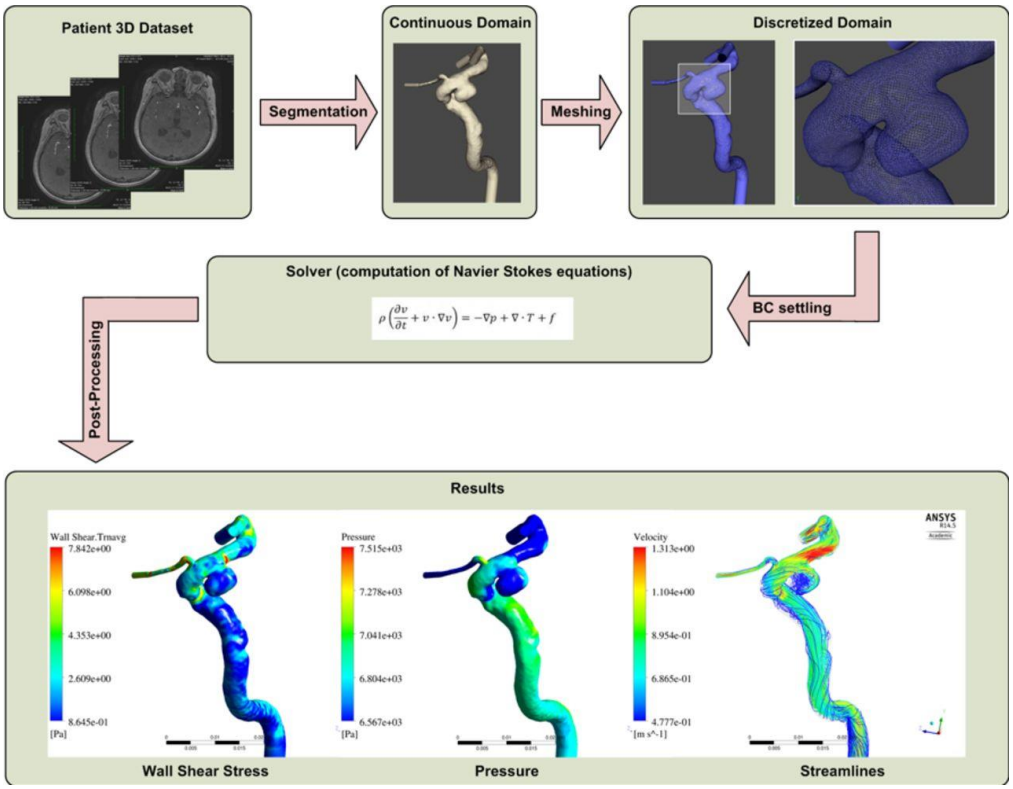

Figure 27: CFD workflow

First, a 3D data set of the patient's cerebral angiogram is obtained. Then the area of interest, which in this case is the cerebral aneurysm, is cut off the rest of the geometry, through a process called segmentation. This results to a continuous domain, which is afterwards divided into numerous small segments through the meshing process. The result is a discretized domain, called a mesh. Given the mesh, the final step in the computational pipeline is the simulation of blood flow through the patient's cerebral aneurysm, which is achieved by solving the Navier-Stokes equations. Once the procedure is over, hemodynamic parameters of interest are calculated and depicted.

For the implementation of those stages, specialized software is required. In the following sections, we present the specific steps along with the software used for the needs of this thesis.

7.3.1 3D Object creation/optimization

The first step of the CFD workflow is the isolation of the cerebral aneurysm from the rest of the angiogram and afterwards it's optimization. This must be done in order to create a 3D object as close to the real aneurysm geometry as possible. As previously noted, the DSA results are exported in WRL format (i.e a 3D object) while the MRA results in DICOM format. Therefore the DICOM data set of Pictures must be converted into a 3D object in order to be optimized subsequently.

Mimics Medical is the software used to initially insert the 3D data set of the MRA and finally end up to a 3D object. The steps for this process are:

1. The tab *Segment* is the first to be used. Then *New Mask* is selected which gives a 3 dimensional view of all the brain arteries, including the aneurysm. This is done by defining the *Threshold* for the gray values (Figure 28).

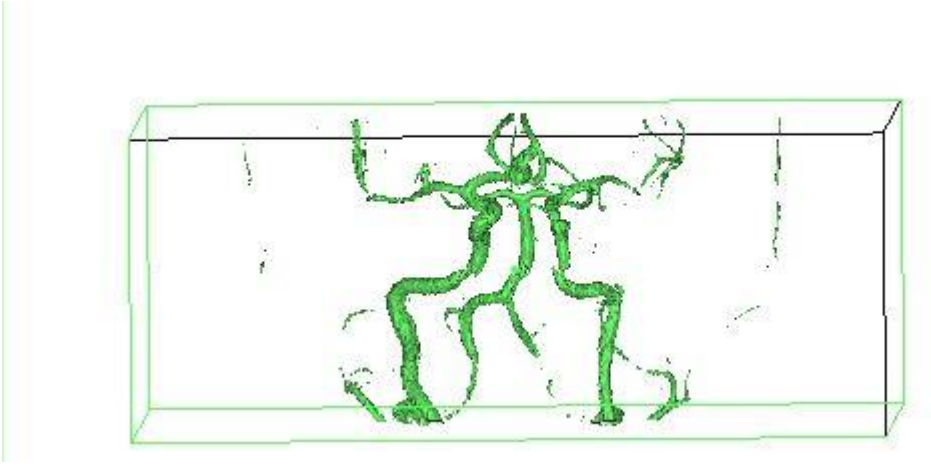

Figure 28: 3D view of the brain arteries

2. From the *Segment* tab, *Region grow* is selected. This removes the floating pixels from the region of interest and depicts the aneurysm with less noise (Figure 29).

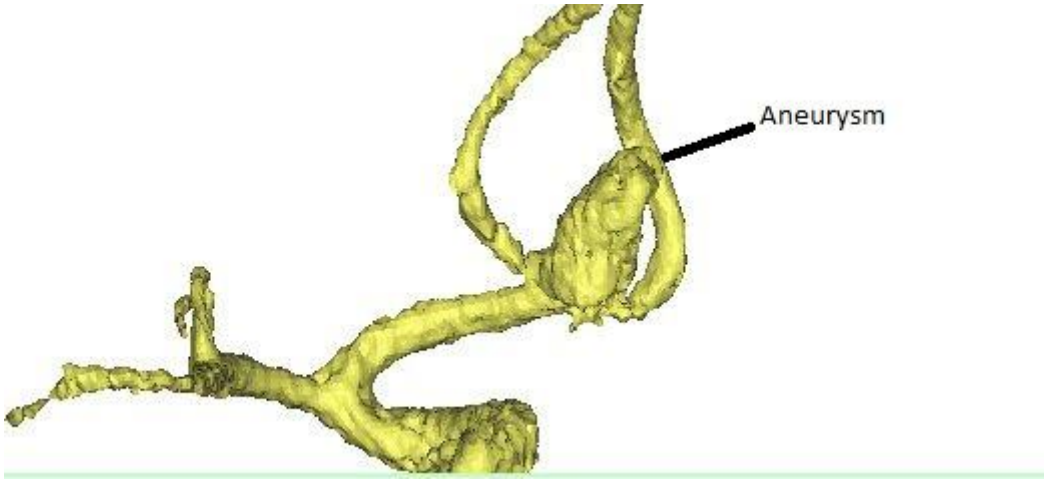

Figure 29: Reduced noise helps isolate the aneurysm from the rest of the brain angiogram

3. With the *Segment* tab still opened, the *Edit Masks* option allow for the unwanted regions to be erased (Figure 30). *Smooth Mask* is then used to filter existing artifacts of the mask and improve the borders quality.

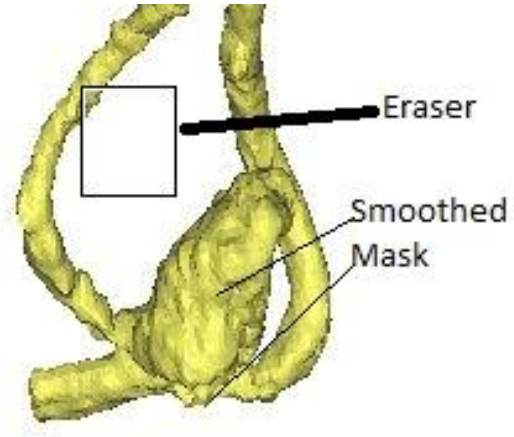

Figure 30: Mask after the Erasement of the unwanted region has been removed and the smoothing has been applied

4. Finally the 3D object is created by selecting the option *Calculate.* The resulting image is one of better quality ready to be exported in WRL format and further optimized (Figure 31).

Figure 31: The 3D object has been created, ready to be exported in WRL format.

A DSA angiogram is exported in WRL format, so these steps do not need to be applied.

The next stage, for the WRL files derived both from the DSA and the MRA examinations, is their optimization. This is a preliminary step and aims to reduce the noise of the 3D object, smooth it's shape and end up with a premature surface Mesh that replicates the real aneurysm's scheme.

Geomagic Design X is the software used for this stage. Obviously, the steps followed are the same for both imaging techniques since the file inserted in this software is in WRL format. The steps followed in this stage are:

1. In the *Polygons* tab, *Mesh Build up Wizard* is selected. The Mesh Buildup Wizard command is a wizard style interface for creating defect-free and watertight mesh models from raw 3D scan data. *Small/Medium Size Object Scanner* option is selected suitable for the size of our 3D object, an aneurysm. Then the aneurysm is isolated from the unwanted arterial branches with the *Define Wanted Area by Box* option (Figure 32, Figure 33).

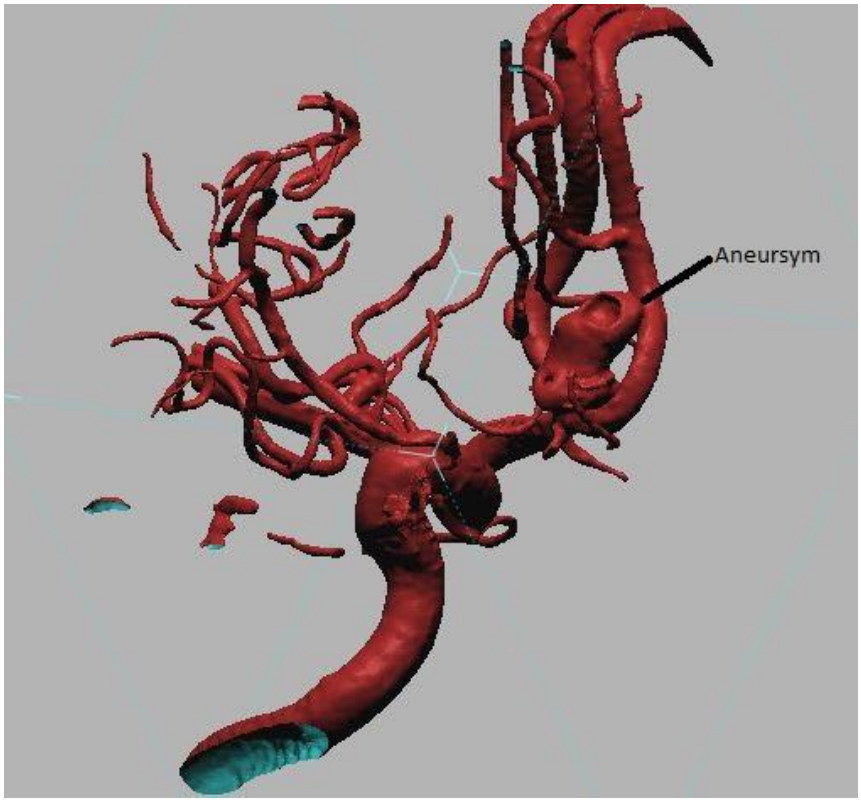

Figure 31: Aneurysm and arterial branch of DSA angiogram

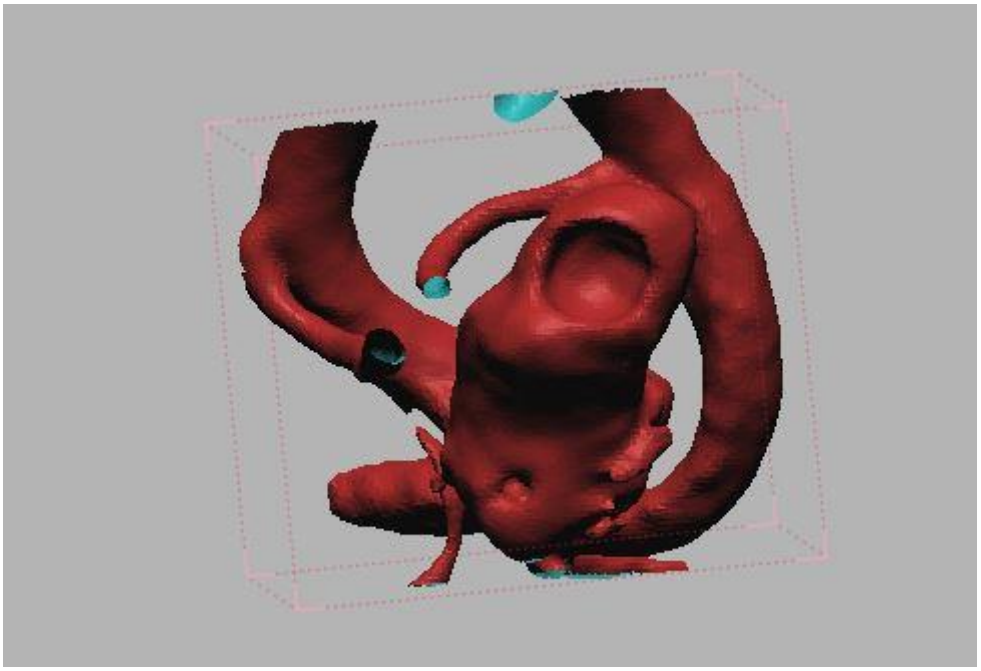

Figure 33: The aneurysm has been isolated

2. The noise is reduced by selecting the *Noise Reduction Level* option and the *HD Mesh Construction* option is used.
3. A series of steps follows, which aim at improving the preliminary Mesh quality and making it smoother without edges*. Global Remesh, Rewrap* and *Smooth* are some of the options under the *Polygons* tab which accomplish this scope (Figure 34).

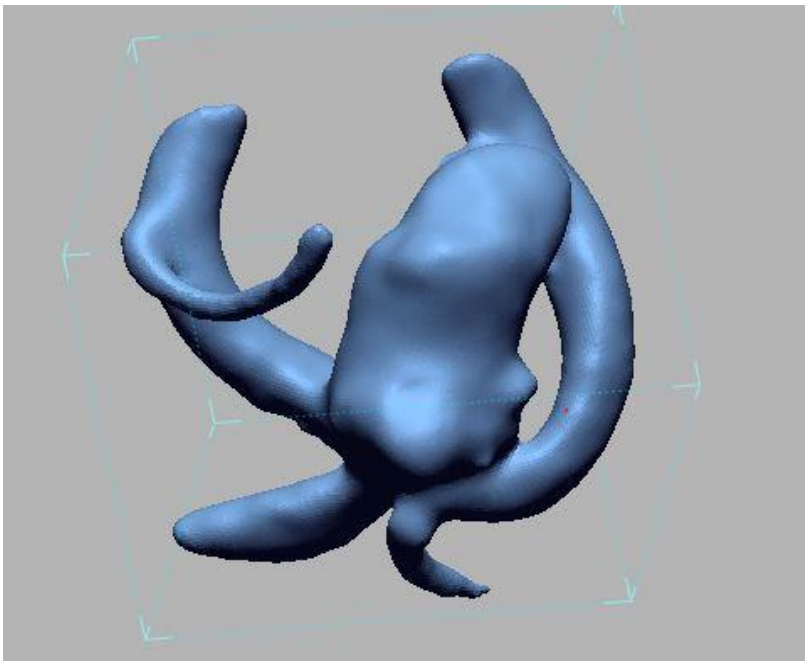

Figure 34: Smoothed out and Higher Quality preliminary Mesh

4. The long branches which are the inlets and outlets of the aneurysm are first trimmed. This is achieved by using the *Trim* option at the *Polygons* tab and Afterwards they are extended using the *Edit Boundaries*, *Extrude* option. This is an obligatory step in order to achieve a non turbulent and fully developed blood flow towards the aneurysm. The resulting preliminary surface Mesh is shown.

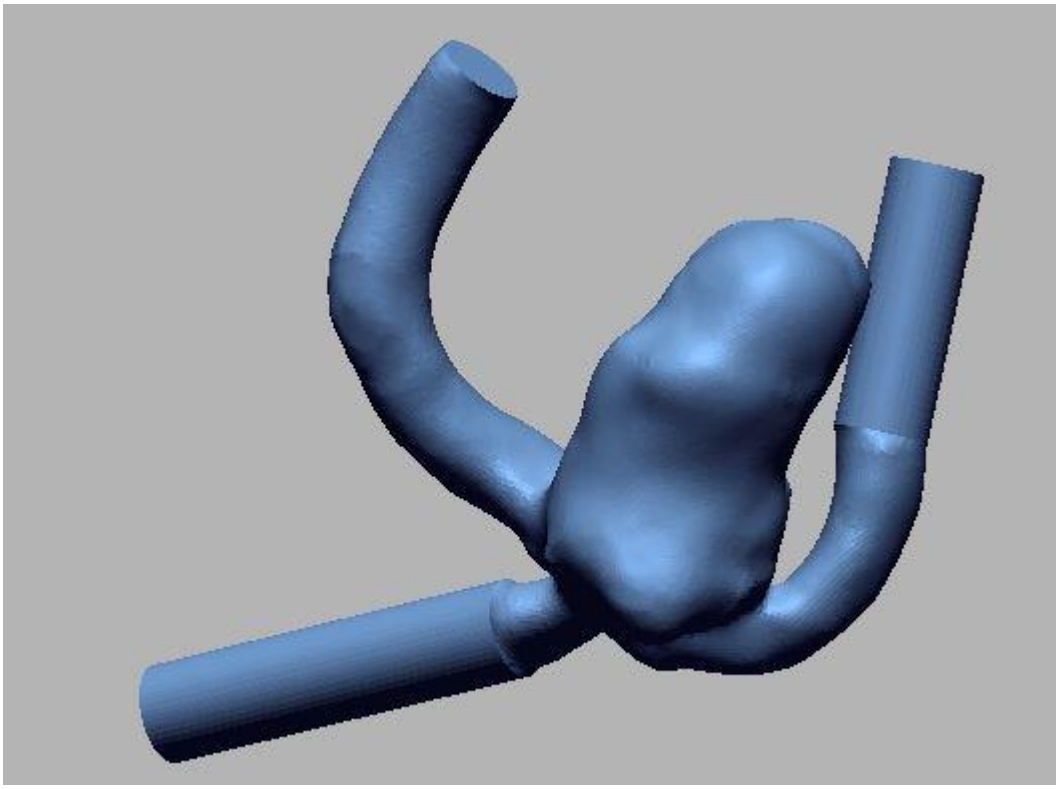

Figure 35: The rsulting preliminary mesh

5. The final step is the *Auto Surface* option. It creates curve networks on the existing preliminary Mesh and fits surface patches to the network which maintain accuracy to the underlying mesh (Figure 36).

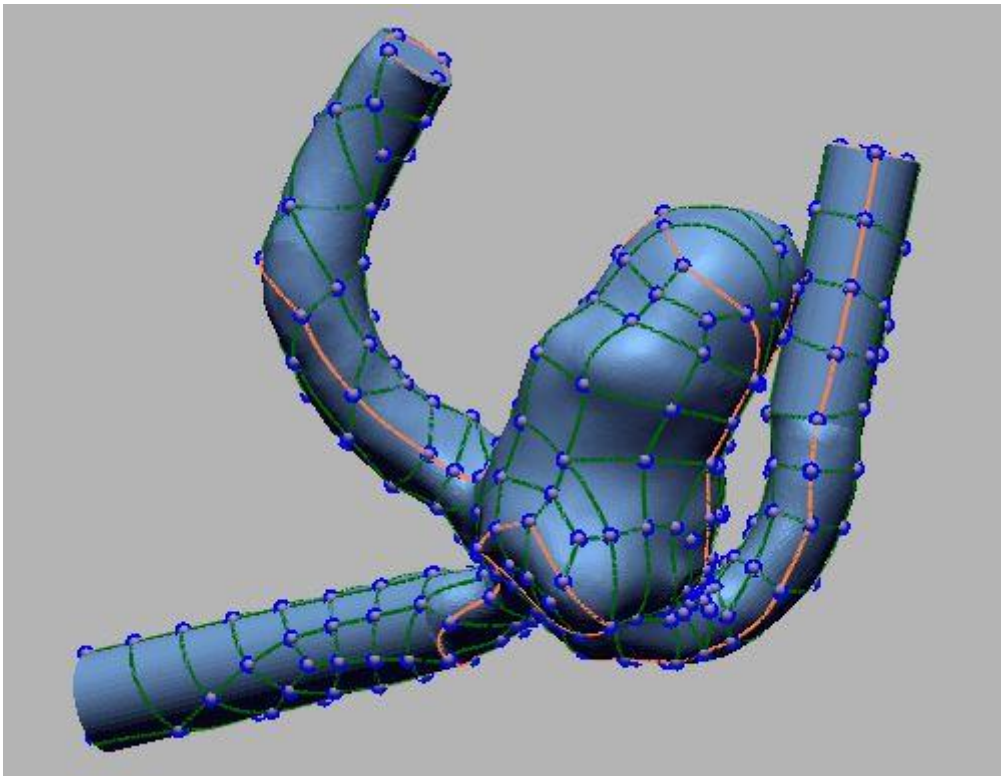

Figure 36: Auto surface stage

7.3.2 Mesh generation

The partial differential equations that govern fluid flow are not usually amenable to analytical solutions, except for very simple cases. Therefore, in order to analyze fluid flows, flow domains are split into smaller subdomains (made up of geometric primitives like hexahedra and tetrahedra in 3D and quadrilaterals and triangles in 2D). The governing equations are then discretized and solved inside each of these subdomains. Typically, one of three methods is used to solve the approximate version of the system of equations: finite volumes, finite elements, or finite differences. Caution should be taken in order to ensure appropriate continuity of solution across the common interfaces between two subdomains, so that the approximate solutions inside various portions can be put together to provide a complete picture of fluid flow in the entire domain. The subdomains are often called elements or cells, and the collection of all elements or cells is called a mesh or grid. [52].

The software used for the final meshing of the aneurysms is Ansys Mechanical Mesh and the steps applied as follows:

1. The aneurysm is divided into its Inlet-s, Outlet-s and Wall. This is done by the *Create Named Selections* option (Figure 37).

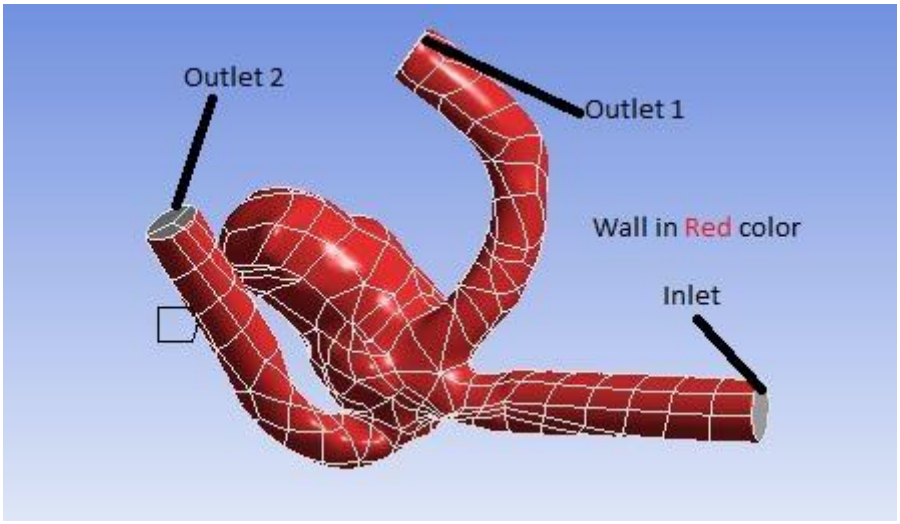

Figure 37: The aneurysm is divided into named selections

This is an essential step that allows the upcoming simulating software “understand” where the blood flow comes from, circulates and exits. More details will be provided in the following section (7.3.3).

2. Regarding the details of the Mesh which will be generated, at the *Physics Preference* tab the CFD option is selected and the *Element Midside Nodes* are *kept.* The first option is obvious and the Midside nodes are necessary to exist in order to predict proper values of stresses [45].
3. The *Tetrahedrons Patch Independent Method* is the meshing method of choice. The Patch Independent mesh method for tetrahedrons is based on the following spatial subdivision algorithm: This algorithm ensures refinement of the mesh where necessary, but maintains larger elements where possible, allowing for faster computation. Once the "root" tetrahedron, which encloses the entire geometry, has been initialized, the Patch Independent mesher subdivides the root tetrahedron until all element size requirements (that is, the prescribed local mesh sizes) are met [46]. The resulting Mesh is shown at *Figure 38.*

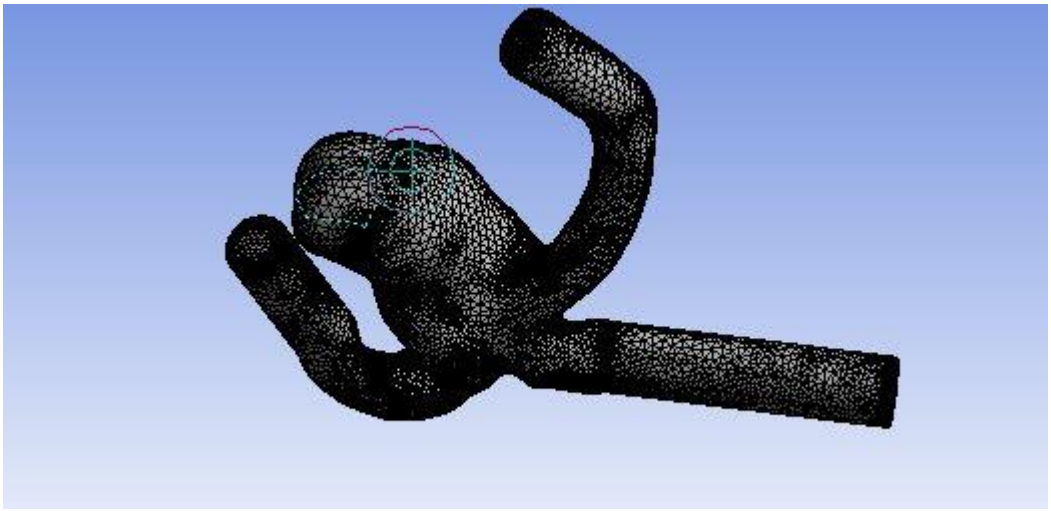

Figure 38: The final stage of the Mesh creation

7.3.3 Simulation

The final stage requires the definition of the fluid's properties, and some necessary boundary conditions in order to simulate the flow of the blood. The software used for this stage is Ansys Fluent. Fluent is a finite volume software that solves conservation equations about mass, momentum and energy, i.e. the Navier Stokes equations.

For the blood flow velocity, a realistic transient inlet velocity model of a patient's right ICA artery was used. The flow is considered laminar and the velocity profile applied at the inlet of the aneurysm is shown at Figure 39. It was created by performing Fourier Analysis and writing a code in C programming language.

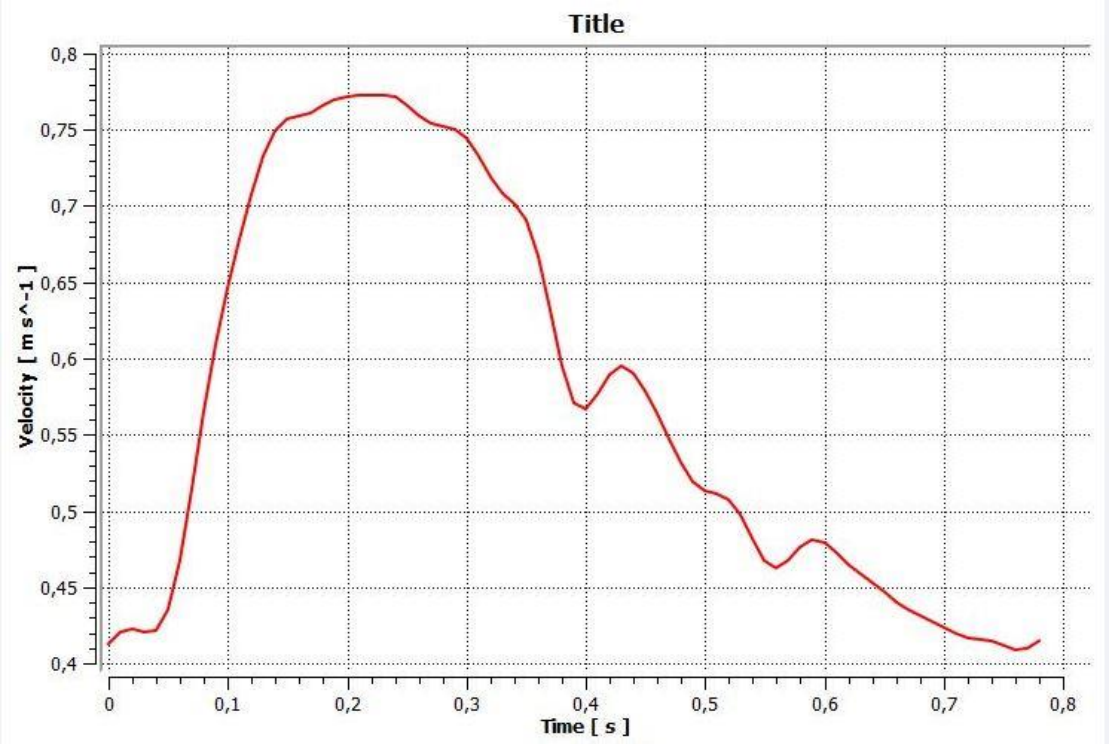

Figure 39: Inlet Velocity profile

The total duration of a cardiac cycle is assumed to be 0.8 sec which is equivalent to a heart rate of 75 beats/minute.

The wall is considered rigid and the no-slip boundary condition is applied at the wall of the aneurysm. Its density is set at 1050 kg/m^3, while the outlet pressure at 0 Pa [47]. Regarding the fluid's properties, it is necessary to help the software "understand" that the fluid flowing through the aneurysm is the blood. For that reason, the fluid's density and infinite shear viscosity were set at 1060 kg/m^3 and 0.0035 kg/m-s respectively.

The blood is known to be a shear thinning non-Newtonian fluid. Despite that, many researchers are modeling it as a Newtonian fluid to simplify the computational

simulation [48]. It must be noted though that this assumption causes a discrepancy especially at low velocity regions such as the aneurysm's dome [49].

7.4 Virtual Treatment Scenarios

Sometimes partial occlusion [50,51] is intended or inevitable while treating an aneurysm. The cerebral aneurysms that are examined in this thesis were treated with coiling and stent placement and all were completely occluded.

Two virtual treatment scenarios were carried out. One of 50% occlusion and one of a nearly complete-90% occlusion. The purpose of this virtual experiment is to discover the changes in key hemodynamic parameters like the WSS and OSI. This was achieved by trimming the aneurysm in half and 90% of its height, in Geomagic Design X. The resulting shapes from the full aneurysm up to 90% occlusion are shown at Figures 40 41 and 42 respectively.

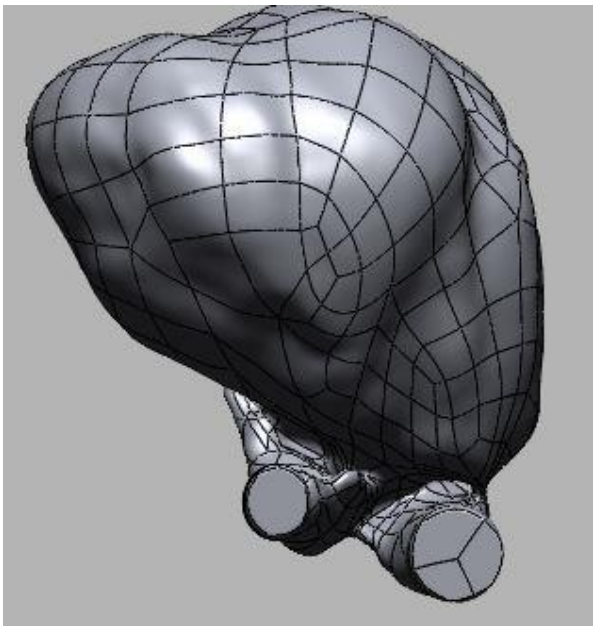

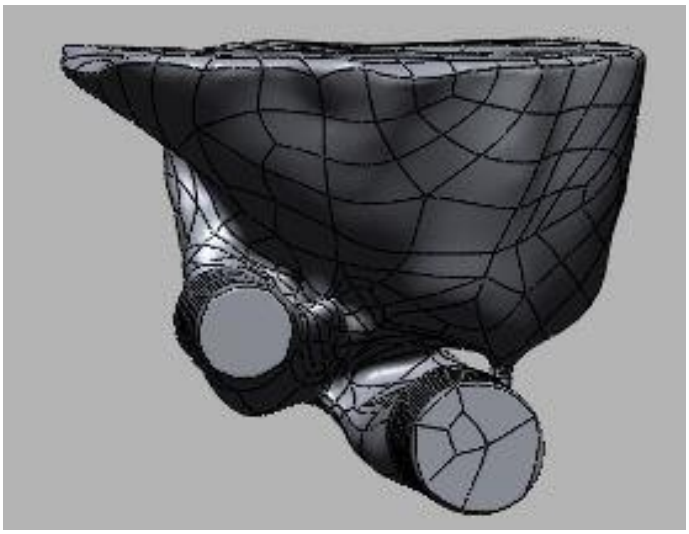

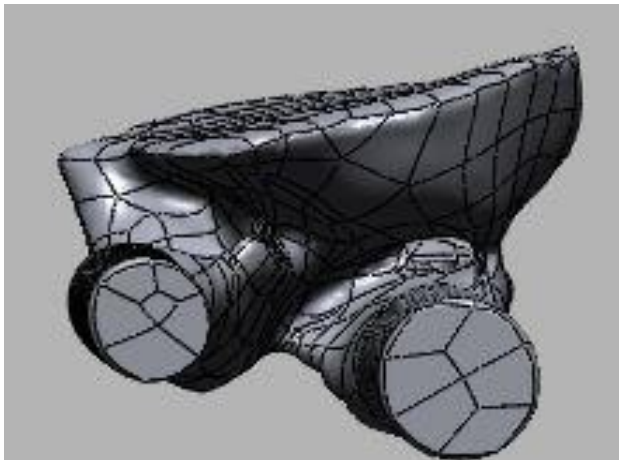

Figures 40,41 and 42: Full, half and 10% aneurysm size respectively

8. Results and Discussion

Six patients were examined. Each of them was found with one cerebral aneurysm. In the following section a comparison of the geometric and hemodynamic characteristics is made, in an attempt to find out if the use of different imaging techniques leads to different results.

8.1 Geometric and hemodynamic results

For each aneurysm a series of comparisons is made. At first the diameter and height of each aneurysm is presented. Then the cardiac cycle is discretized in four different time steps (0.05 sec, 0.2 sec, 0.4 sec, 0.6 sec) and for each one of them, a numeric and schematic comparison of the pressure and WSS is made. At the end of the cardiac cycle, which is the 0.8 sec mark, the parameter of OSI is depicted and finally a series of pathline Figures is presented at each timestep in order to simulate the path along which the blood flows.

At the end of each patient's case, a video of the WSS and the pathlines throughout the cardiac cycle is provided.

1st patient DSA vs MRA

- Diameter derived from the DSA examination: **21** mm
- Diameter derived from the MRA examination: **18.5** mm
- Height derived from the DSA examination: **20,5** mm
- Height derived from the MRA examination: **20** mm
- 1 inlet and 1 outlet of blood

The velocity profile applied at the inlet of all the cerebral aneurysms during the computational simulation at the Ansys Fluent software, is the following.

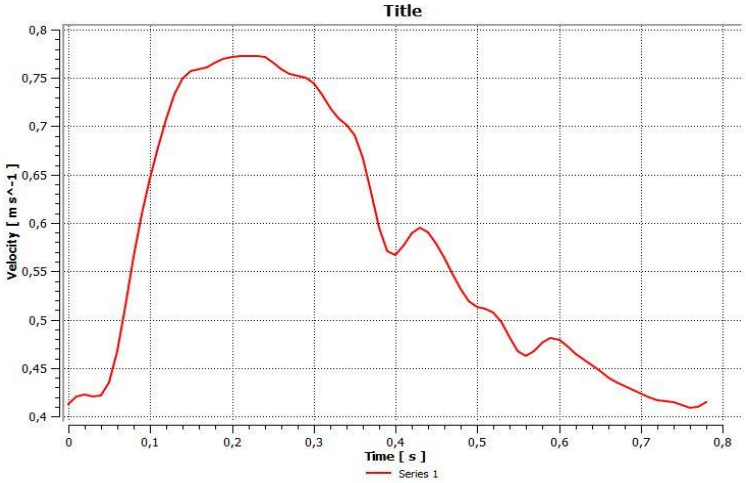

t = 0.05 sec

	DSA	MRA
Pressure	-20 to 298 Pa	-22 to 345 Pa
WSS	0 to 140 Pa	0 to 177 Pa
Area Average WSS	1.26 Pa	1.61 Pa

Pressure 0.05

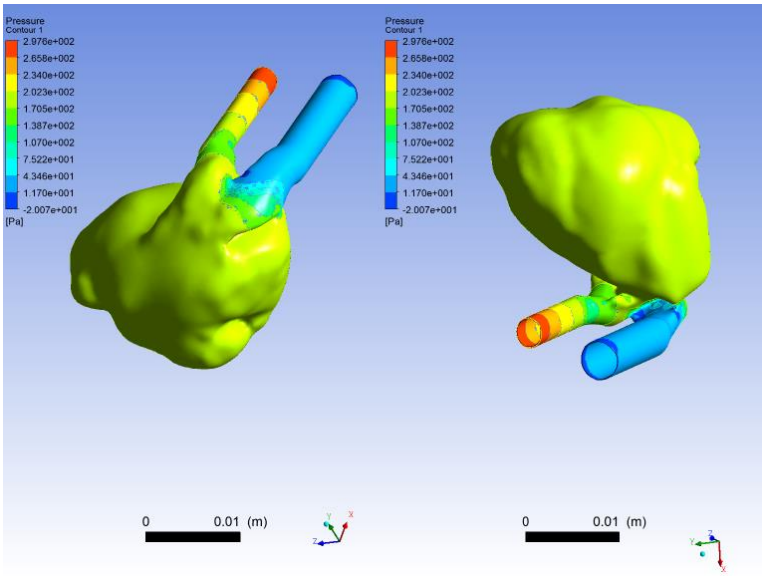

DSA

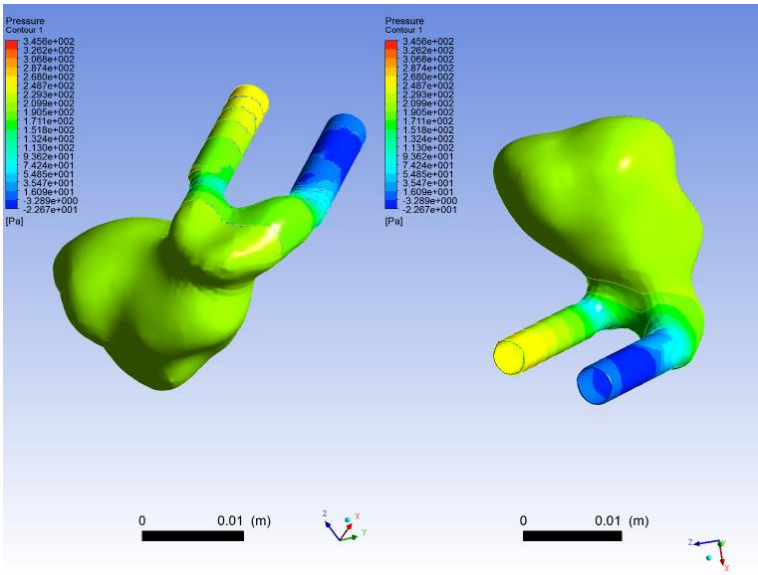

MRA

WSS 0.05

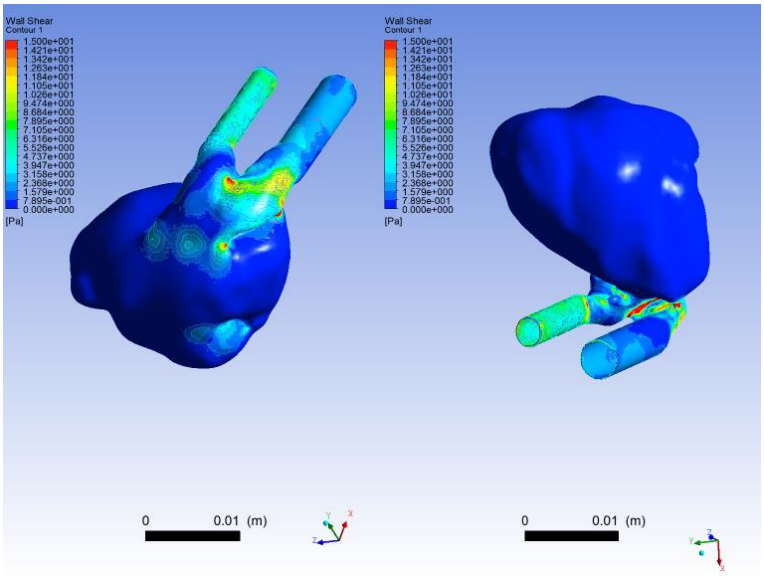

DSA

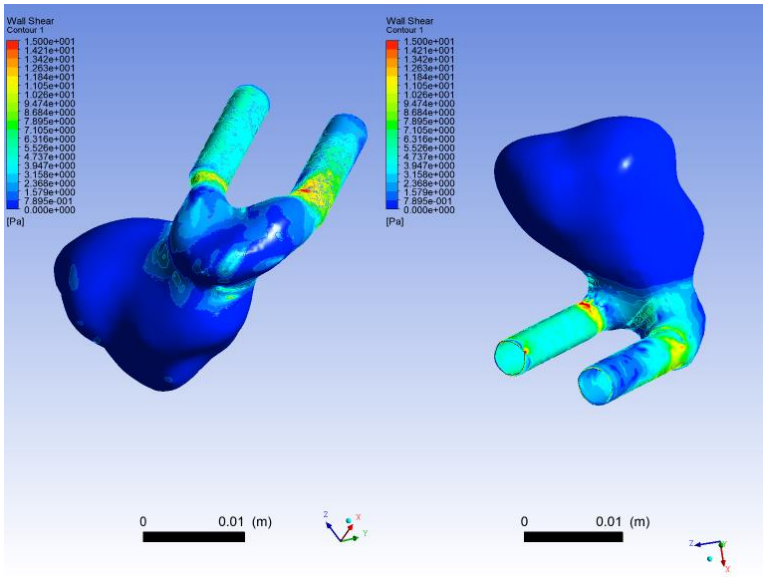

MRA

Pathlines (coloured by velocity magnitude) 0.05

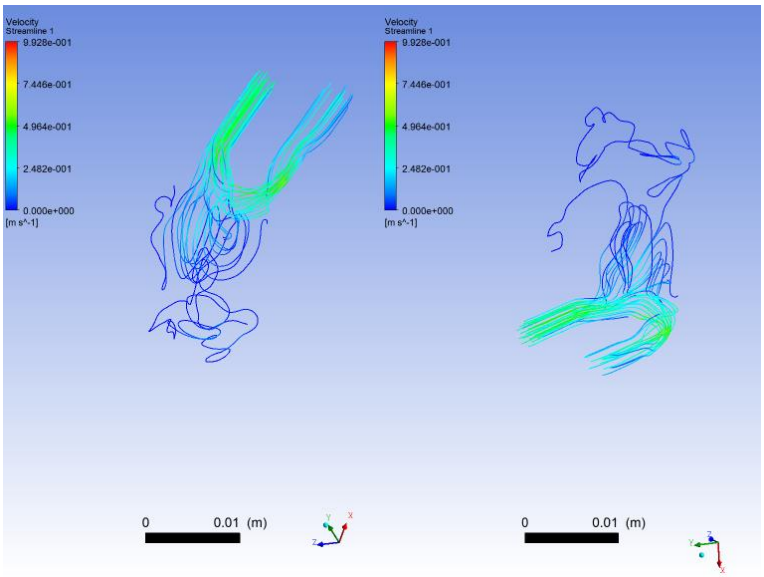

DSA

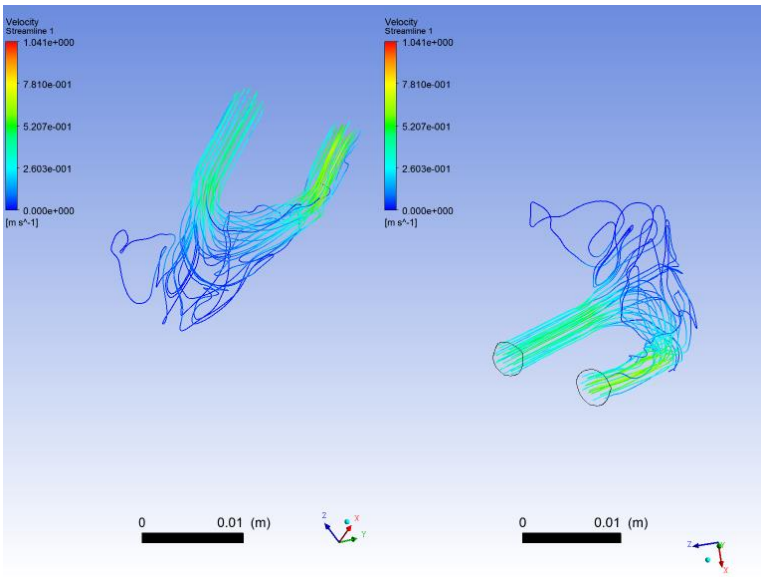

MRA

t = 0.2 sec

	DSA	MRA
Pressure	-203 to 634 Pa	0 to 790 Pa
WSS	0 to 282 Pa	0 to 334 Pa
Area Average WSS	2.84 Pa	4.21 Pa

Pressure 0.2

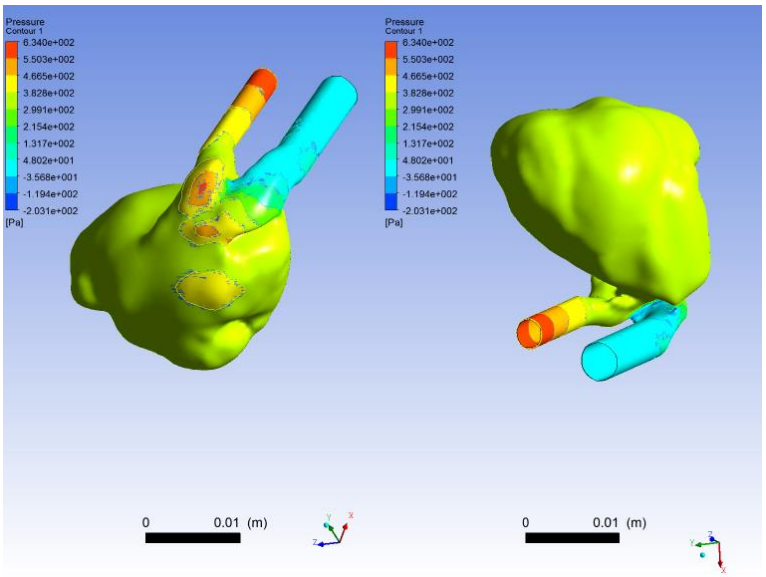

DSA

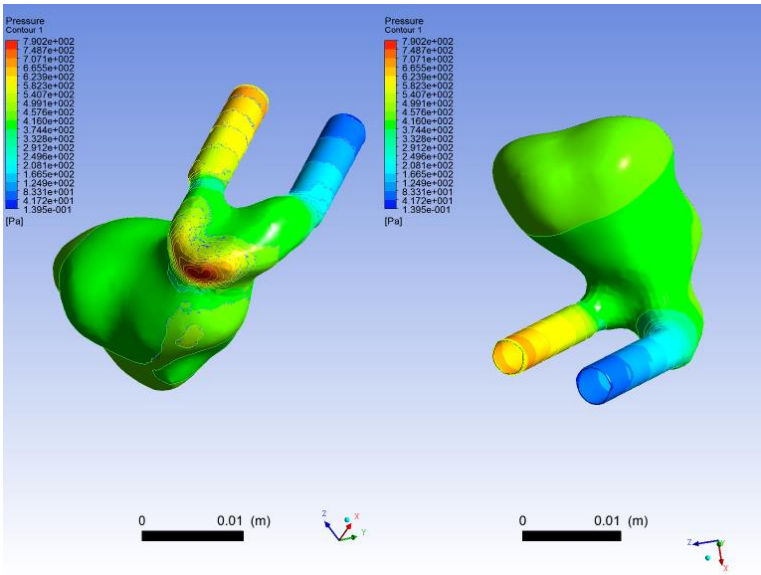

MRA

WSS 0.2

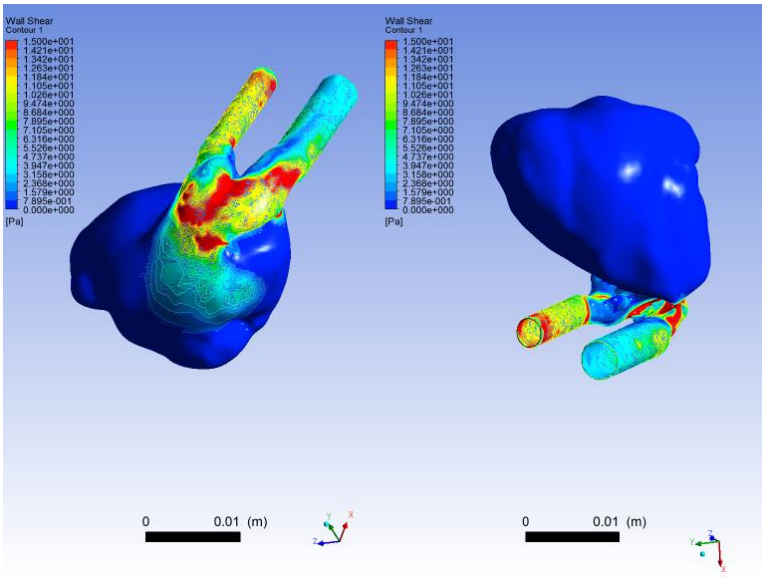

DSA

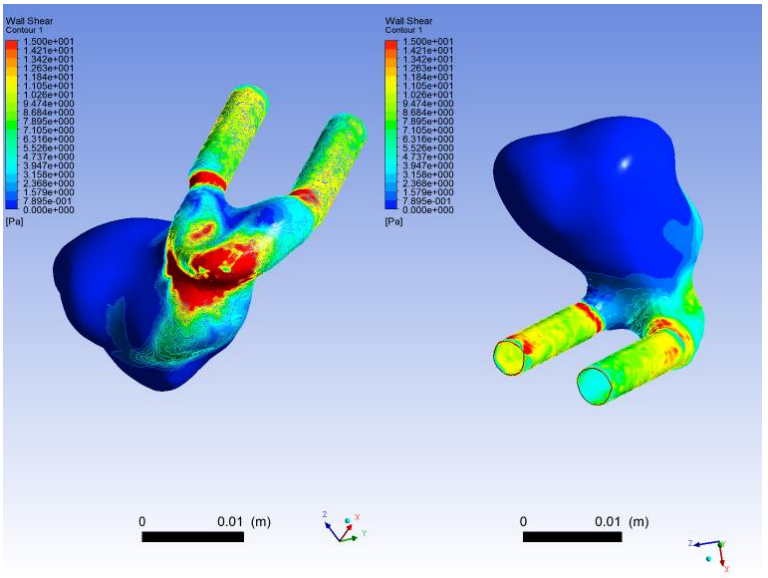

MRA

Pathlines 0.2

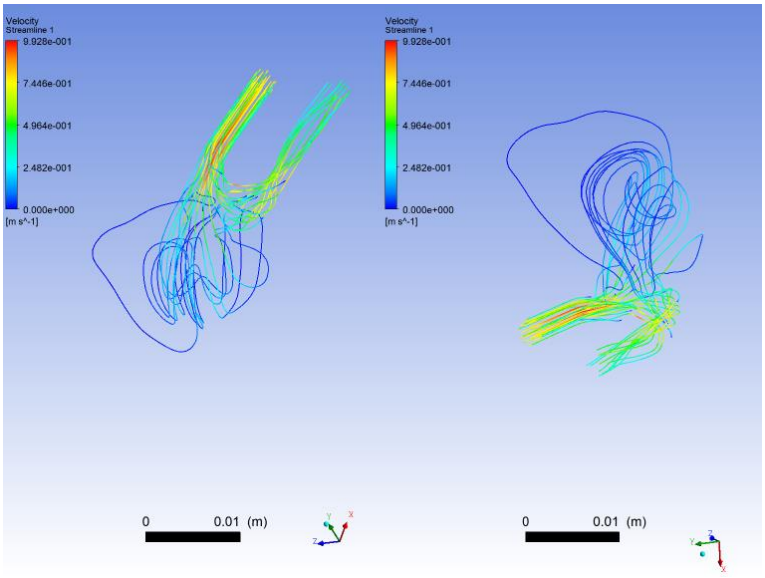

DSA

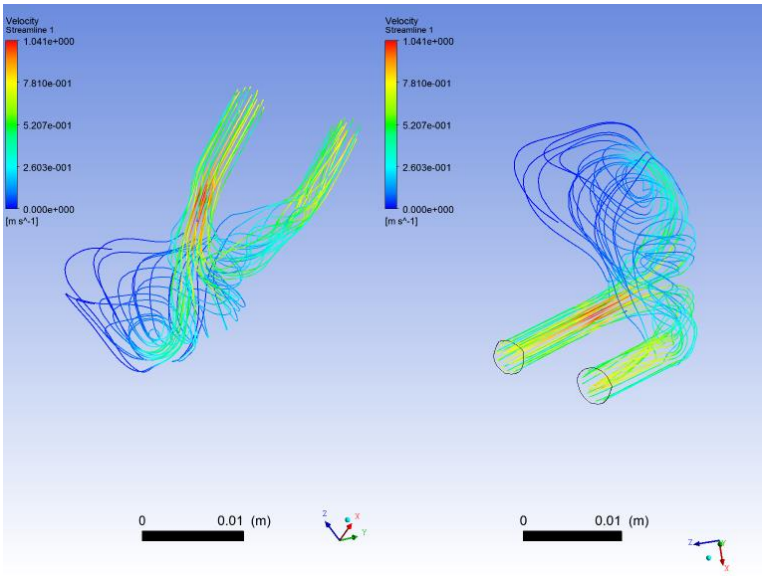

MRA

t = 0.4 sec

	DSA	MRA
Pressure	-97 to 420 Pa	-3 to 536 Pa
WSS	0 to 192 Pa	0 to 237 Pa
Area Average WSS	2.26 Pa	3.75 Pa

Pressure 0.4

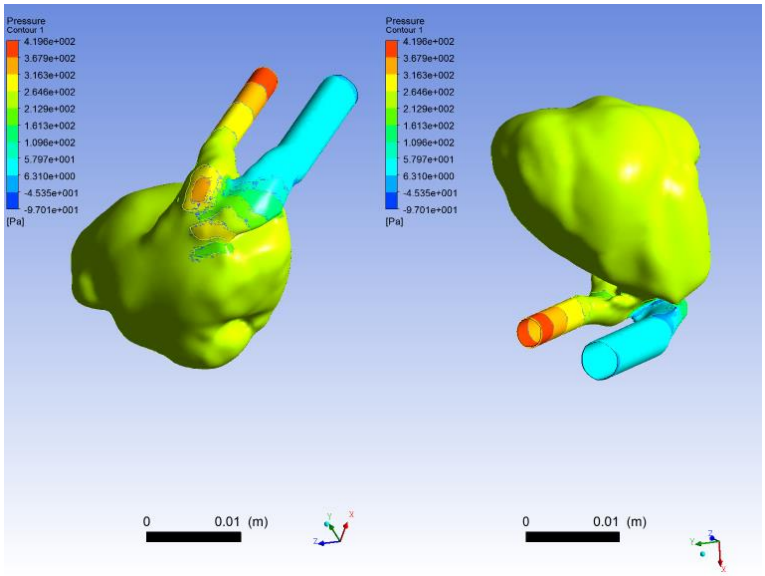

DSA

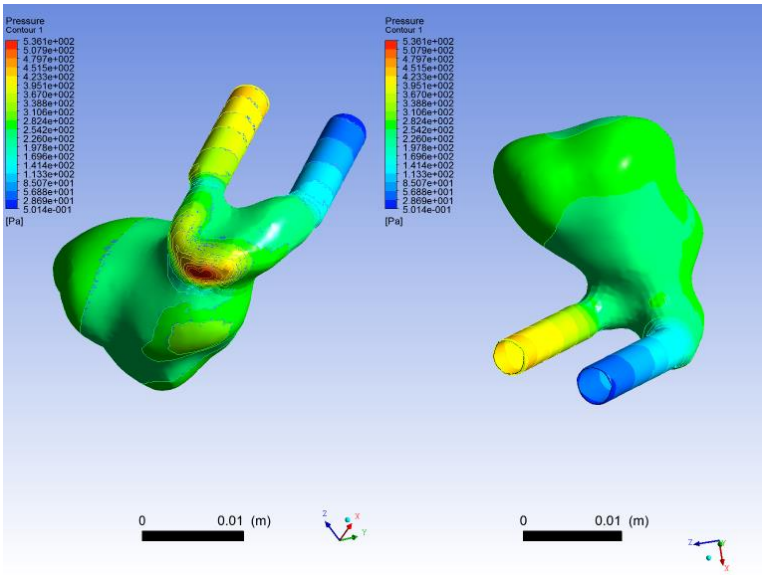

MRA

WSS 0.4

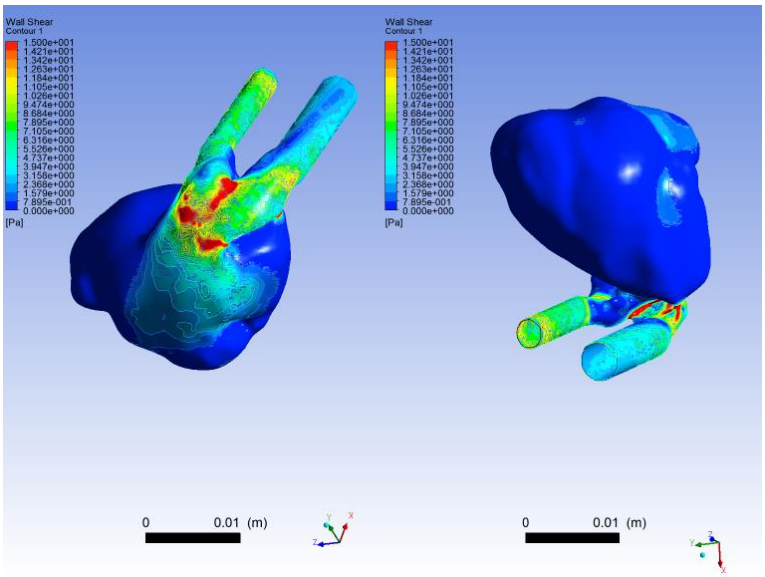

DSA

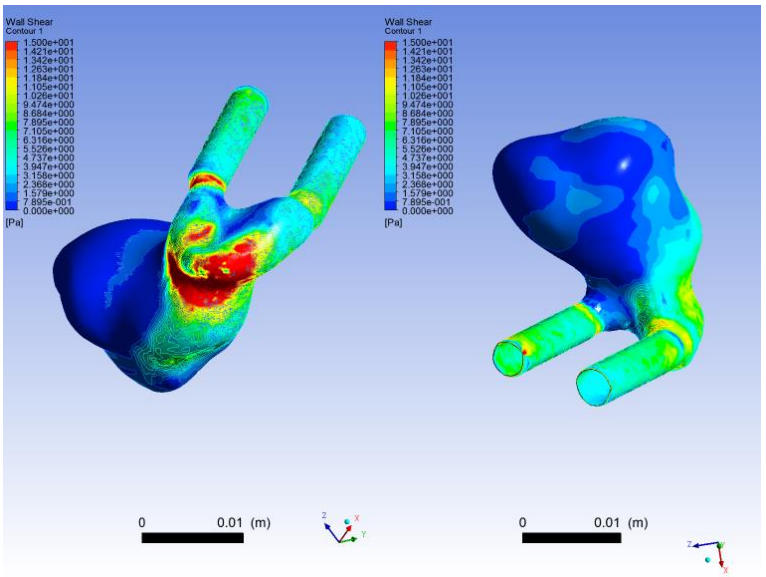

MRA

Pathlines 0.4

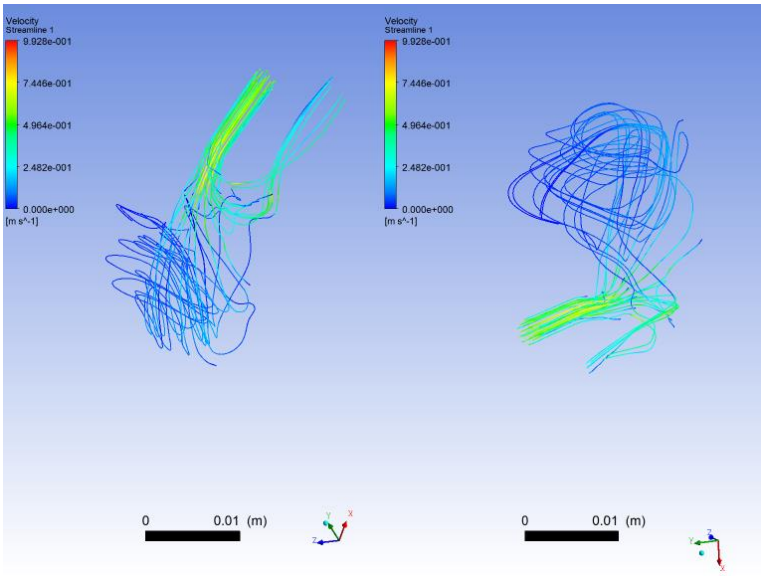

DSA

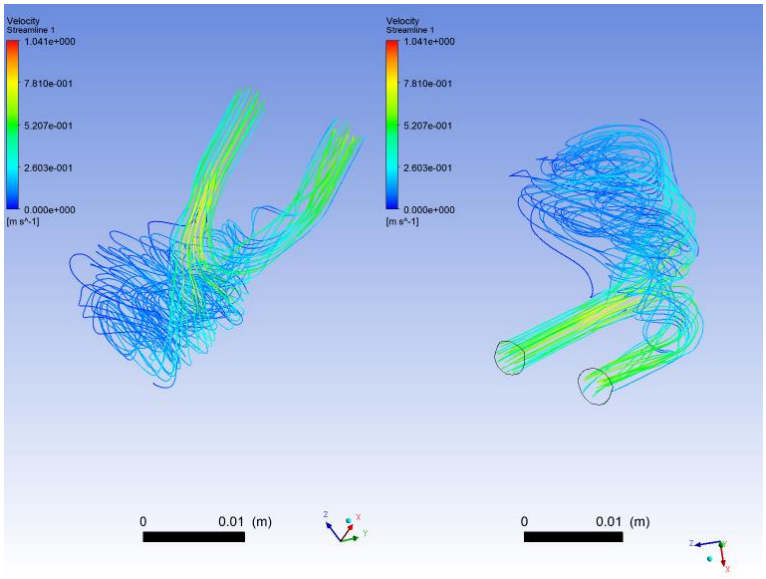

MRA

t = 0.6 sec

	DSA	MRA
Pressure	-74 to 275 Pa	0 to 372 Pa
WSS	0 to 157 Pa	0 to 197 Pa
Area Average WSS	1.60 Pa	2.57 Pa

Pressure 0.6

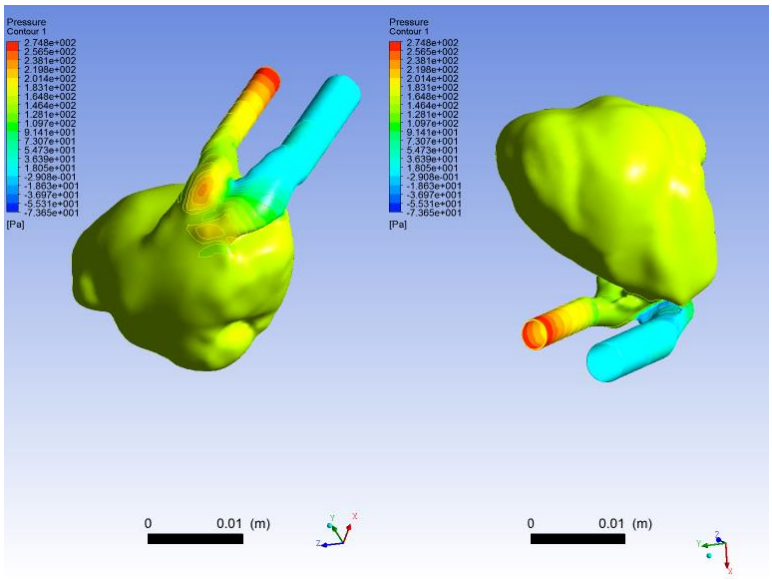

DSA

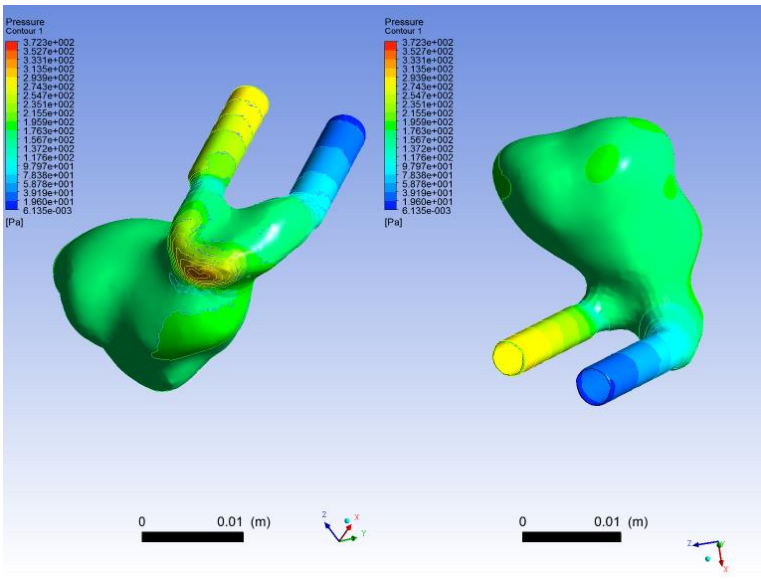

MRA

WSS 0.6

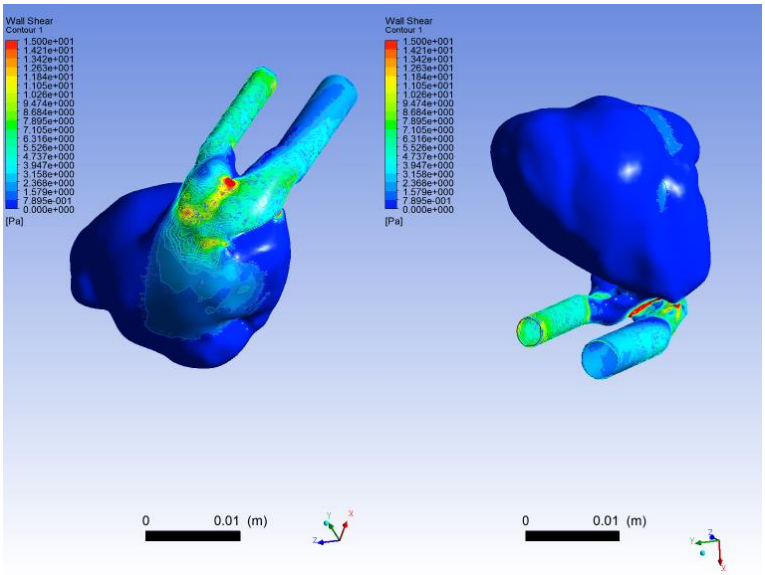

DSA

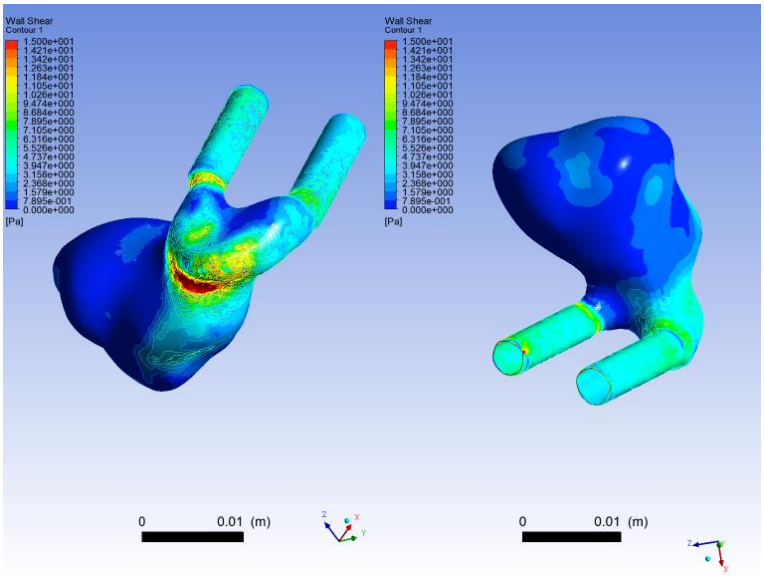

MRA

Pathlines 0.6

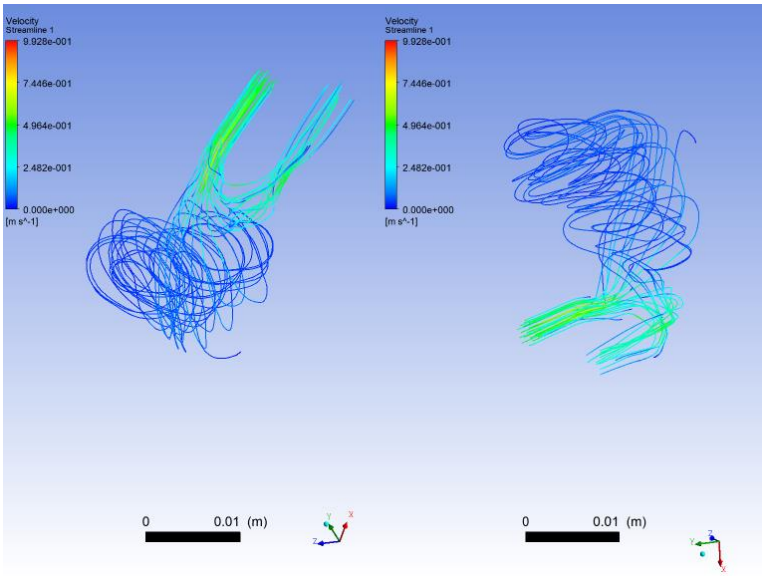

DSA

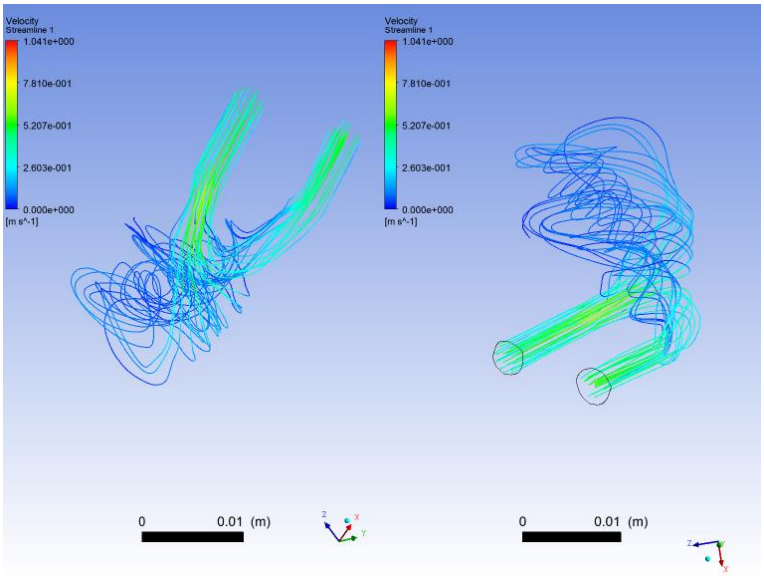

MRA

OSI 0.8

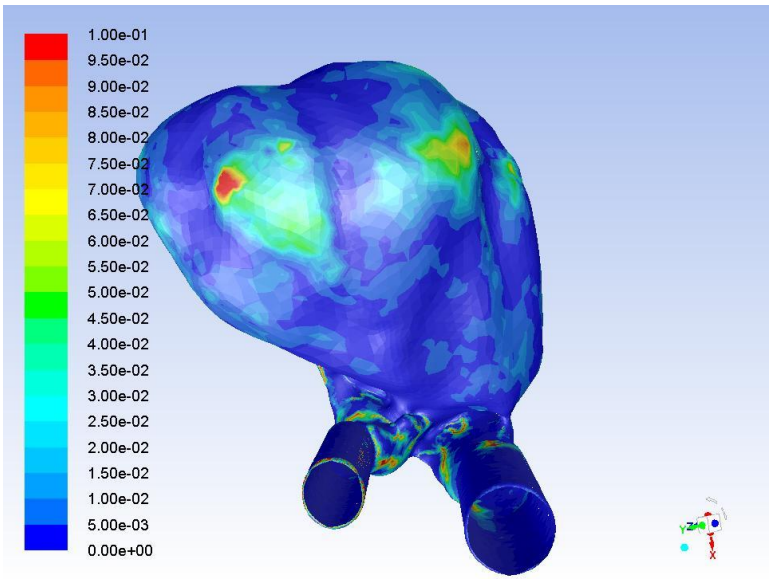

DSA front view

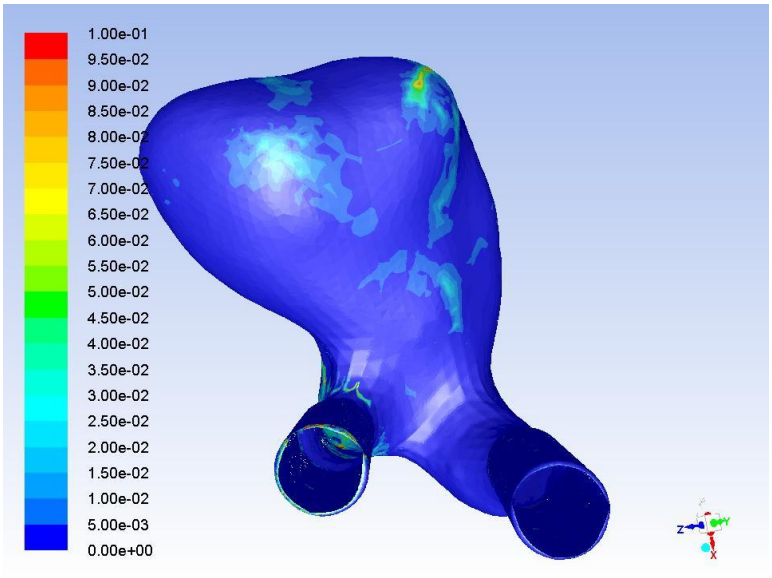

MRA front view

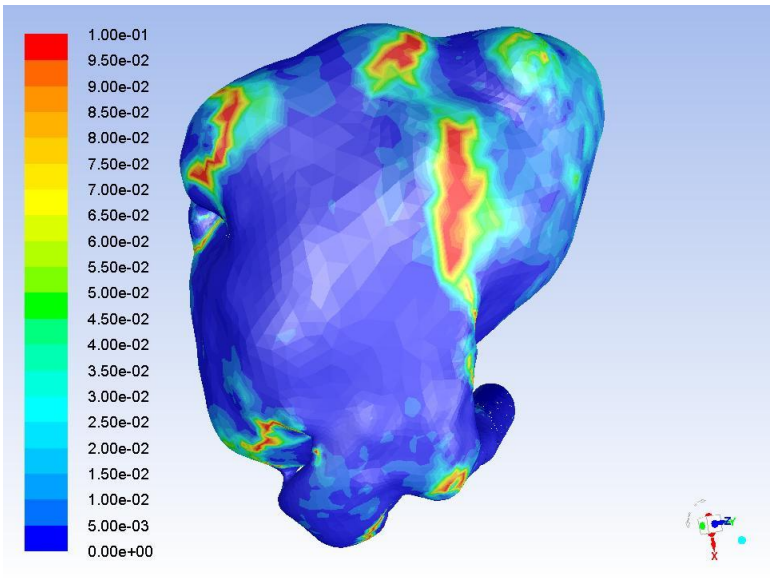

DSA rear view

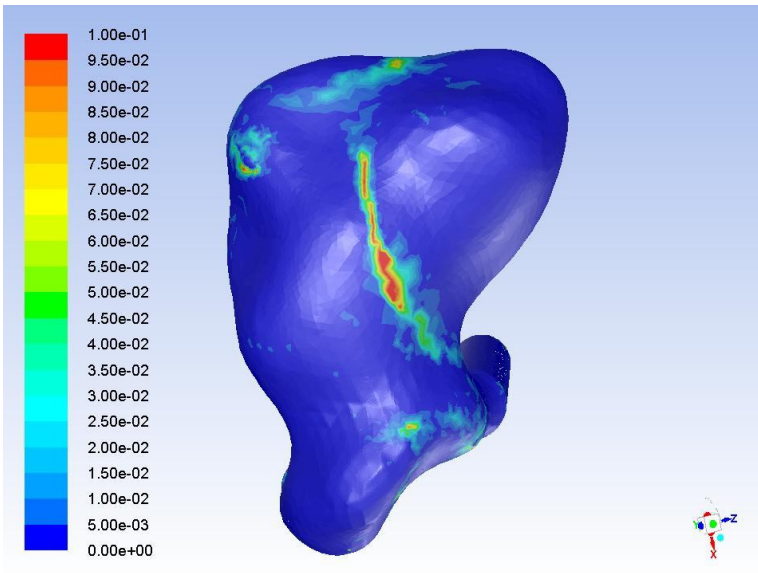

MRA rear view

1st patient results

- There is a notable difference in the shape and size of the aneurysm.
- The pathlines have different density but extend at the same regions of the aneurysm dome
- The minimum and maximum regions of WSS and OSI have some common regions
- The maximum values of pressure are always less at the DSA simulated aneurysm, with a margin as big as 26 %
- The maximum values of WSS are always less at the DSA simulated aneurysm with a margin as big as 21 %
- The area averaged WSS value is always less at the DSA simulated aneurysm and the margin is as big as 40 %

2nd patient DSA vs MRA

- Diameter derived from the DSA examination: **6** mm
- Diameter derived from the MRA examination: **6** mm
- Height derived from the DSA examination: **12** mm
- Height derived from the MRA examination: **12** mm
- 1 inlet and 2 outlets of blood

t=0.05 sec

	DSA	MRA
Pressure	-100 to 462 Pa	-9 to 553 Pa
WSS	0 to 226 Pa	0 to 252 Pa
Area Average WSS	3.66 Pa	4.71 Pa

Pressure 0.05

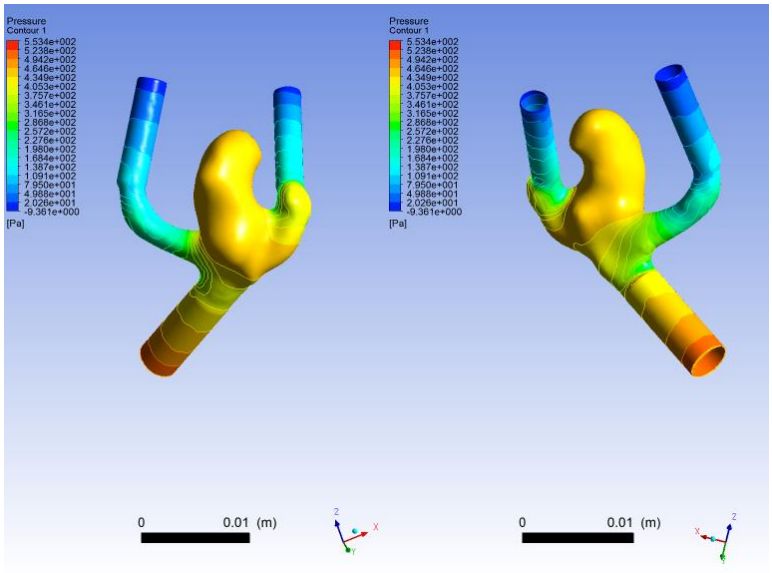
Pressure
Contour 1
5.534e+002
5.238e+002
4.942e+002
4.646e+002
4.349e+002
4.053e+002
3.757e+002
3.461e+002
3.165e+002
2.868e+002
2.572e+002
2.276e+002
1.980e+002
1.684e+002
1.387e+002
1.091e+002
7.950e+001
4.988e+001
2.026e+001
-9.361e+000
[Pa]
0
0.01 (m)
Pressure
Contour 1
5.534e+002
5.238e+002
4.942e+002
4.646e+002
4.349e+002
4.053e+002
3.757e+002
3.461e+002
3.165e+002
2.868e+002
2.572e+002
2.276e+002
1.980e+002
1.684e+002
1.387e+002
1.091e+002
7.950e+001
4.988e+001
2.026e+001
-9.361e+000
[Pa]
0
0.01 (m)

DSA

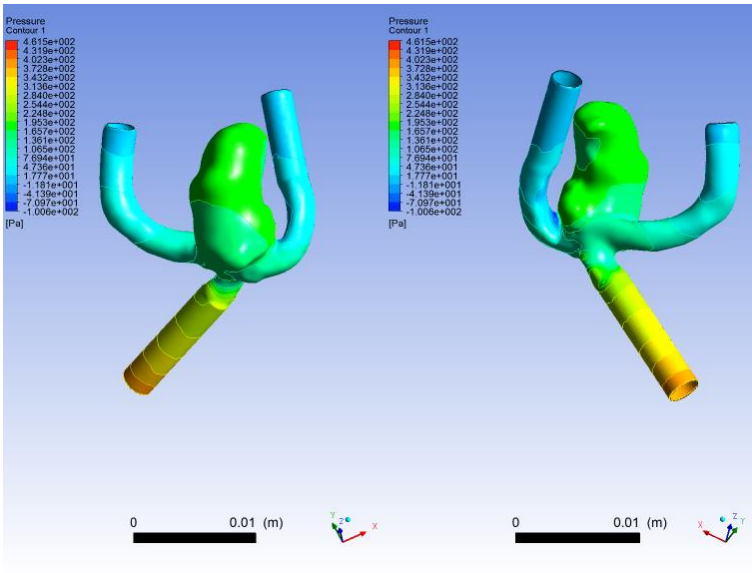
Pressure
Contour 1
4.615e+002
4.319e+002
4.023e+002
3.728e+002
3.432e+002
3.136e+002
2.840e+002
2.544e+002
2.248e+002
1.953e+002
1.657e+002
1.361e+002
1.065e+002
7.694e+001
4.736e+001
1.777e+001
-1.181e+001
-4.139e+001
-7.097e+001
-1.006e+002
[Pa]
0
0.01 (m)
Pressure
Contour 1
4.615e+002
4.319e+002
4.023e+002
3.728e+002
3.432e+002
3.136e+002
2.840e+002
2.544e+002
2.248e+002
1.953e+002
1.657e+002
1.361e+002
1.065e+002
7.694e+001
4.736e+001
1.777e+001
-1.181e+001
-4.139e+001
-7.097e+001
-1.006e+002
[Pa]
0
0.01 (m)

MRA

WSS 0.05

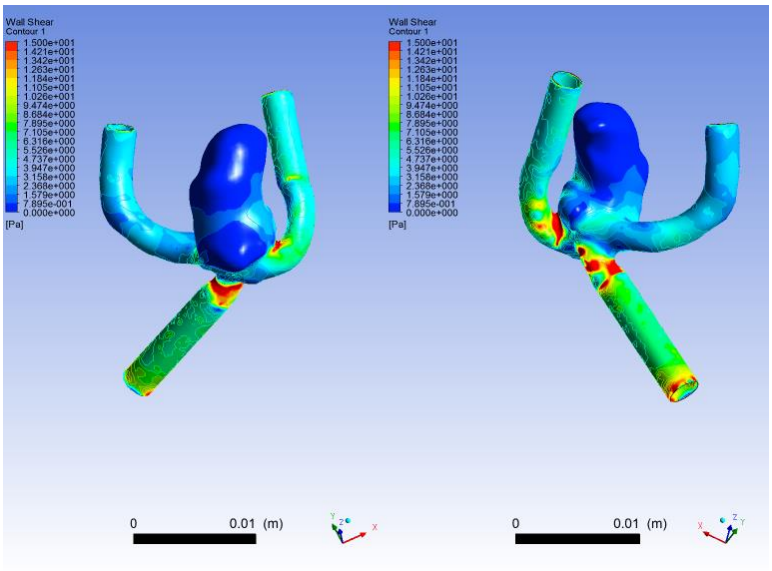

DSA

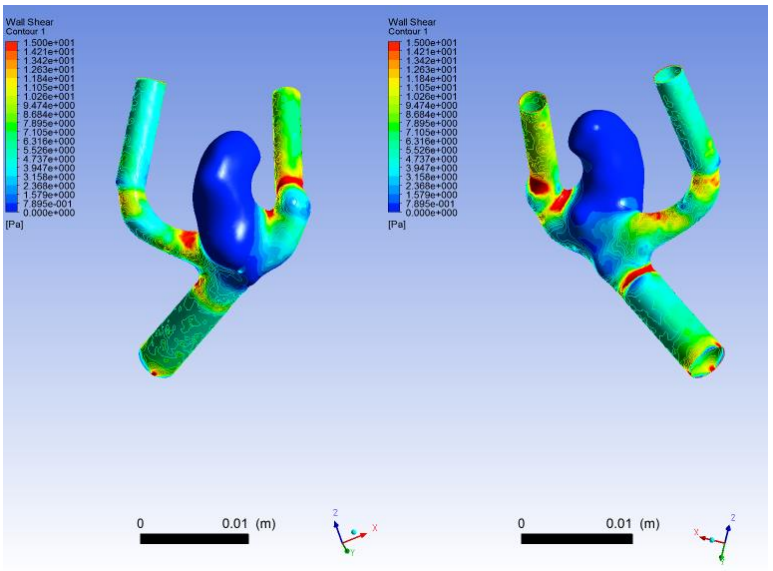

MRA

Pathlines 0.05

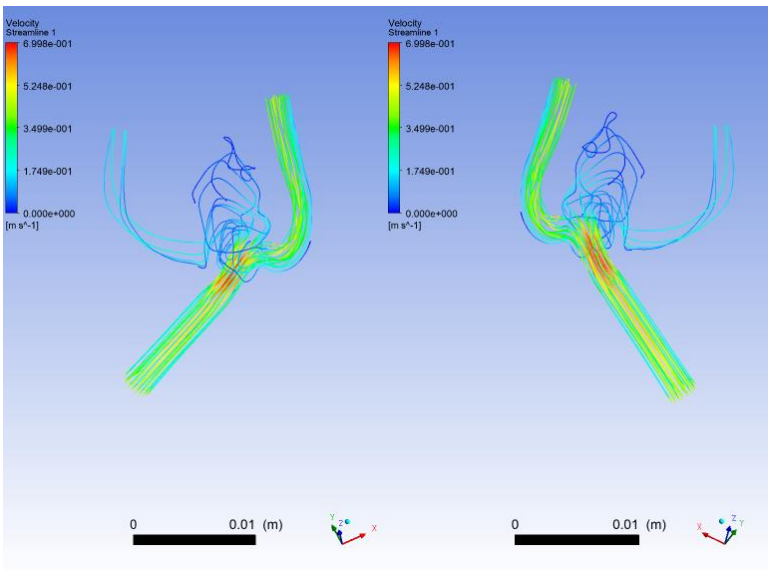

DSA

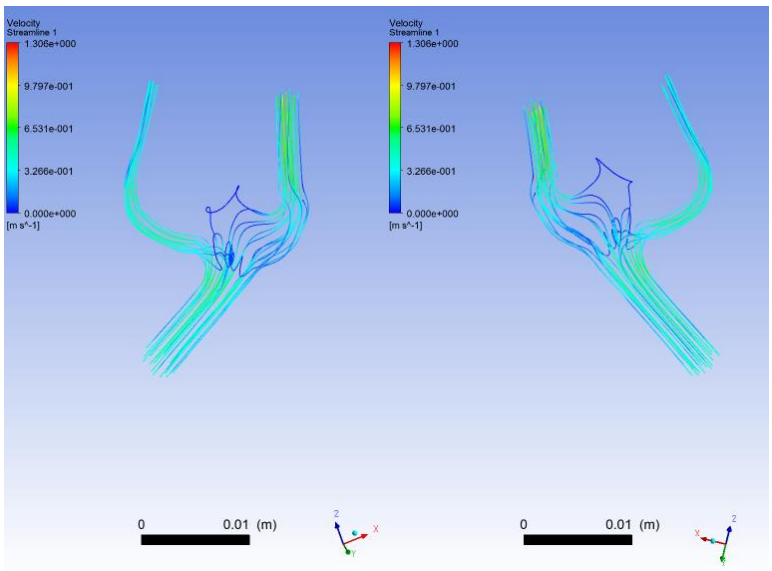

MRA

t=0.2 sec

	DSA	MRA
Pressure	-216 to 1017 Pa	-1 to 1238 Pa
WSS	0 to 420 Pa	0 to 452 Pa
Area Average WSS	10.16 Pa	12.15 Pa

Pressure 0.2

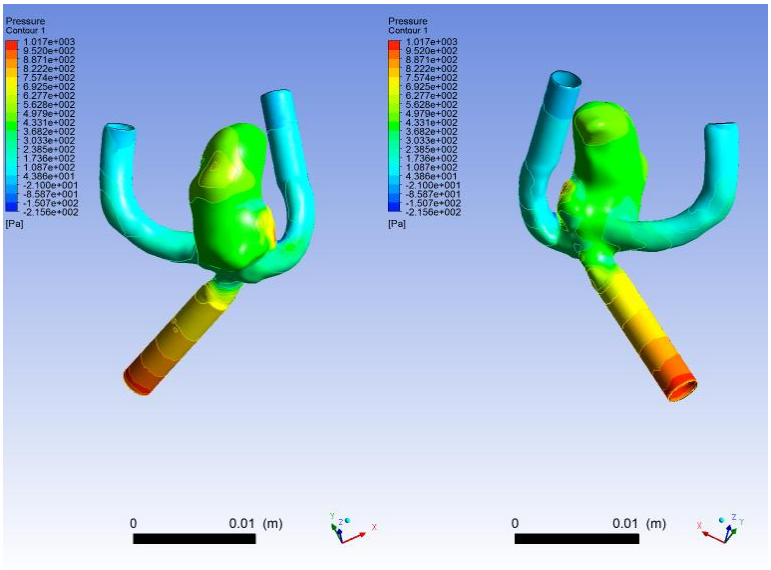

DSA

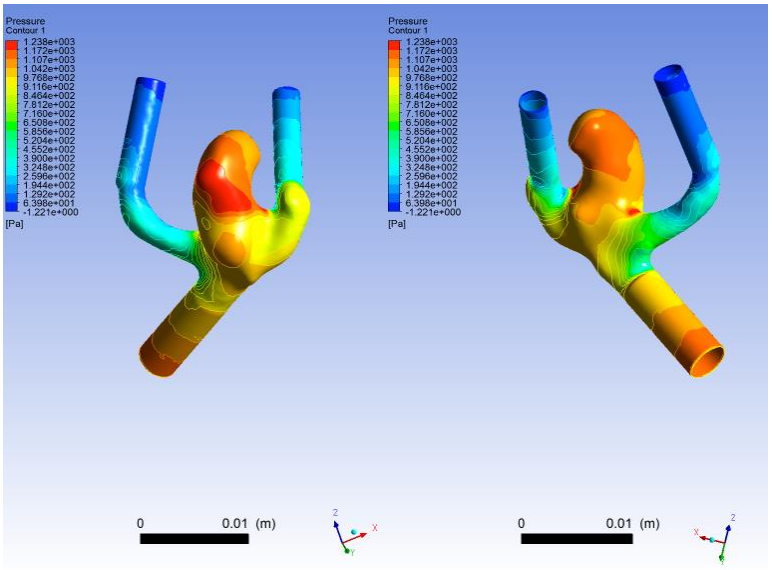

MRA

WSS 0.2

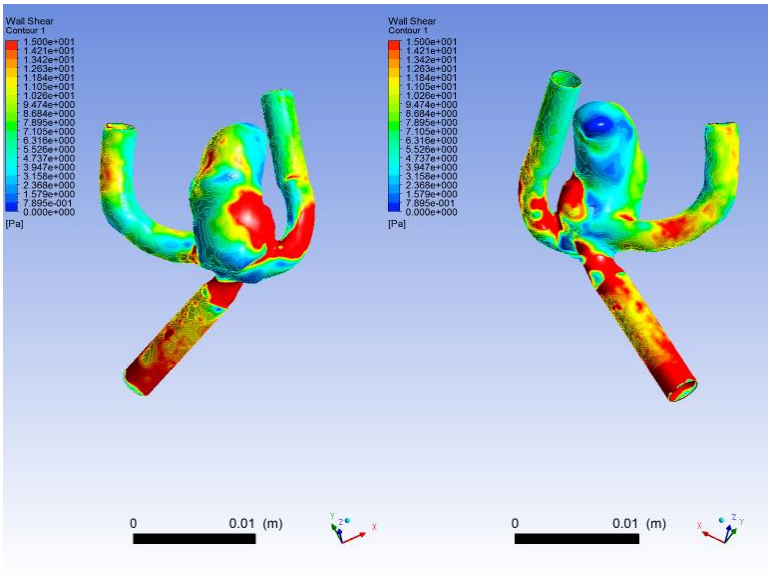

DSA

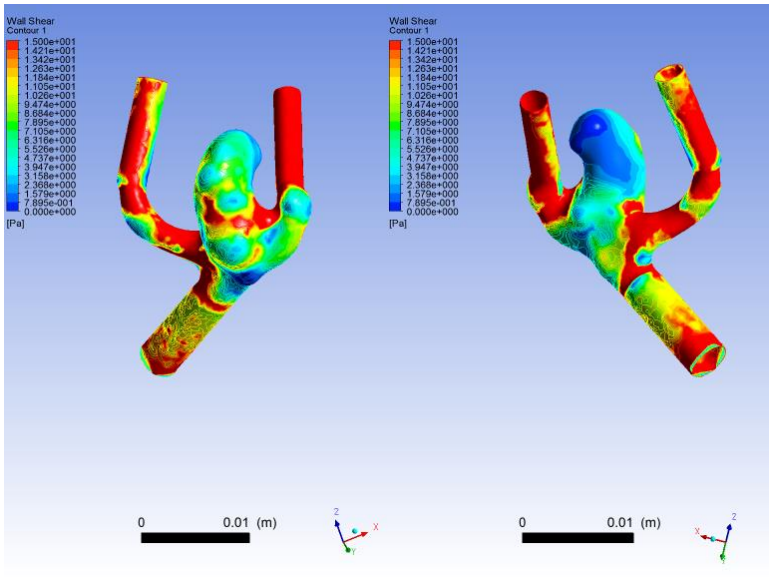

MRA

Pathlines 0.2

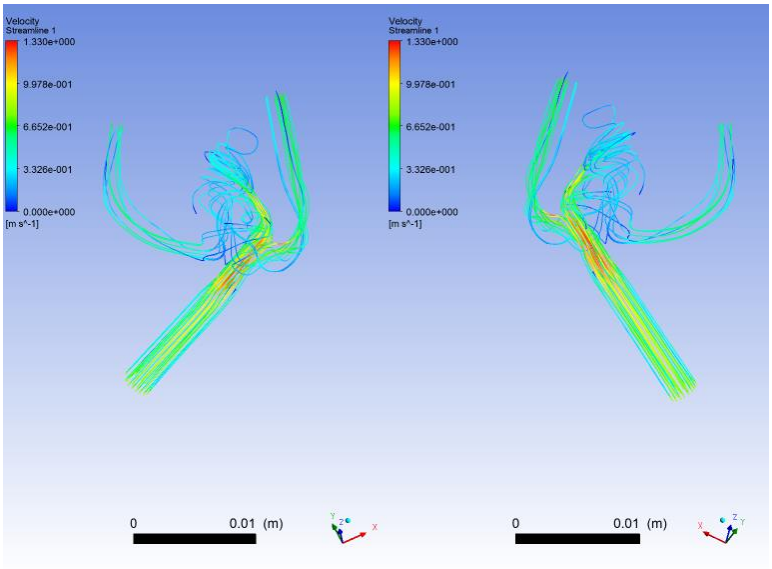

DSA

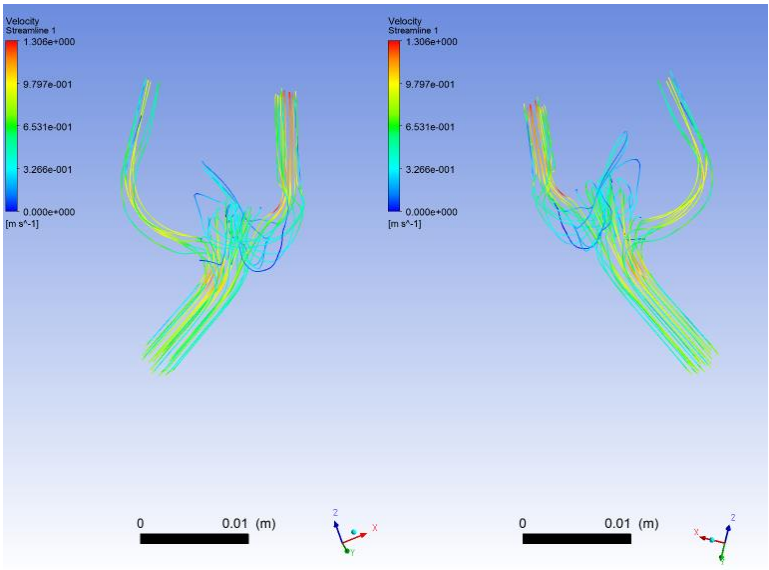

MRA

t=0.4 sec

	DSA	MRA
Pressure	-152 to 743 Pa	-0.5 to 804 Pa
WSS	0 to 300 Pa	0 to 330 Pa
Area Average WSS	7.49 Pa	8.53 Pa

Pressure 0.4

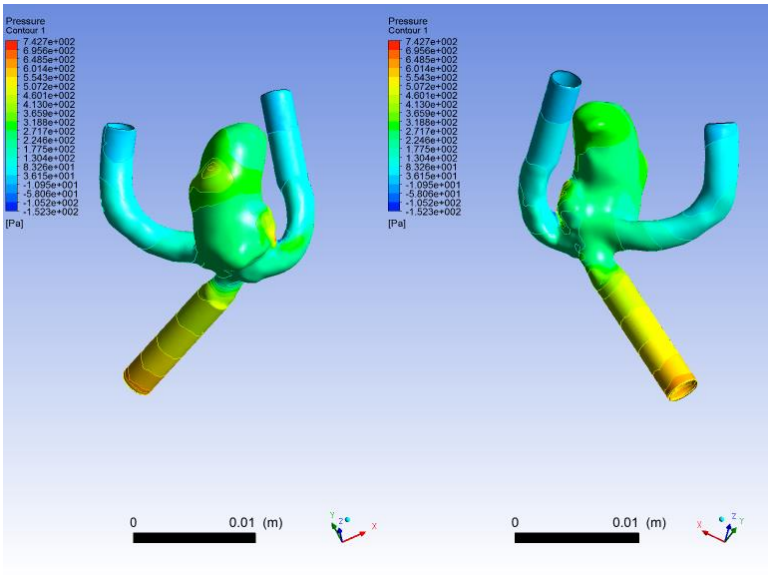

DSA

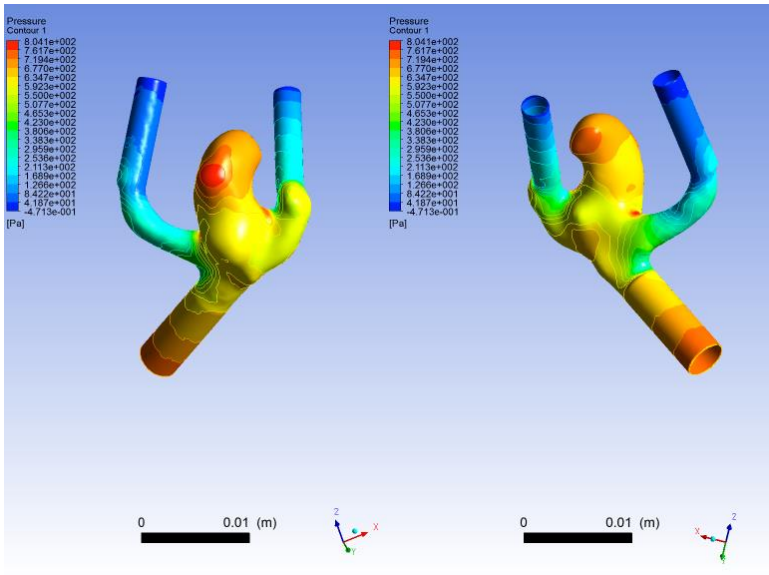

MRA

WSS 0.4

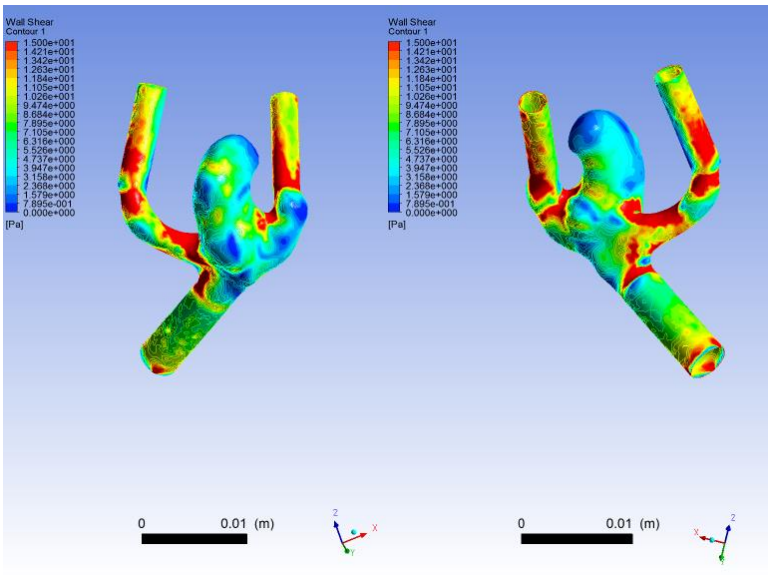

DSA

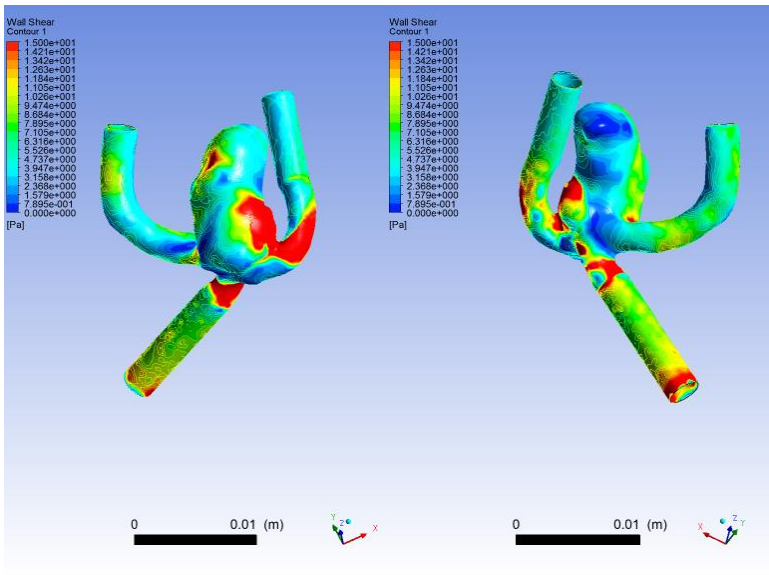

MRA

Pathlines 0.4

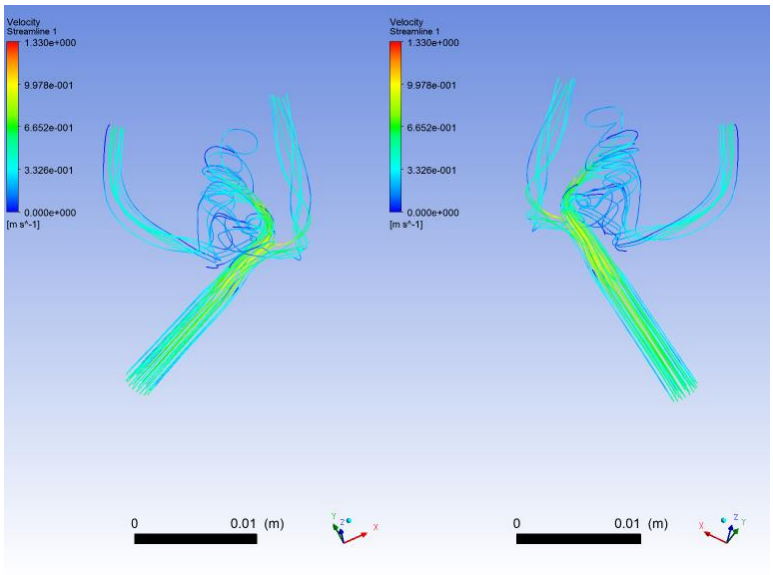

DSA

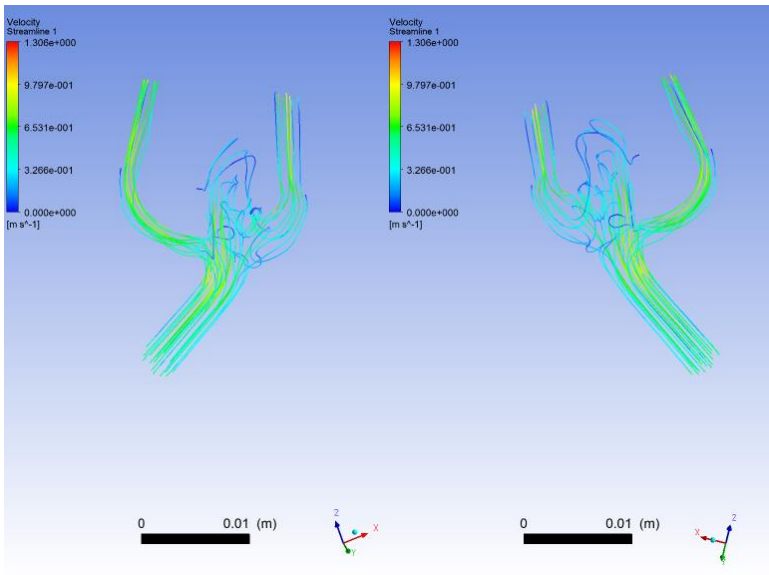

MRA

t=0.6 sec

	DSA	MRA
Pressure	-85 to 504 Pa	-0.85 to 597 Pa
WSS	0 to 251 Pa	0 to 278 Pa
Area Average WSS	5.14 Pa	6.69 Pa

Pressure 0.6

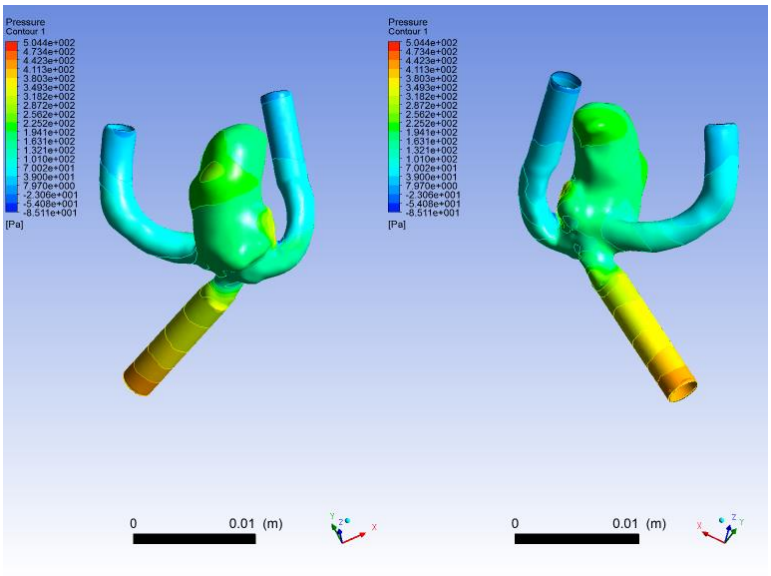

DSA

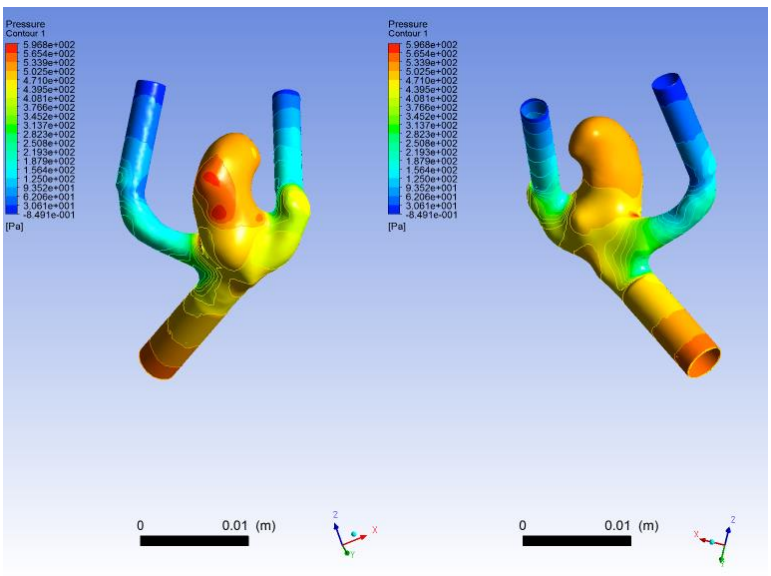

MRA

WSS 0.6

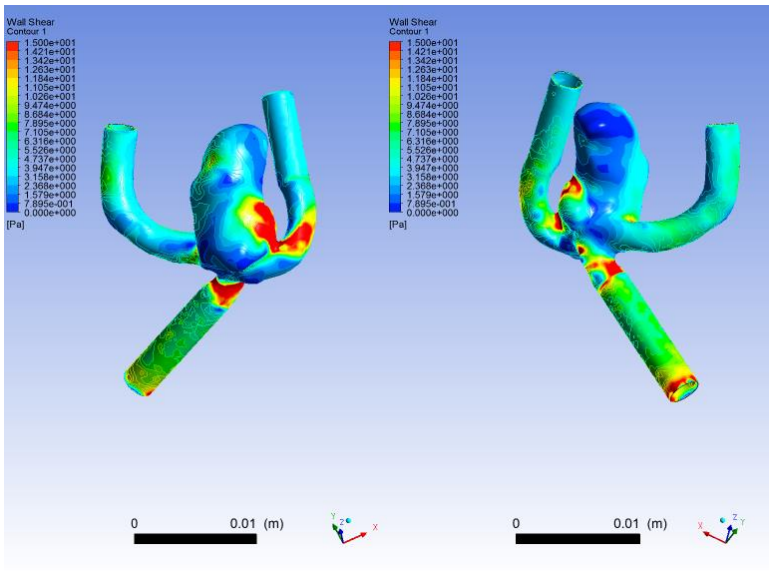

DSA

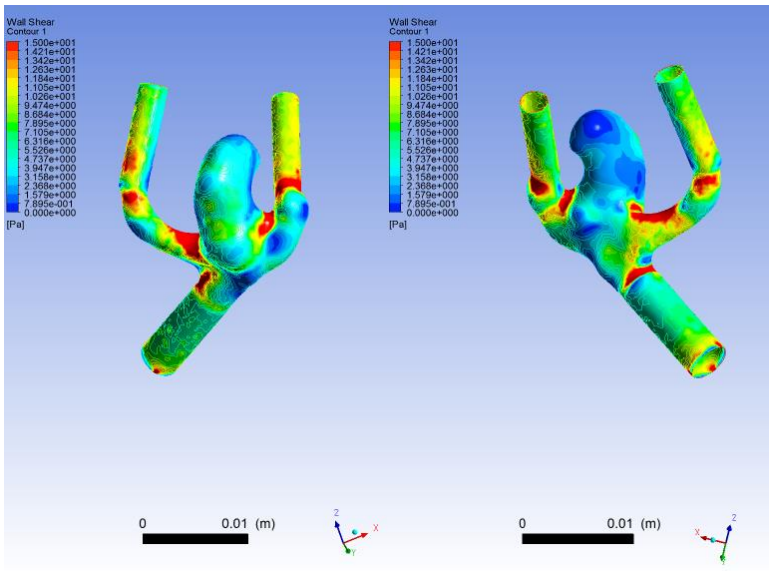

MRA

Pathlines 0.6

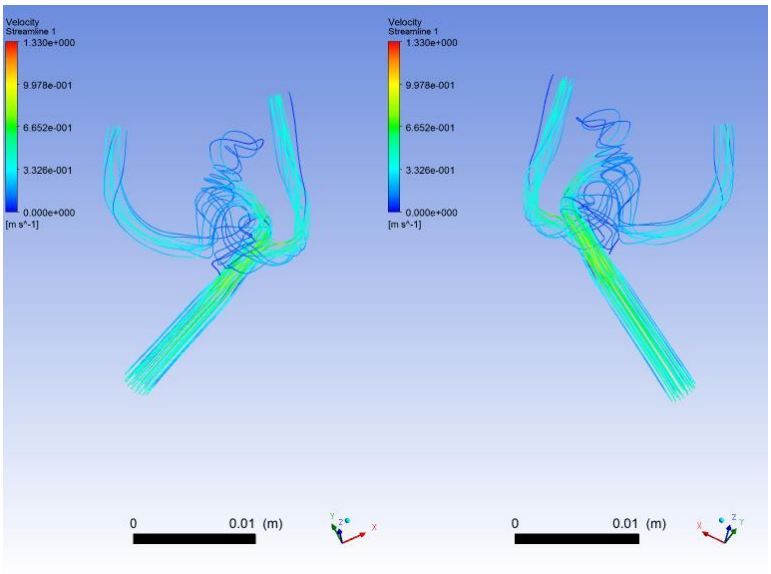

DSA

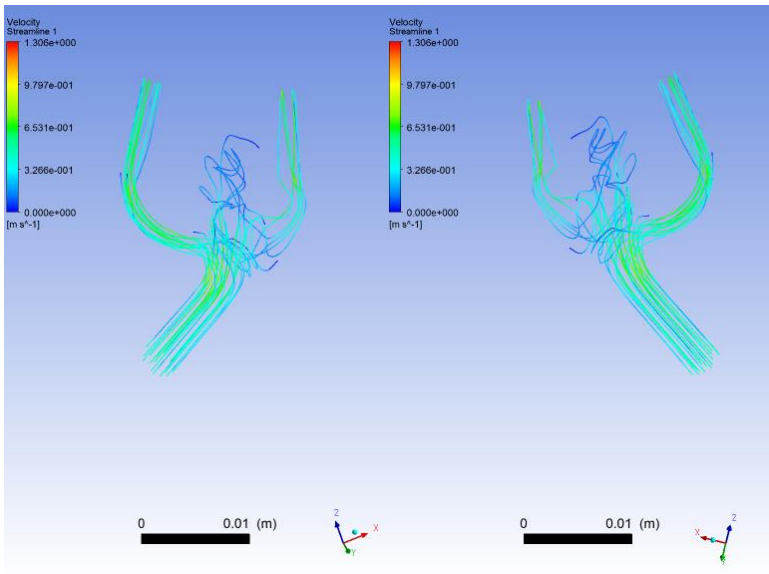

MRA

OSI 0.8

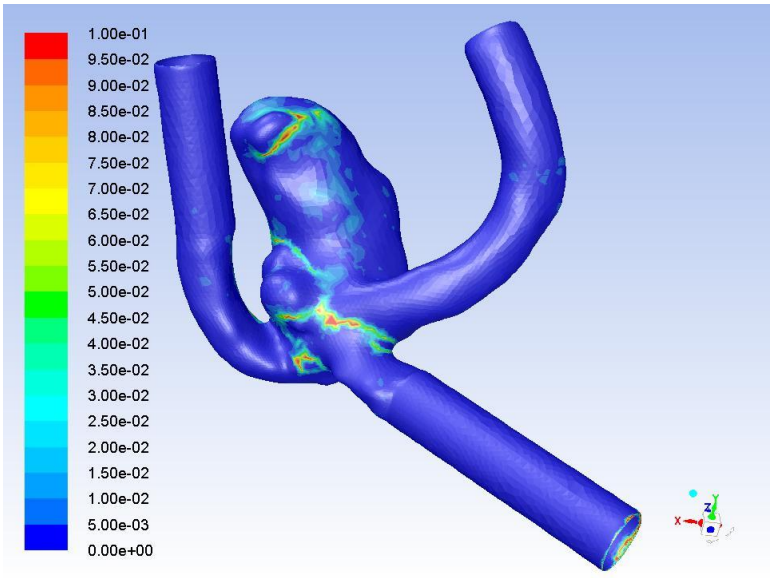

DSA front view

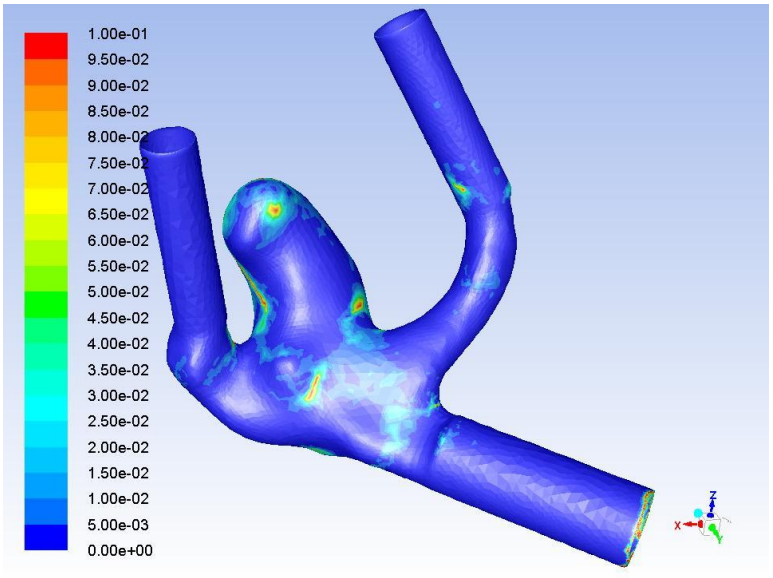

MRA first view

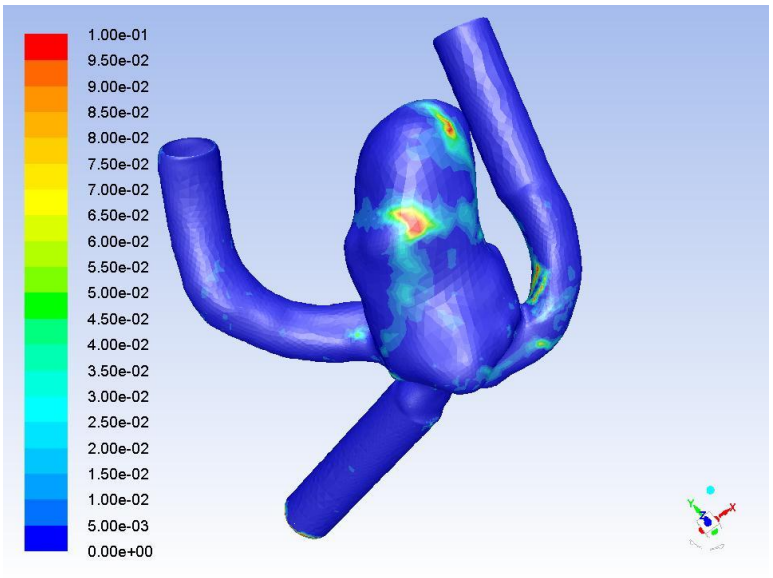

MRA rear view

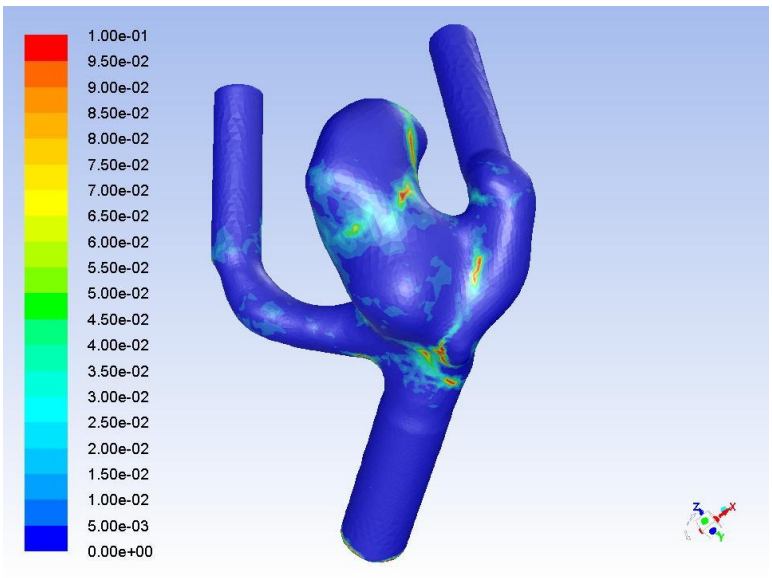

MRA rear view

2nd patient results

- There is a notable difference in the shape and size of the aneurysm.
- The pathlines have different density and shape as a result of the different geometric characteristics of the aneurysms
- The minimum and maximum regions of WSS and OSI have some common regions despite not being exactly the same.
- The maximum values of pressure are always less at the DSA simulated aneurysm, with a margin as big as 18 %
- The maximum values of WSS are always less at the DSA simulated aneurysm, with a margin as big as 10 %
- The area averaged WSS value is always less at the DSA simulated aneurysm and the margin is as big as 23 %

3rd patient DSA vs MRA

- Diameter derived from the DSA examination: **10** mm
- Diameter derived from the MRA examination: **10** mm
- Height derived from the DSA examination: **12.5** mm
- Height derived from the MRA examination: **13** mm
- 1 inlet and 2 outlets of blood

t = 0.05 sec

	DSA	MRA
Pressure	-16 to 491 Pa	-4.6 to 919 Pa
WSS	0 to 223 Pa	0 to 244 Pa
Area Average WSS	3.49 Pa	4.57 Pa

Pressure 0.05

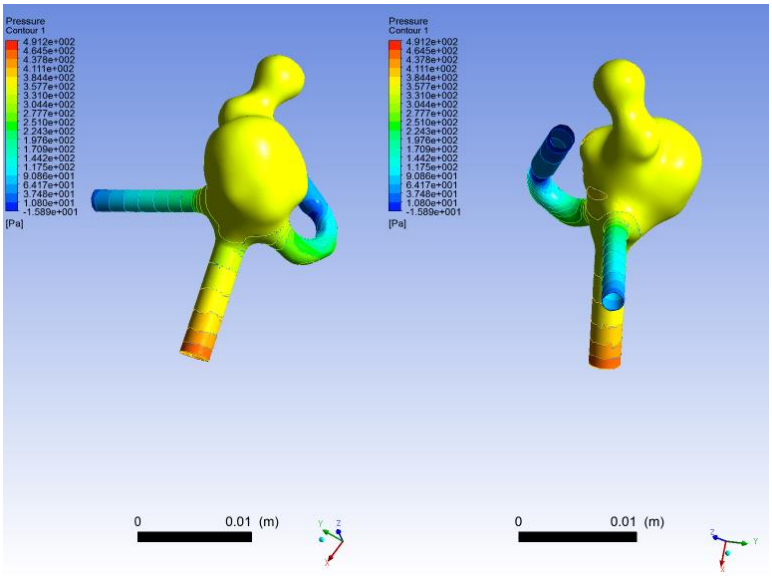

DSA

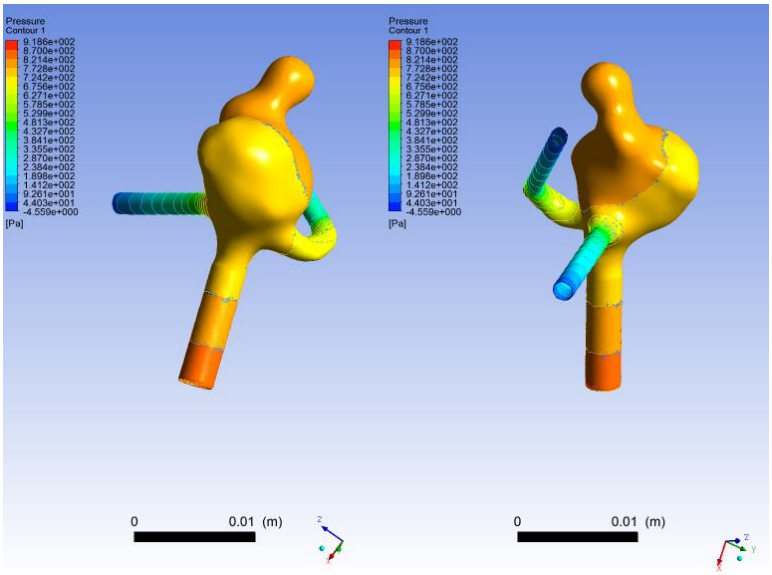

MRA

WSS 0.05

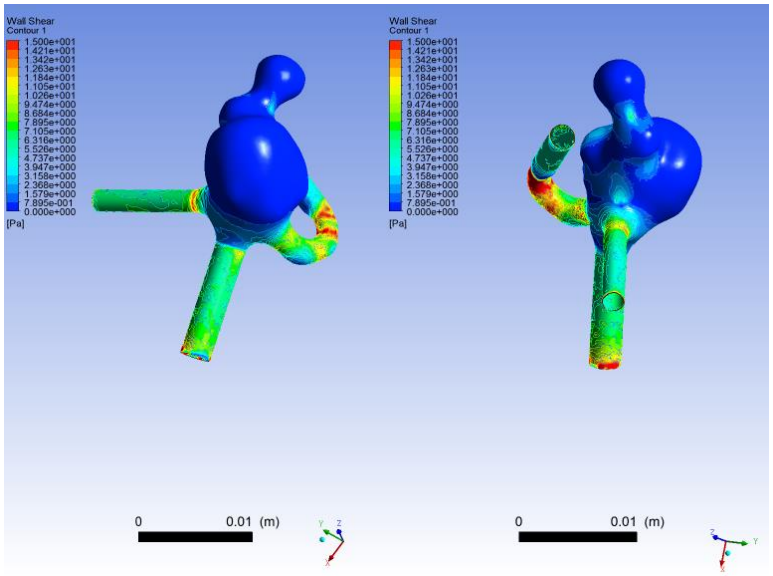

DSA

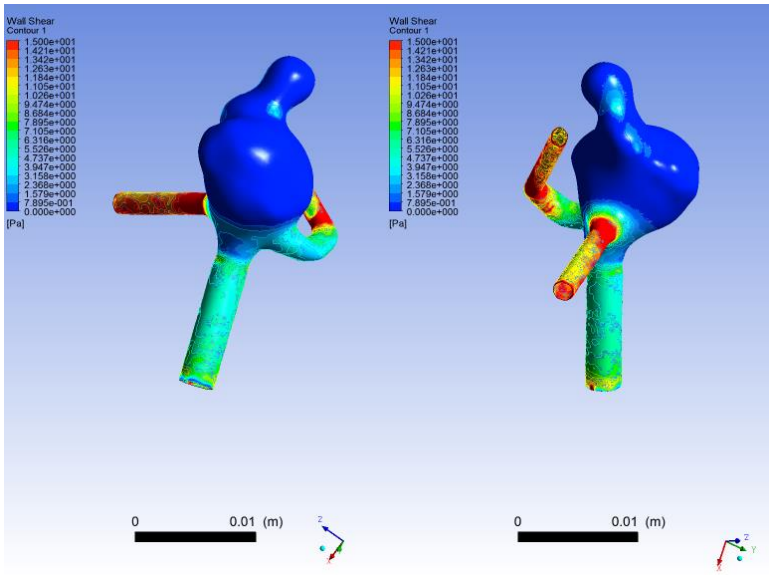

MRA

Pathlines 0.05

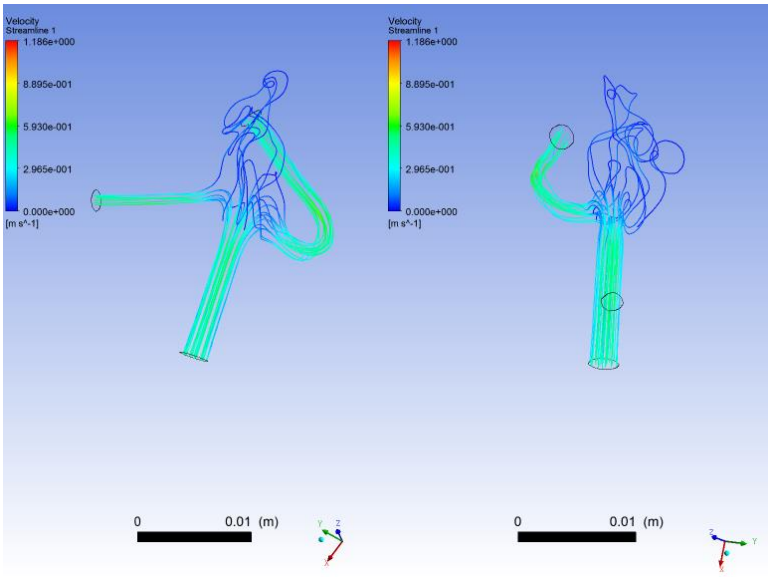

DSA

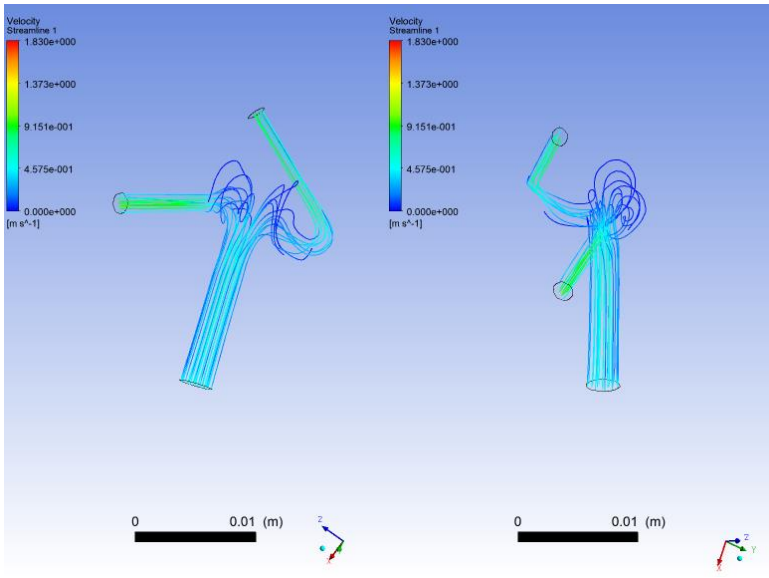

MRA

t = 0.2 sec

	DSA	MRA
Pressure	-0 to 1070 Pa	-90 to 2487 Pa
WSS	0 to 413 Pa	0 to 472 Pa
Area Average WSS	8.67 Pa	11.35 Pa

Pressure 0.2

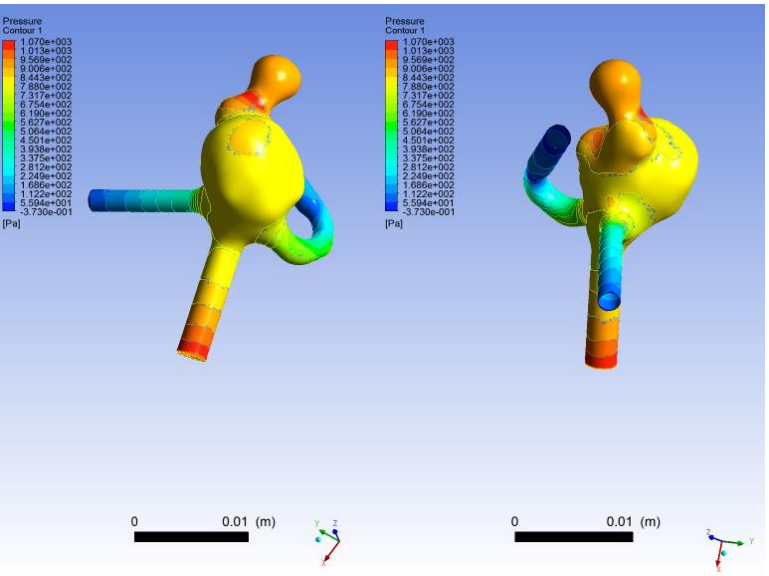

DSA

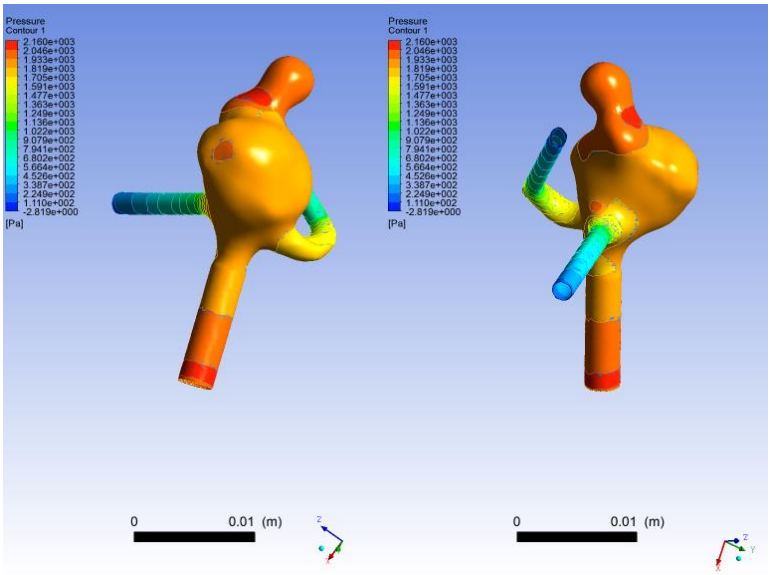

MRA

WSS 0.2

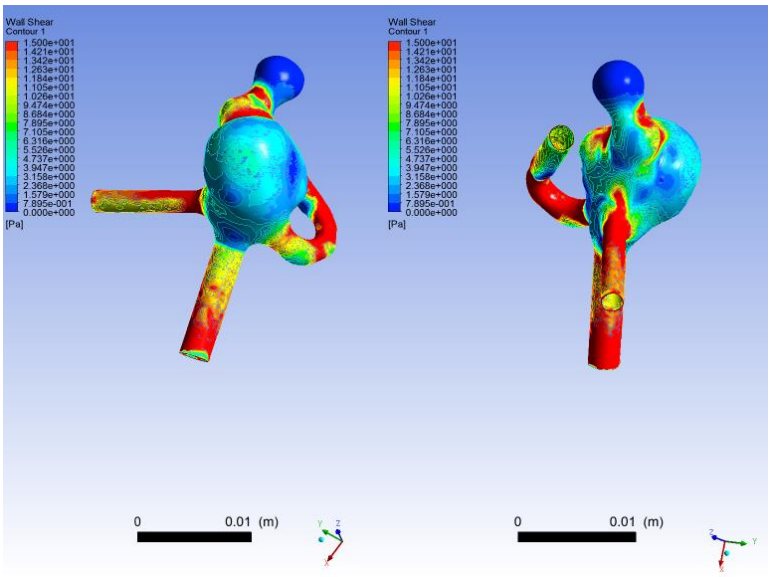

DSA

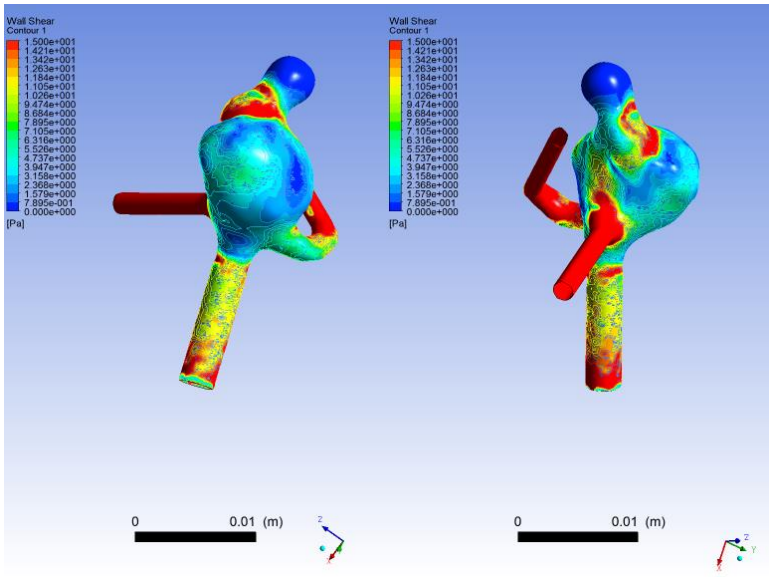

MRA

Pathlines 0.2

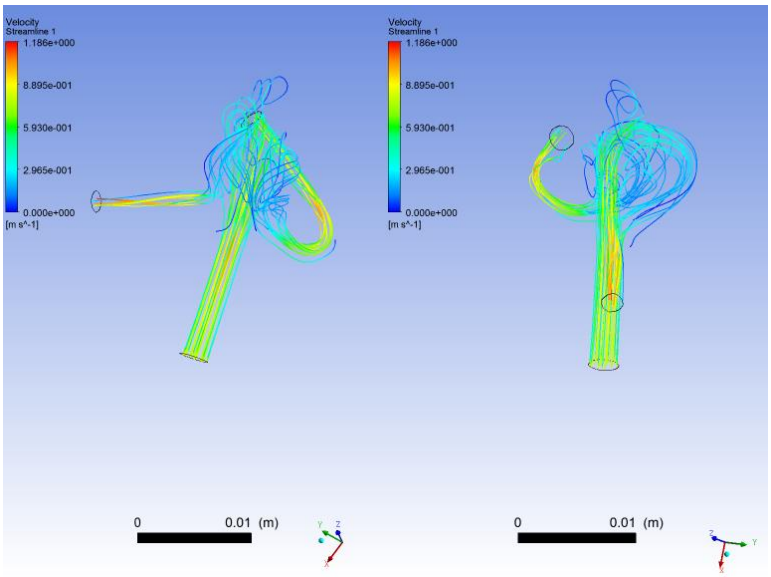

DSA

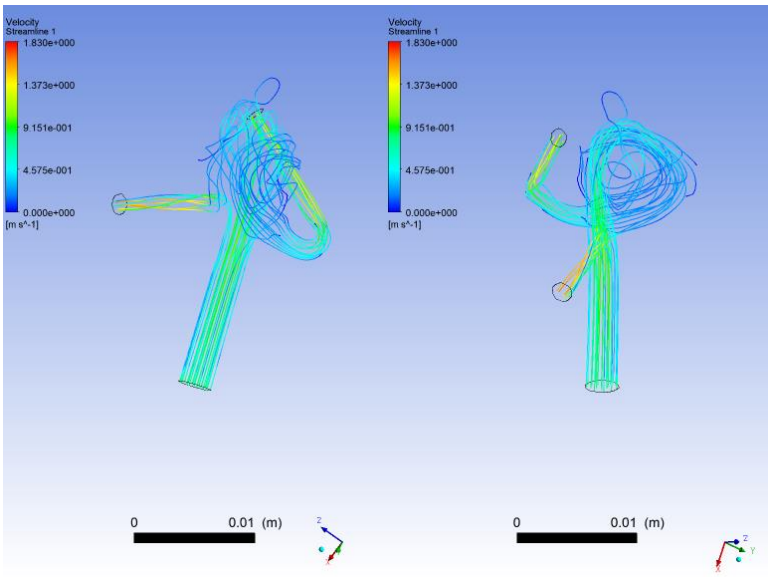

MRA

t = 0.4 sec

	DSA	MRA
Pressure	-1 to 707 Pa	-2 to 1410 Pa
WSS	0 to 296 Pa	0 to 327 Pa
Area Average WSS	6.22 Pa	8.34 Pa

Pressure 0.4

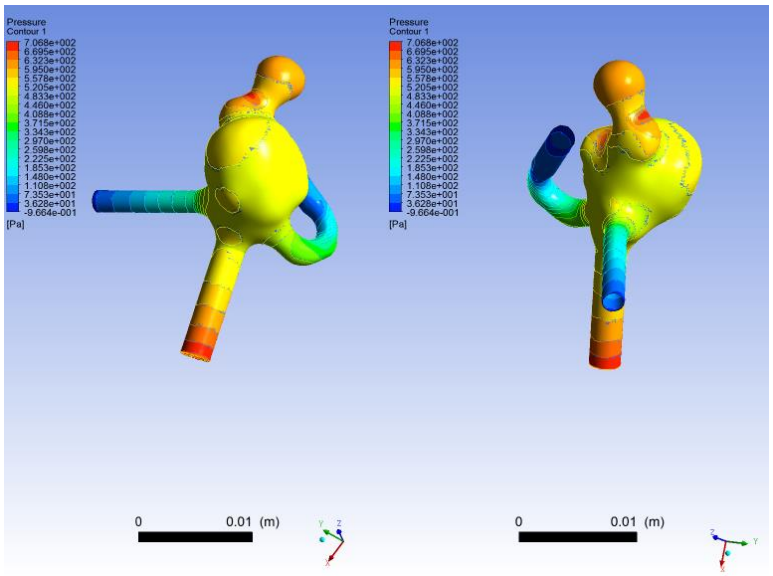

DSA

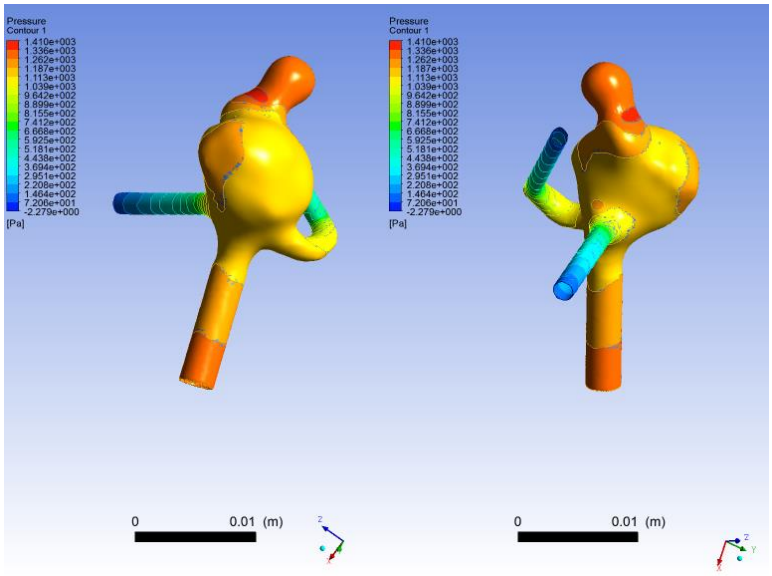

MRA

WSS 0.4

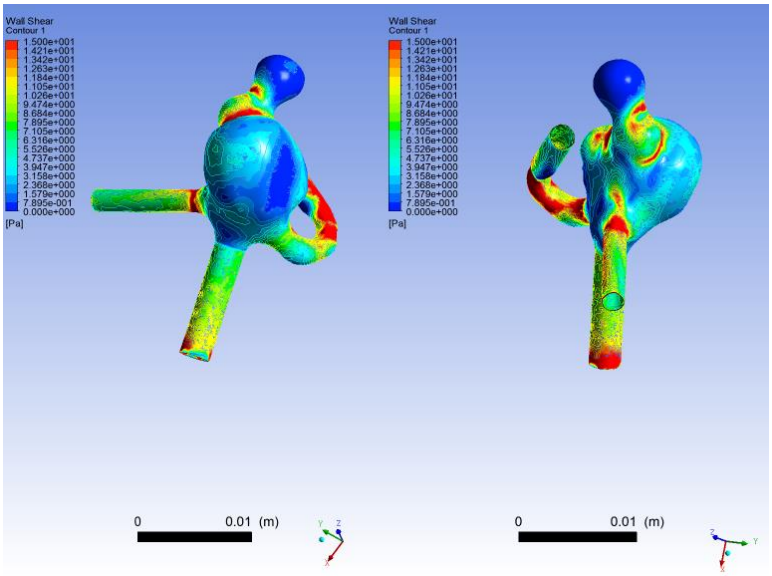

DSA

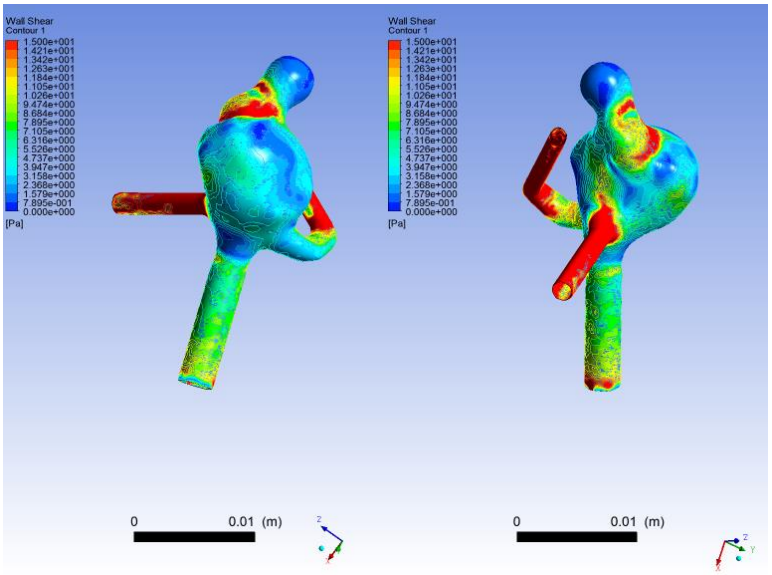

MRA

Pathlines 0.4

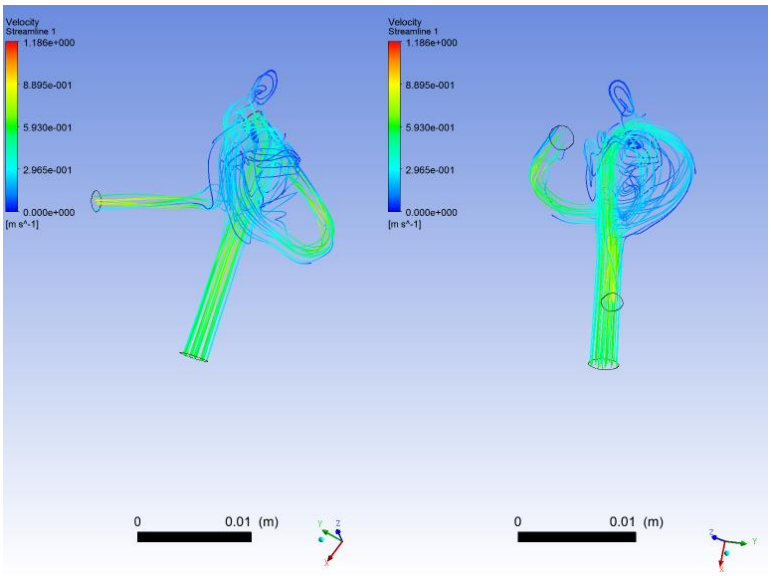

DSA

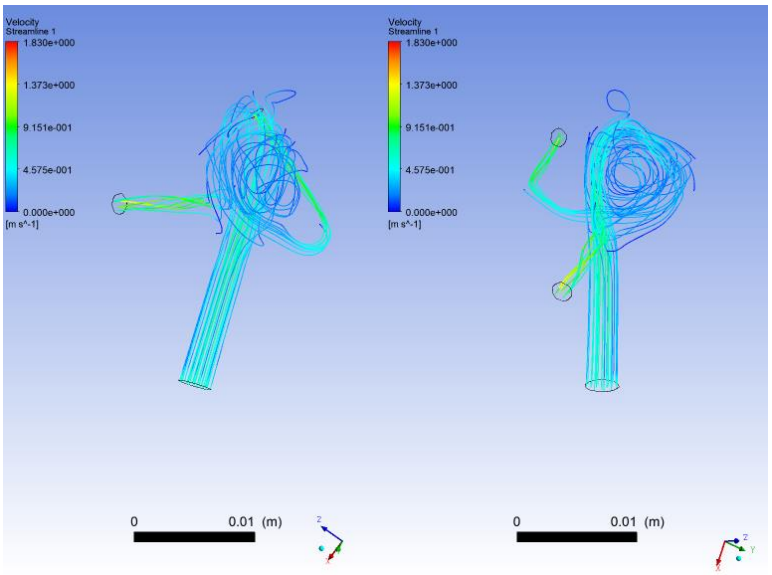

MRA

t = 0.6 sec

	DSA	MRA
Pressure	-1 to 525 Pa	-3 to 1004 Pa
WSS	0 to 247 Pa	0 to 272 Pa
Area Average WSS	4.53 Pa	6.08 Pa

Pressure 0.6

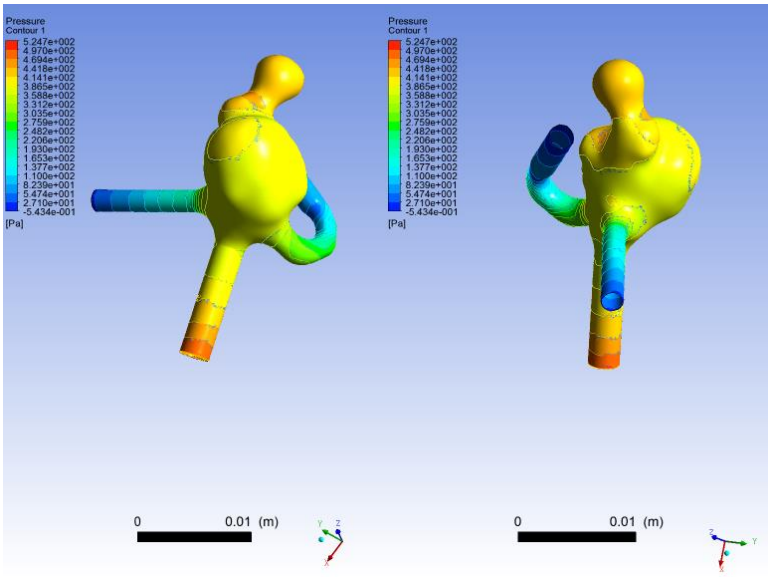

DSA

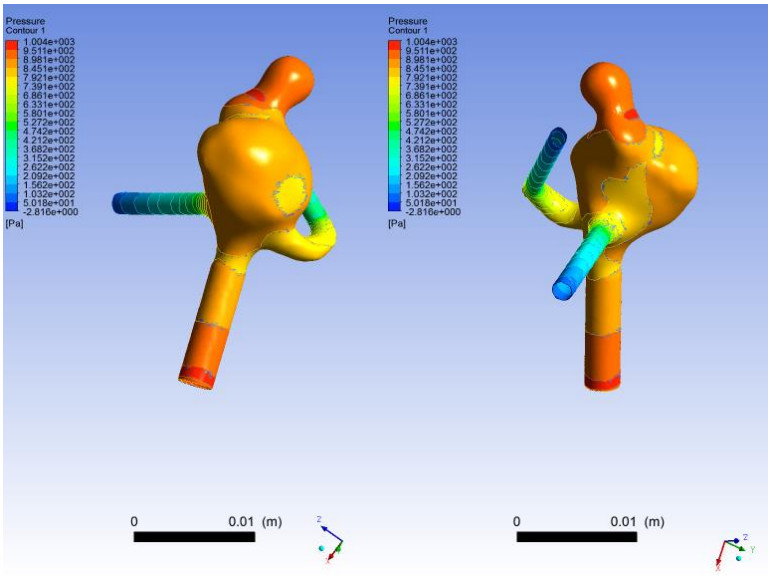

MRA

WSS 0.6

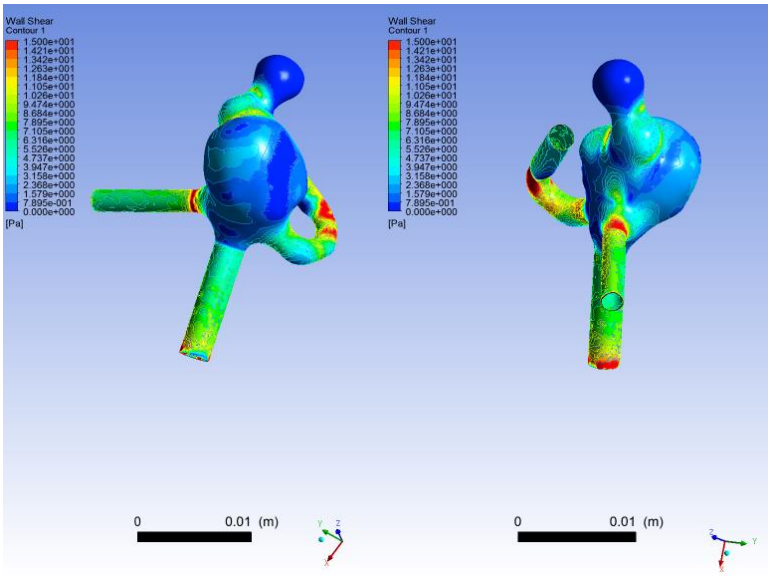

DSA

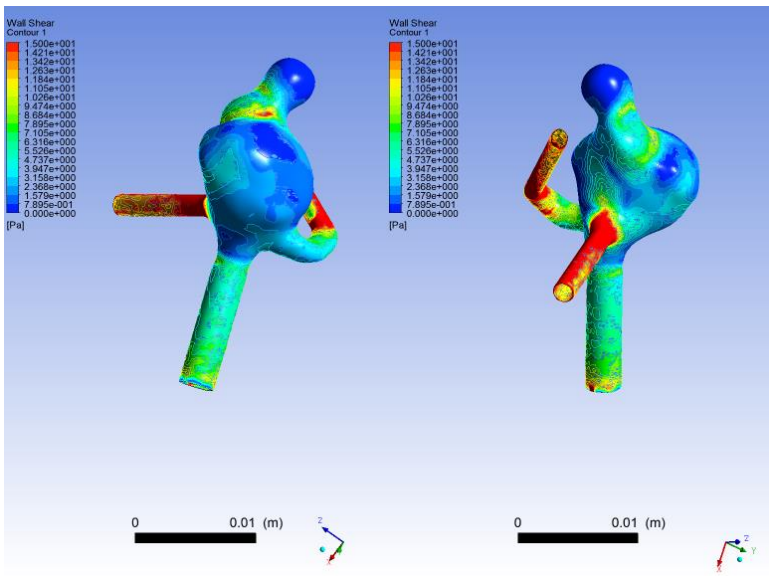

MRA

Pathlines 0.6

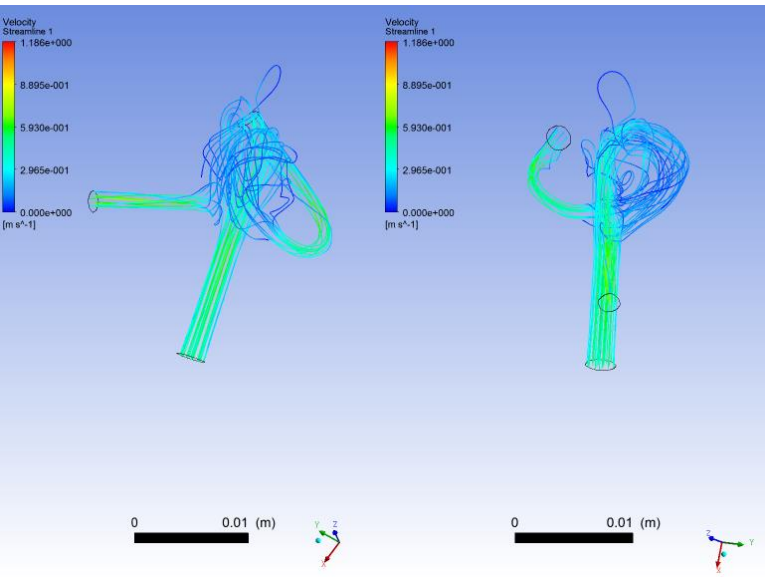

DSA

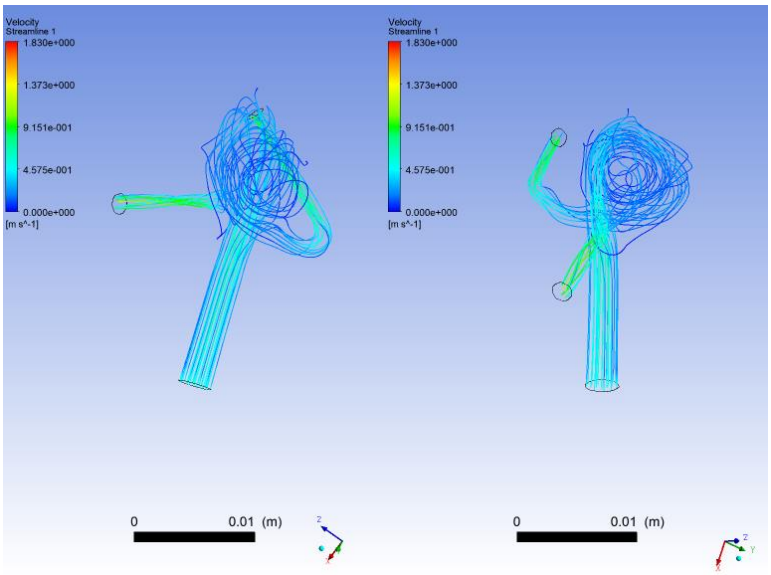

MRA

OSI 0.8

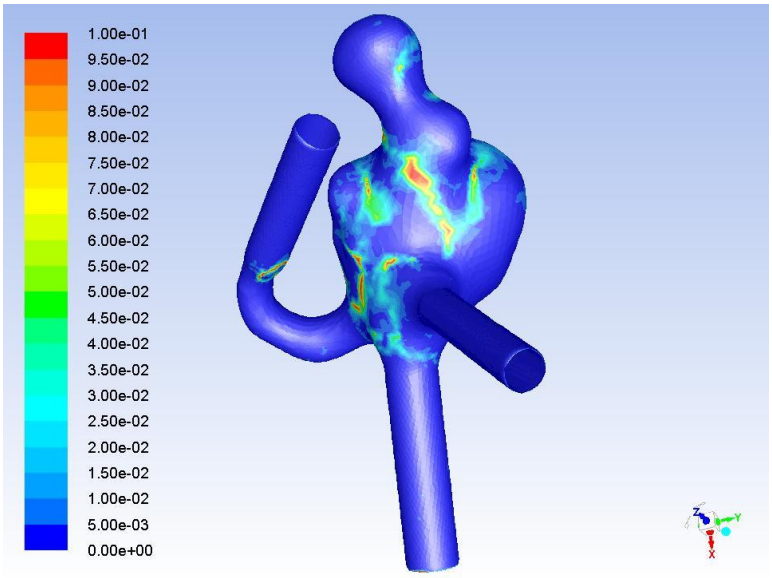

DSA front view

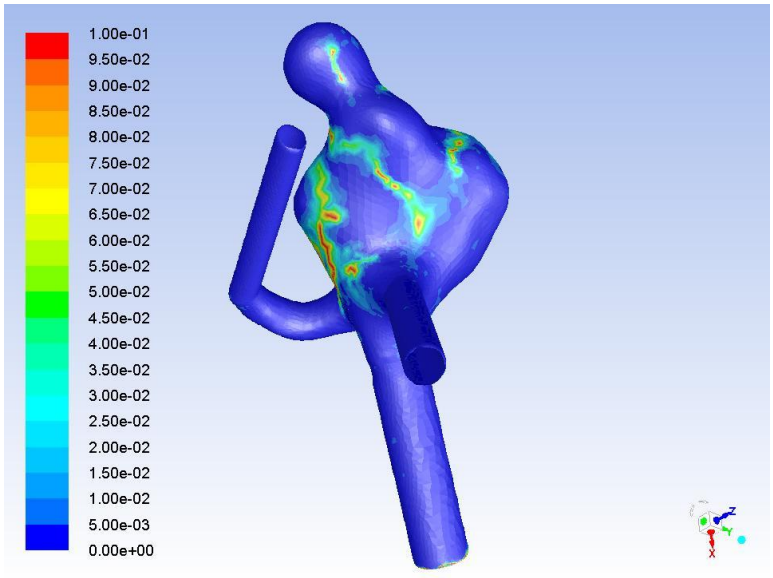

MRA front view

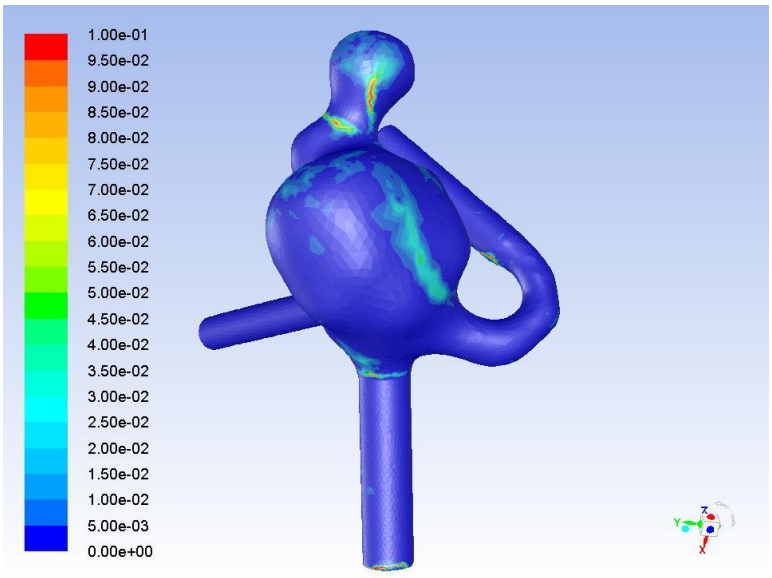

DSA rear view

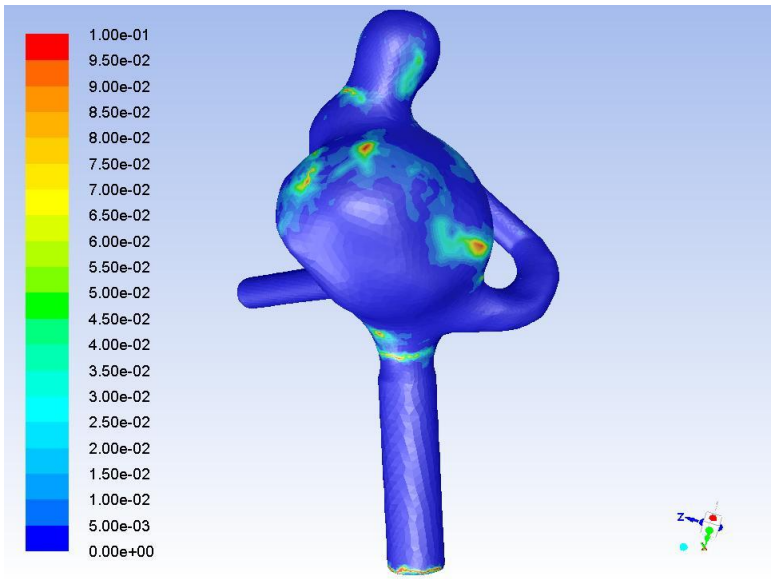

MRA rear view

3rd patient results

- There is not a notable difference in the shape and size of the aneurysm.
- The pathlines extend at the same regions of the aneurysm dome
- The minimum and maximum regions of WSS and OSI have many similarities
- The maximum values of pressure are always less at the DSA simulated aneurysm, with a margin that ranges between 47 and 57 %
- The maximum values of WSS are always less at the DSA simulated aneurysm, with a margin that ranges between 9 and 11 %
- The area averaged WSS value is always less at the DSA simulated aneurysm and the margin is as big as 25 %

4th patient DSA vs MRA

- Diameter derived from the DSA examination: **6.5** mm
- Diameter derived from the MRA examination: **7** mm
- Height derived from the DSA examination: **10** mm
- Height derived from the MRA examination: **10** mm
- 2 inlets and 2 outlets of blood

t=0.05 sec

	DSA	MRA
Pressure	-2 to 545 Pa	-4 to 604 Pa
WSS	0 to 219 Pa	0 to 231 Pa
Area Average WSS	3.74 Pa	4.88 Pa

Pressure 0.05

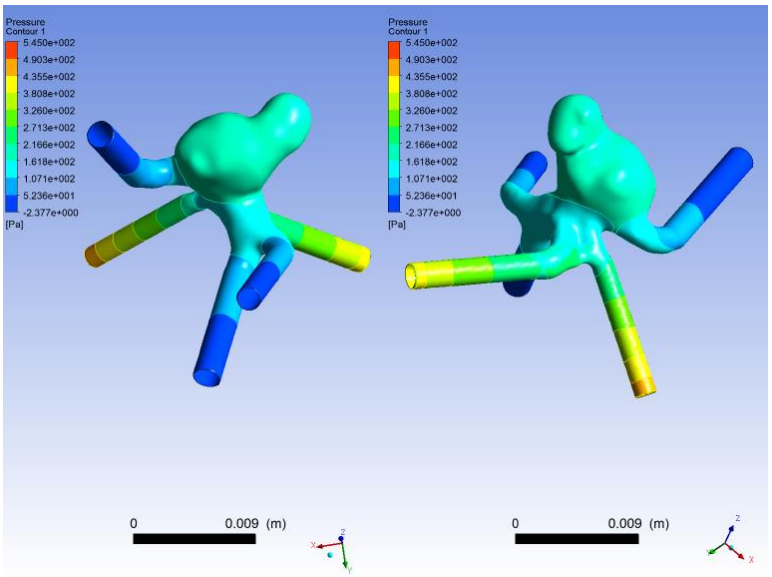

DSA

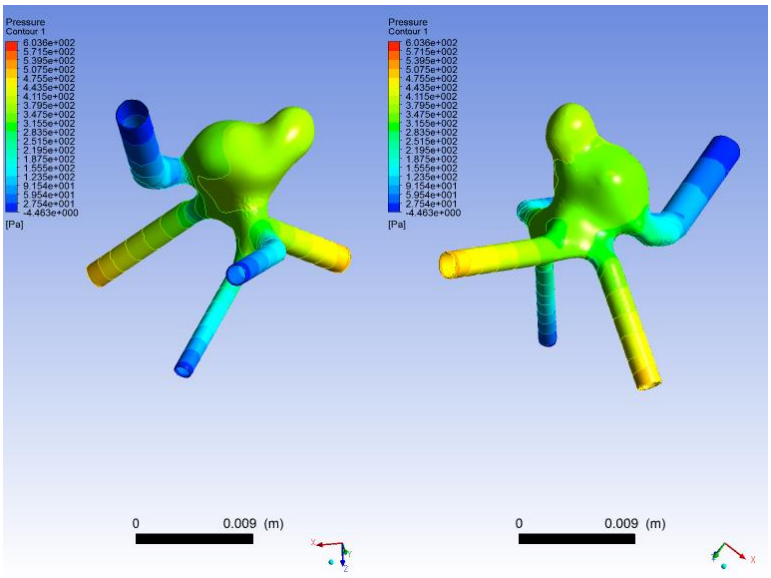

MRA

WSS 0.05

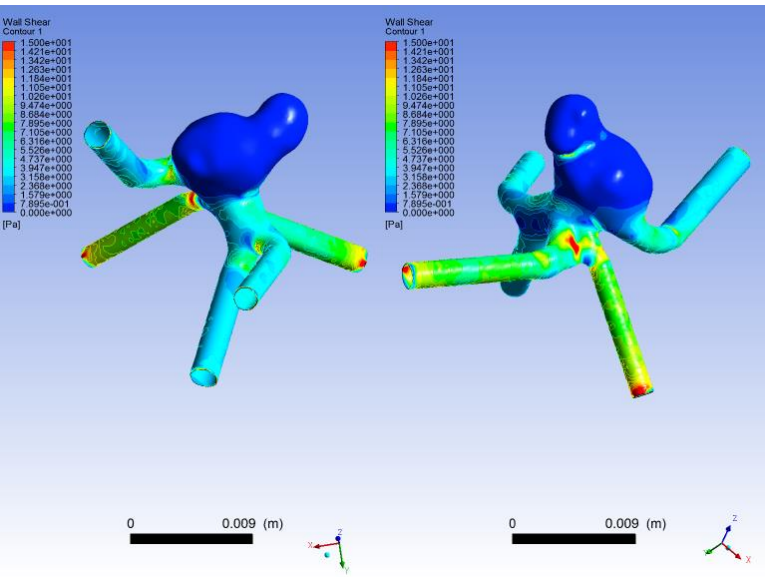

DSA

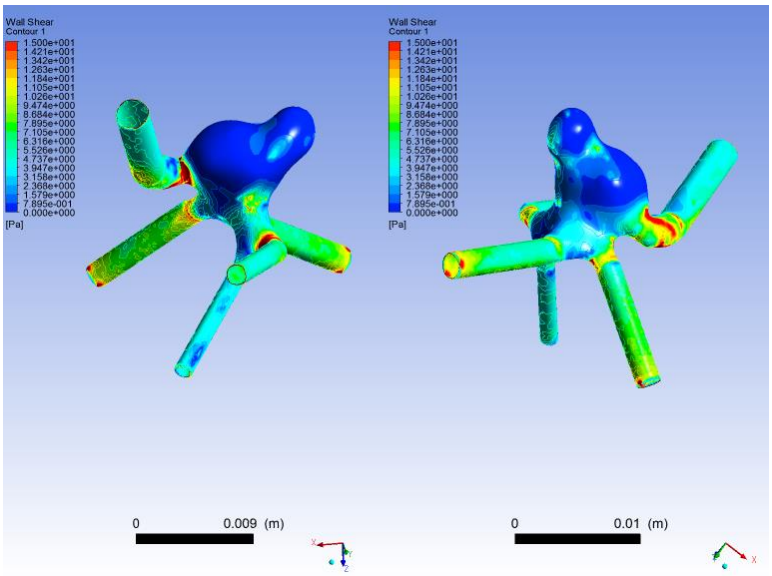

MRA

Pathlines 0.05

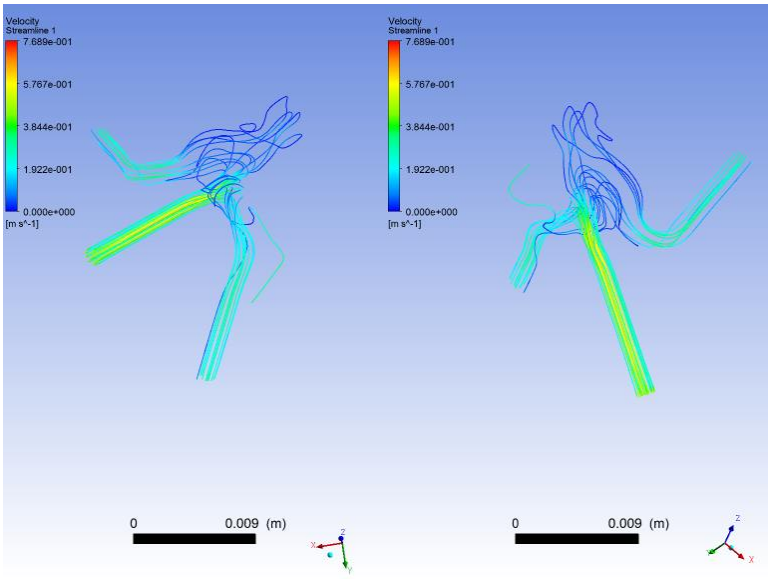

DSA

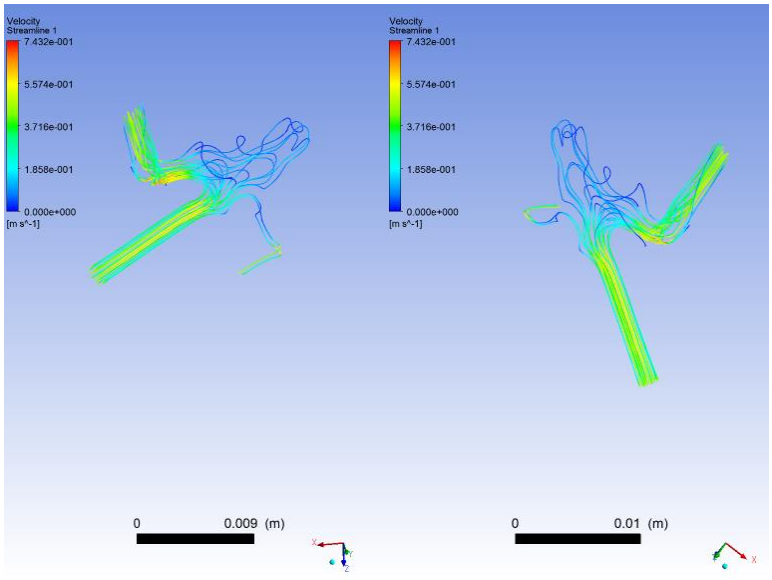

MRA

t=0.2 sec

	DSA	MRA
Pressure	-55 to 1001 Pa	-219 to 1185 Pa
WSS	0 to 413 Pa	0 to 433 Pa
Area Average WSS	8.59 Pa	10.94 Pa

Pressure 0.2

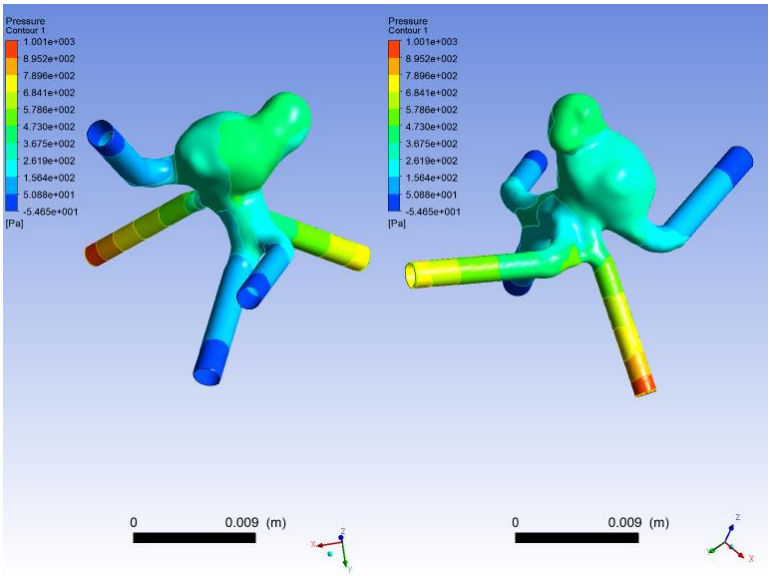

DSA

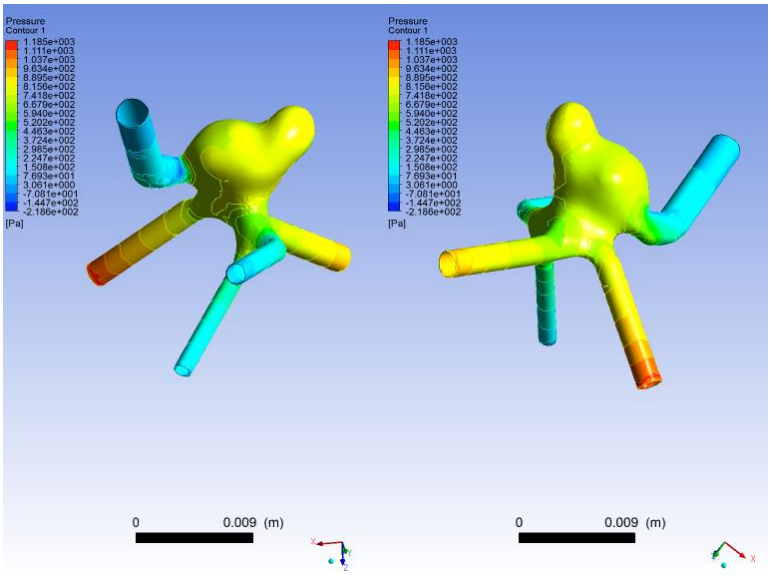

MRA

WSS 0.2

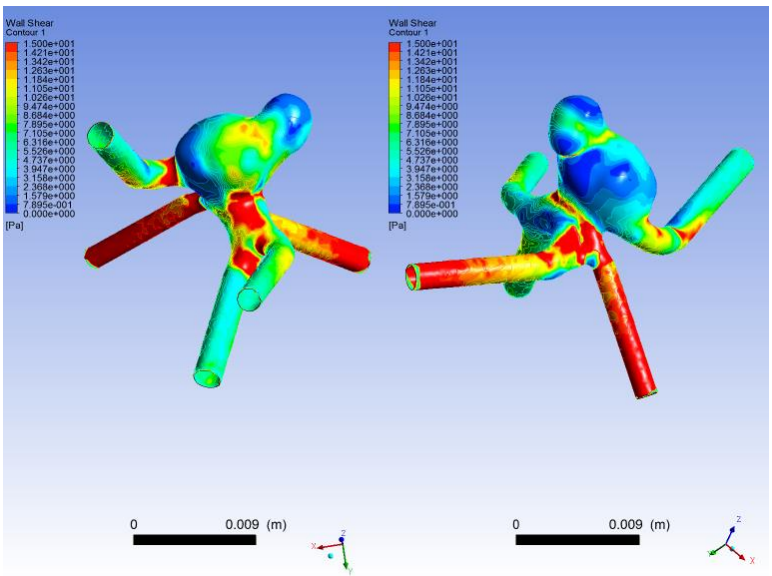

DSA

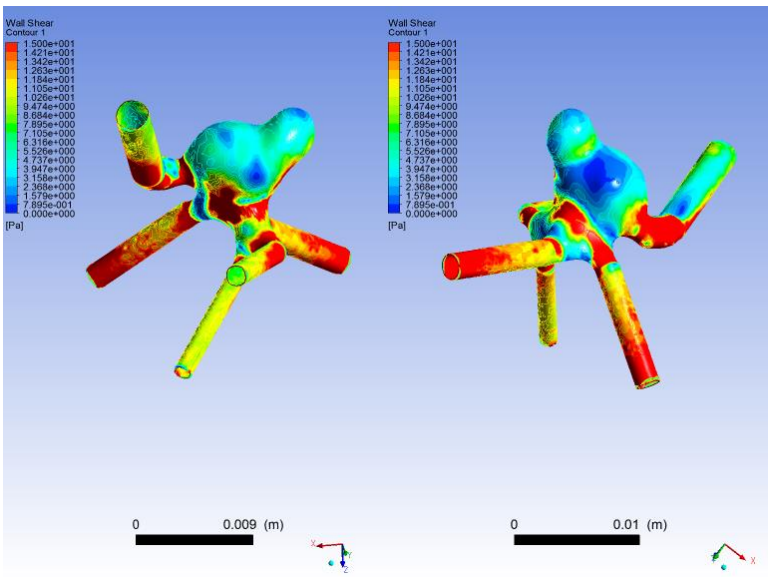

MRA

Pathlines 0.2

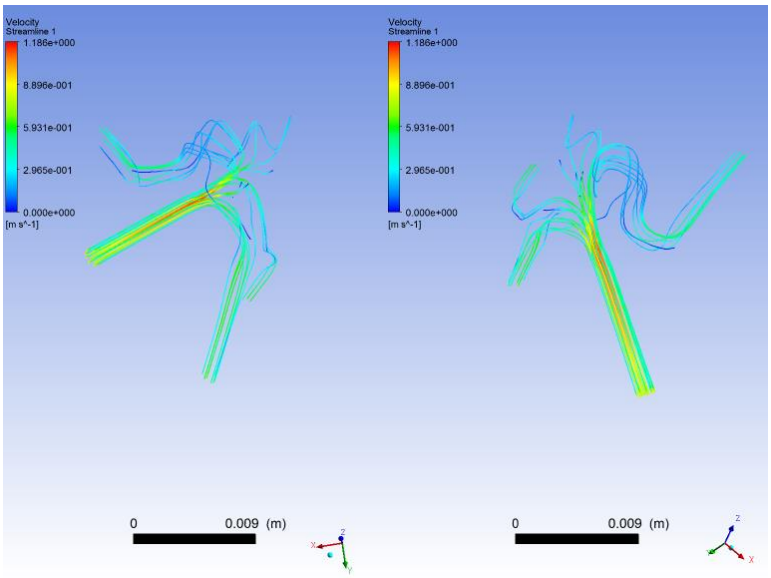

DSA

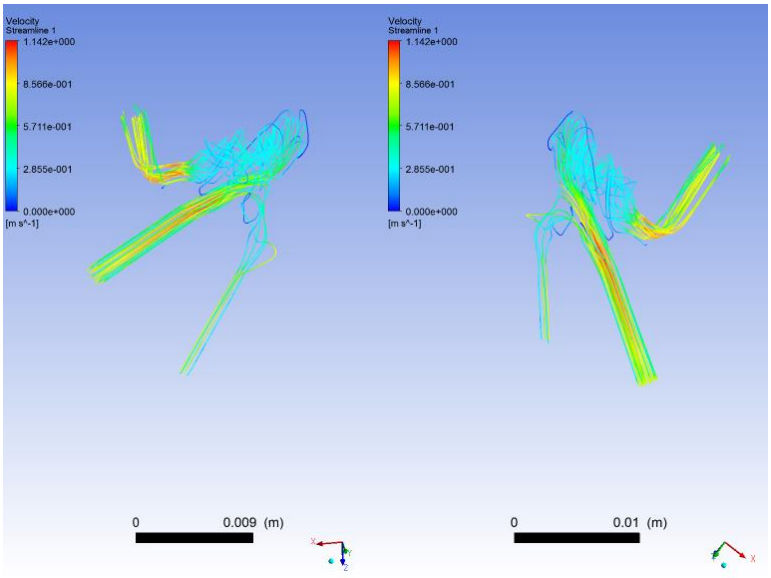

MRA

t=0.4 sec

	DSA	MRA
Pressure	0 to 726 Pa	-103 to 846 Pa
WSS	0 to 293 Pa	0 to 307 Pa
Area Average WSS	5.84 Pa	8.16 Pa

Pressure 0.4

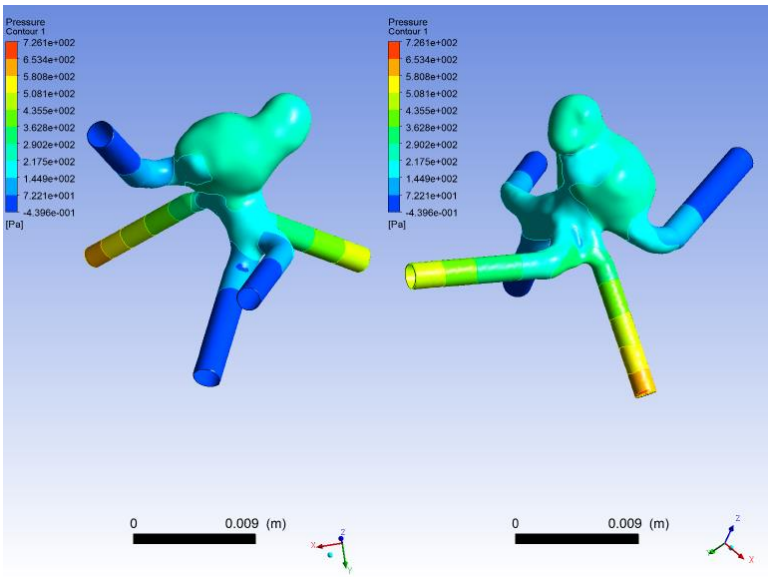

DSA

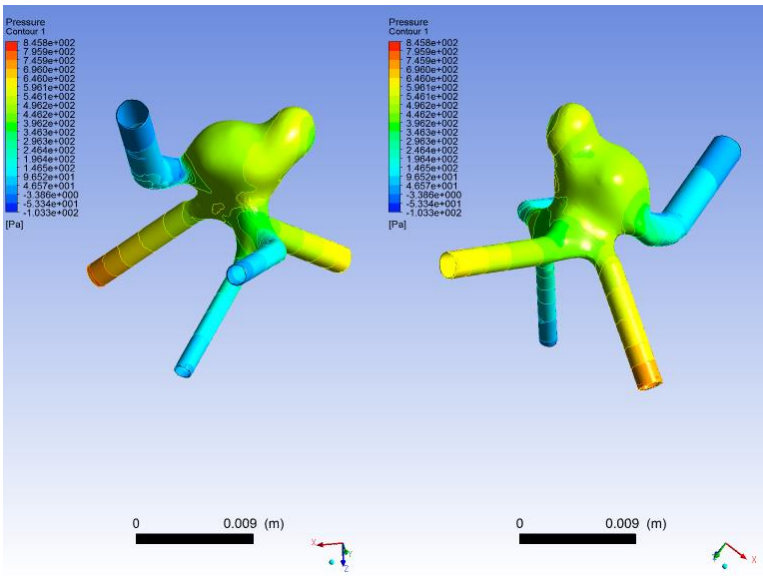

MRA

WSS 0.4

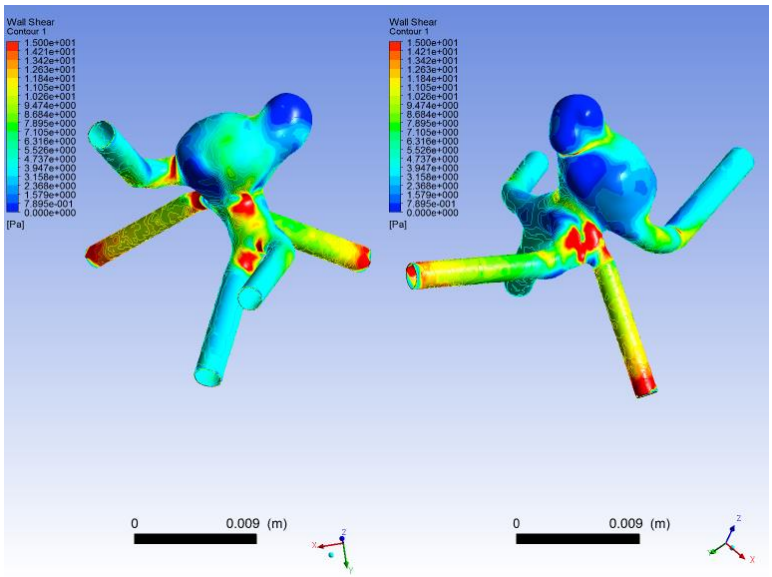

DSA

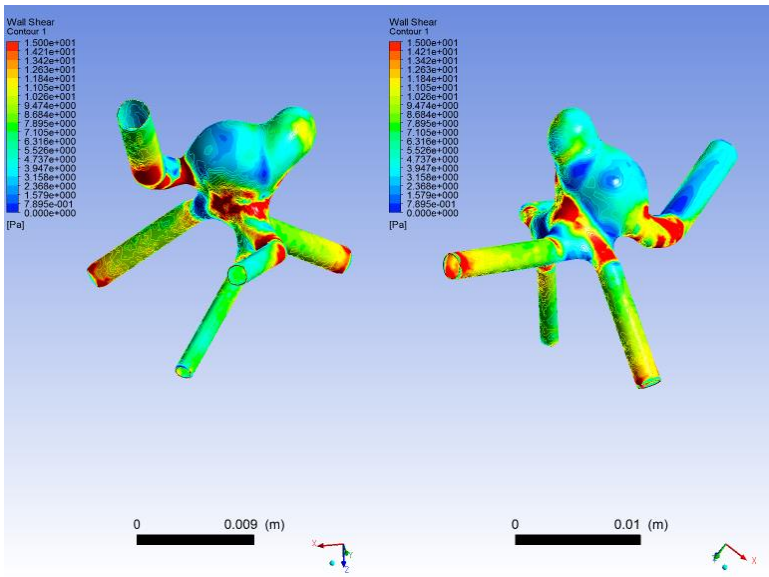

MRA

Pathlines 0.4

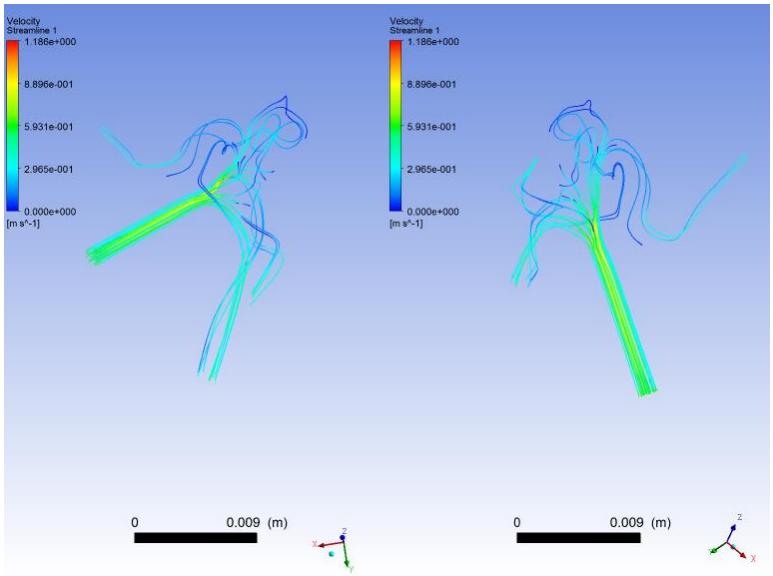

DSA

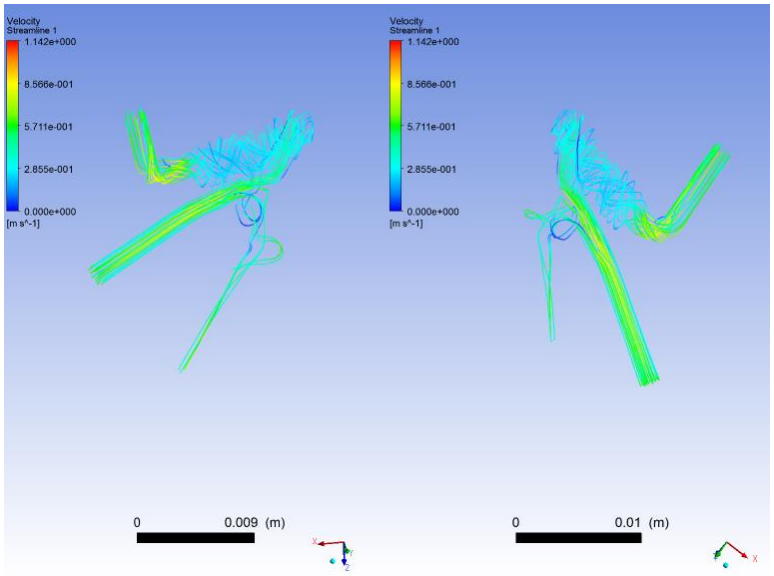

MRA

t=0.6 sec

	DSA	MRA
Pressure	0 to 561 Pa	-79 to 645 Pa
WSS	0 to 244 Pa	0 to 257 Pa
Area Average WSS	4.53 Pa	5.93 Pa

Pressure 0.6

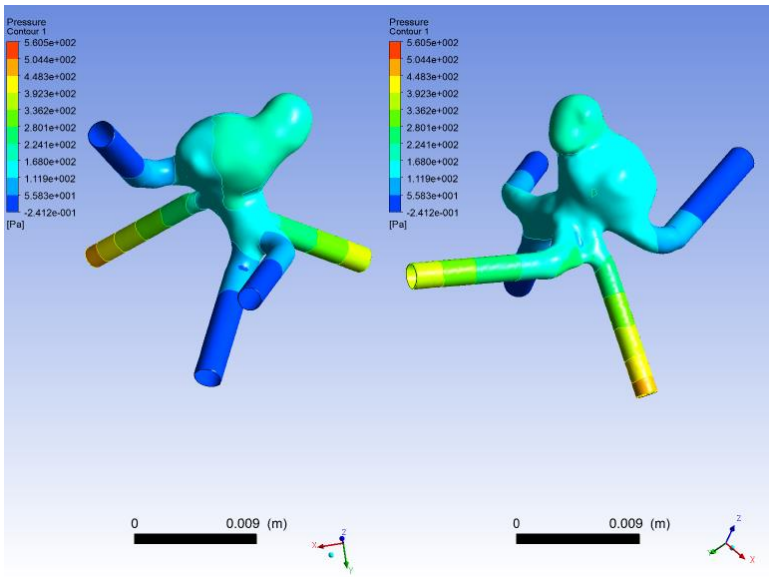

DSA

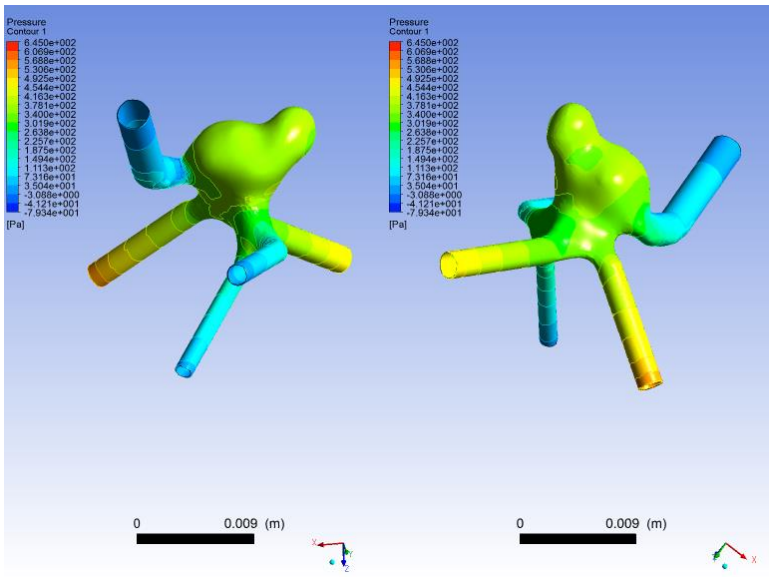

MRA

WSS 0.6

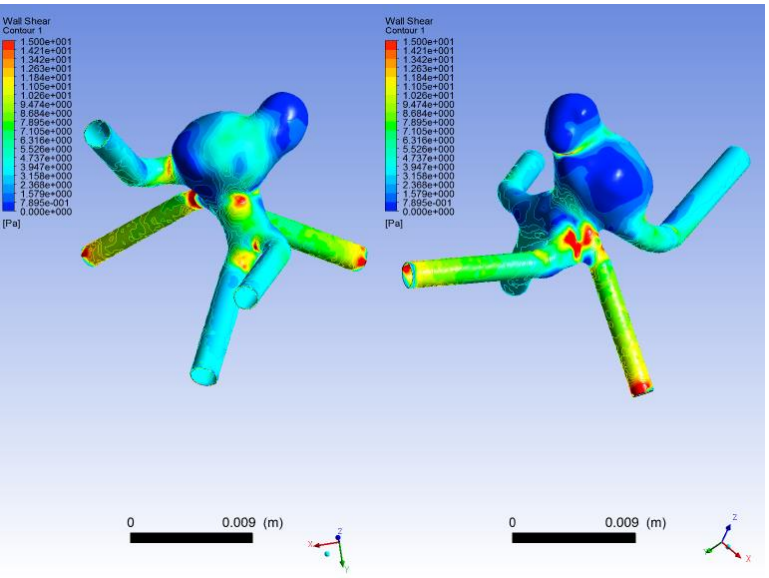

DSA

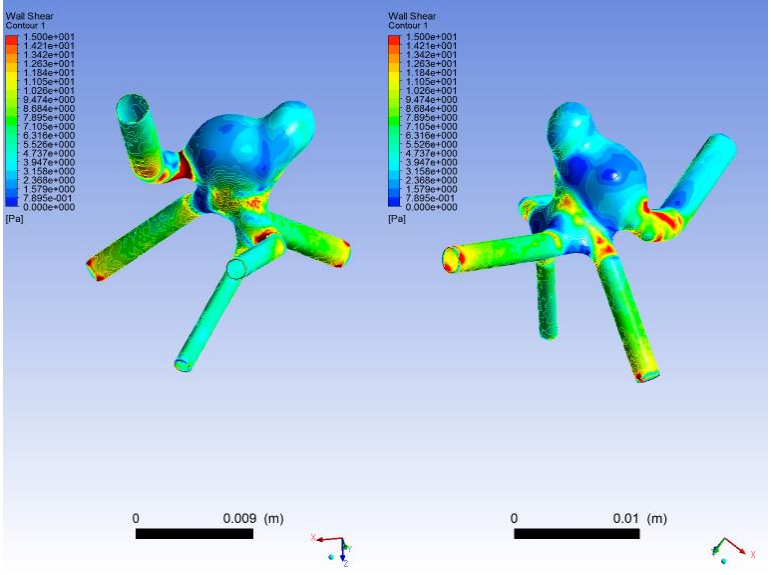

MRA

Pathlines 0.6

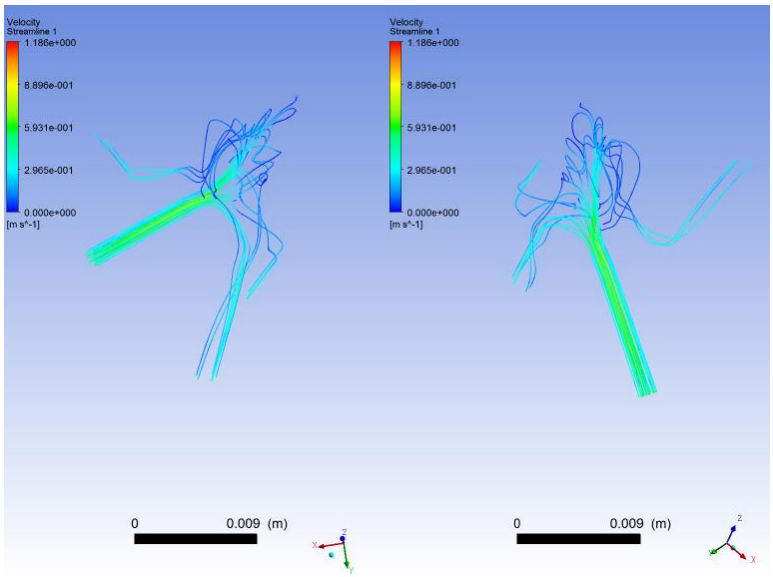

DSA

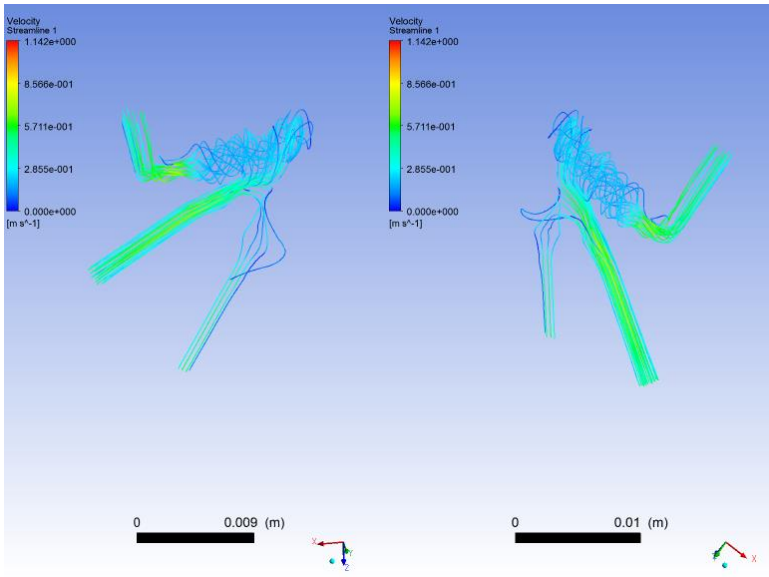

MRA

OSI 0.8

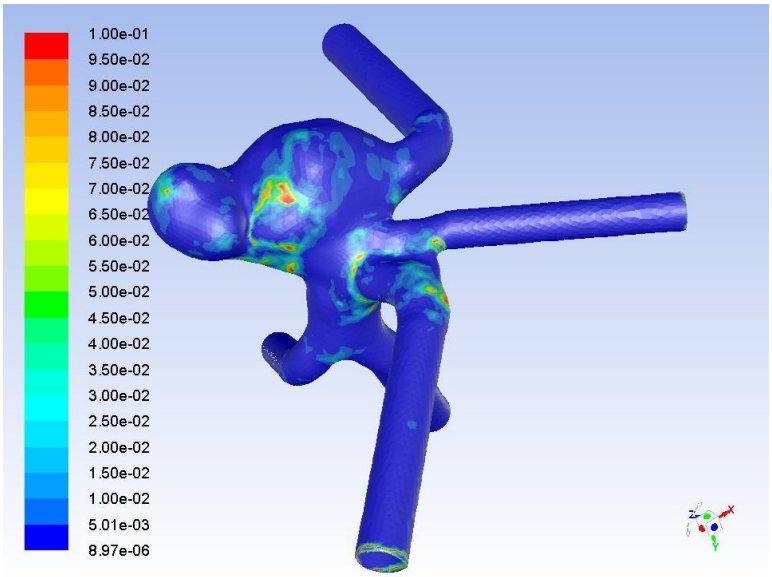

DSA front view

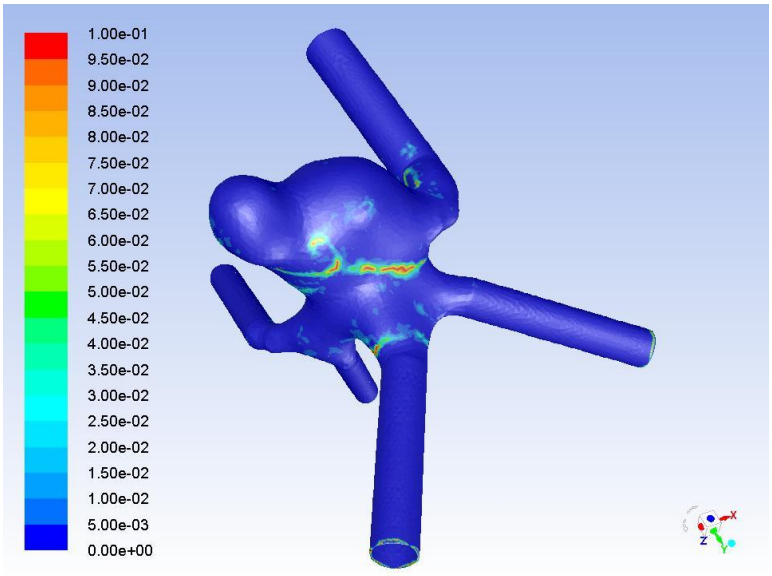

MRA front view

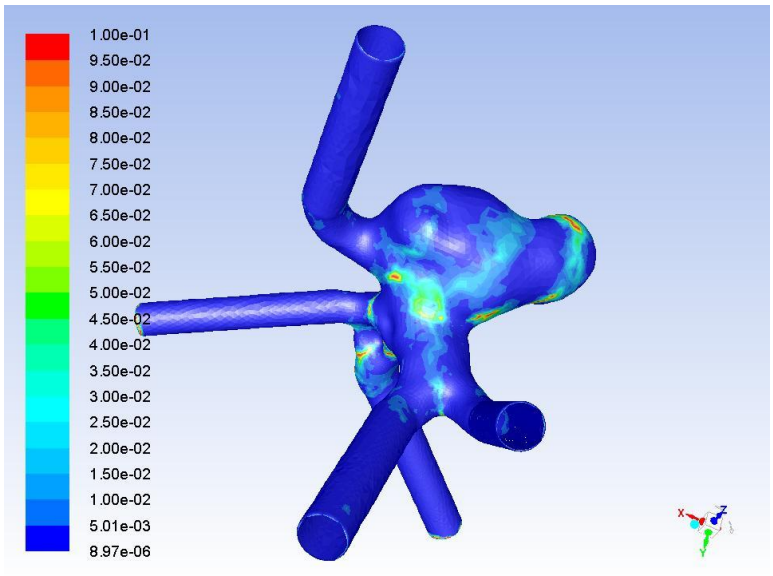

DSA rear view

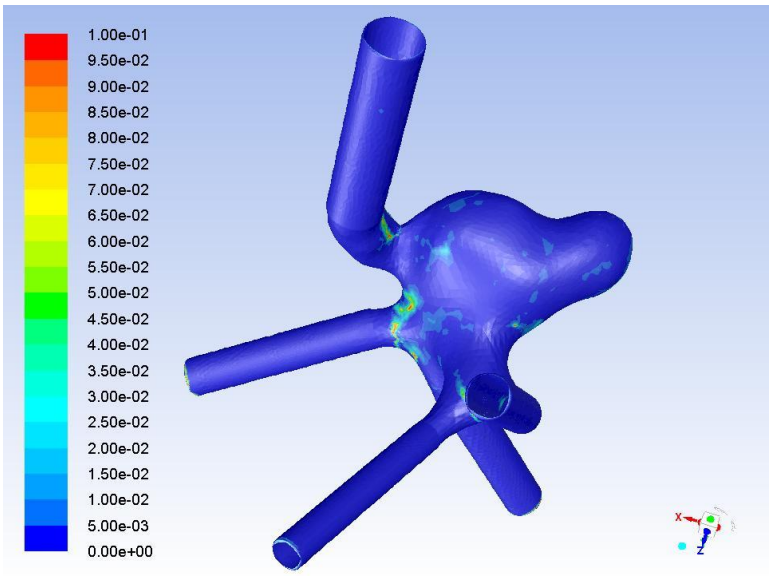

MRA rear view

4th patient results

- There is not a notable difference in the shape and size of the aneurysm.
- The pathlines extend at different regions both in the aneurysm dome and in the aneurysm outlets
- The minimum and maximum regions of WSS and OSI have similarities only to a certain extent
- The maximum values of pressure are always less at the DSA simulated aneurysm, with a margin that ranges between 10 and 15 %
- The maximum values of WSS are always less at the DSA simulated aneurysm, with a margin that ranges between 5 and 6 %
- The area averaged WSS value is always less at the DSA simulated aneurysm and the margin is as big as 28 %

5th patient DSA vs MRA

- Diameter derived from the DSA examination: **7**mm
- Diameter derived from the MRA examination: **7** mm
- Height derived from the DSA examination: **14.9** mm
- Height derived from the MRA examination: **15.5** mm
- 1 inlet and 2 outlets of blood

t=0.05 sec

	DSA	MRA
Pressure	-26 to 519 Pa	-30 to 736 Pa
WSS	0 to 208 Pa	0 to 230 Pa
Area Average WSS	3.58 Pa	3.72 Pa

Pressure 0.05

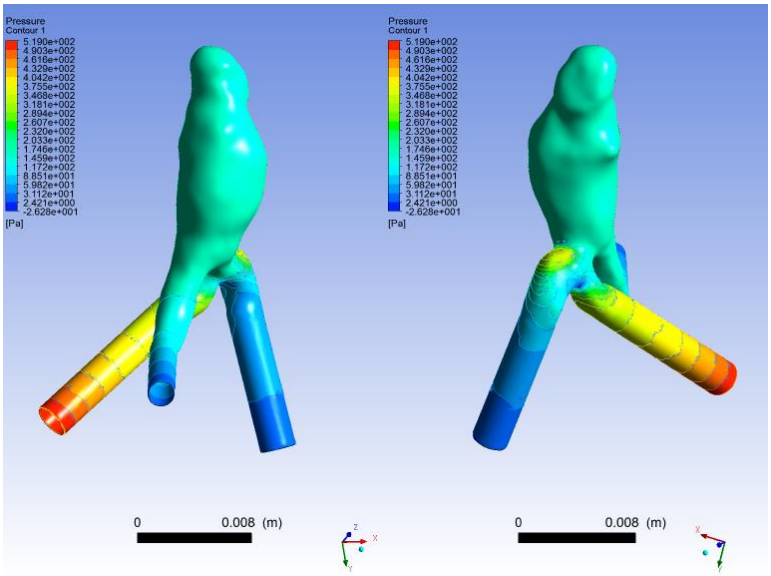
Pressure
Contour 1
5.190e+002
4.903e+002
4.616e+002
4.329e+002
4.042e+002
3.755e+002
3.468e+002
3.181e+002
2.894e+002
2.607e+002
2.320e+002
2.033e+002
1.746e+002
1.459e+002
1.172e+002
8.851e+001
5.982e+001
3.112e+001
2.421e+000
-2.628e+001
[Pa]
0
0.008 (m)
Pressure
Contour 1
5.190e+002
4.903e+002
4.616e+002
4.329e+002
4.042e+002
3.755e+002
3.468e+002
3.181e+002
2.894e+002
2.607e+002
2.320e+002
2.033e+002
1.746e+002
1.459e+002
1.172e+002
8.851e+001
5.982e+001
3.112e+001
2.421e+000
-2.628e+001
[Pa]
0
0.008 (m)

DSA

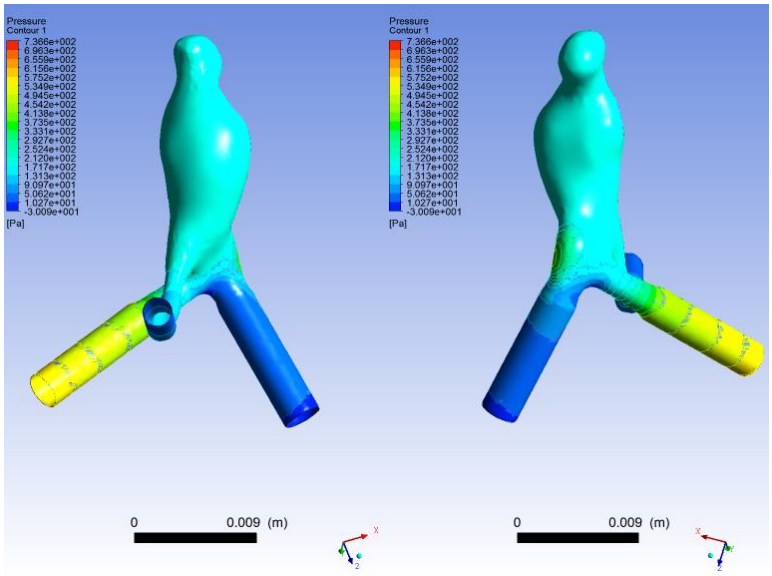
Pressure
Contour 1
7.366e+002
6.963e+002
6.559e+002
6.156e+002
5.752e+002
5.349e+002
4.945e+002
4.542e+002
4.138e+002
3.735e+002
3.331e+002
2.927e+002
2.524e+002
2.120e+002
1.717e+002
1.313e+002
9.097e+001
5.062e+001
1.027e+001
-3.009e+001
[Pa]
0
0.009 (m)
Pressure
Contour 1
7.366e+002
6.963e+002
6.559e+002
6.156e+002
5.752e+002
5.349e+002
4.945e+002
4.542e+002
4.138e+002
3.735e+002
3.331e+002
2.927e+002
2.524e+002
2.120e+002
1.717e+002
1.313e+002
9.097e+001
5.062e+001
1.027e+001
-3.009e+001
[Pa]
0
0.009 (m)

MRA

WSS 0.05

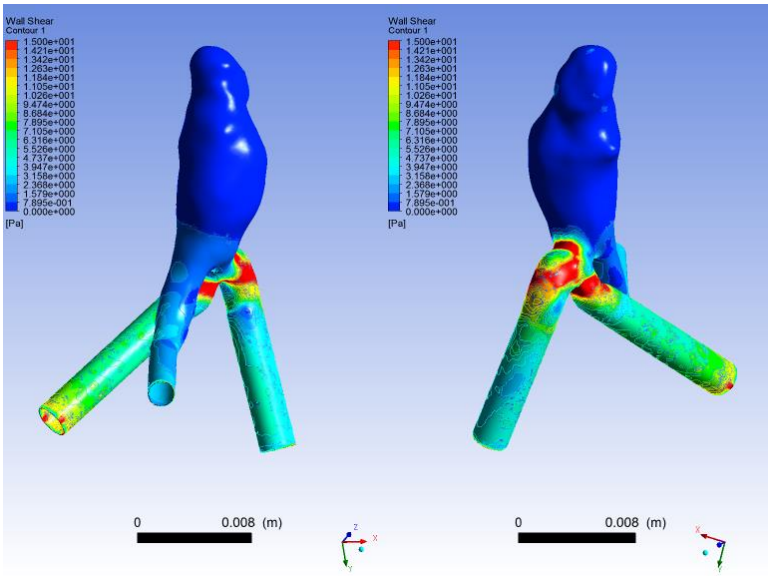

DSA

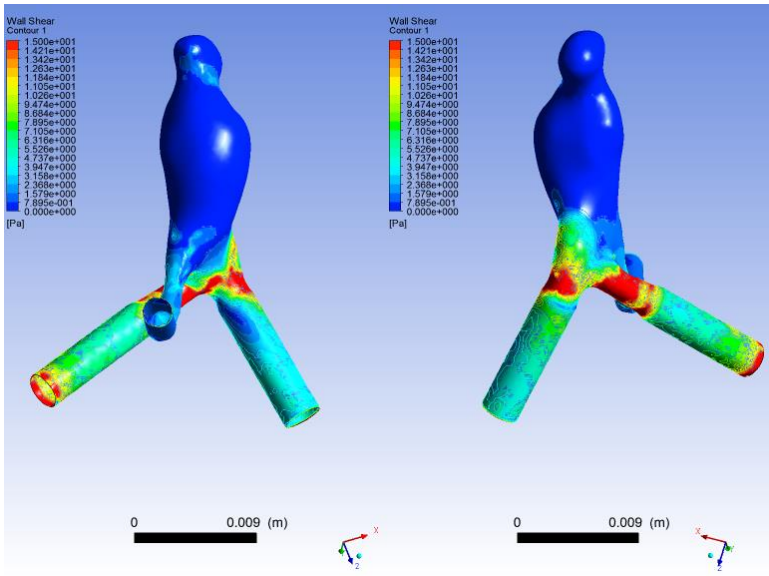

MRA

Pathlines 0.05

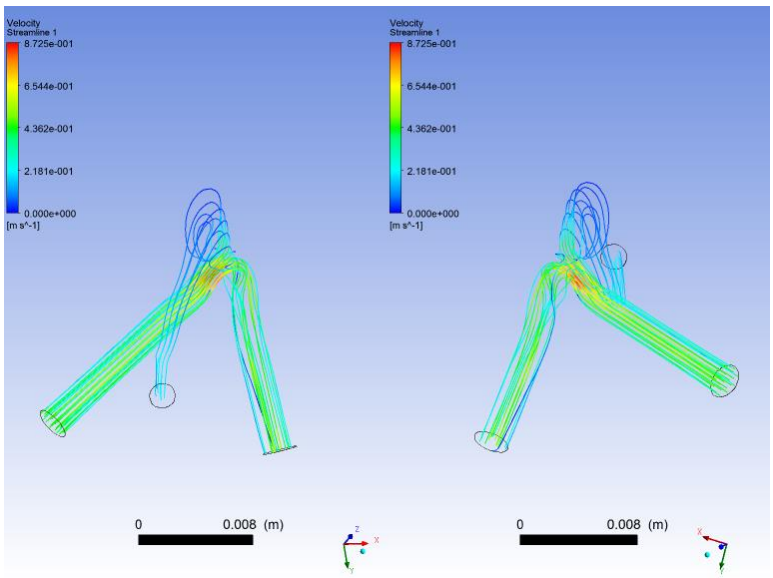

DSA

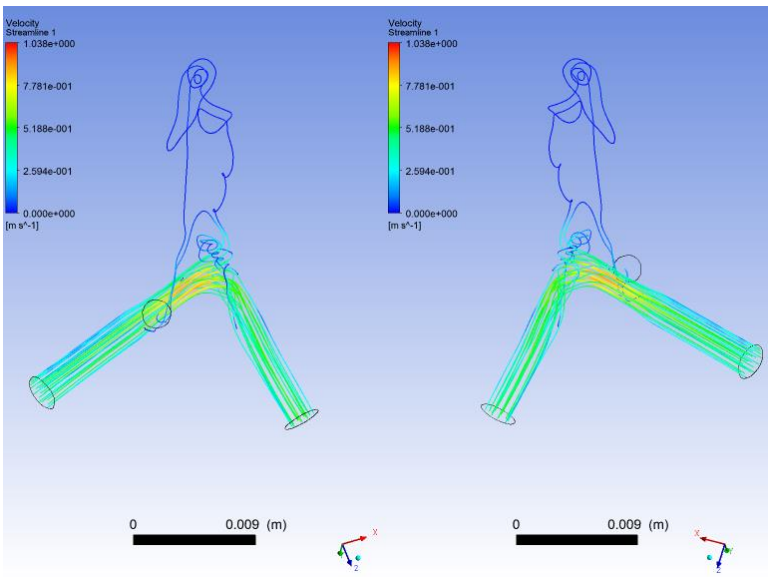

MRA

t=0.2 sec

	DSA	MRA
Pressure	-144 to 1243 Pa	-2 to 1671 Pa
WSS	0 to 398 Pa	0 to 435 Pa
Area Average WSS	9.02 Pa	10.48 Pa

Pressure 0.2

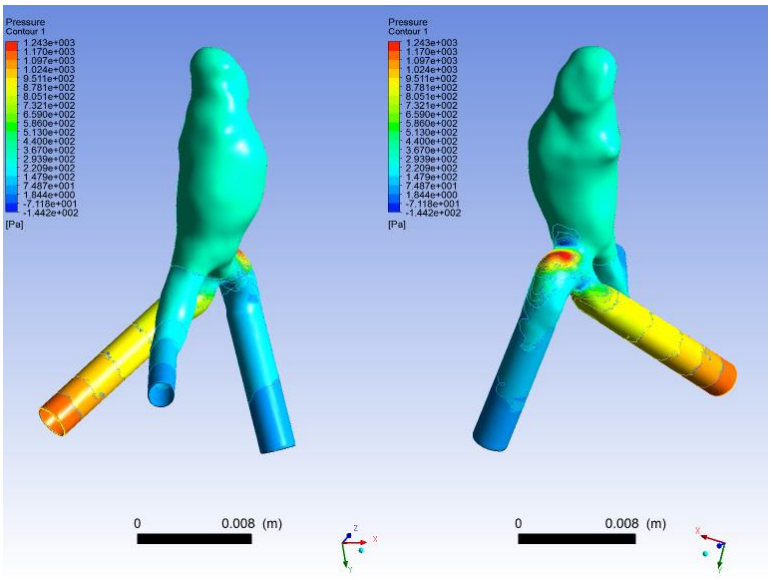

DSA

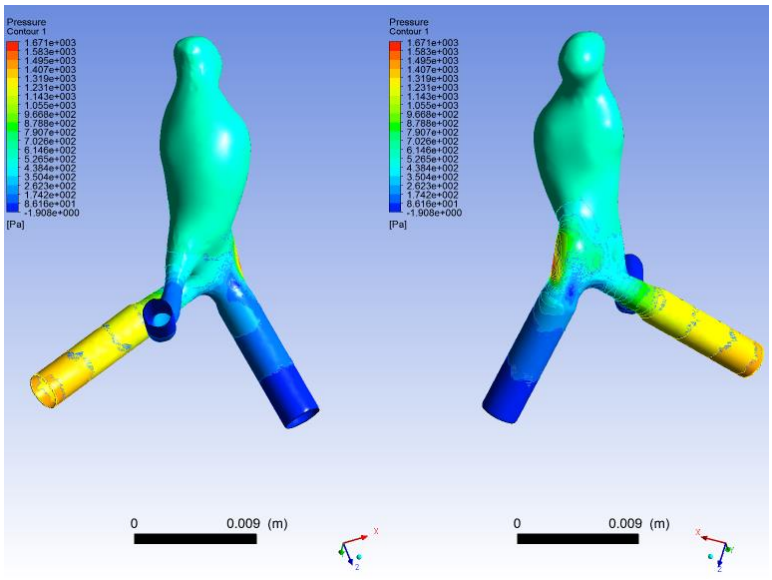

MRA

WSS 0.2

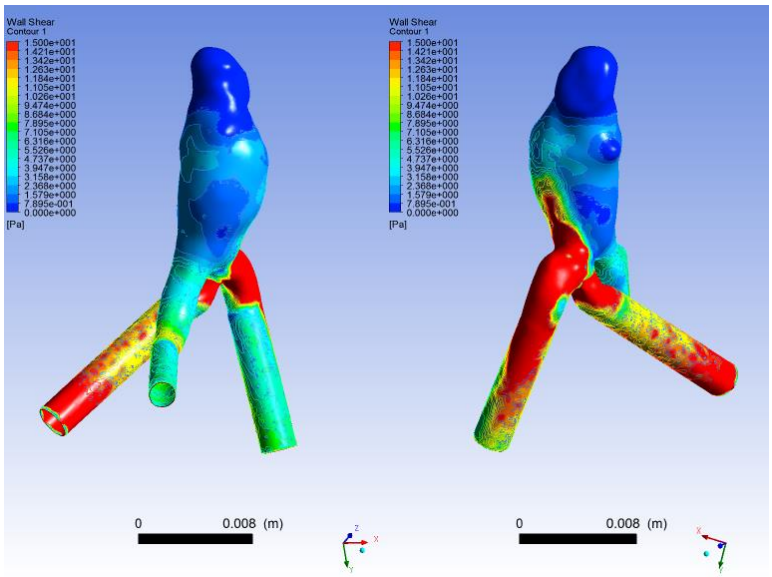

DSA

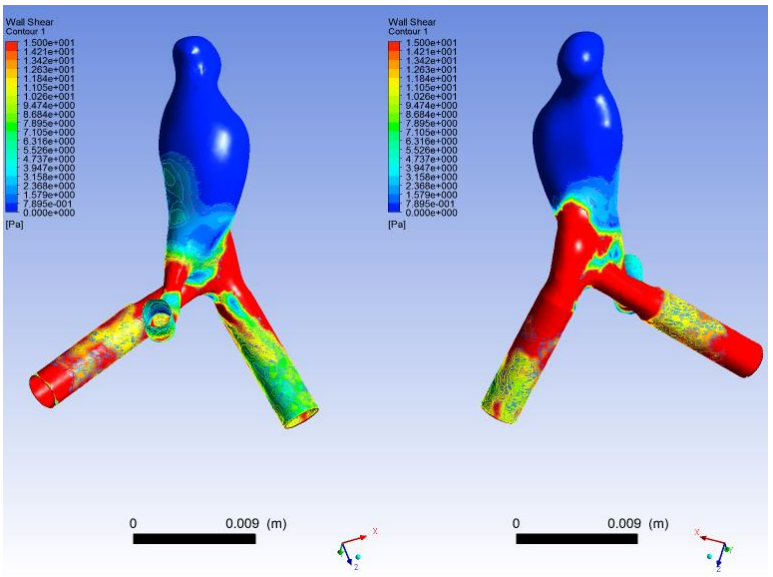

MRA

Pathlines 0.2

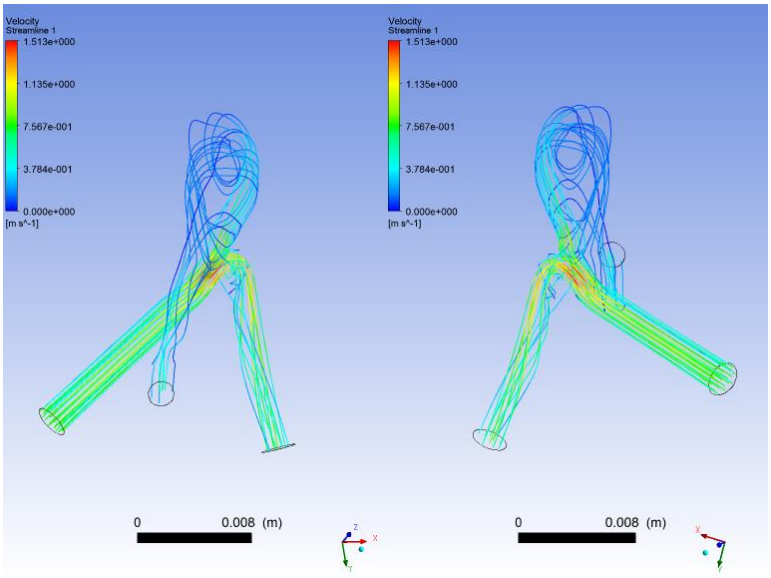

DSA

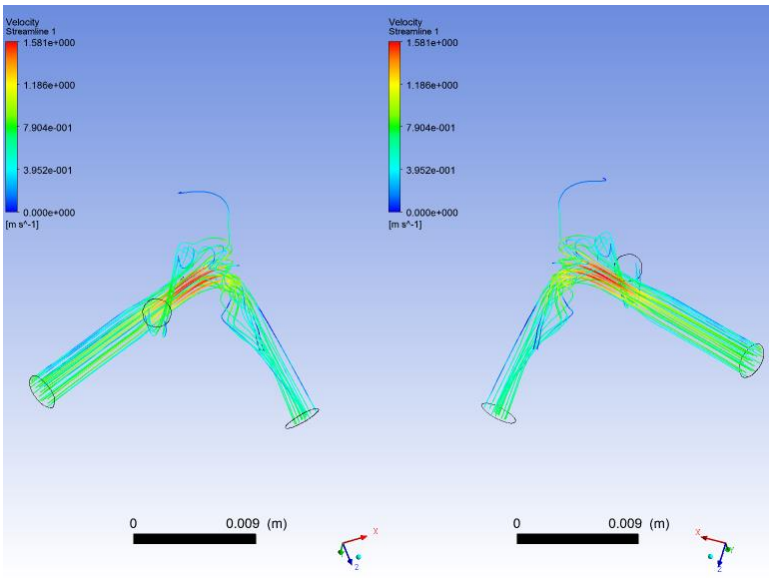

MRA

t=0.4 sec

	DSA	MRA
Pressure	-72 to 771 Pa	-1 to 1089 Pa
WSS	0 to 279 Pa	0 to 307 Pa
Area Average WSS	6.56 Pa	7.51 Pa

Pressure 0.4

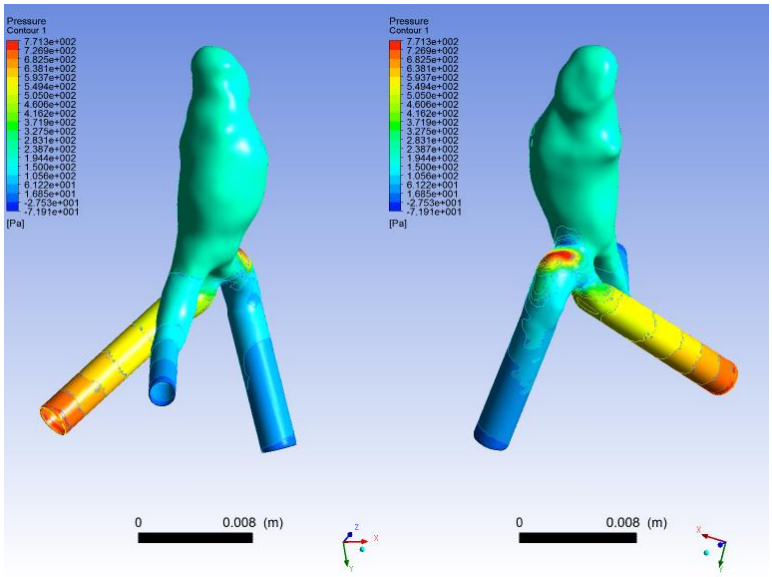

DSA

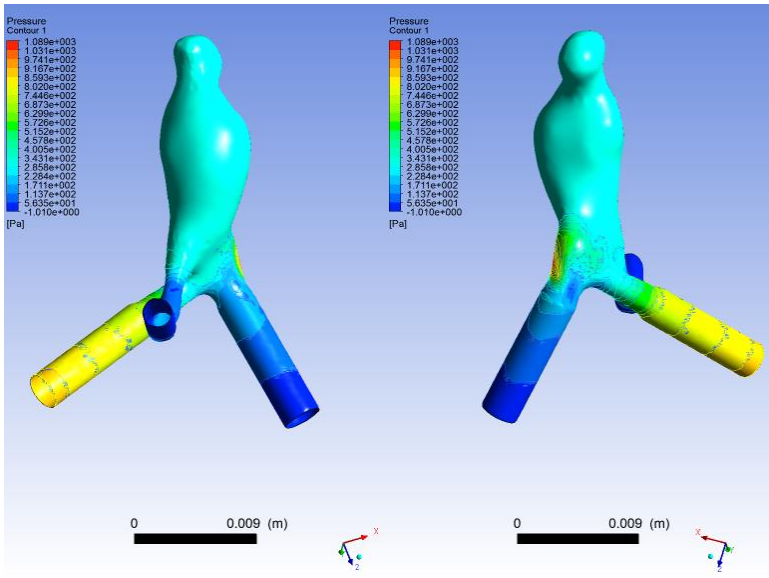

MRA

WSS 0.4

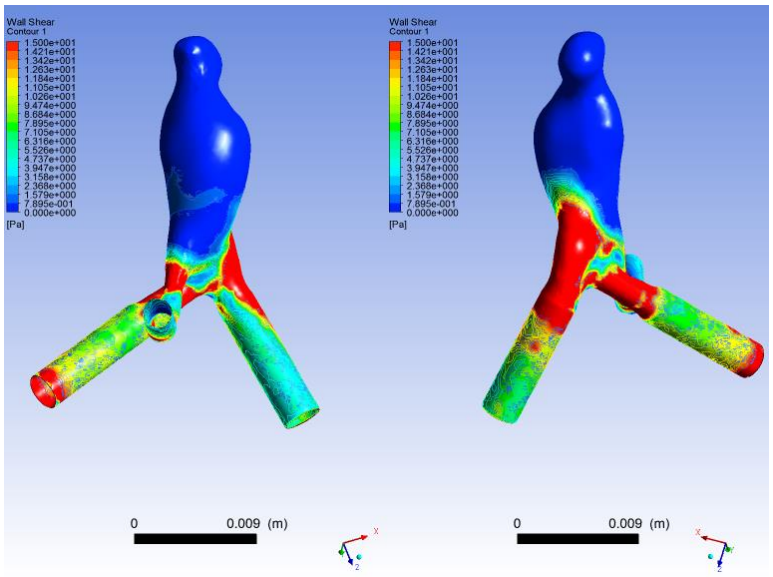

DSA

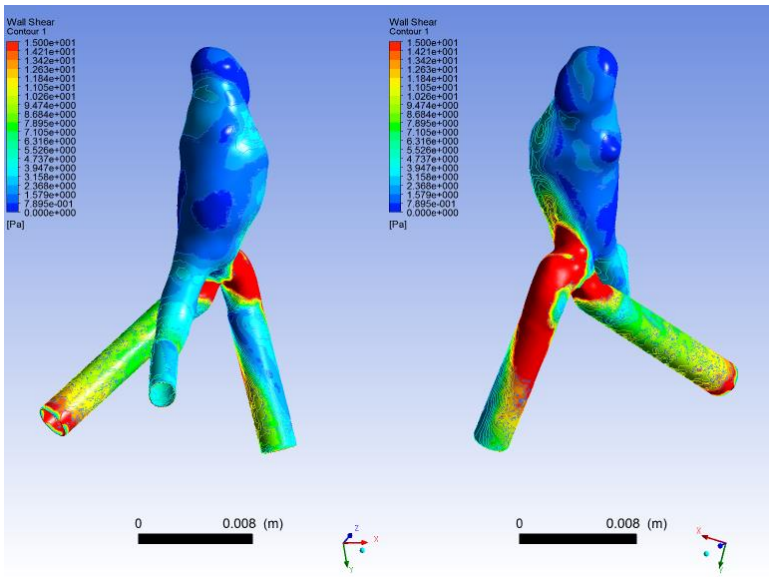

MRA

Pathlines 0.4

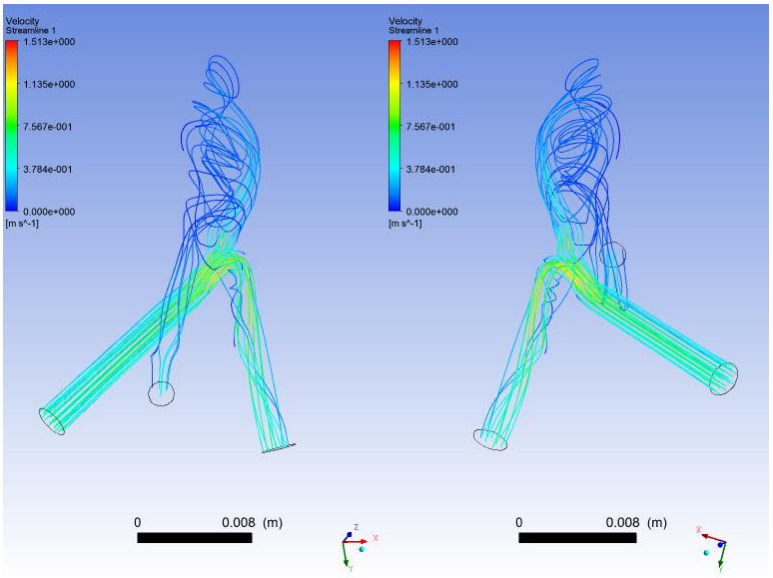

DSA

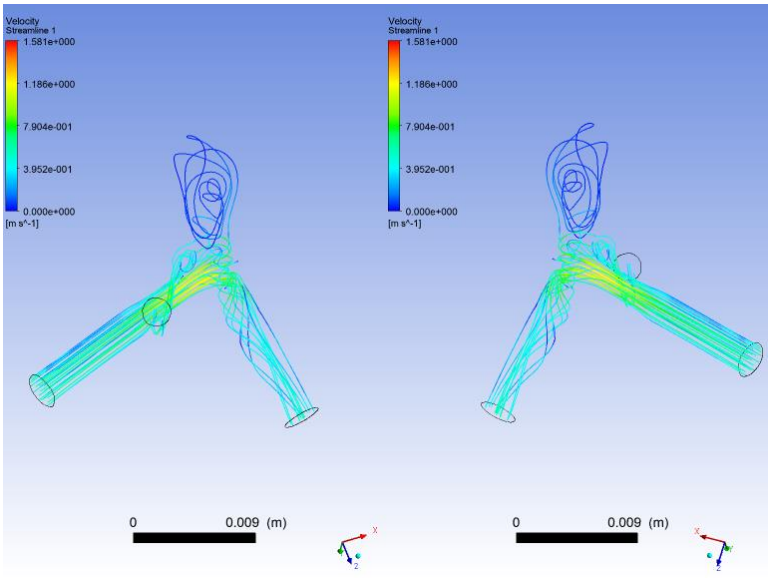

MRA

t=0.6 sec

	DSA	MRA
Pressure	-43 to 536 Pa	-1 to 821 Pa
WSS	0 to 232 Pa	0 to 256 Pa
Area Average WSS	4.74 Pa	5.39 Pa

Pressure 0.6

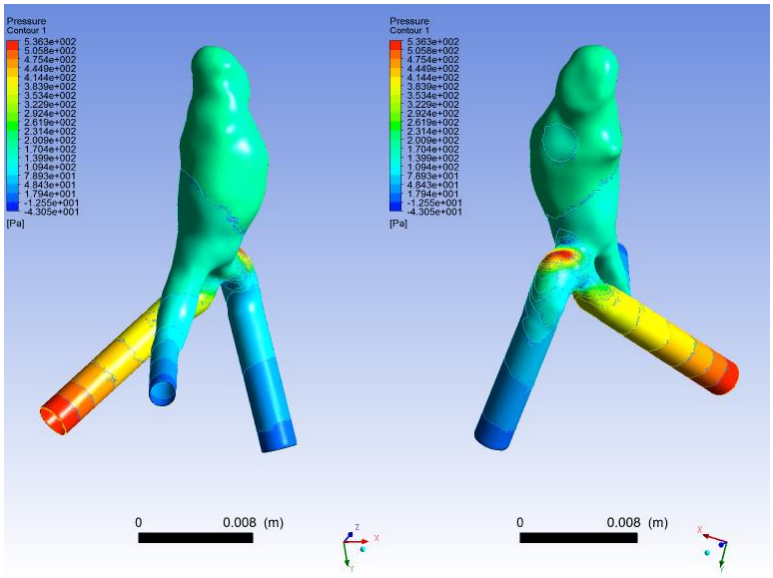

DSA

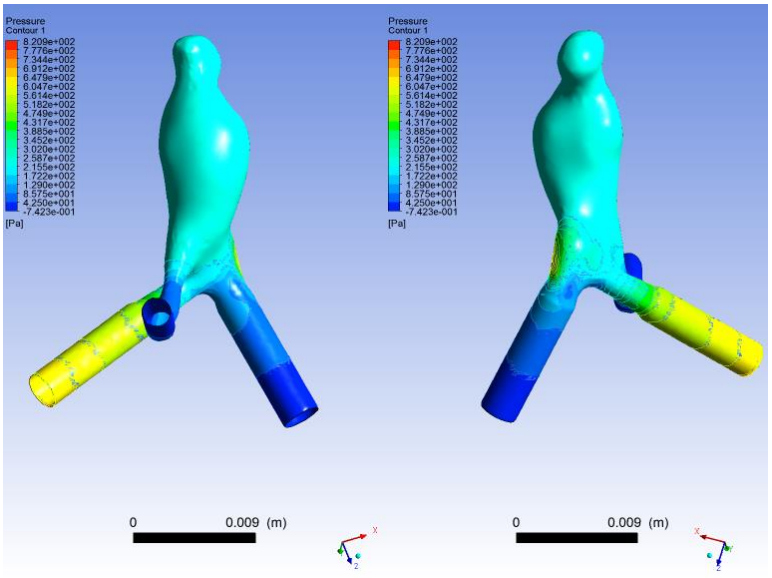

MRA

WSS 0.6

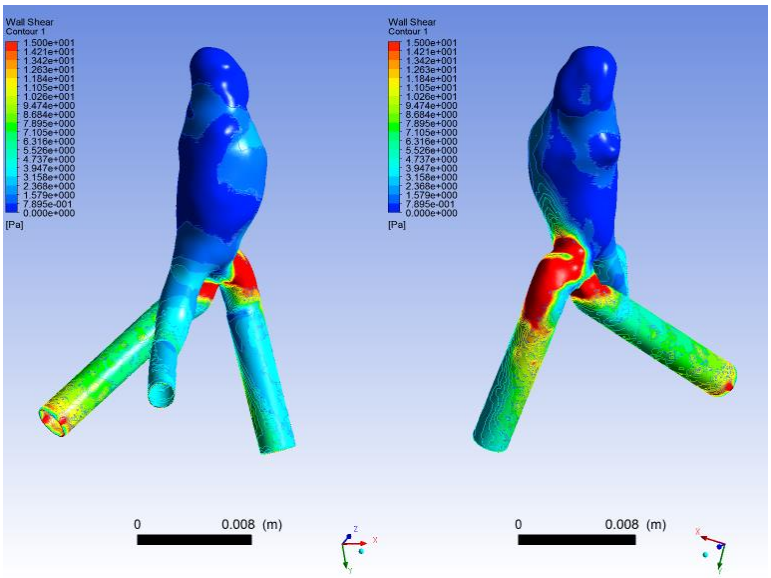

DSA

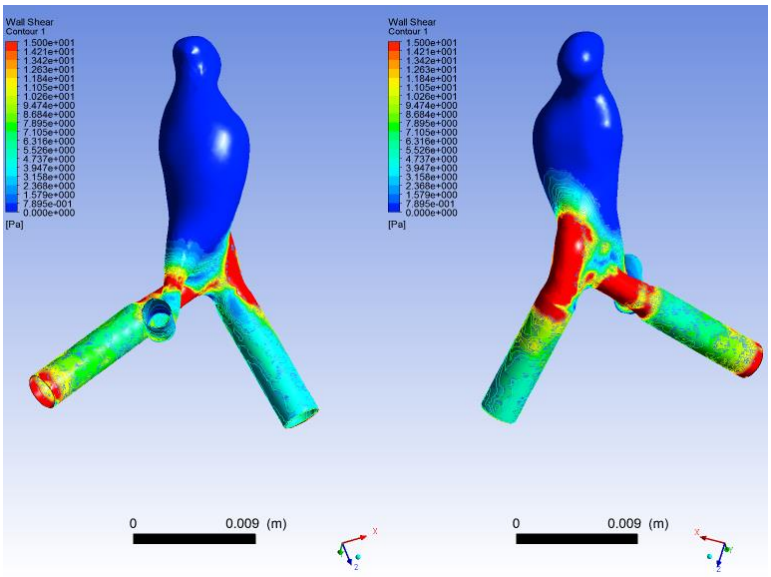

MRA

Pathlines 0.6

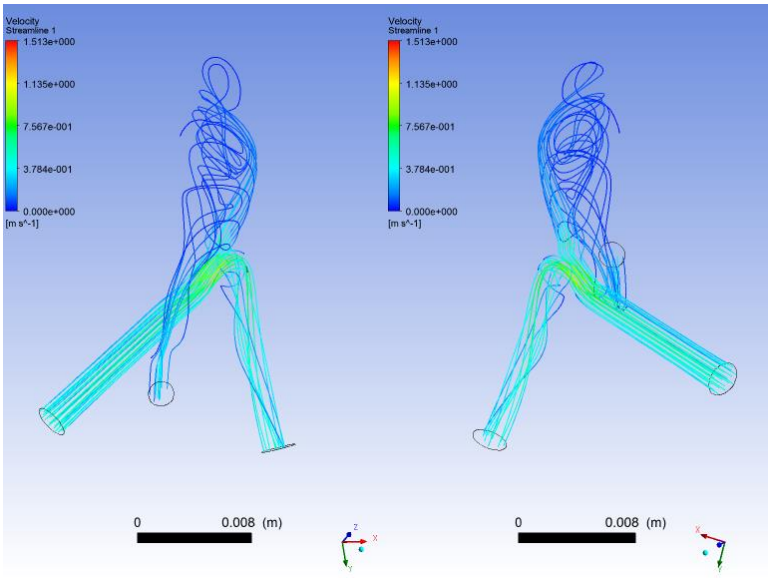

DSA

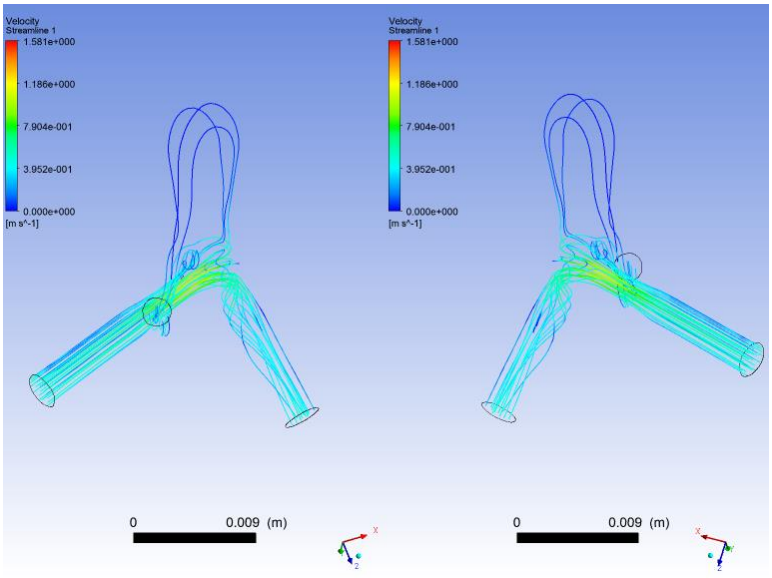

MRA

OSI 0.8

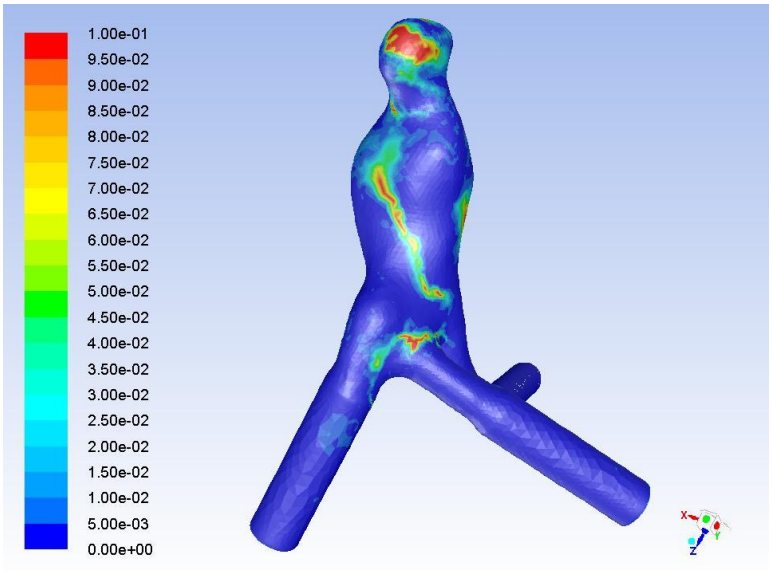

DSA front view

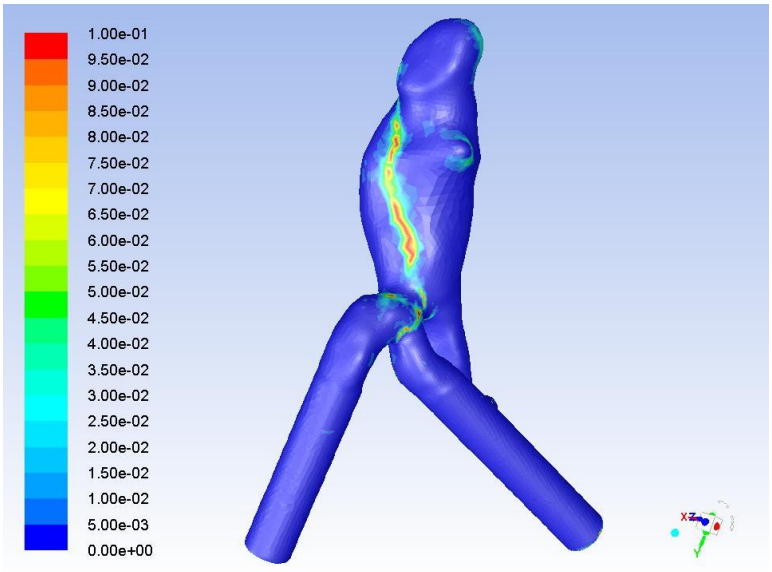

MRA front view

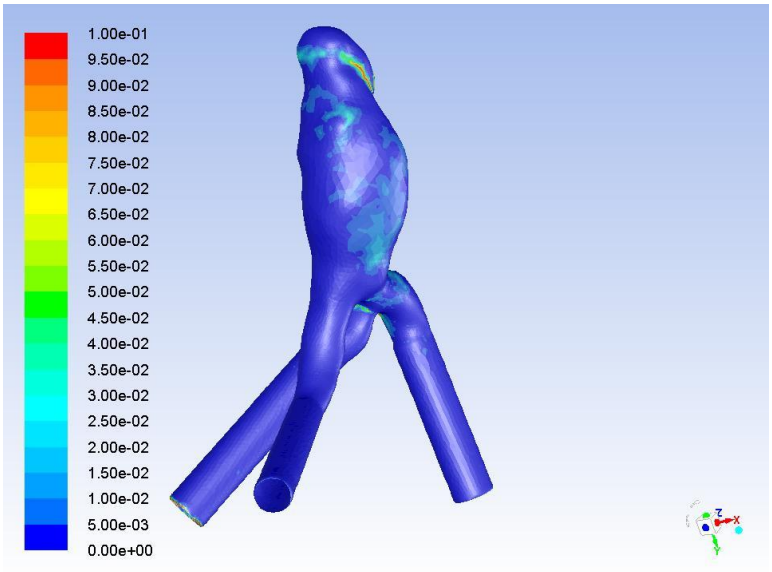

DSA rear view

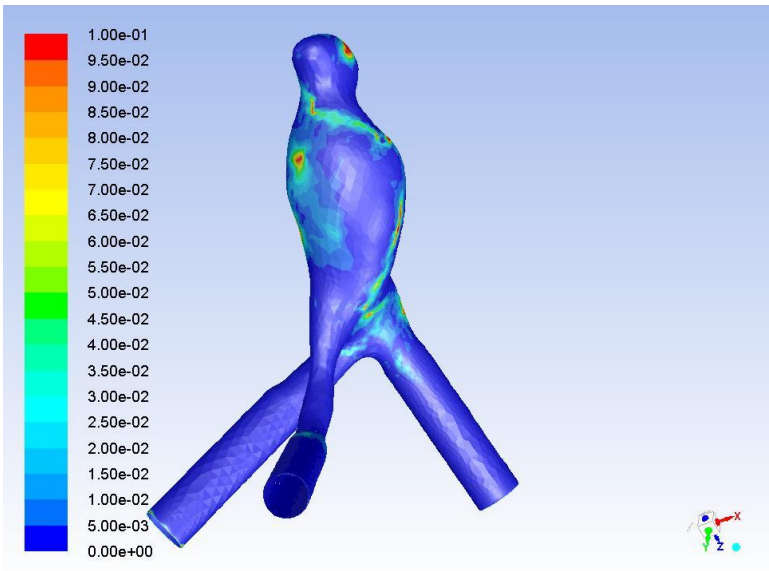

MRA rear view

5th patient results

- There is a notable difference in the shape and size of the aneurysm.
- The pathlines extend at different regions in the aneurysm dome.
- The minimum and maximum regions of WSS and OSI have similarities only to a certain extent
- The maximum values of pressure are always less at the DSA simulated aneurysm, with a margin of 10 %
- The maximum values of WSS are always less at the DSA simulated aneurysm, with a margin of 10 %
- The area averaged WSS value is always less at the DSA simulated aneurysm and the margin is as big as 13 %

6th patient DSA vs MRA

- Diameter derived from the DSA examination: **6.8** mm
- Diameter derived from the MRA examination: **5.9** mm
- Height derived from the DSA examination: **3** mm
- Height derived from the MRA examination: **3.2** mm
- 1 inlet and 3 outlets of blood

t=0.05 sec

	DSA	MRA
Pressure	-17 to 522 Pa	-11 to 609 Pa
WSS	0 to 270 Pa	0 to 280 Pa
Area Average WSS	4.16 Pa	5.34 Pa

Pressure 0.05

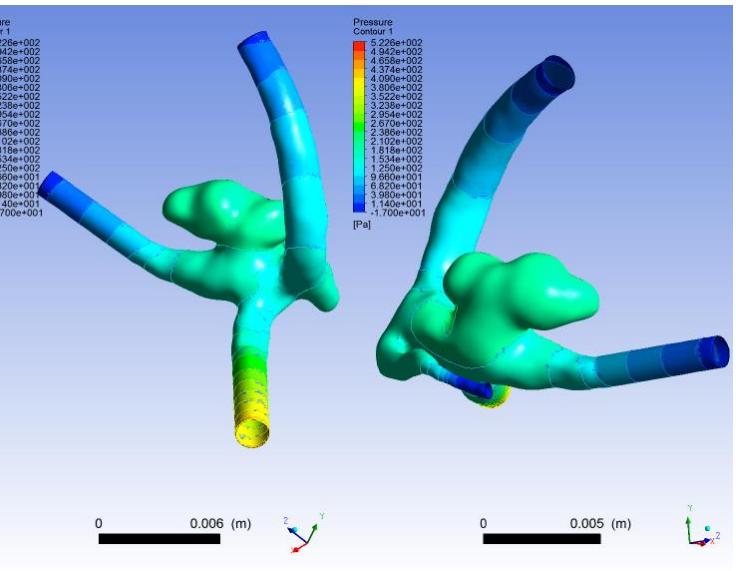
Pressure
Contour 1
5.226e+002
4.942e+002
4.658e+002
4.374e+002
4.090e+002
3.806e+002
3.522e+002
3.238e+002
2.954e+002
2.670e+002
2.385e+002
2.102e+002
1.818e+002
1.534e+002
1.250e+002
9.660e+001
6.820e+001
3.980e+001
1.140e+001
-1.700e+001
[Pa]
0
0.006 (m)
0
0.005 (m)

DSA

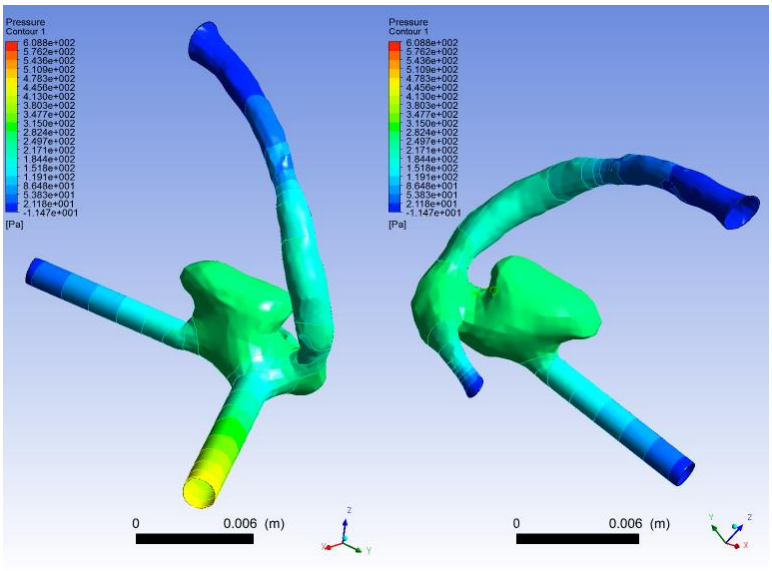
Pressure
Contour 1
6.088e+002
5.762e+002
5.436e+002
5.109e+002
4.783e+002
4.456e+002
4.130e+002
3.803e+002
3.477e+002
3.150e+002
2.824e+002
2.497e+002
2.171e+002
1.844e+002
1.518e+002
1.191e+002
8.648e+001
5.383e+001
2.118e+001
-1.147e+001
[Pa]
0
0.006 (m)
0
0.006 (m)

MRA

WSS 0.05

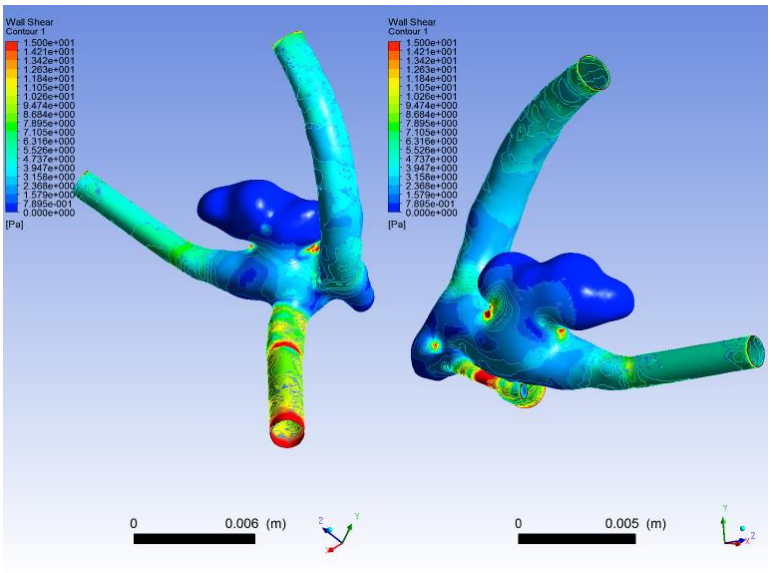

DSA

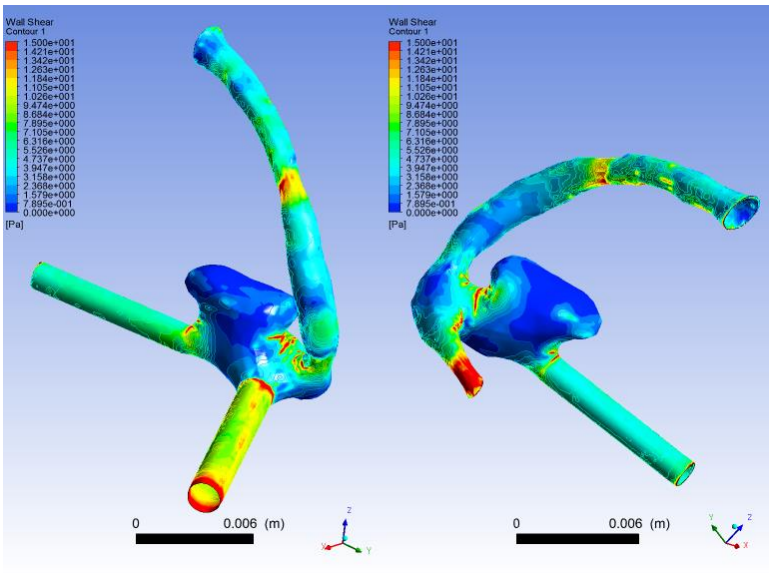

MRA

Pathlines 0.05

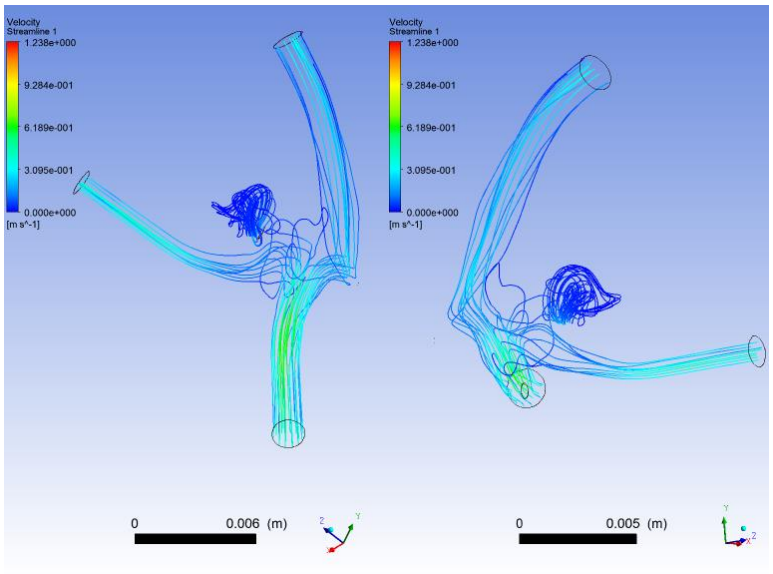

DSA

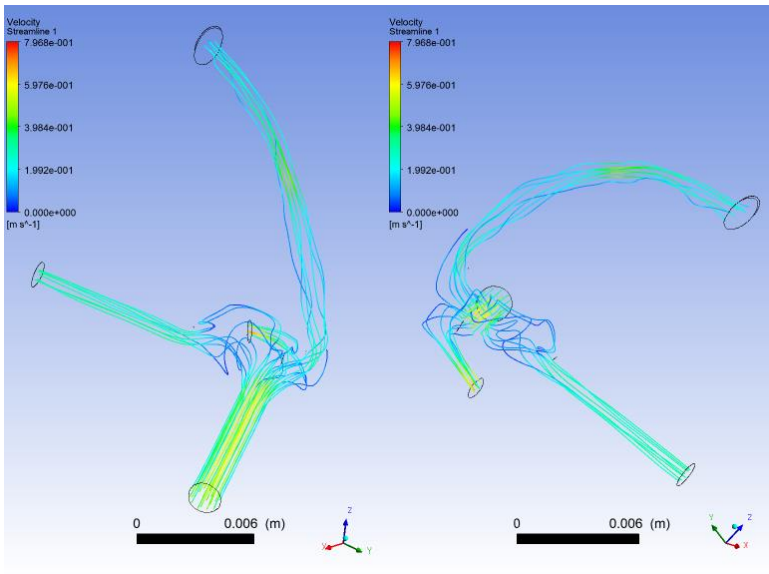

MRA

t=0.2 sec

	DSA	MRA
Pressure	-5 to 1019 Pa	-18 to 1215 Pa
WSS	0 to 499 Pa	0 to 524 Pa
Area Average WSS	9.9 Pa	10.52 Pa

Pressure 0.2

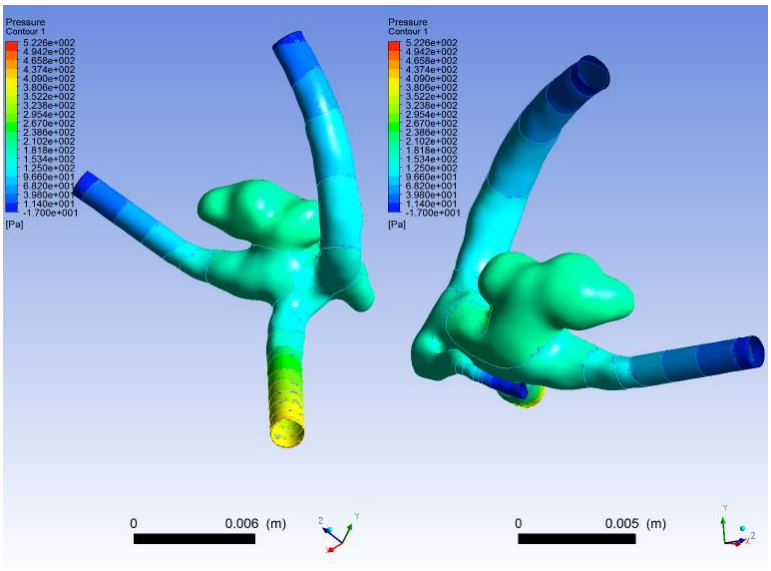

DSA

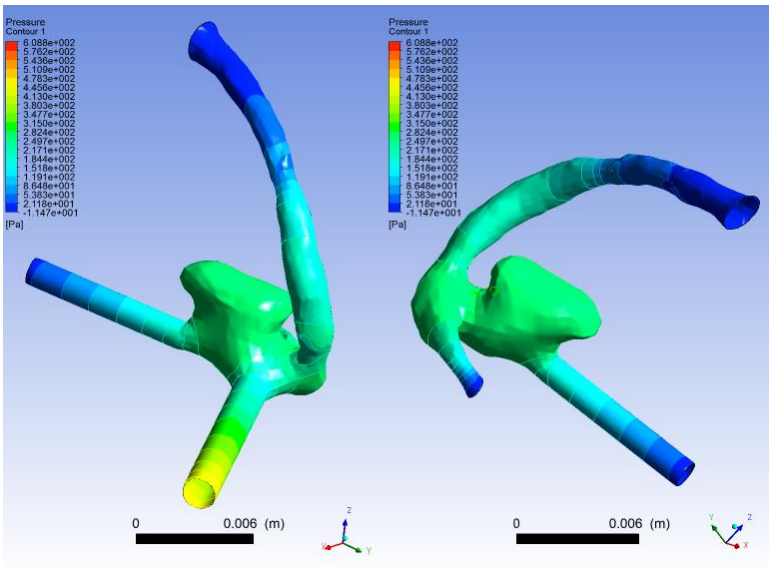

MRA

WSS 0.2

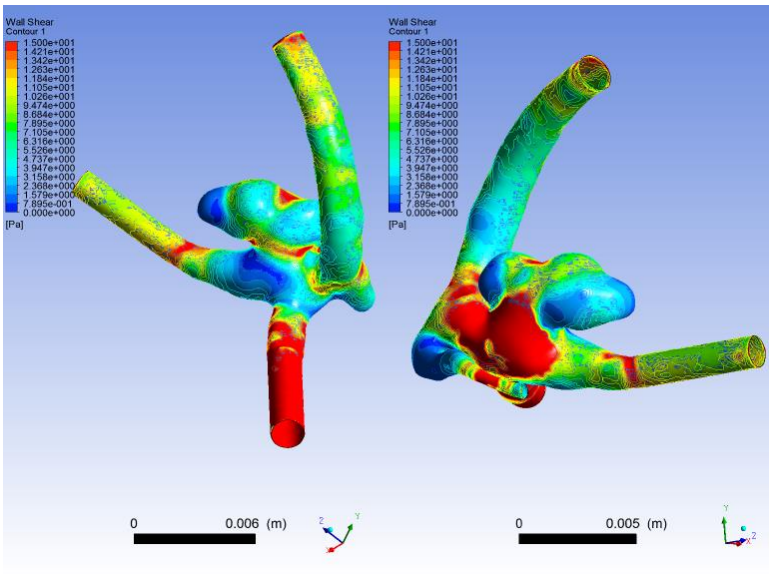

DSA

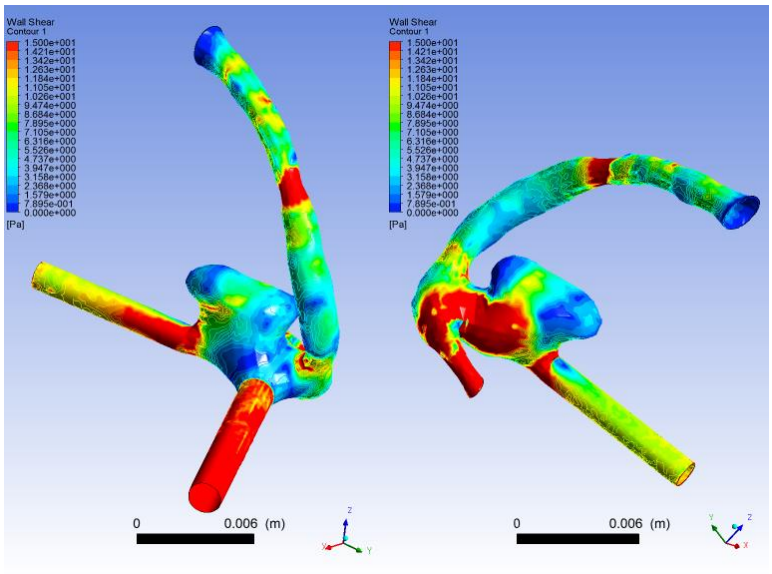

MRA

Pathlines 0.2

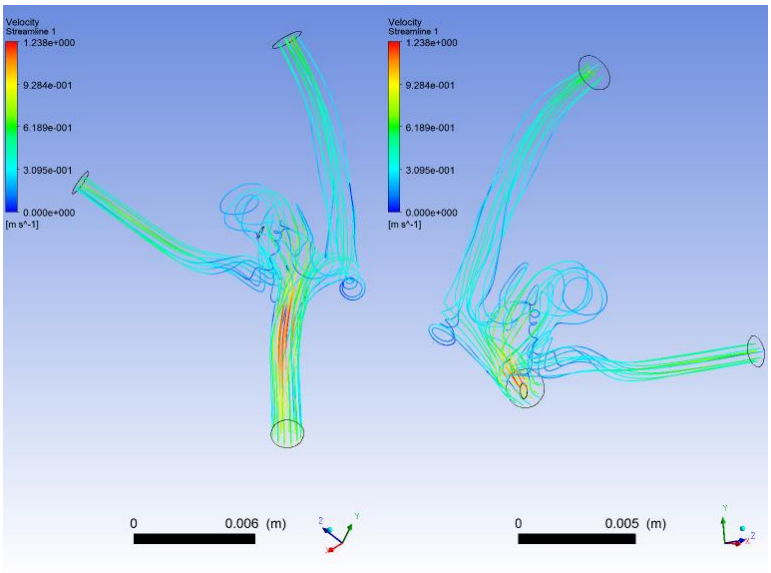

DSA

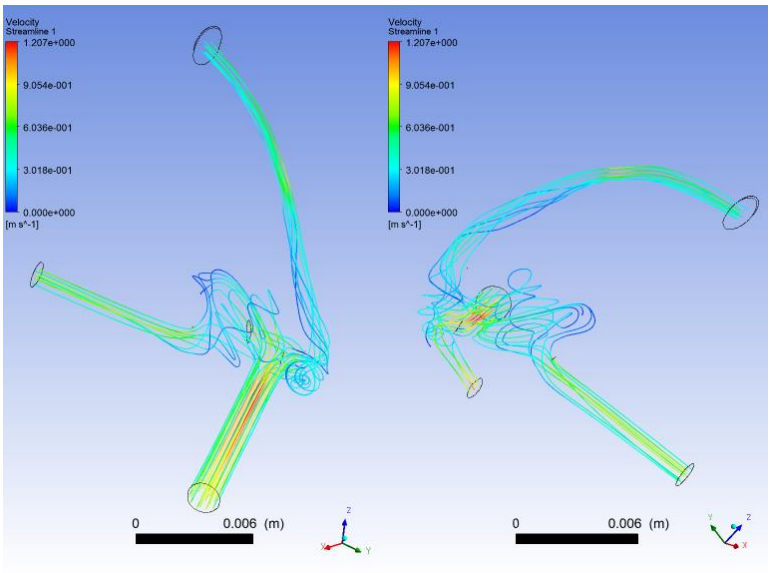

MRA

t=0.4 sec

	DSA	MRA
Pressure	-1 ως 735 Pa	-9 ως 864 Pa
WSS	0 to 358 Pa	0 to 372 Pa
Area Average WSS	7.06 Pa	7.94 Pa

Pressure 0.4

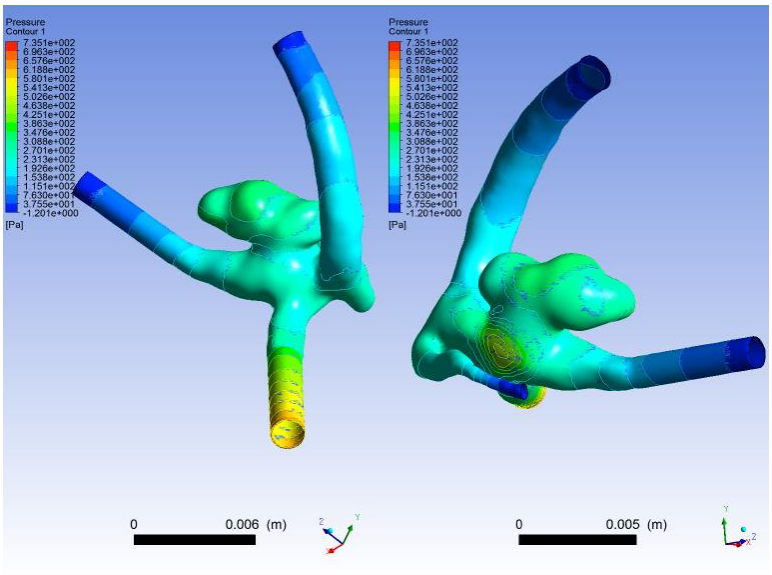

DSA

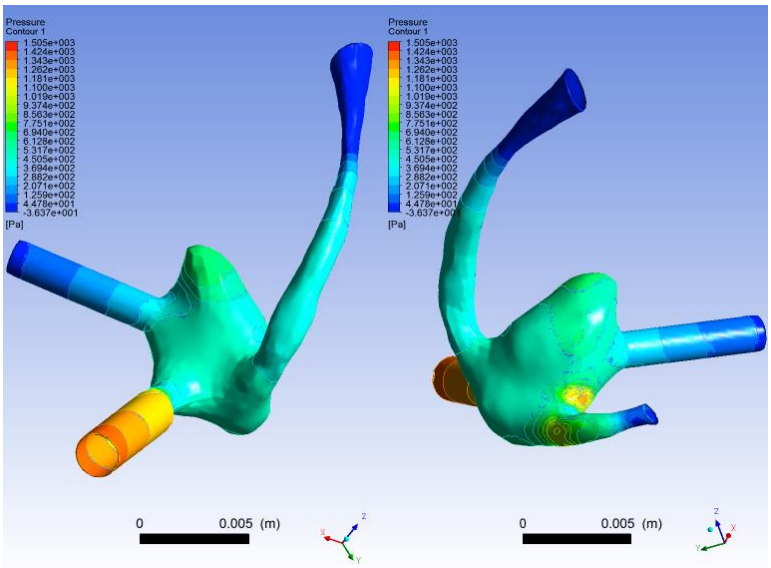

MRA

WSS 0.4

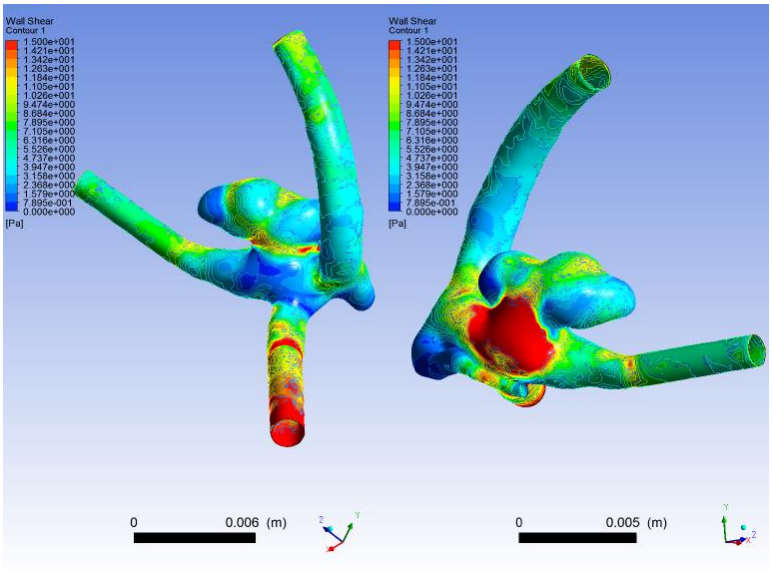

DSA

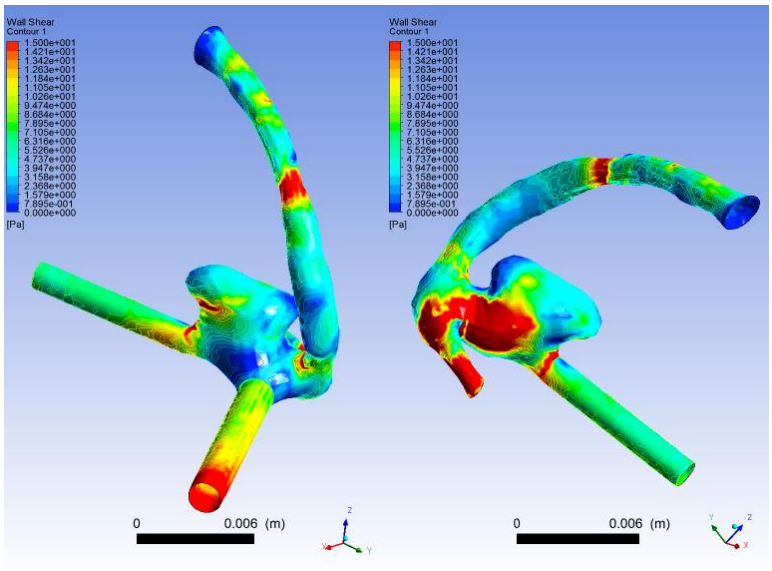

MRA

Pathlines 0.4

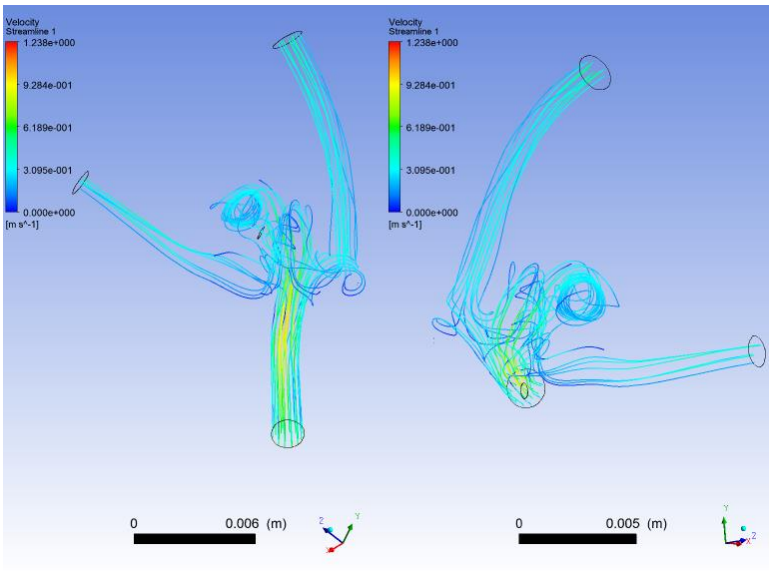

DSA

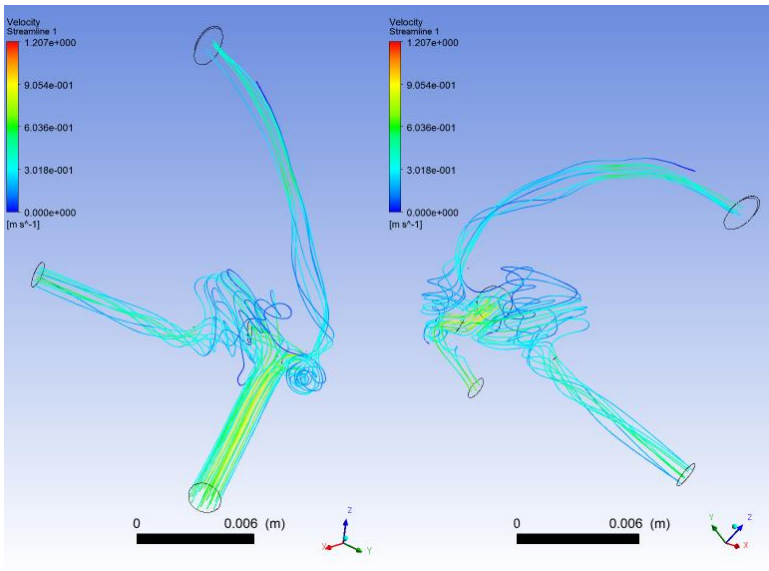

MRA

t=0.6 sec

	DSA	MRA
Pressure	-1 to 573 Pa	-6 to 685 Pa
WSS	0 to 300 Pa	0 to 310 Pa
Area Average WSS	5.17 Pa	5.82 Pa

Pressure 0.6

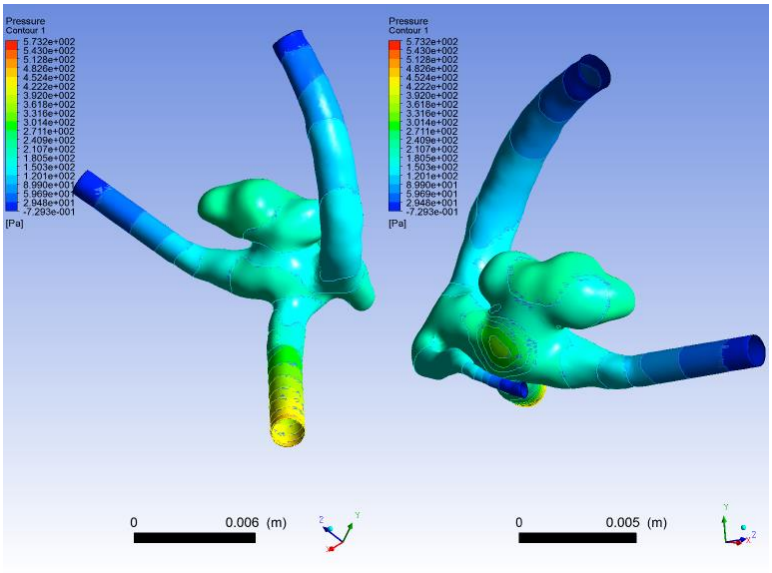

DSA

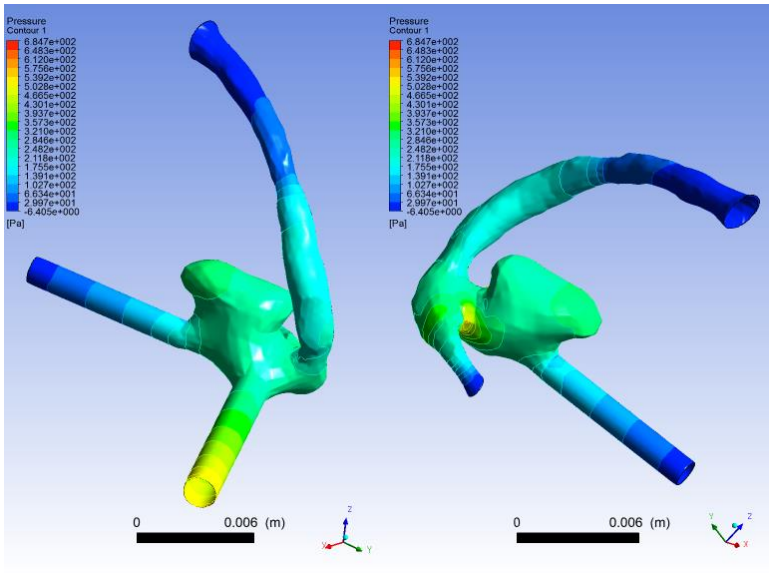

MRA

WSS 0.6

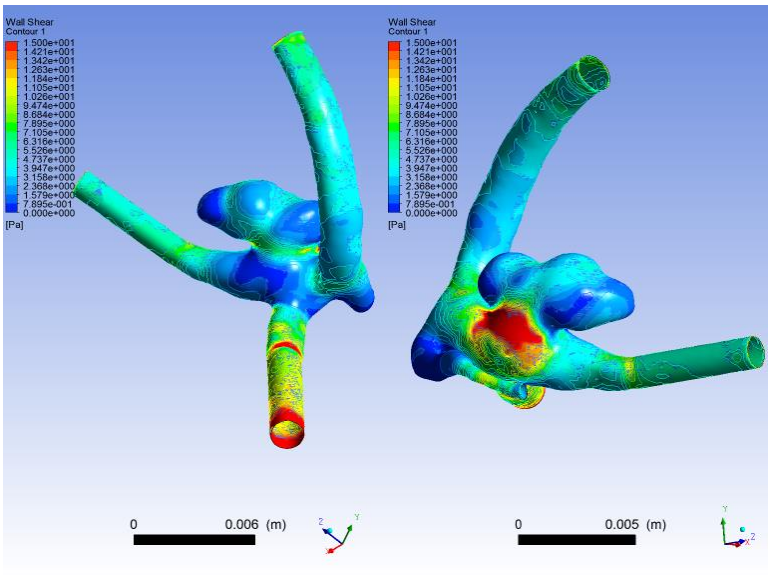

DSA

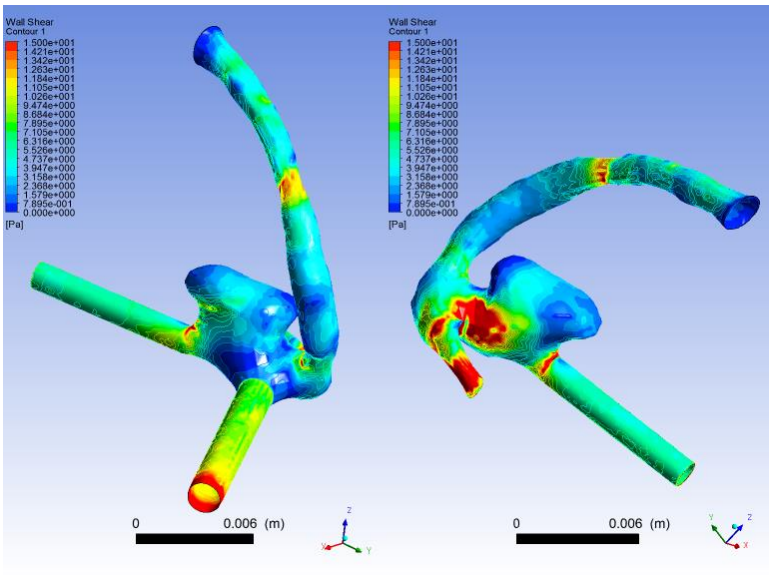

MRA

Pathlines 0.6

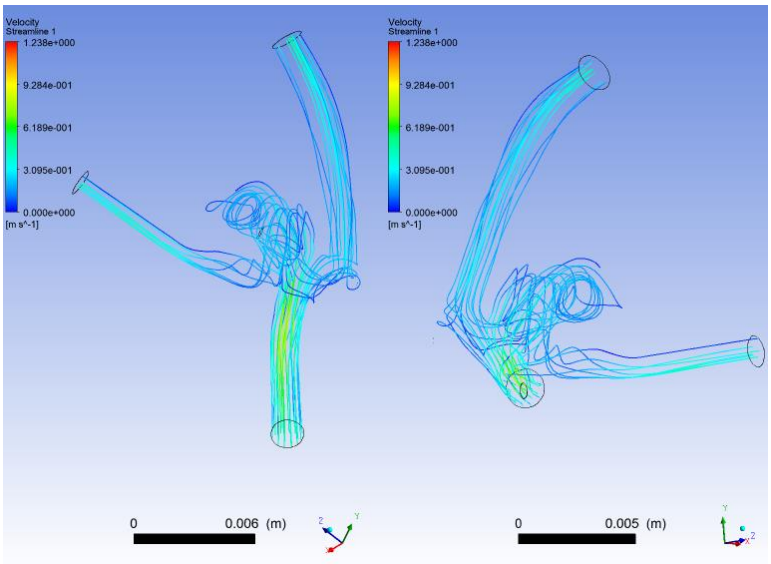

DSA

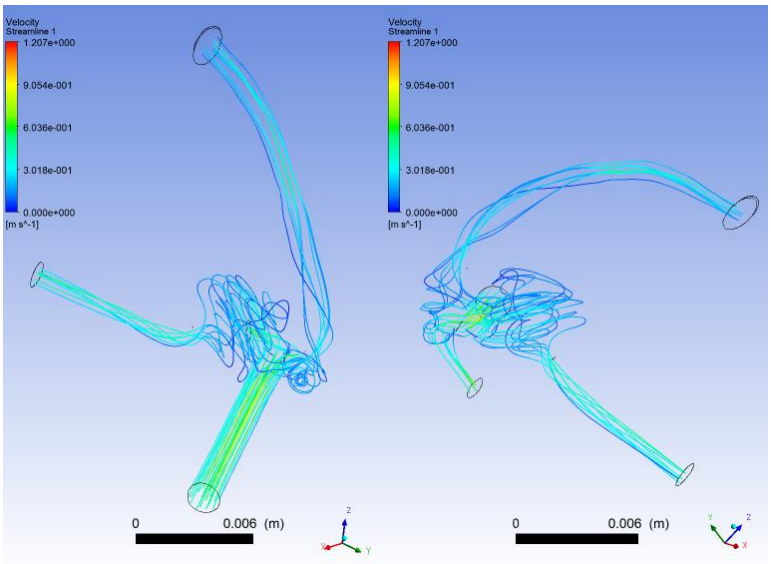

MRA

OSI 0.8

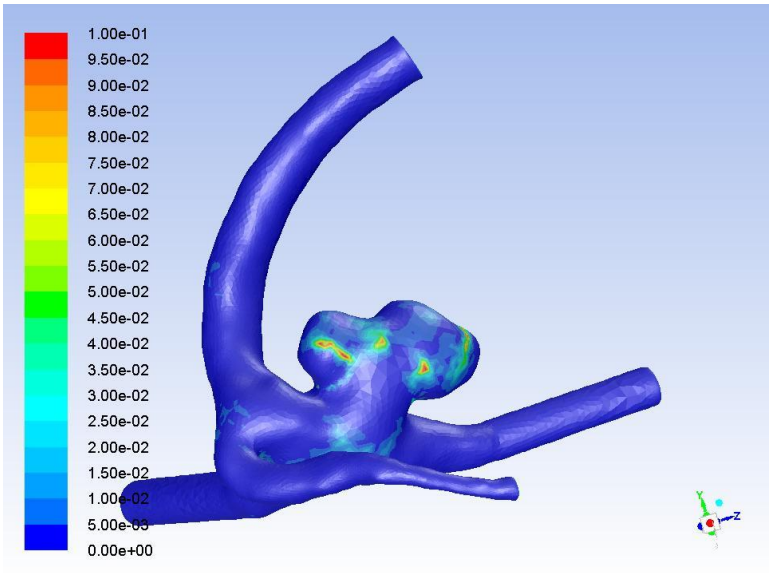

DSA front view

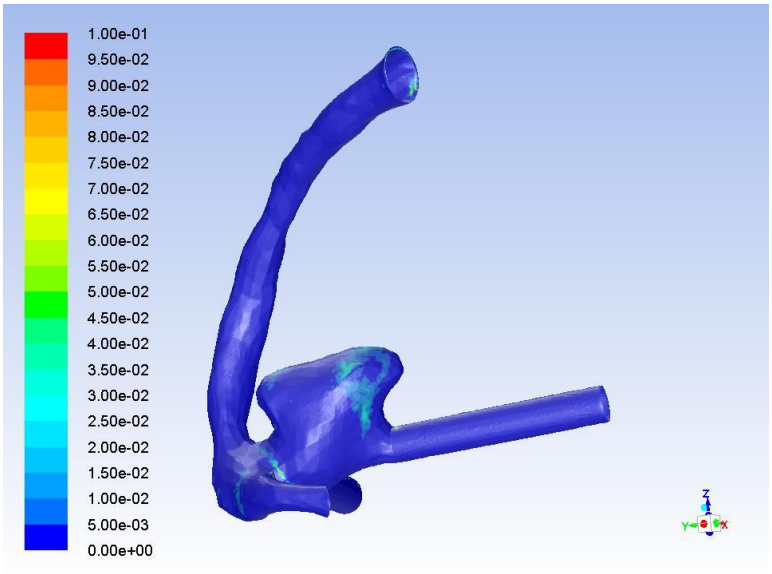

MRA front view

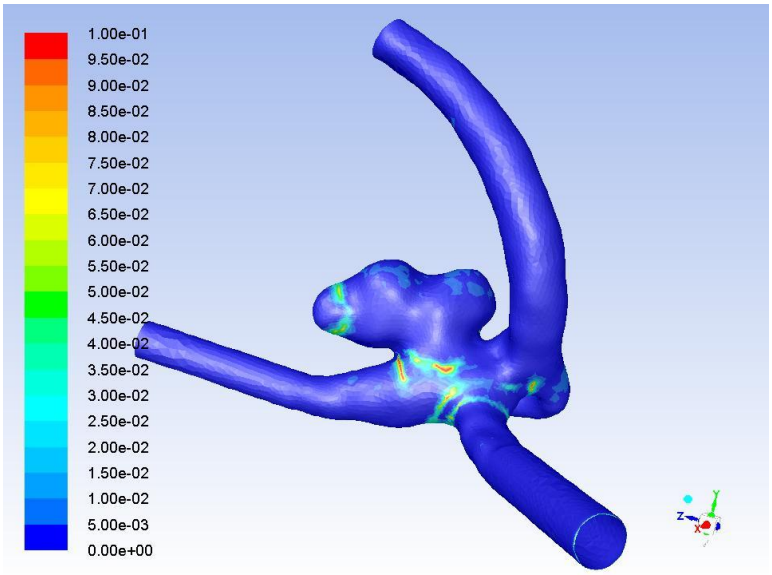

DSA rear view

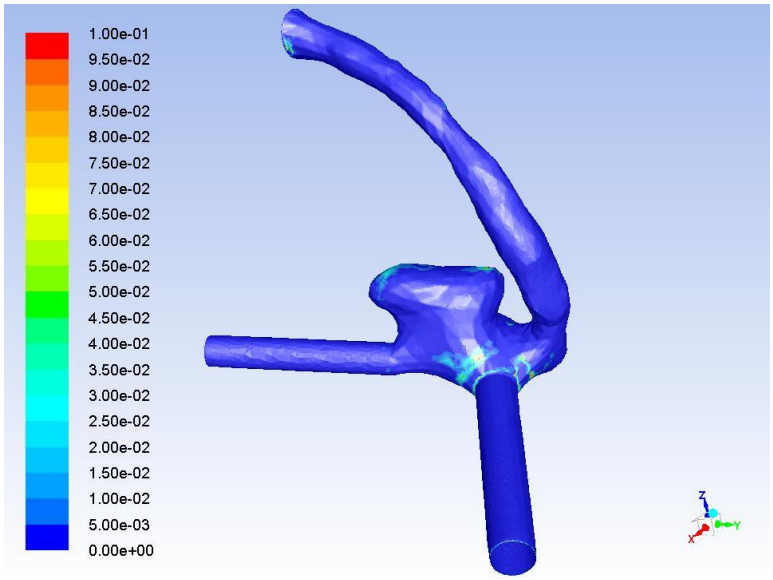

MRA rear view

6th patient results

- This is the smallest aneurysm that was modeled and simulated. The MRA raw data had to undergo important geometric improvements to end up in a shape close to the one from the DSA examination. Thus, the shape of the aneurysms has noticeable discrepancies.
- The pathlines extend at different regions in the aneurysm dome.
- The minimum and maximum regions of WSS and OSI have similarities only to a certain extent
- The maximum values of pressure are always less at the DSA simulated aneurysm, with a margin of 16 %
- The maximum values of WSS are always less at the DSA simulated aneurysm, with a margin of 5 %
- The area averaged WSS value is always less at the DSA simulated aneurysm and the margin is as big as 22%

8.2 Virtual post treatment results

The aim of this section is to examine the changes in pressure, WSS, and pathlines after two virtual treatment scenarios have taken place. One is after 50% occlusion and the other after 90% occlusion. For this purpose, the DSA examinations of the first two aneurysms where used and the fourth to find out what would happen if only the secondary bleb was occluded.

1st patient occlusions

t= 0.05 sec

	Full	Half	1/10
Pressure	-11.7 to 418 Pa	-18 to 507 Pa	-25.2 to 541 Pa
WSS	0 to 140.1 Pa	0 to 176.8 Pa	0 to 240.6 Pa
Area Aver. WSS	1.13	2.065	2.9

Pressure 0.05

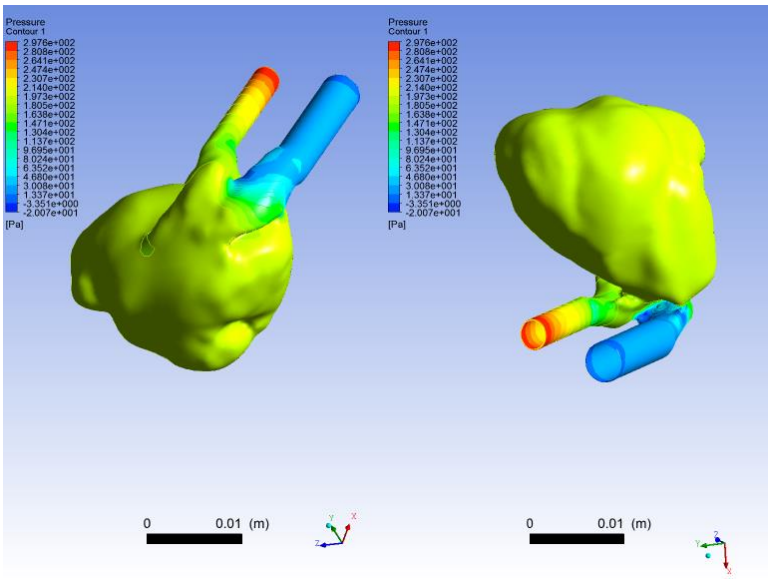

Whole

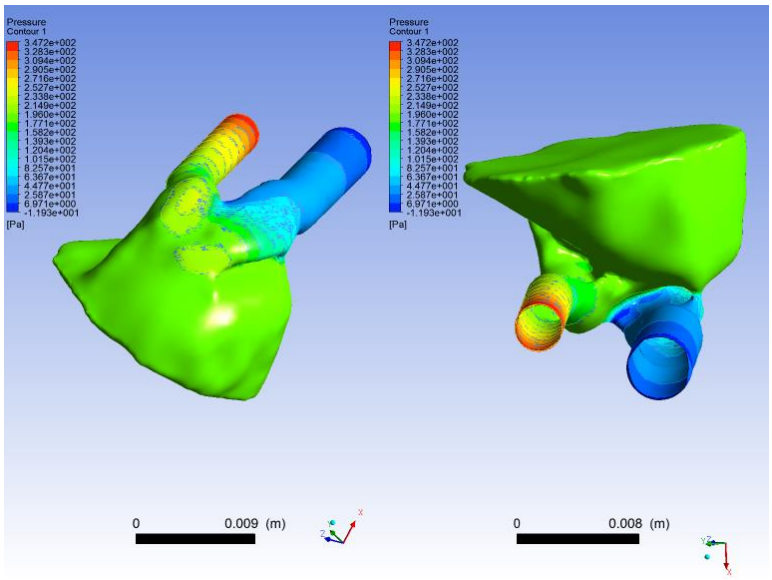

Half

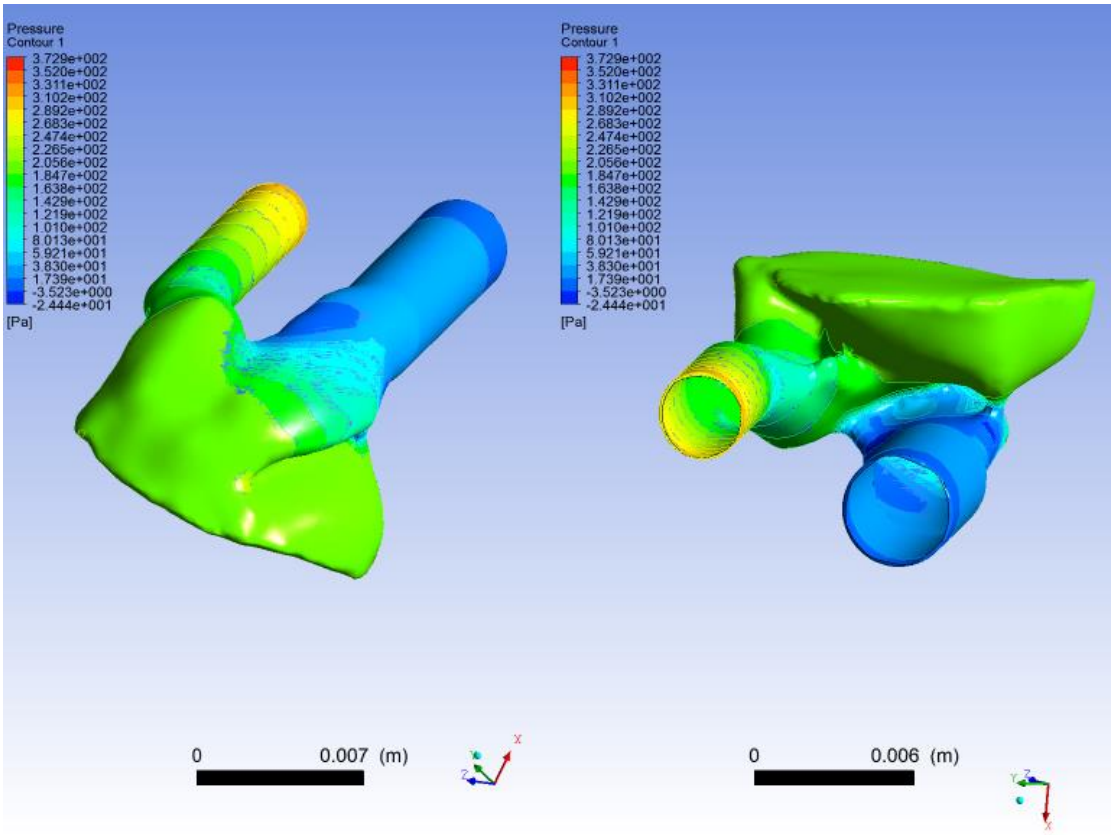

Tenth

WSS 0.05

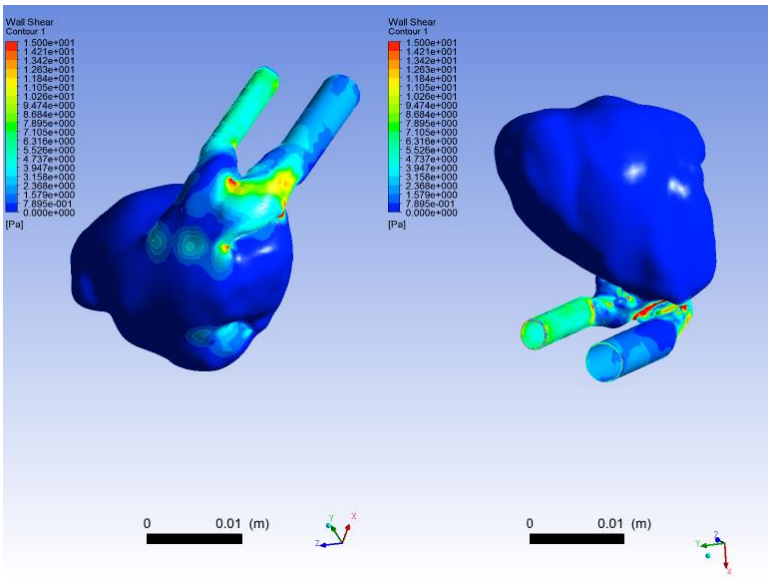

Whole

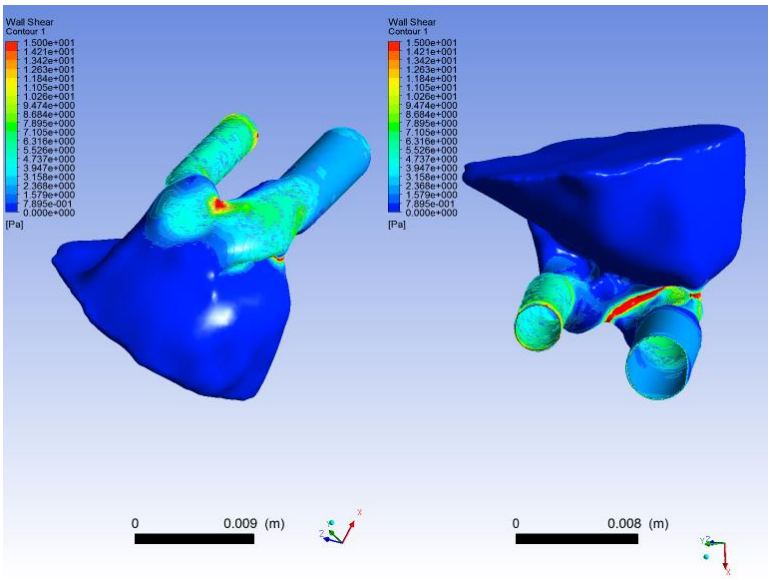

Half

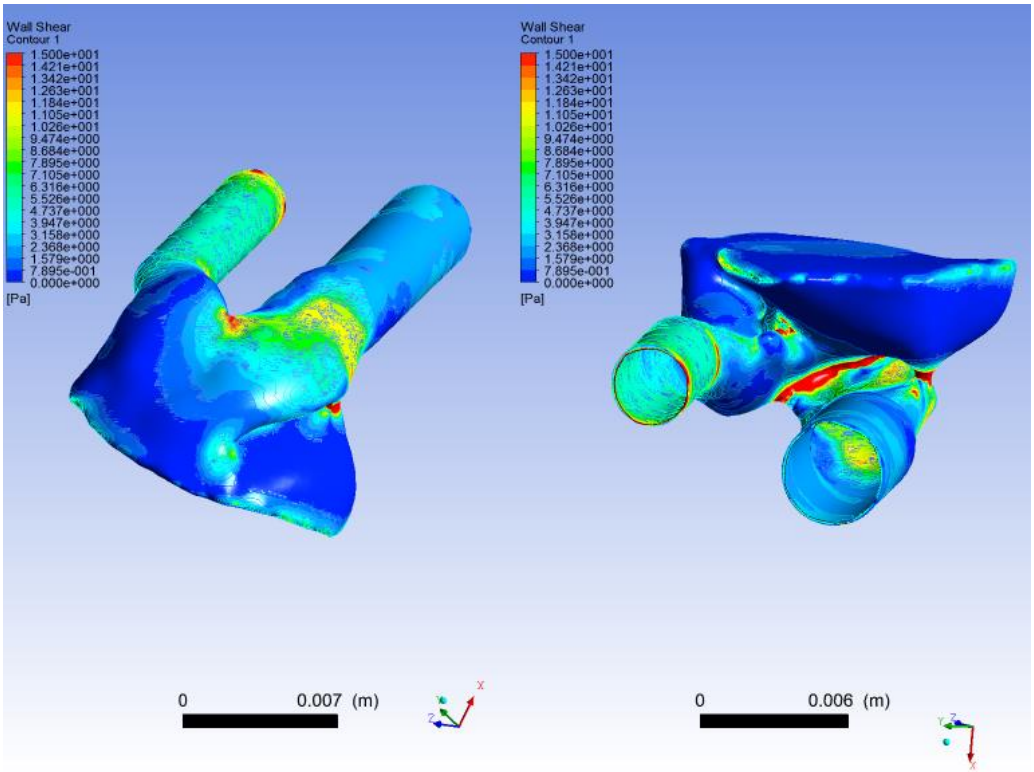

Tenth

Pathlines 0.05

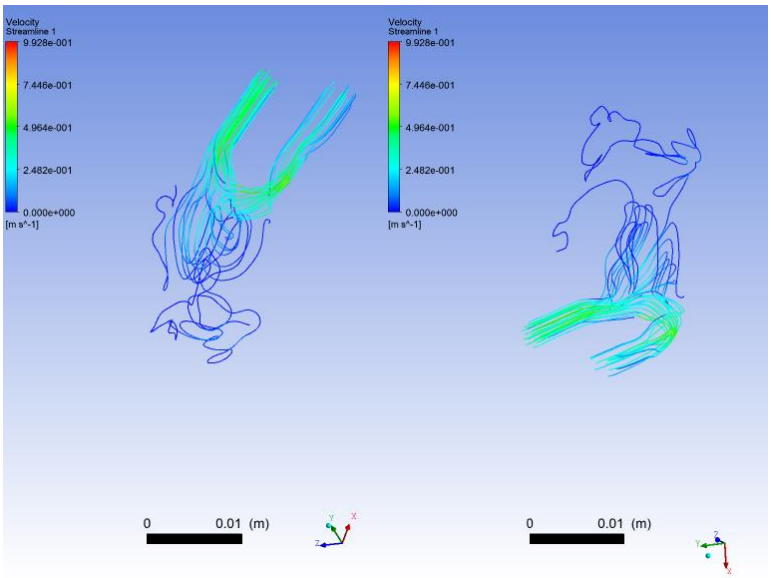

Whole

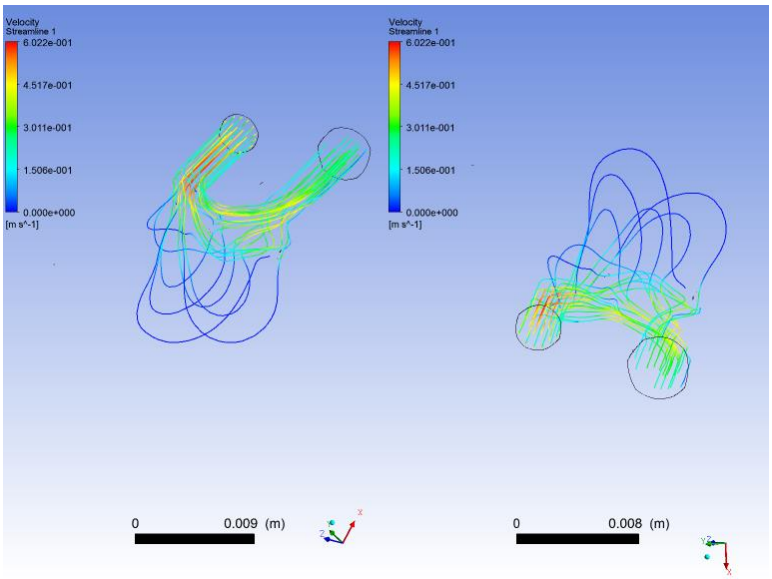

Half

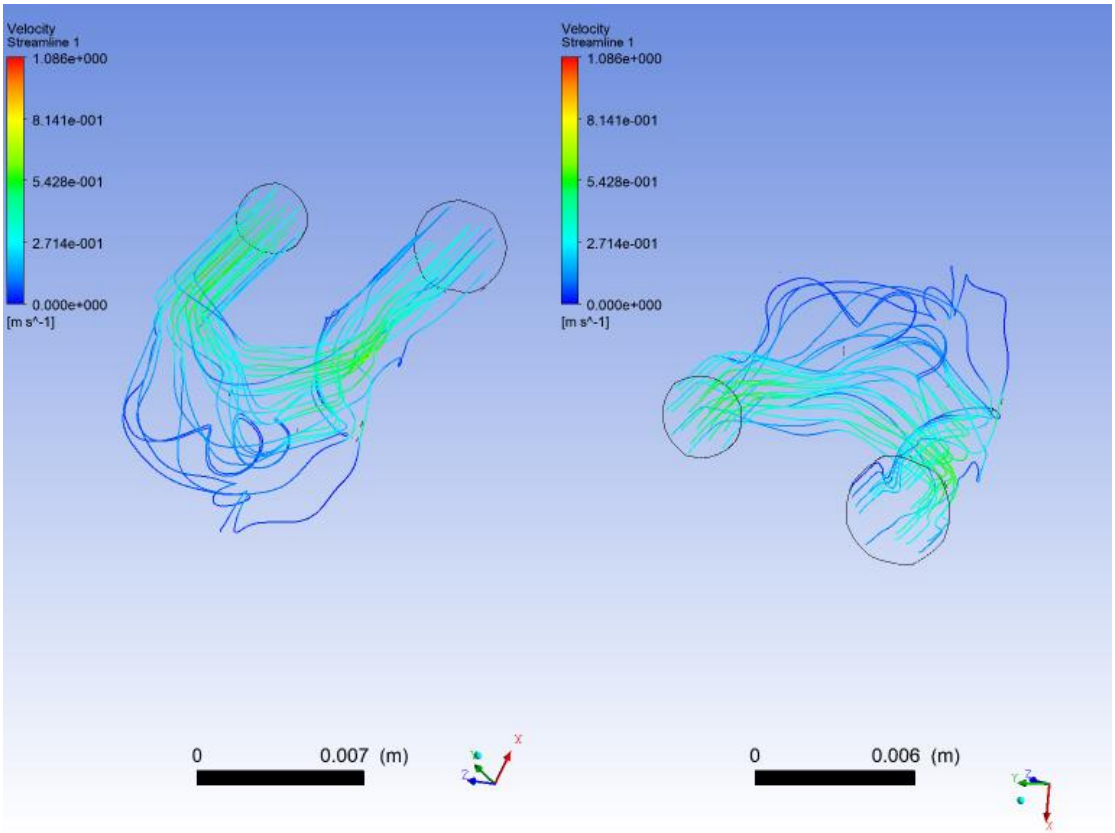

Tenth

t = 0.2 sec

	Full	Half	1/10
Pressure	-154 to 866 Pa	-129 to 911 Pa	-211 to 1200 Pa
WSS	0 to 272.9 Pa	0 to 315.5 Pa	0 to 446.9 Pa
Area Aver. WSS	3.2	4.72	7.56

Pressure 0.2

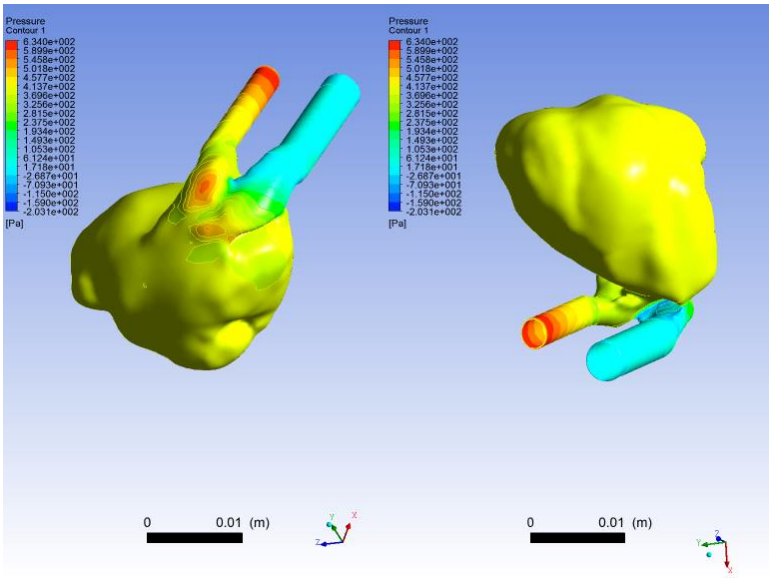

Whole

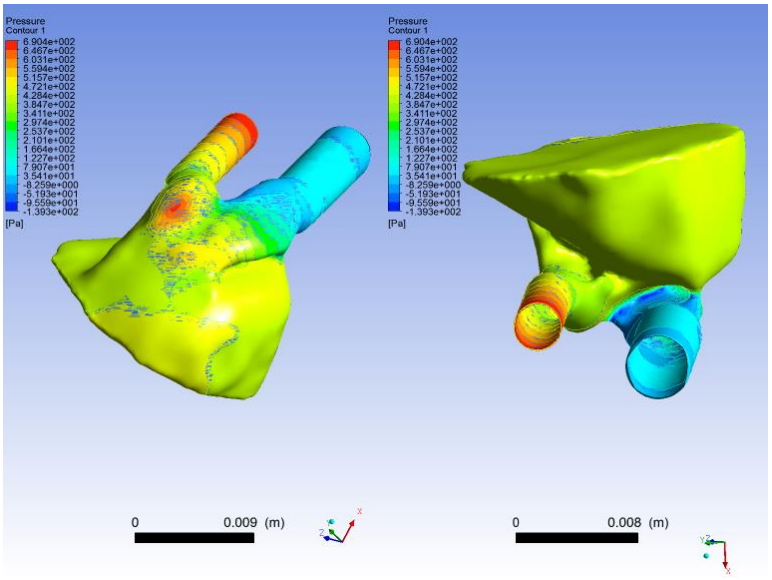

Half

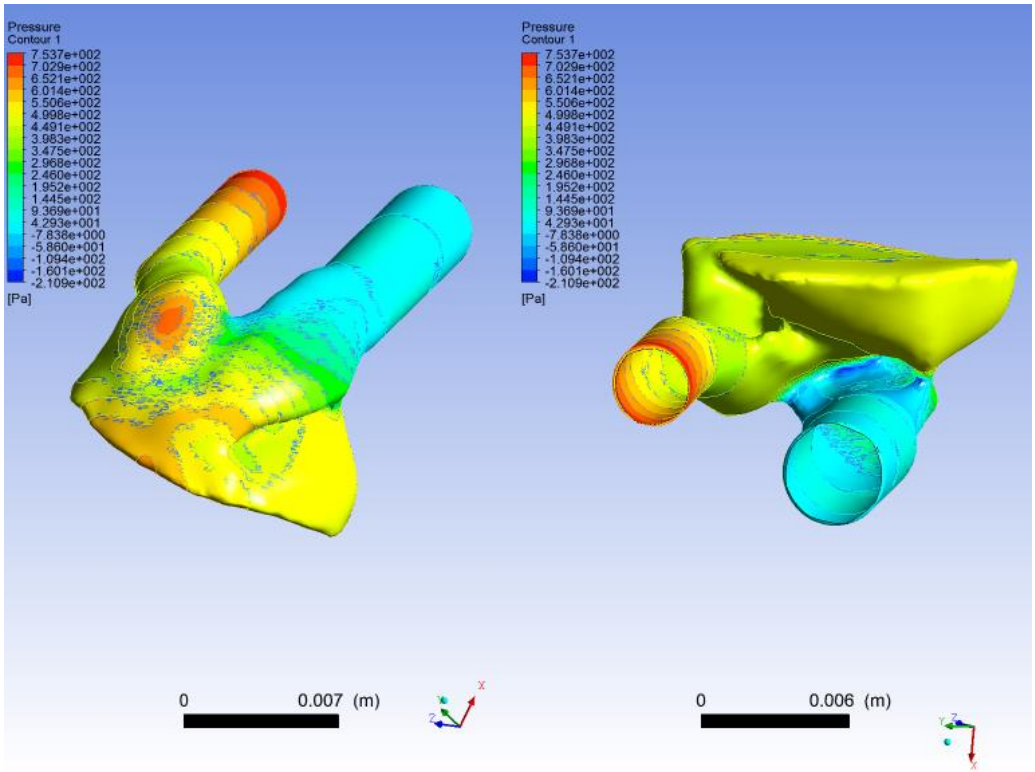

Tenth

WSS 0.2

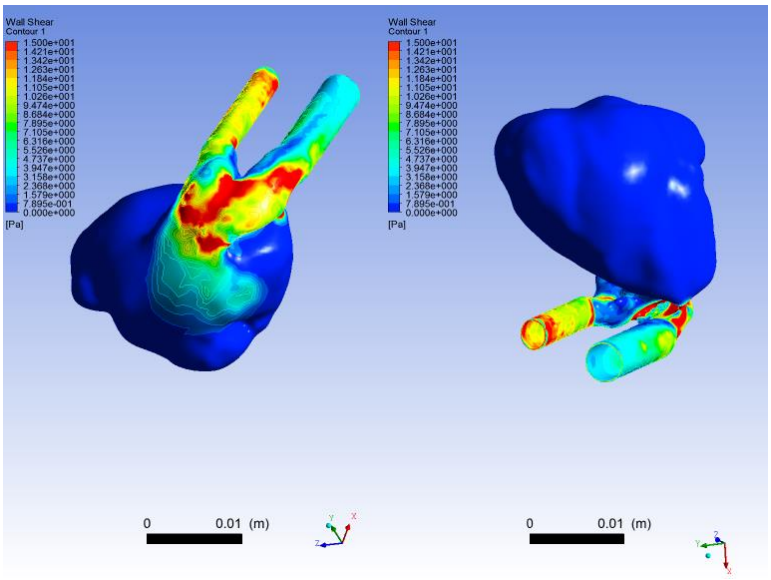

Whole

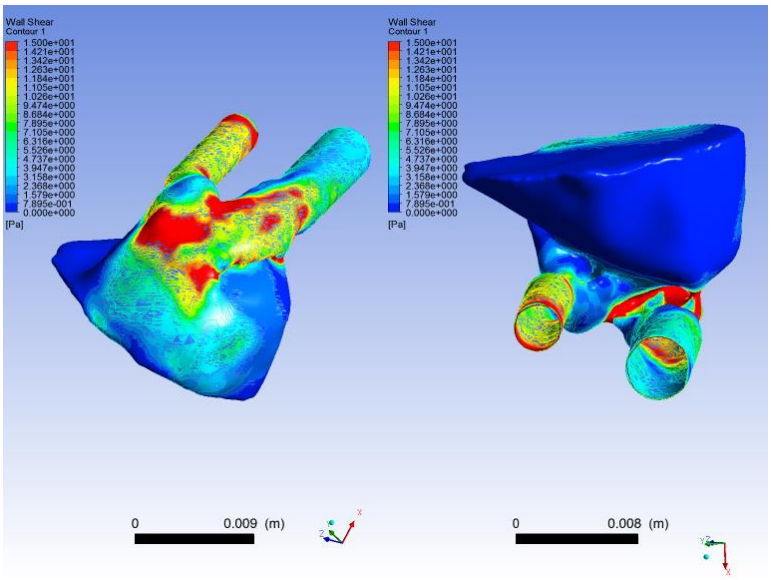

Half

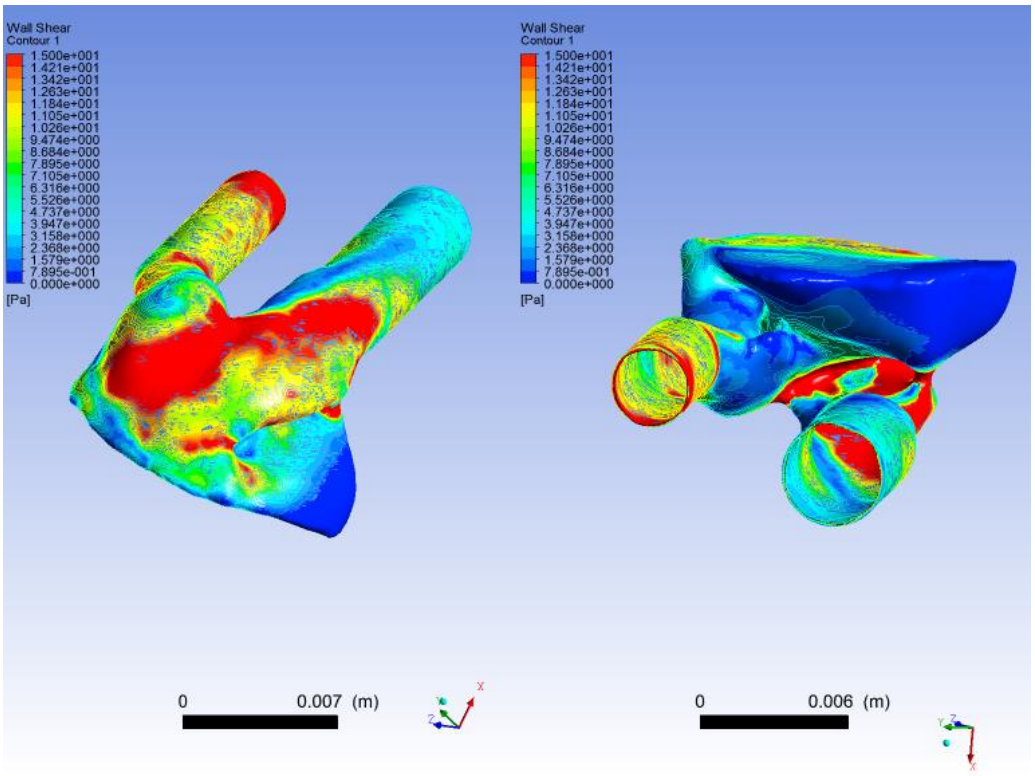

Tenth

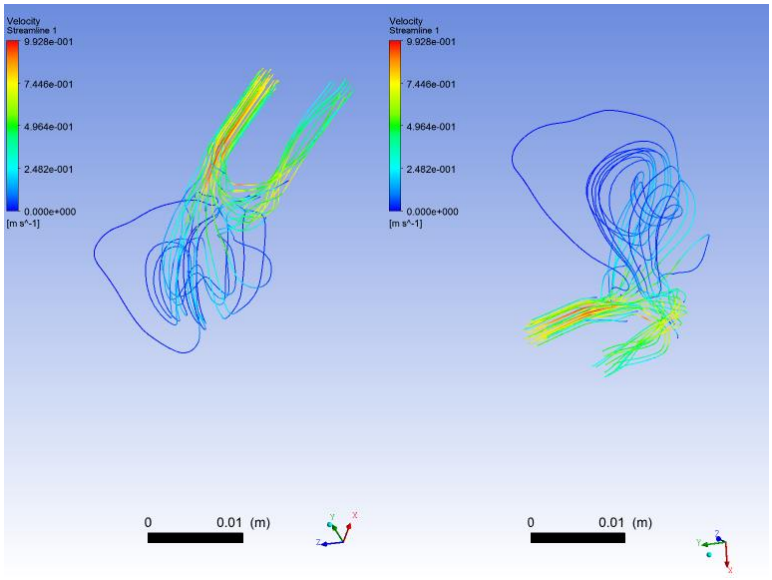

Whole

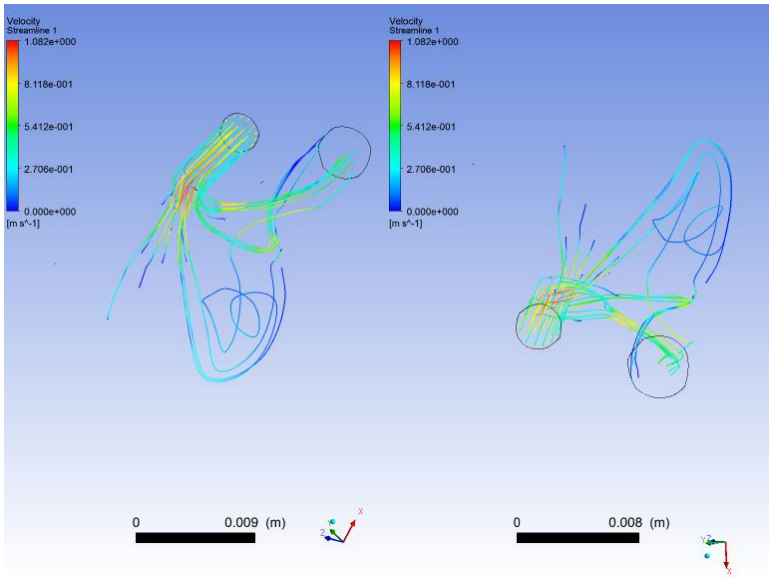

Half

Pathlines 0.2

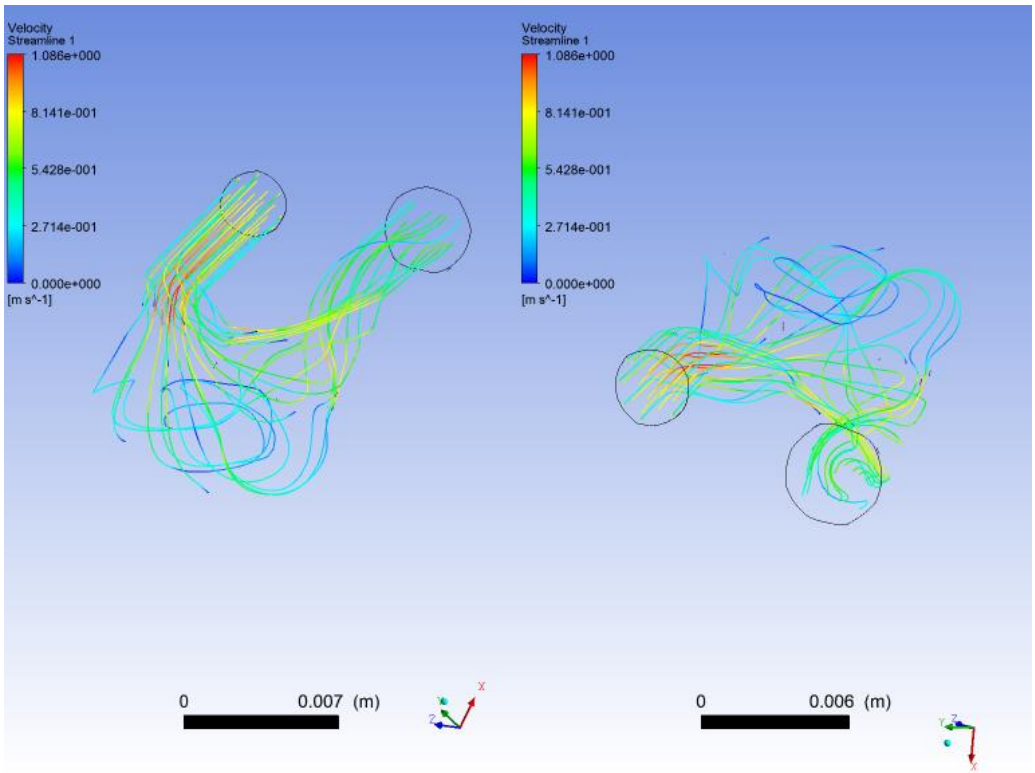

Tenth

t = 0.4 sec

	Full	Half	1/10
Pressure	-97 to 594 Pa	-51 to 664 Pa	-98 to 797 Pa
WSS	0 to 272.9 Pa	0 to 229 Pa	0 to 319.6 Pa
Area Aver. WSS	2.26	3.80	5.71

Pressure 0.4

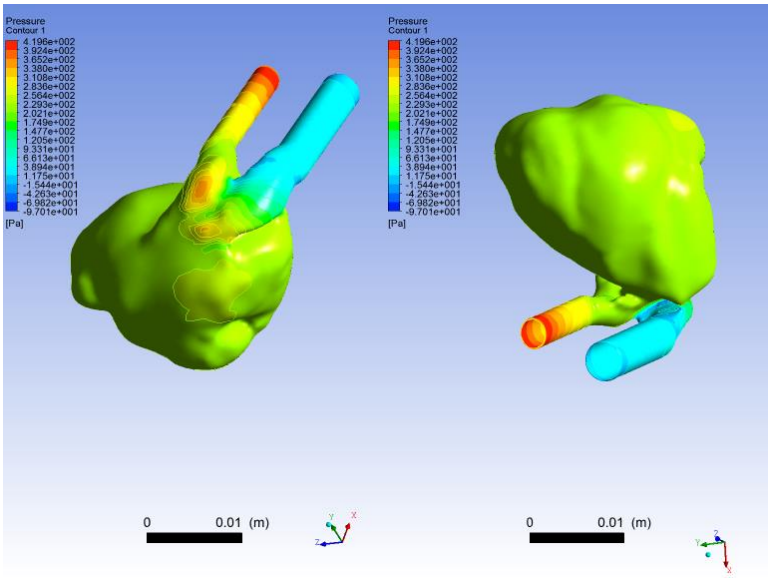

Whole

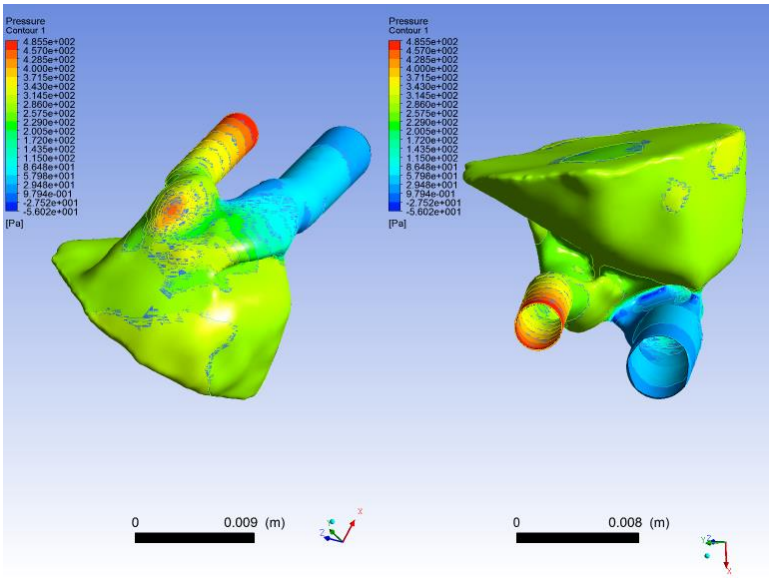

Half

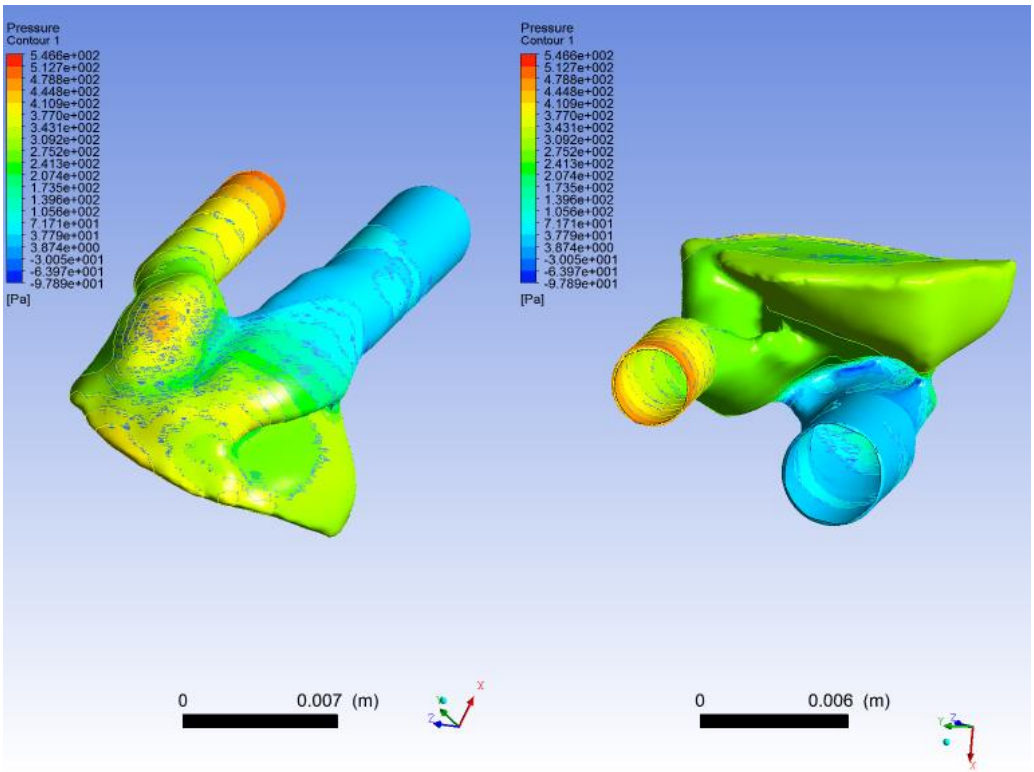

Tenth

WSS 0.4

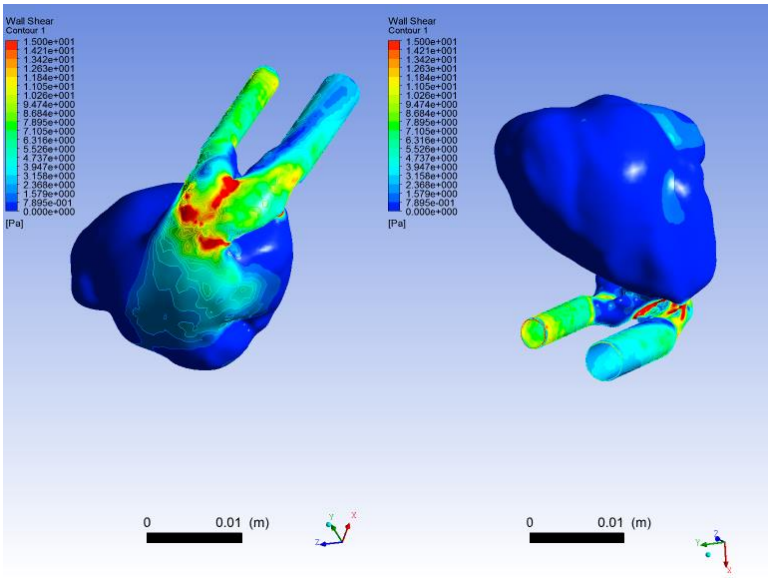

Whole

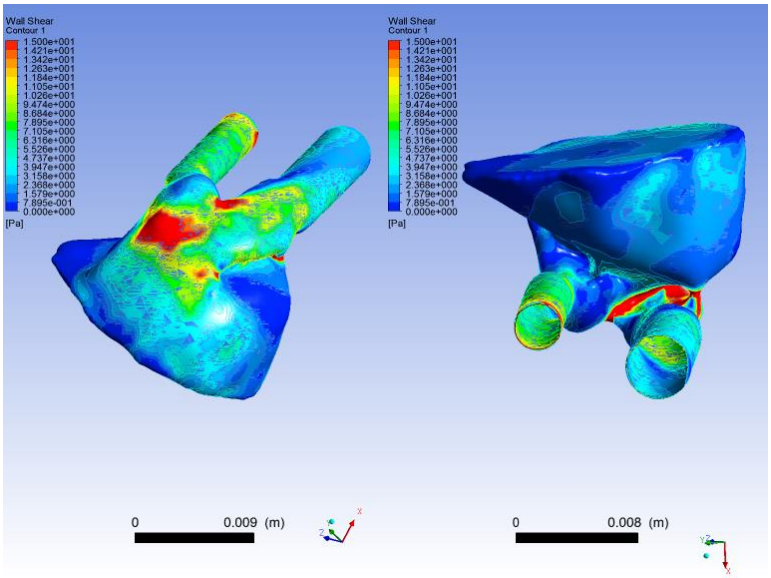

Half

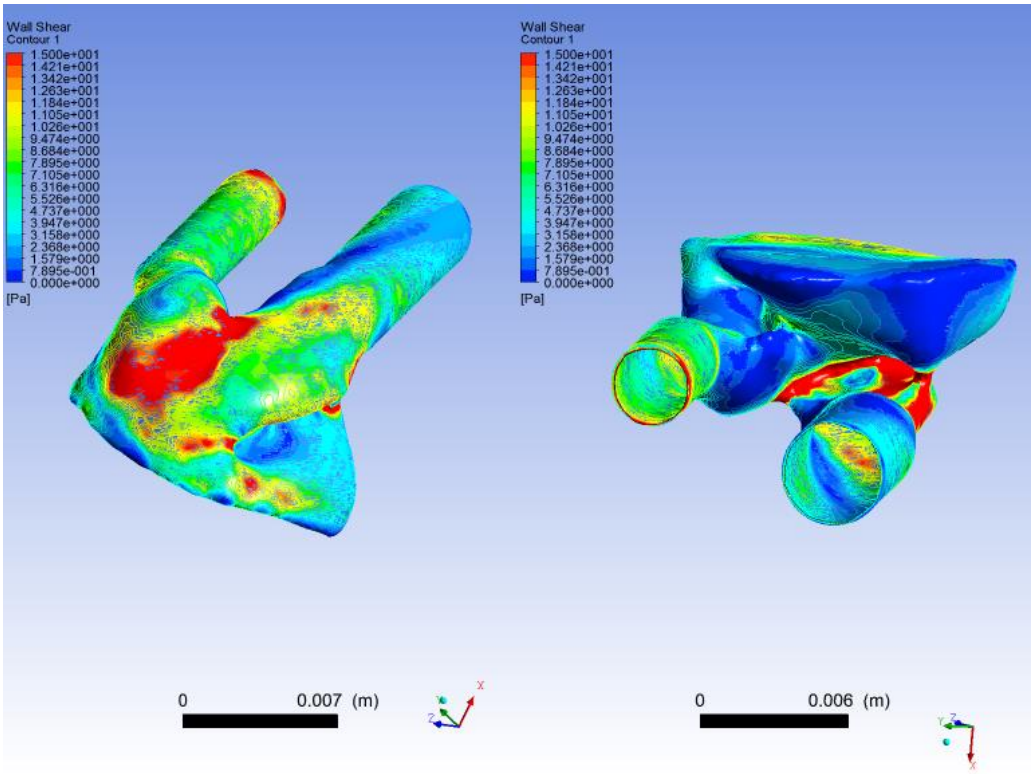

Tenth

Pathlines 0.4

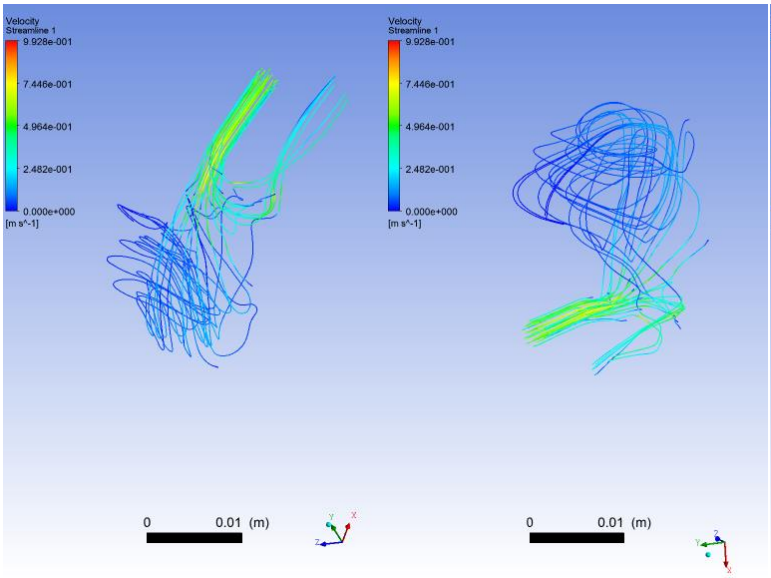

Whole

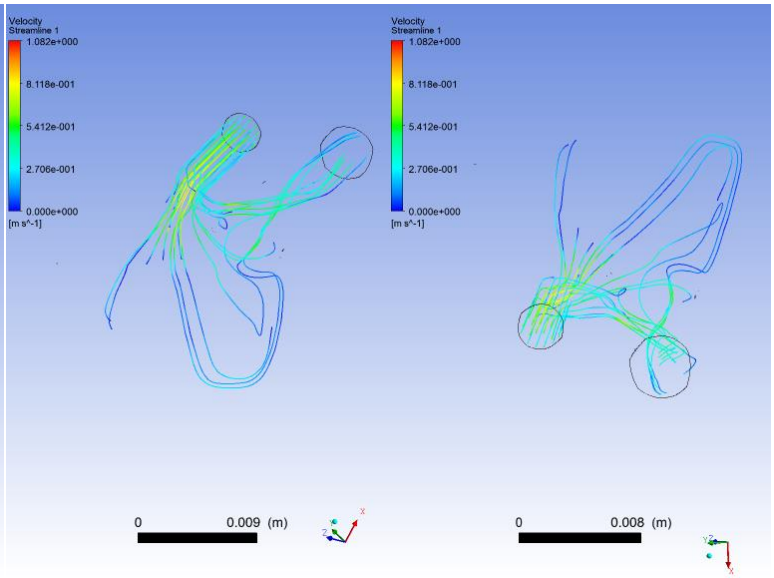

Half

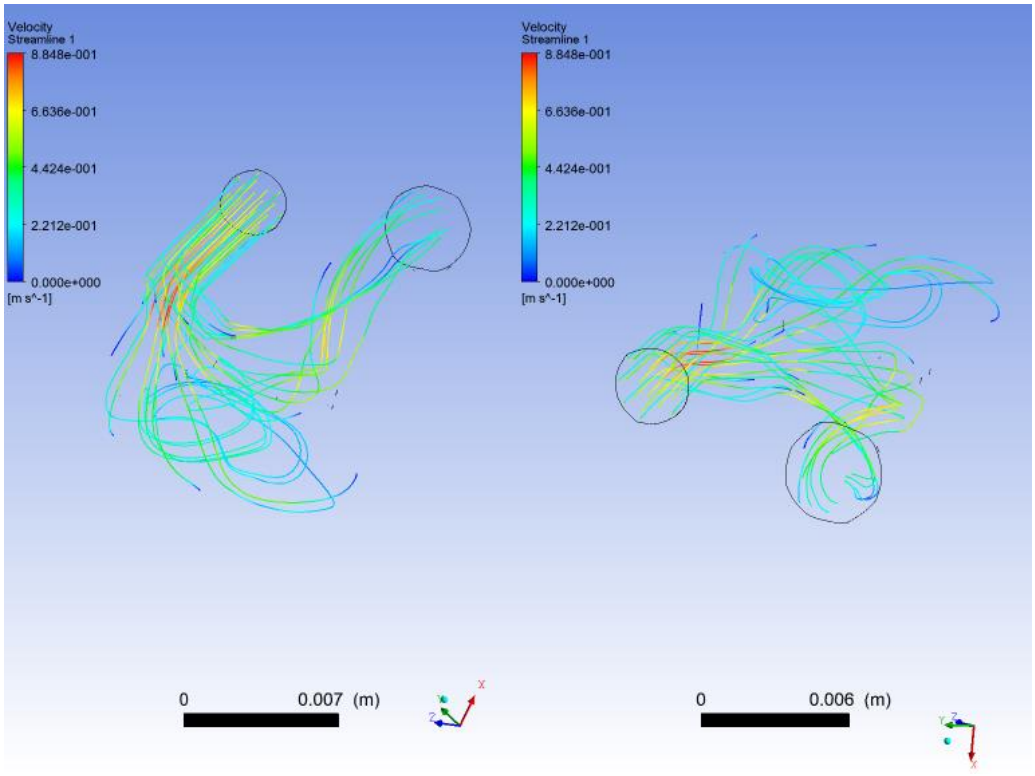

Tenth

t = 0.6 sec

	Full	Half	1/10
Pressure	-74 to 415 Pa	-56 to 472 Pa	-59 to 572 Pa
WSS	0 to 157.2 Pa	0 to 190 Pa	0 to 267 Pa
Area Aver. WSS	1.6	2.74	3.91

Pressure 0.6

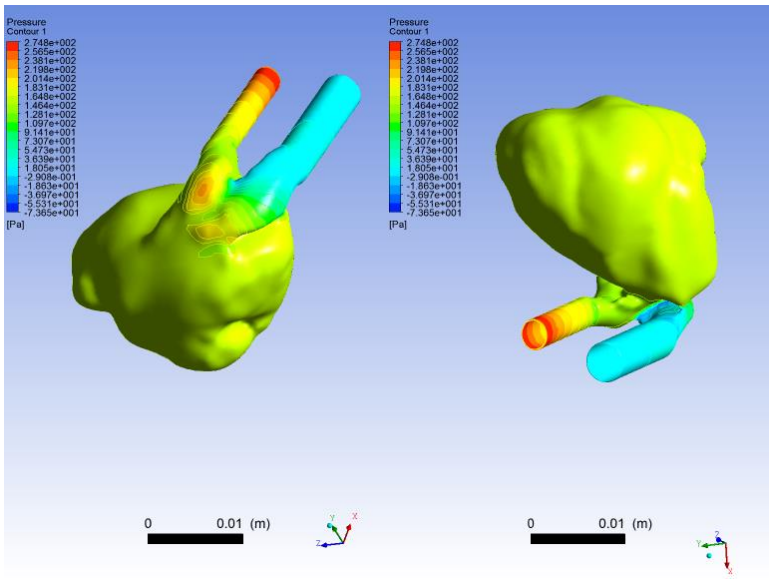

Whole

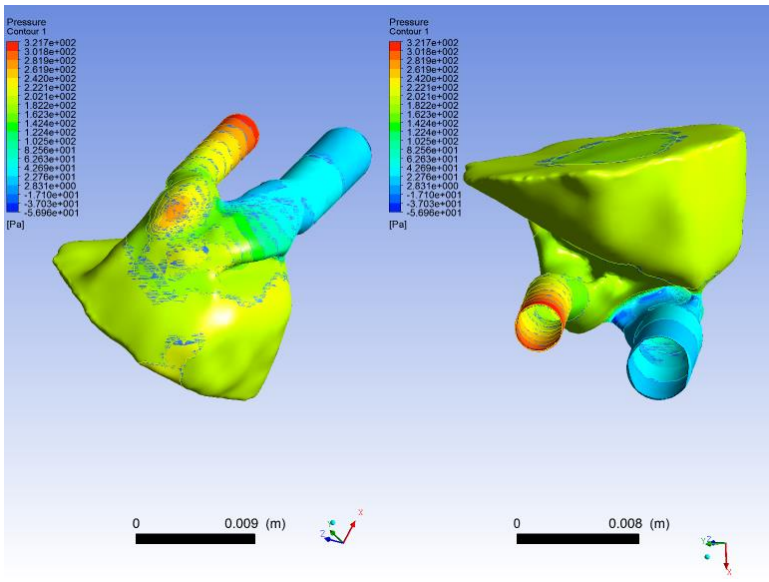

Half

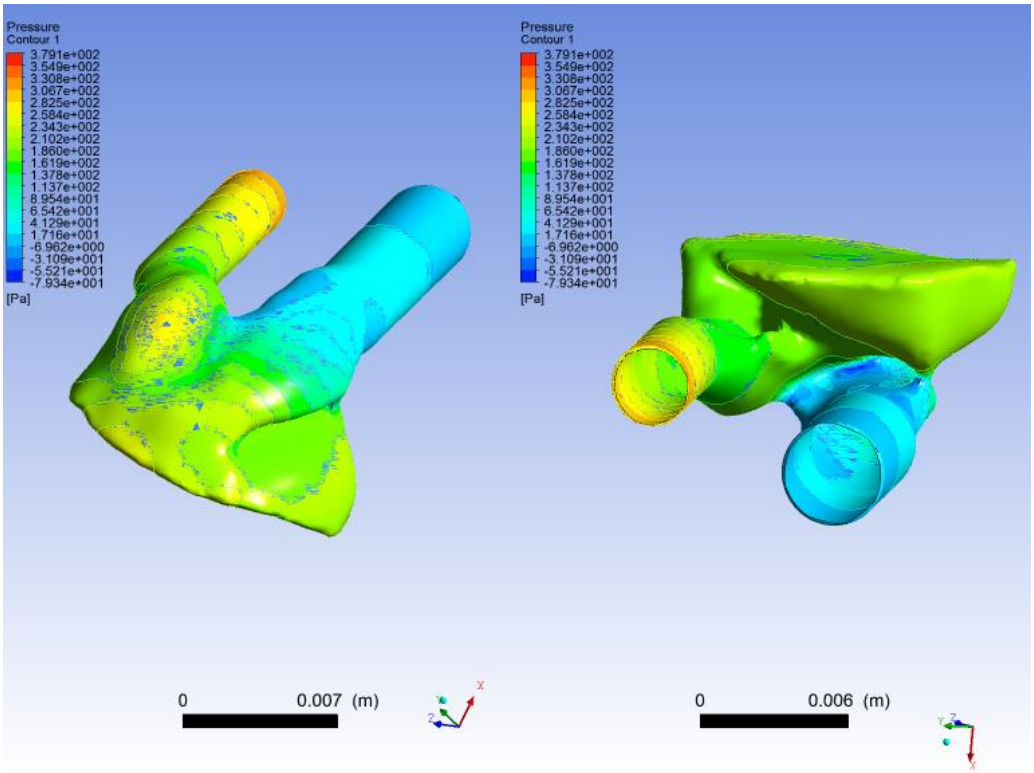

Tenth

WSS 0.6

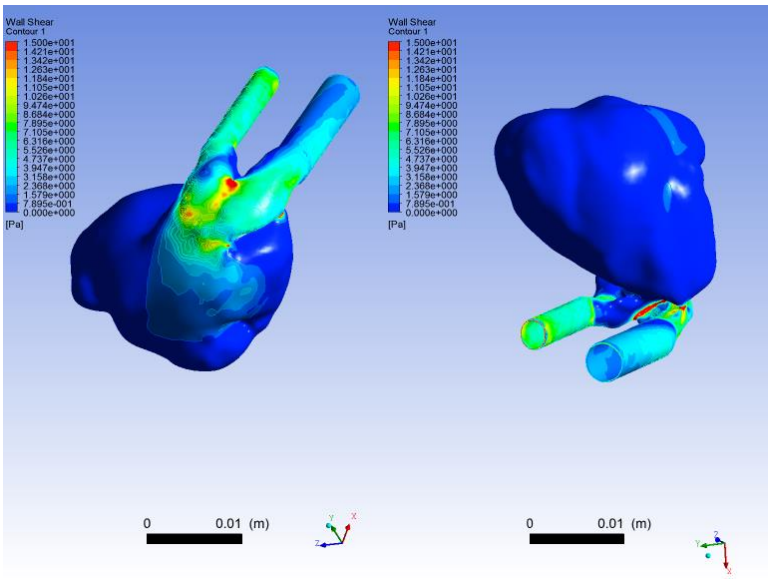

Whole

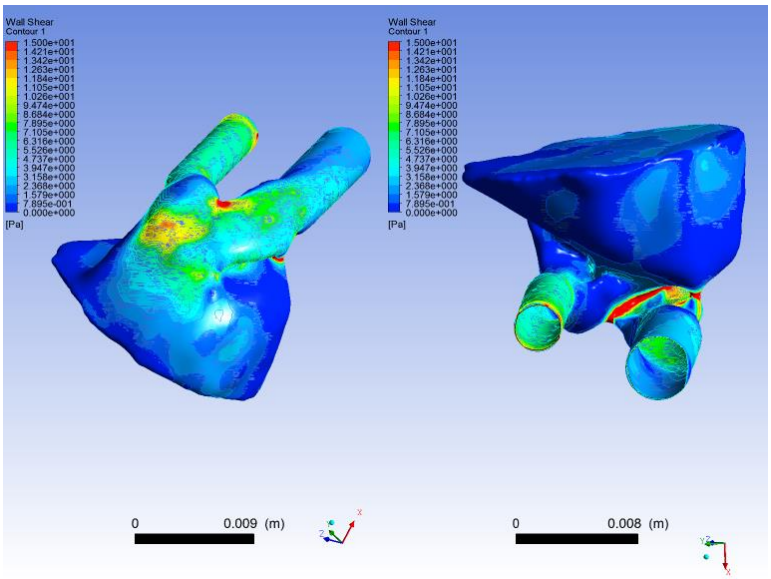

Half

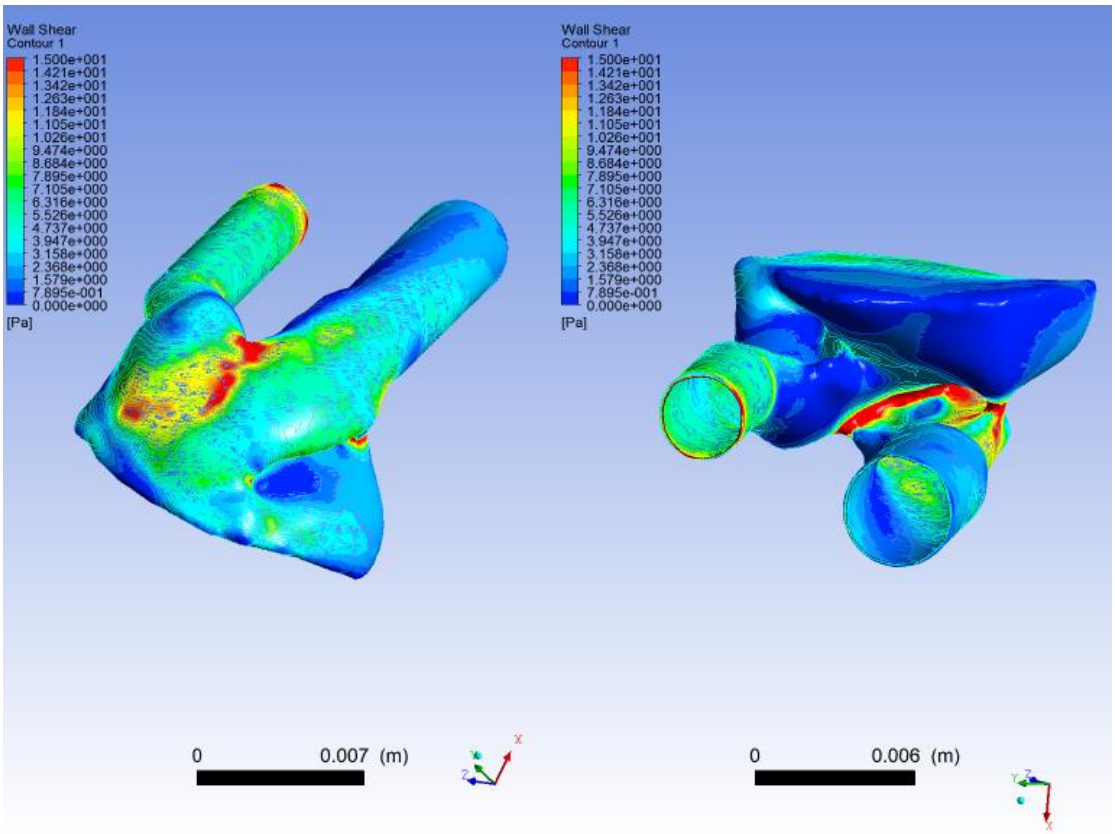
Wall Shear
Contour 1
1.500e+001
1.421e+001
1.342e+001
1.263e+001
1.184e+001
1.105e+001
1.026e+001
9.474e+000
8.684e+000
7.895e+000
7.105e+000
6.316e+000
5.526e+000
4.737e+000
3.947e+000
3.158e+000
2.368e+000
1.579e+000
7.895e-001
0.000e+000
[Pa]
0
0.007 (m)
Wall Shear
Contour 1
1.500e+001
1.421e+001
1.342e+001
1.263e+001
1.184e+001
1.105e+001
1.026e+001
9.474e+000
8.684e+000
7.895e+000
7.105e+000
6.316e+000
5.526e+000
4.737e+000
3.947e+000
3.158e+000
2.368e+000
1.579e+000
7.895e-001
0.000e+000
[Pa]
0
0.006 (m)

Tenth

Pathlines 0.6

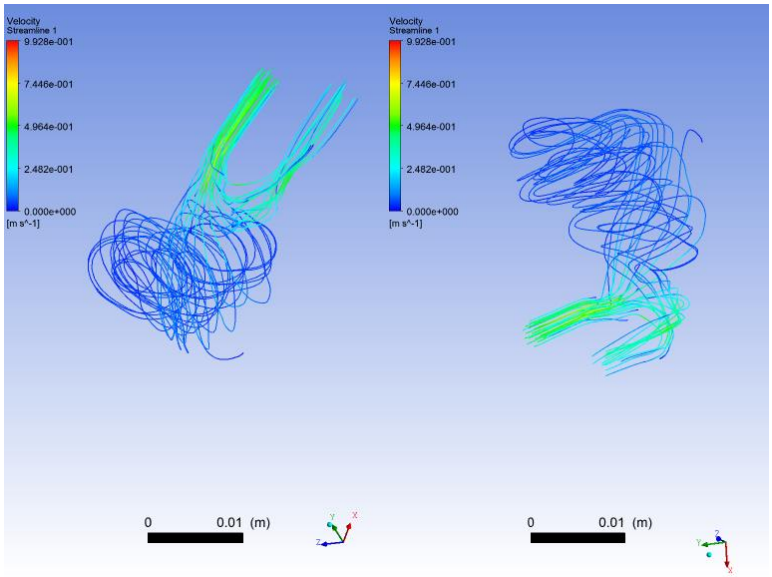

Whole

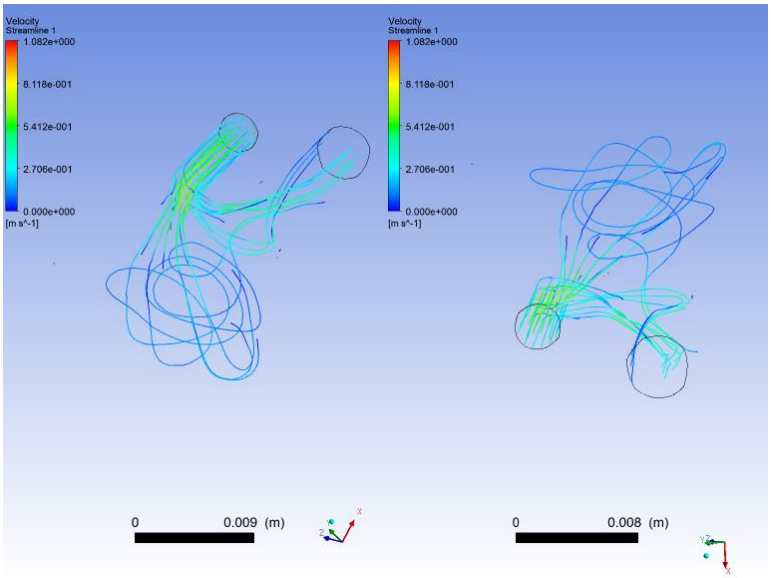

Half

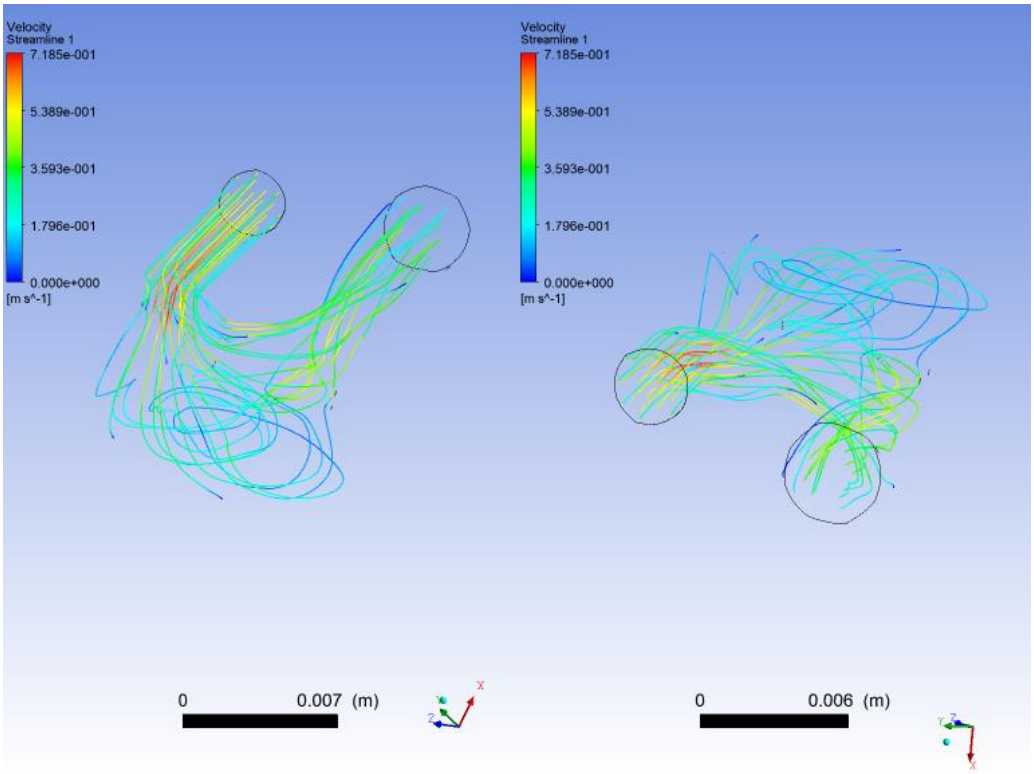

Tenth

OSI 0.8

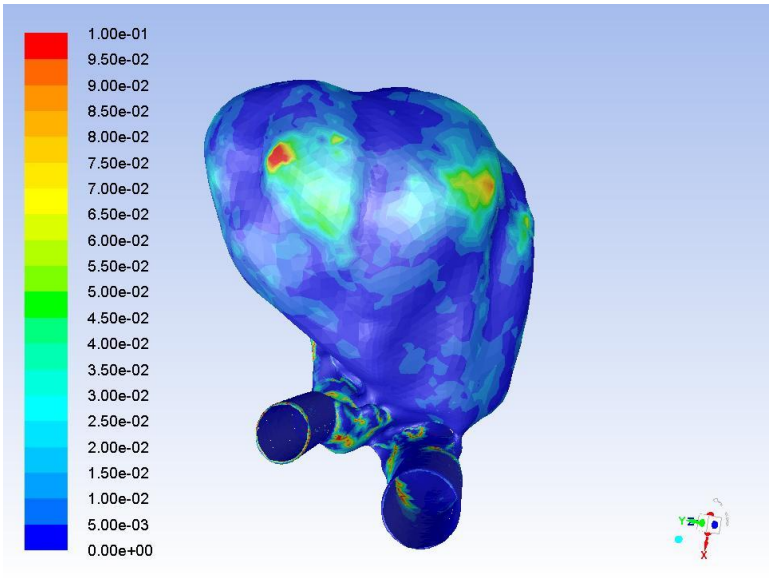

Whole front view

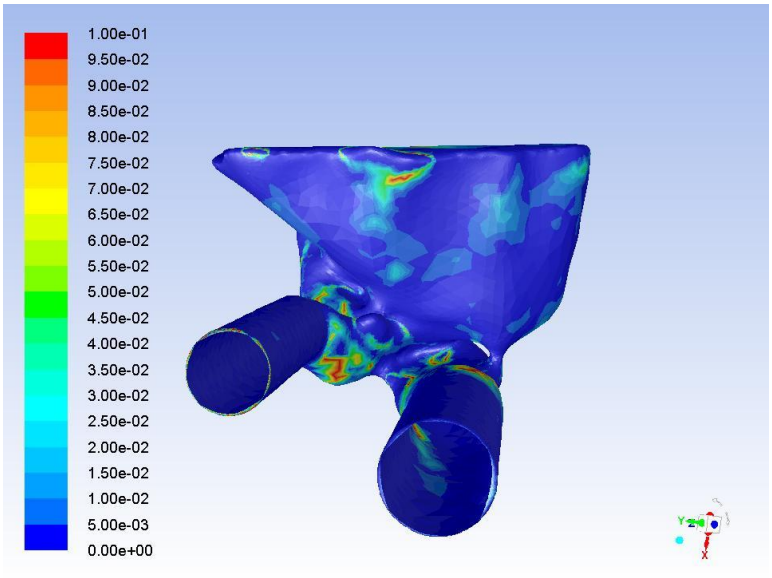

Half front view

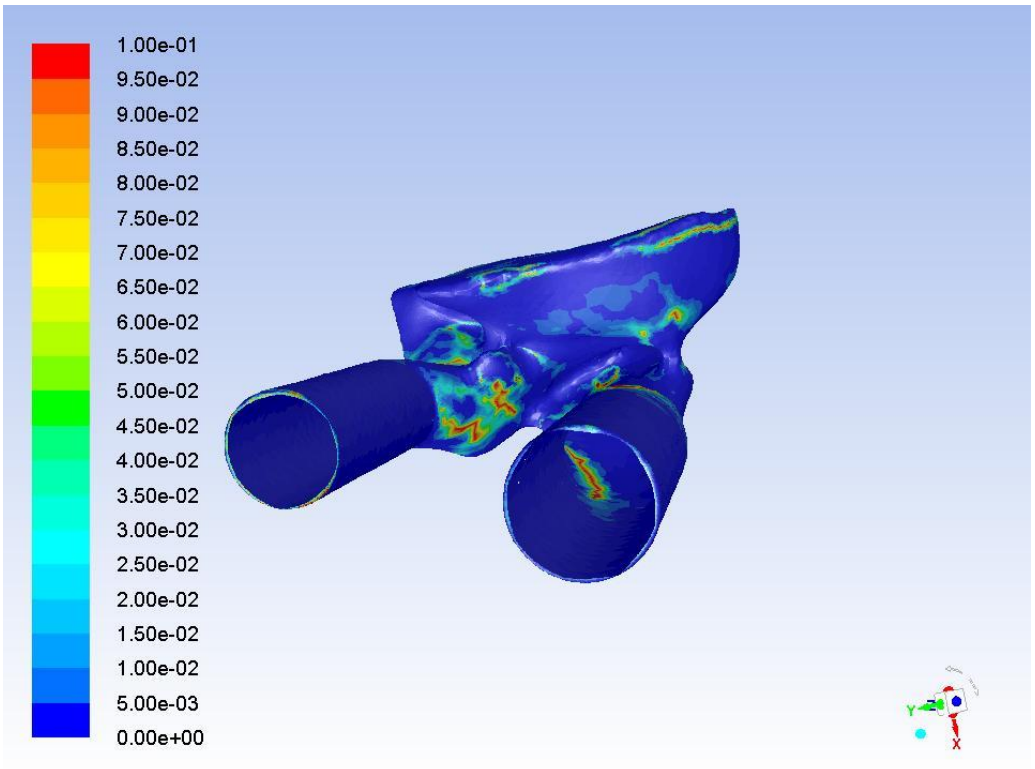

Tenth front view

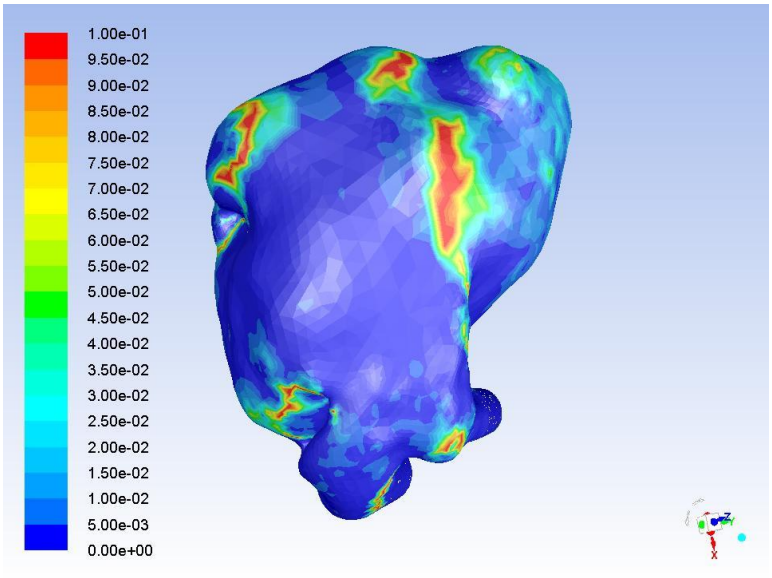

Whole rear view

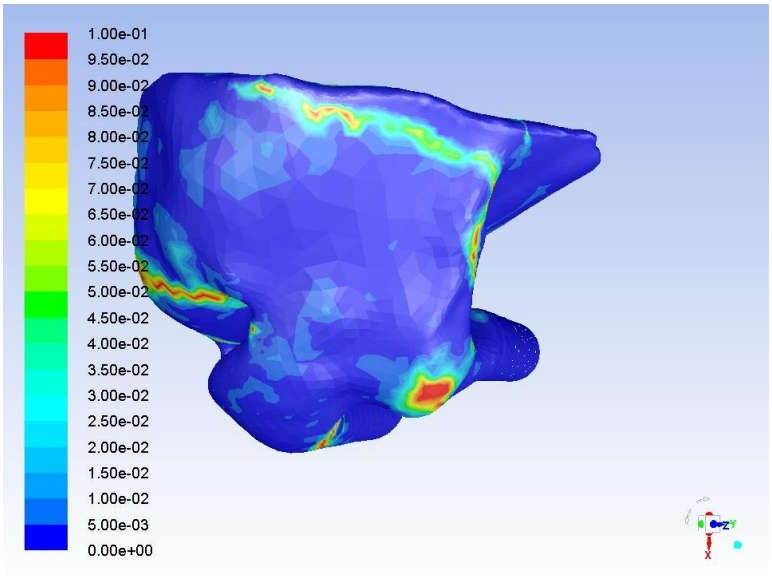

Half rear view

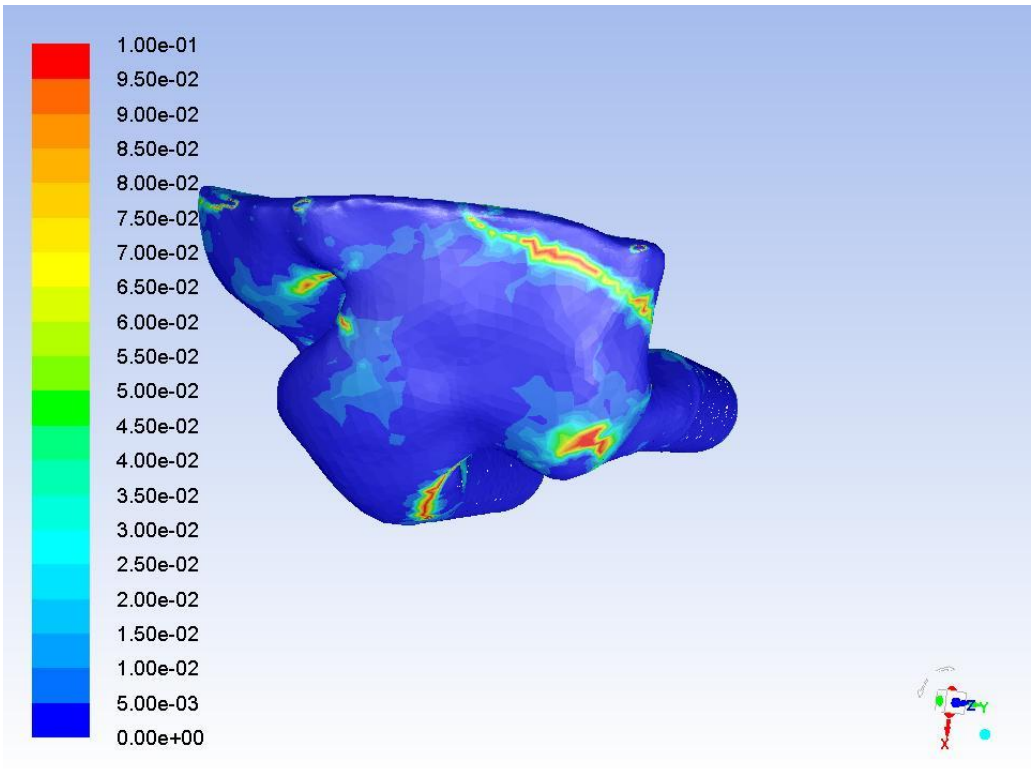

Tenth rear view

1st patient virtual occlusion results

- The values of pressure, WSS and area averaged WSS increase as occlusion level increases.
- The regions of low WSS are less after the occlusions.
- The regions of OSI do not seem to have any significant difference

2nd patient occlusions

t= 0.05 sec

	Full	Half	1/10
Pressure	-100 to 462 Pa	-73 to 462 Pa	-118 to 546 Pa
WSS	0 to 225 Pa	0 to 256 Pa	0 to 240.6 Pa
Area Aver. WSS	3.66	4.17	4.62

Pressure 0.05

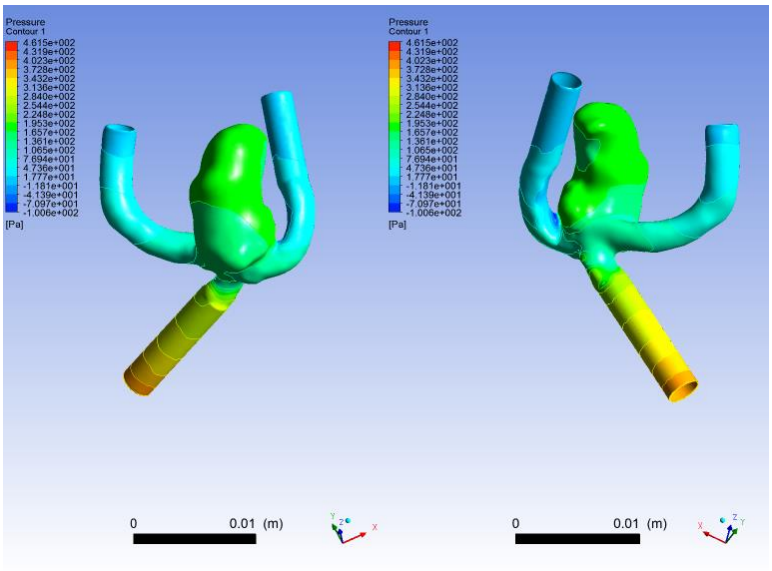

Whole

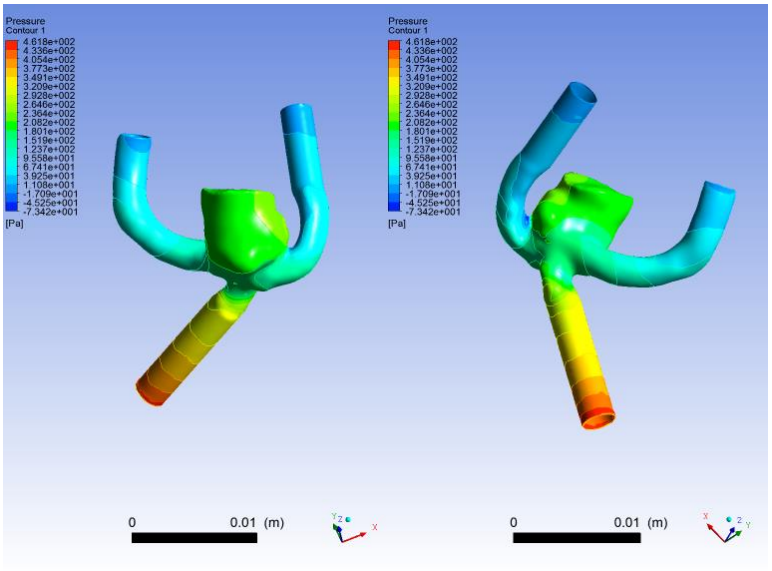

Half

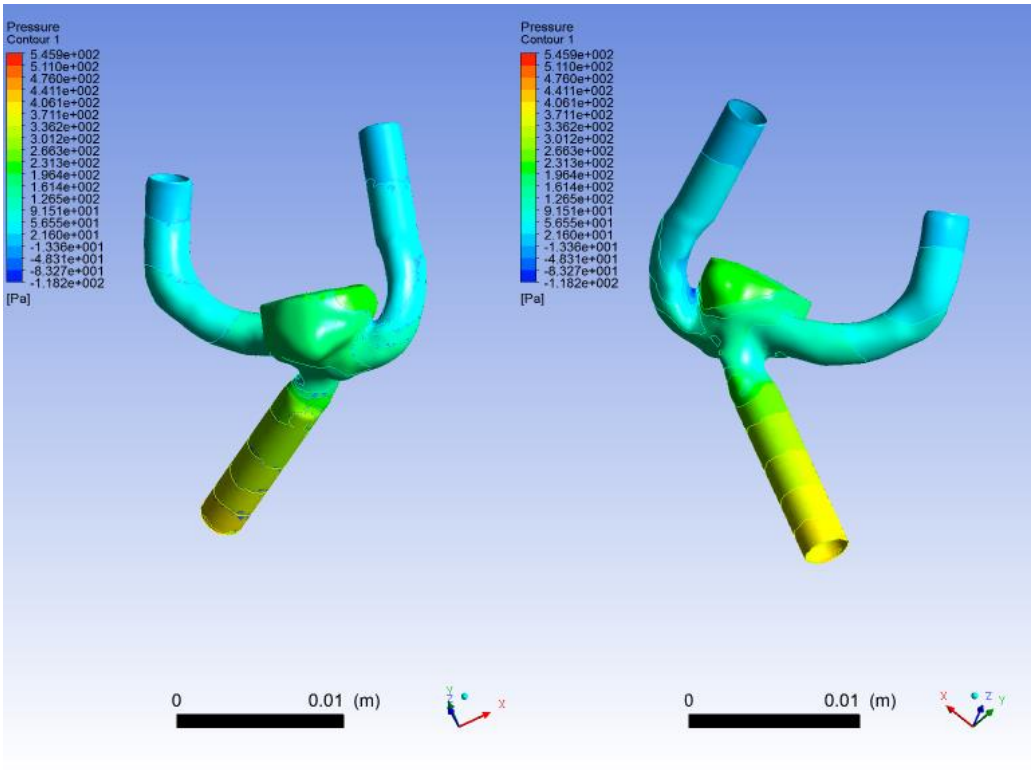

Tenth

WSS 0.05

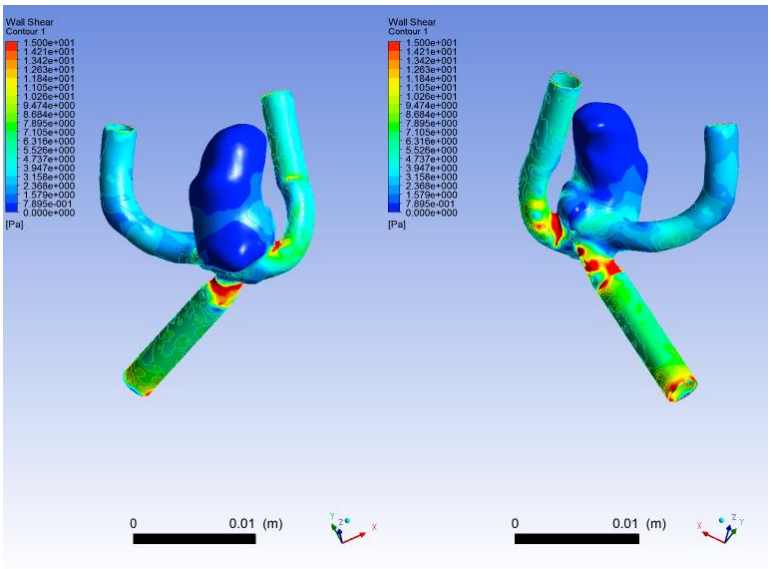

Whole

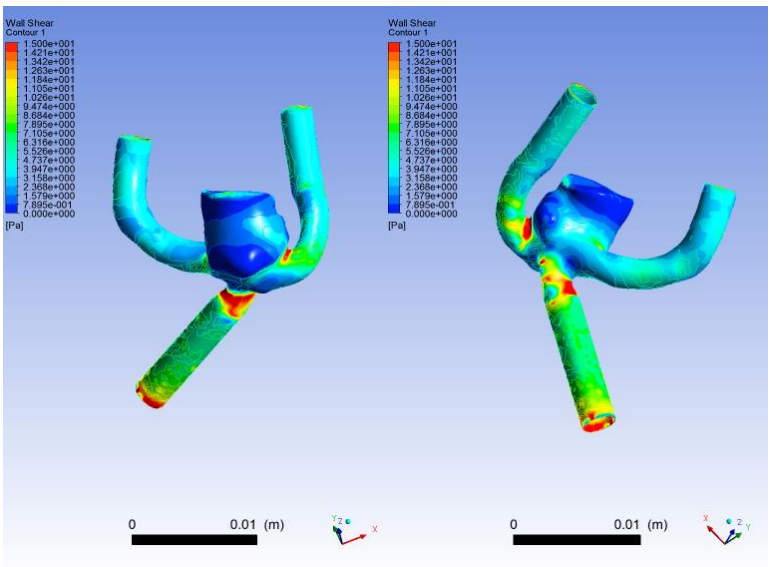

Half

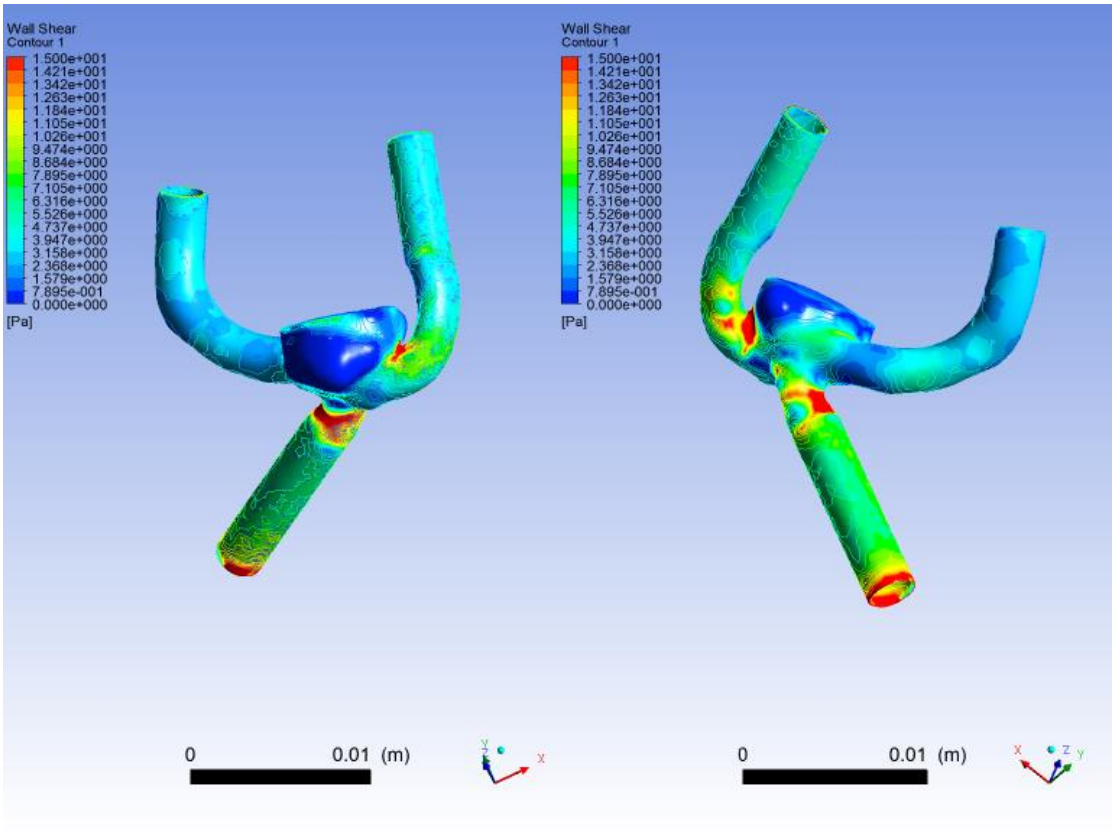

Tenth

Pathlines 0.05

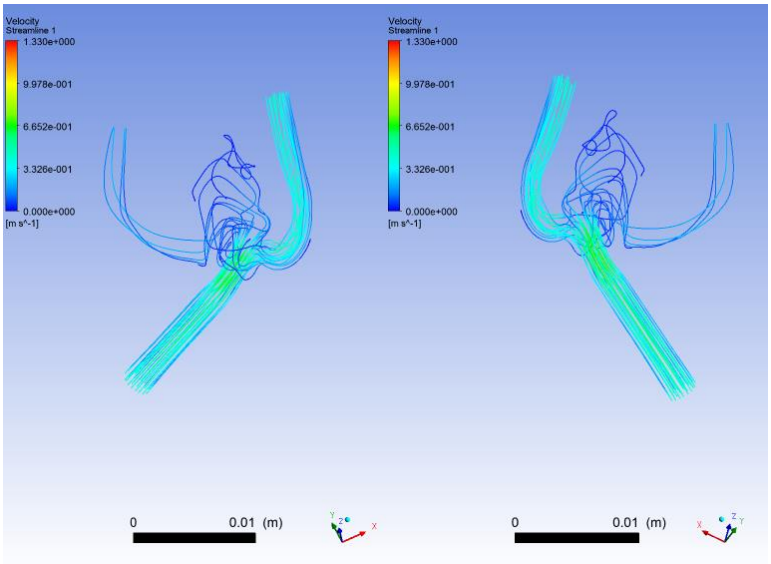

Whole

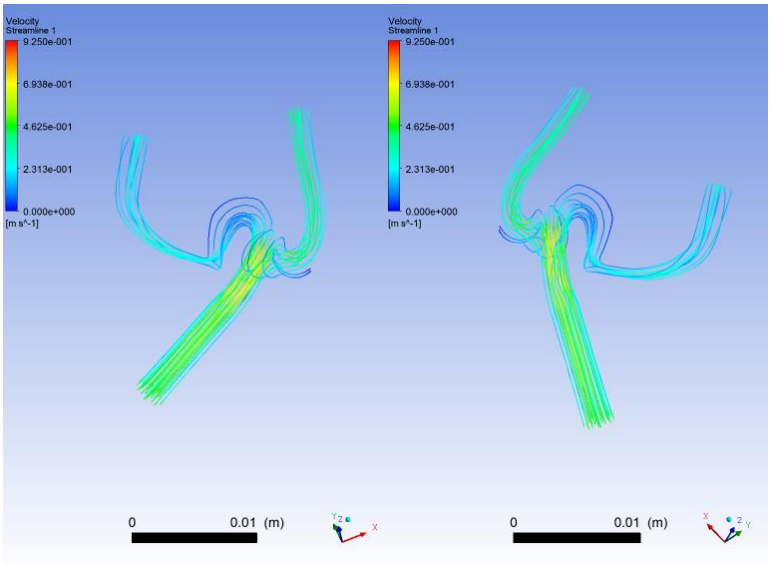

Half

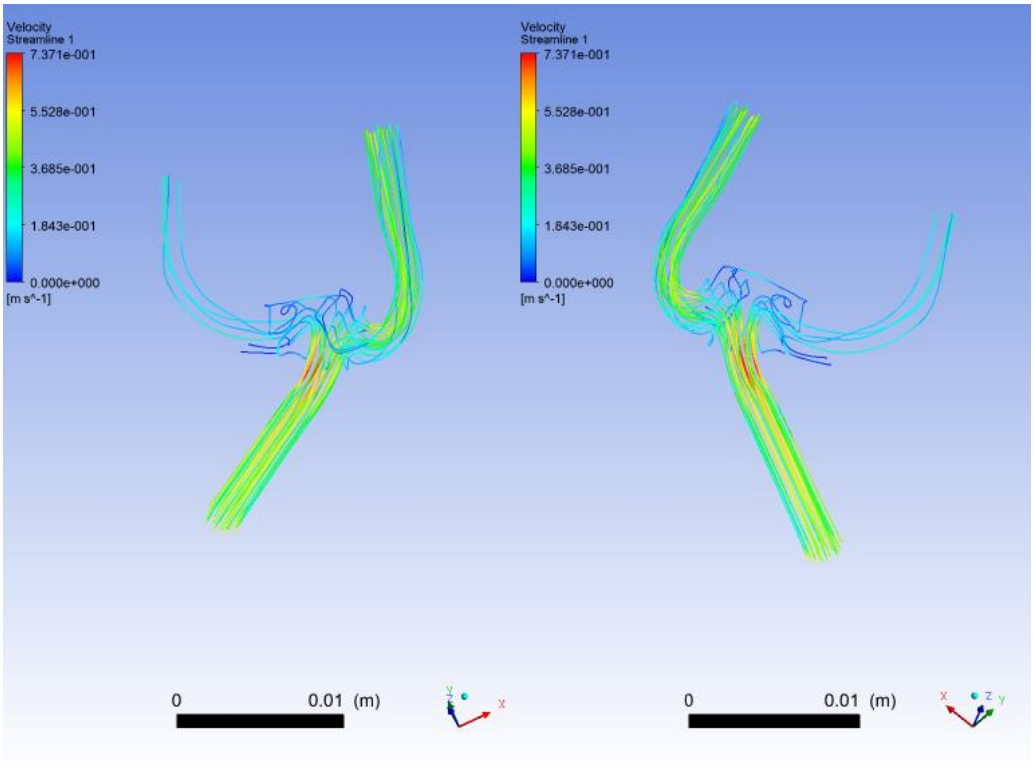

Tenth

t= 0.2 sec

	Full	Half	1/10
Pressure	-216 to 1016 Pa	-362 to 1123 Pa	-243 to 1143 Pa
WSS	0 to 420 Pa	0 to 468 Pa	0 to 486 Pa
Area Aver. WSS	10.16	11.83	12.72

Pressure 0.2

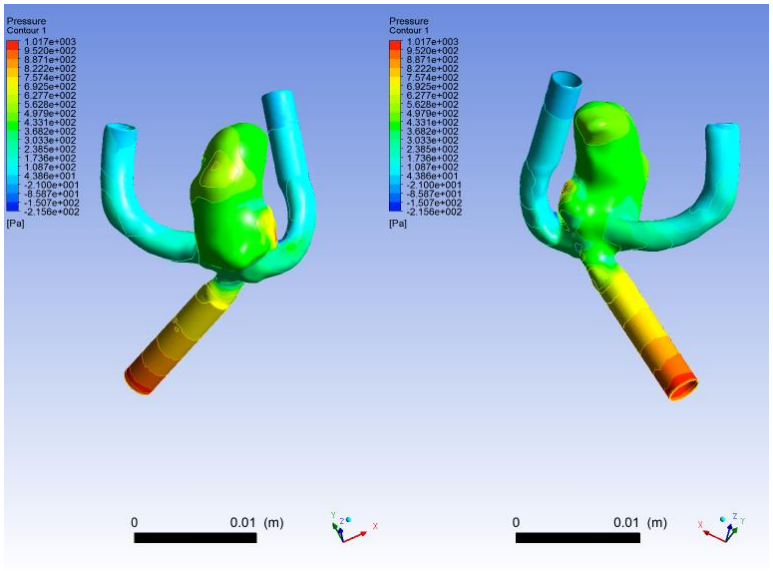

Whole

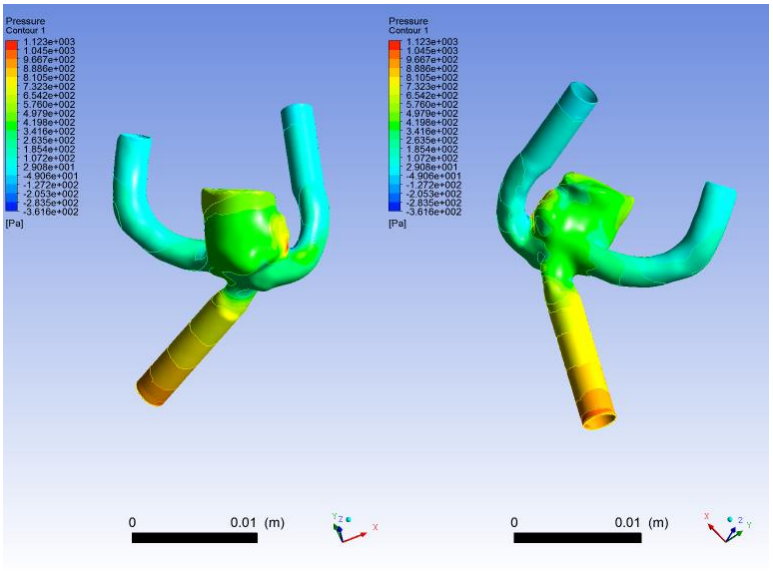

Half

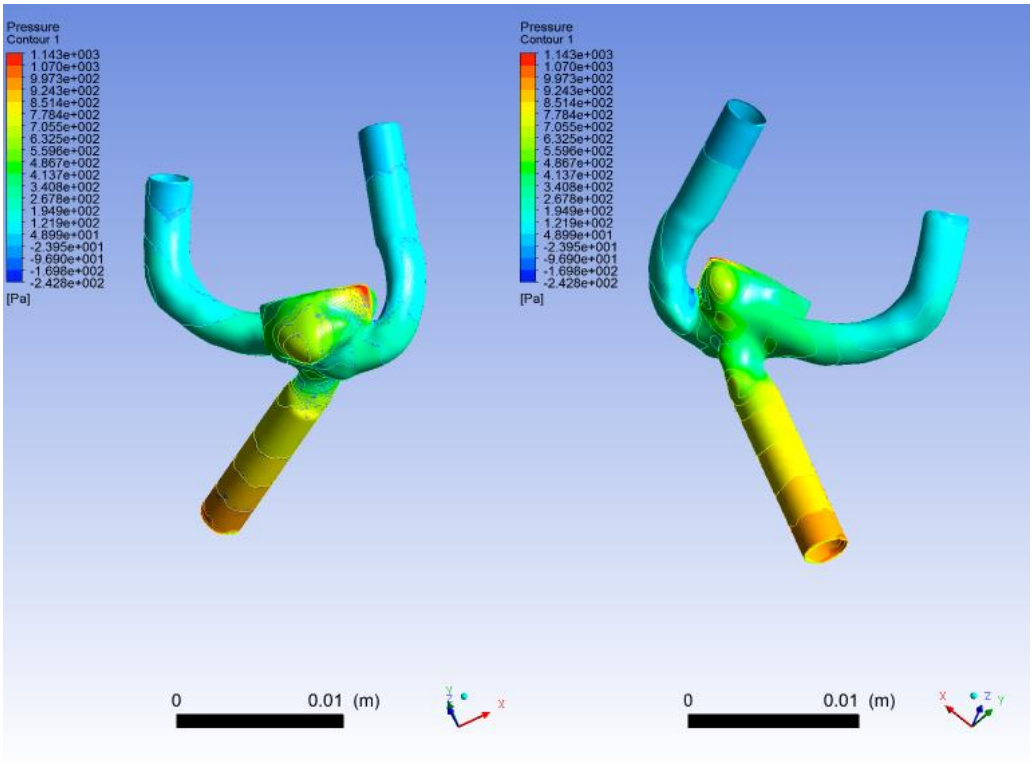

Tenth

WSS 0.2

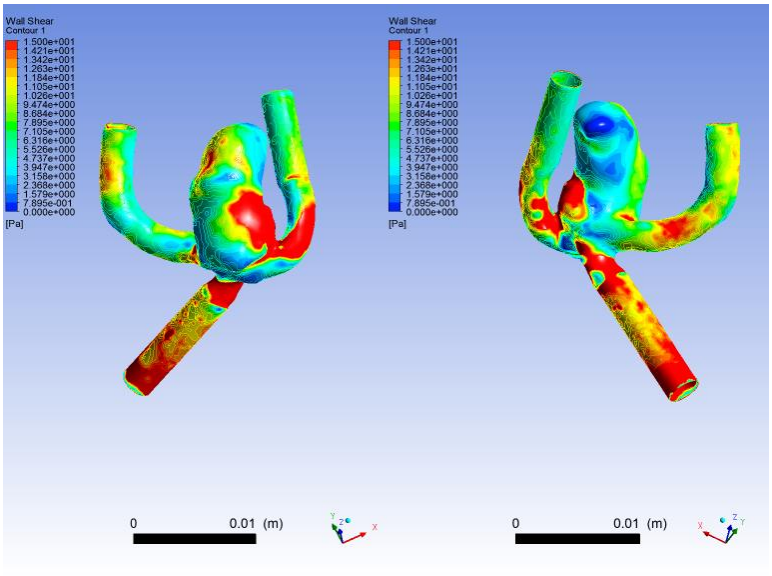

Whole

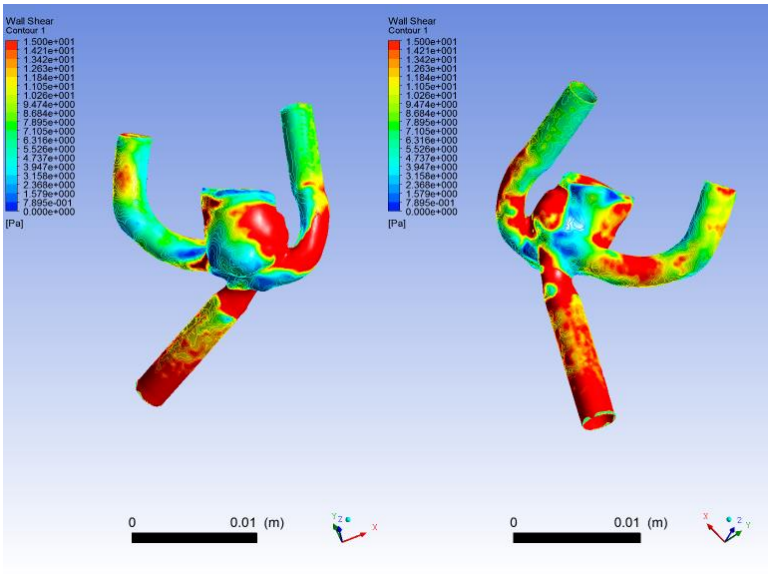

Half

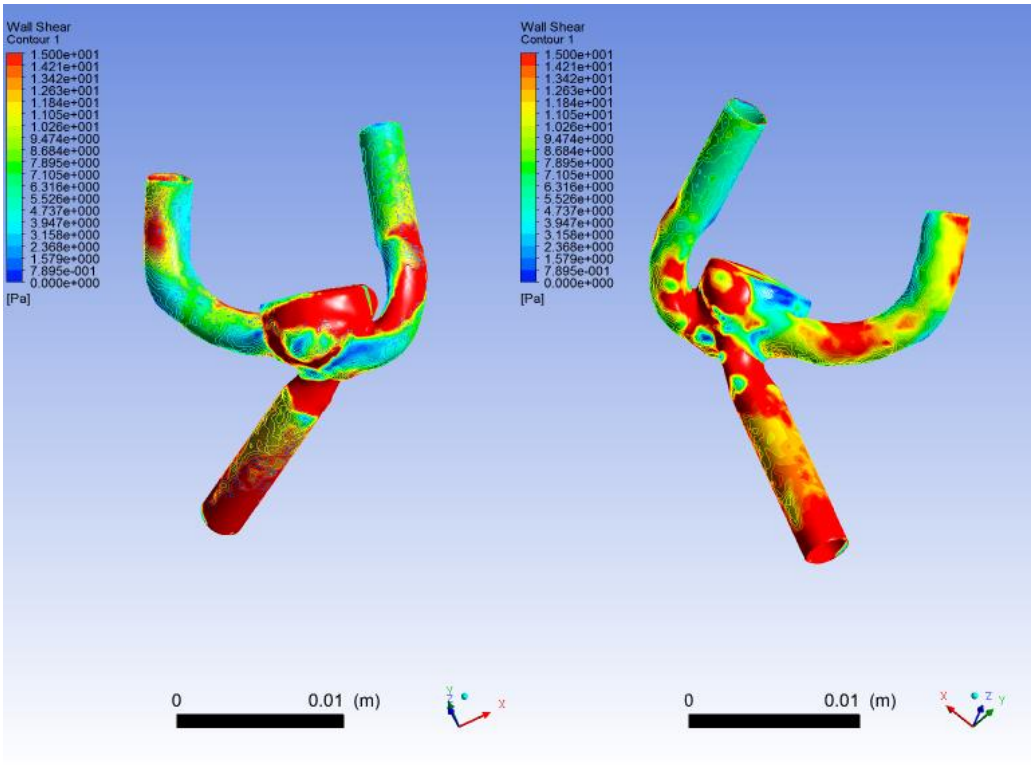

Tenth

Pathlines 0.2

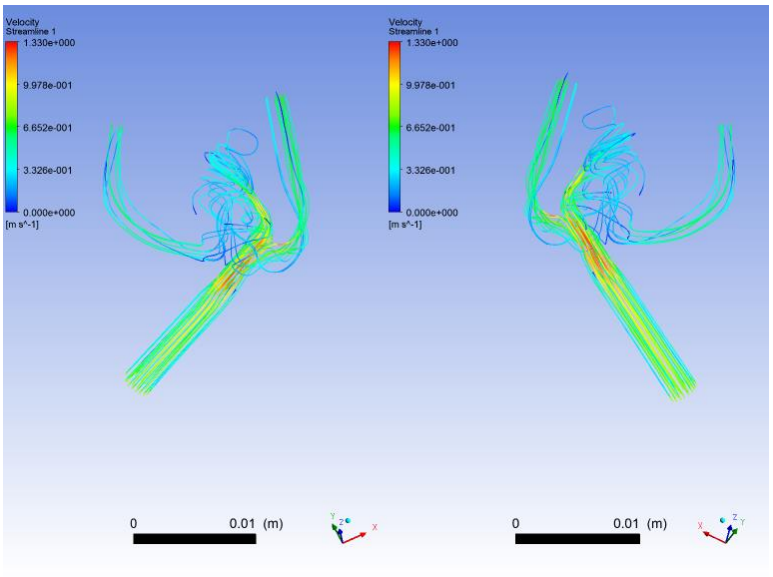

Whole

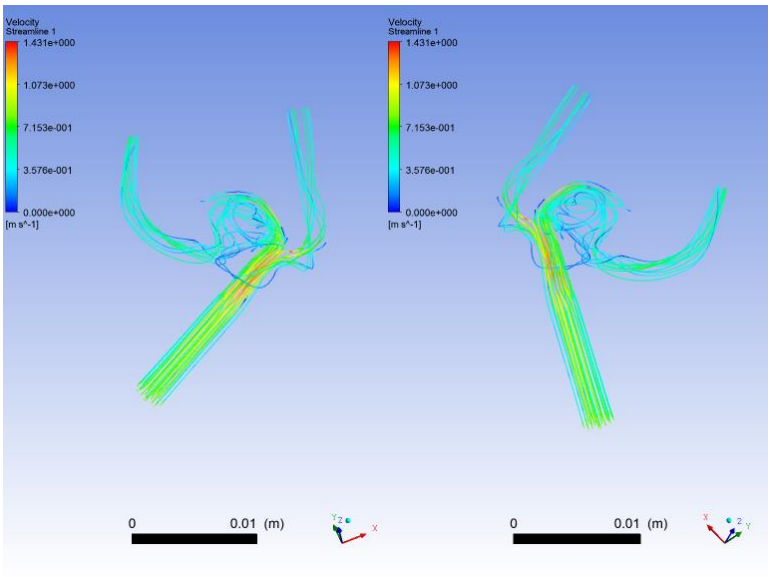

Half

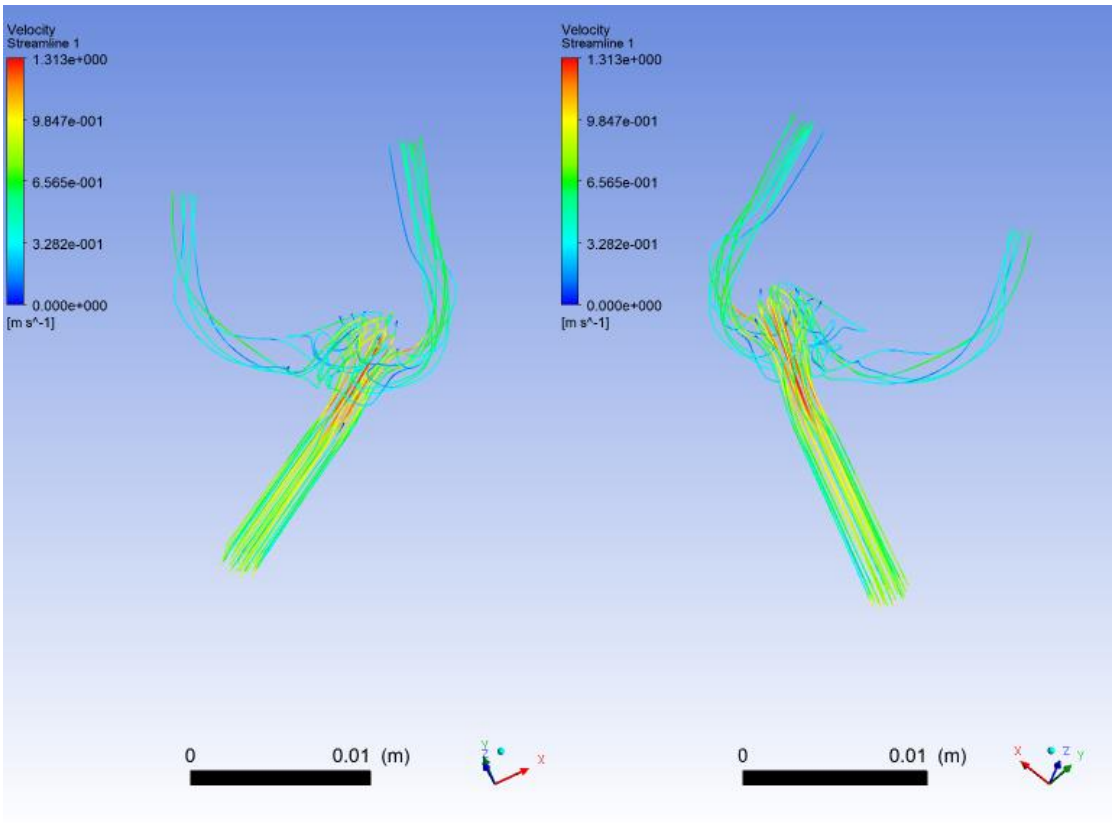

Tenth

t= 0.4 sec

	Full	Half	1/10
Pressure	-152 to 743 Pa	-250 to 800 Pa	-166 to 790 Pa
WSS	0 to 300 Pa	0 to 331 Pa	0 to 343 Pa
Area Aver. WSS	7.46	8.8	9.32

Pressure 0.4

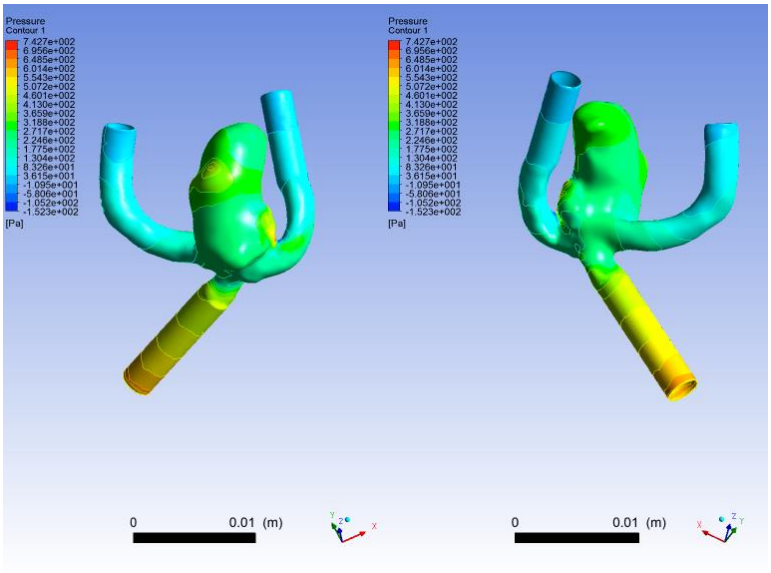

Whole

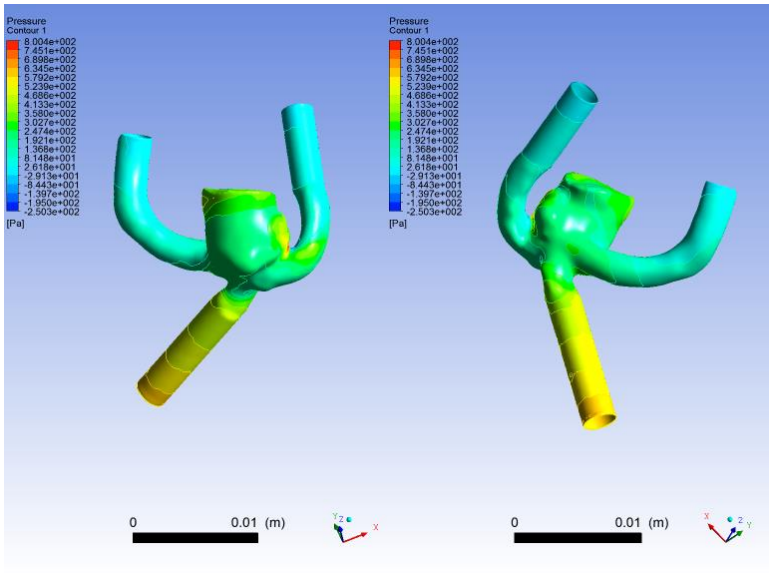

Half

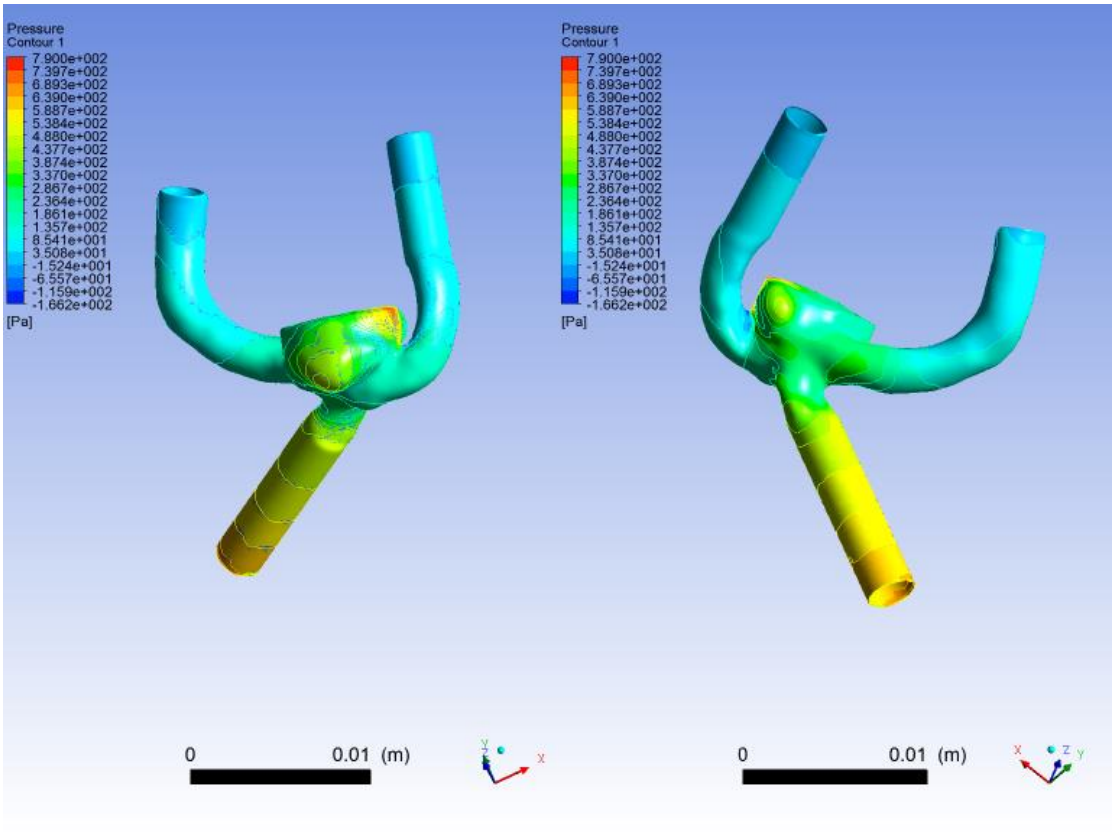

Tenth

WSS 0.4

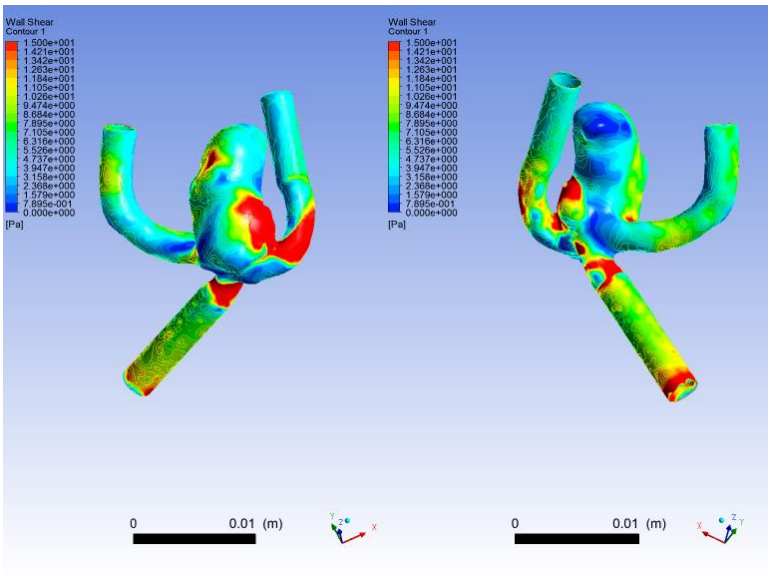

Whole

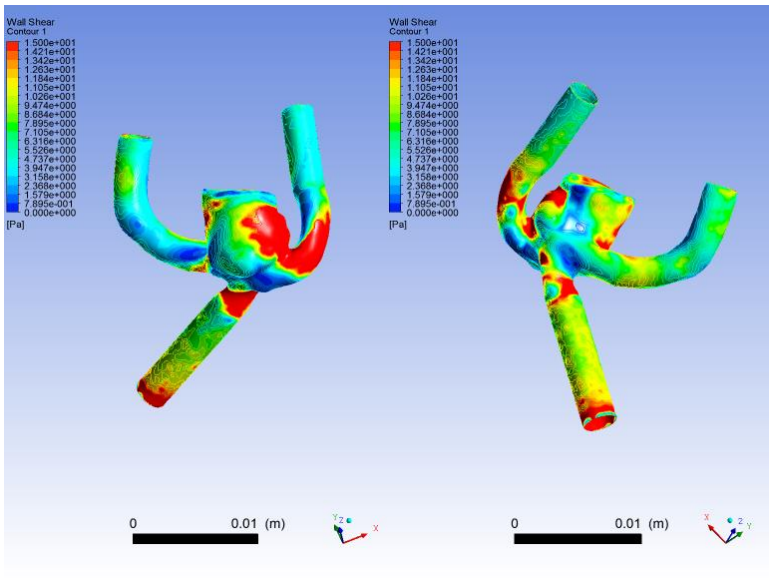

Half

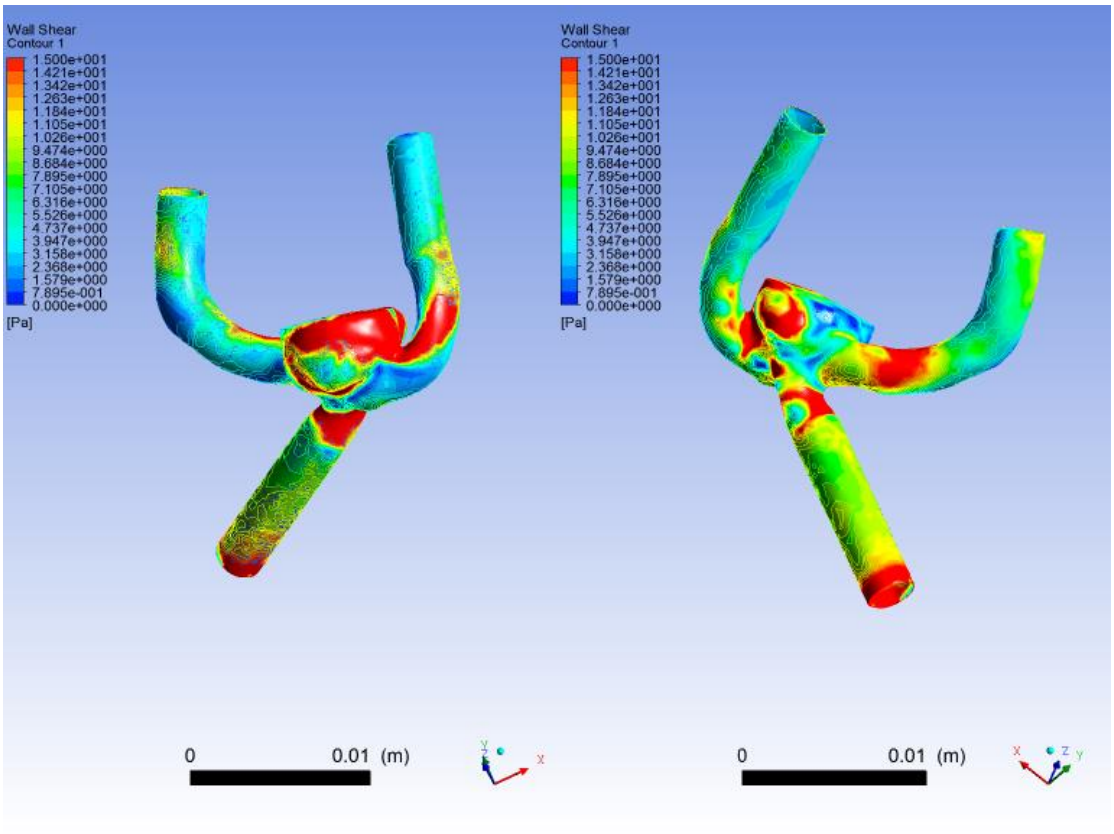

Tenth

Pathlines 0.4

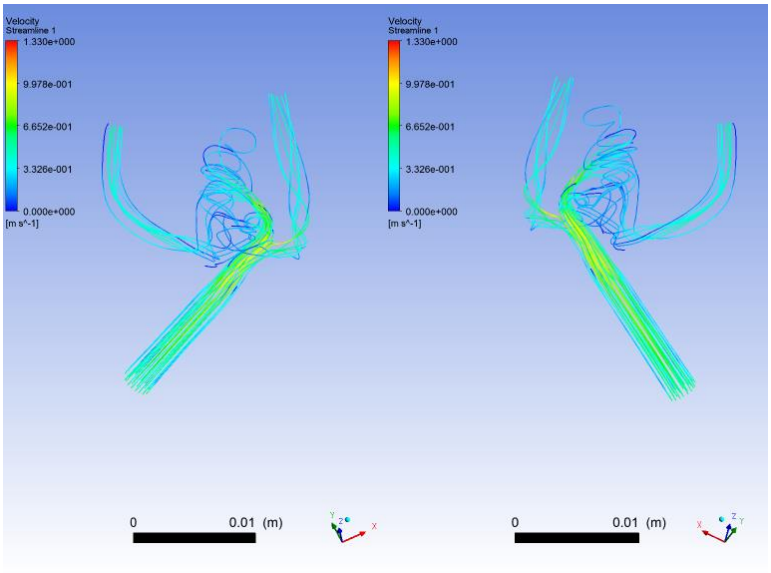

Whole

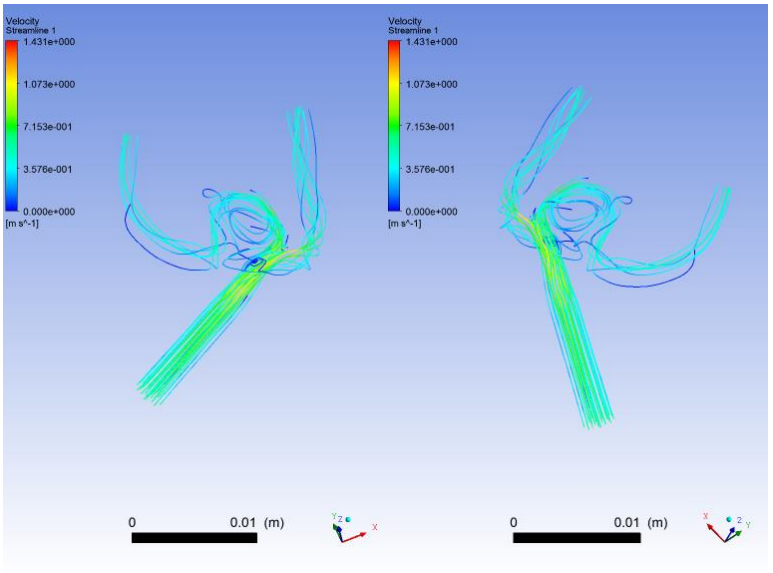

Half

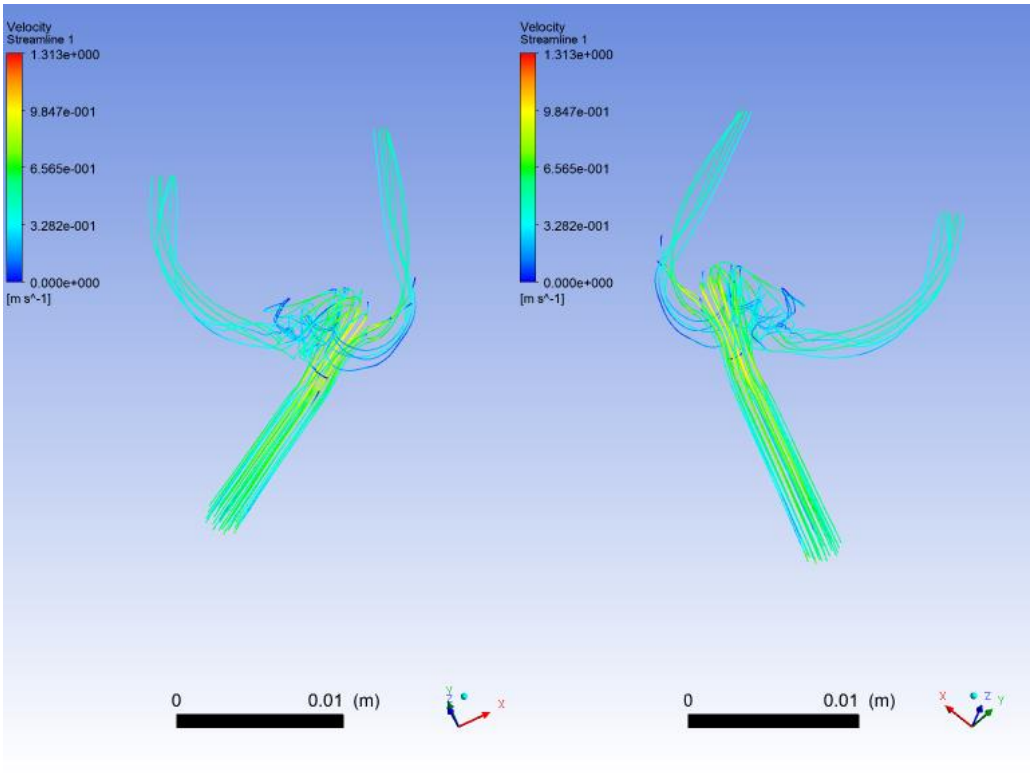

Tenth

t= 0.6 sec

	Full	Half	1/10
Pressure	-85 to 504 Pa	-127 to 480 Pa	-92 to 609 Pa
WSS	0 to 250 Pa	0 to 275 Pa	0 to 285 Pa
Area Aver. WSS	5.14	6	6.44

Pressure 0.6

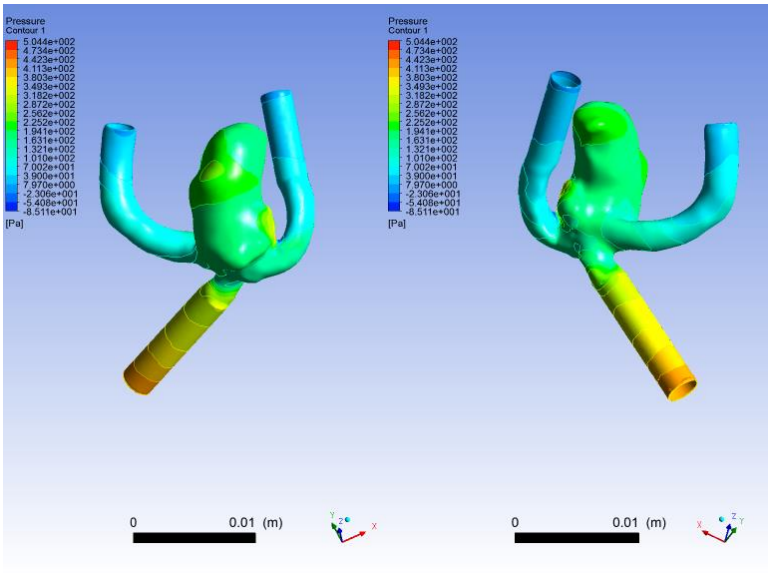

Whole

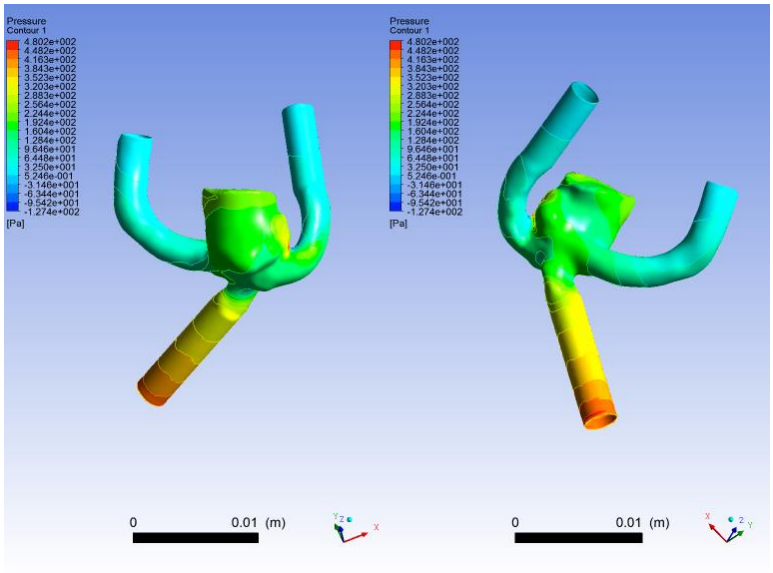

Half

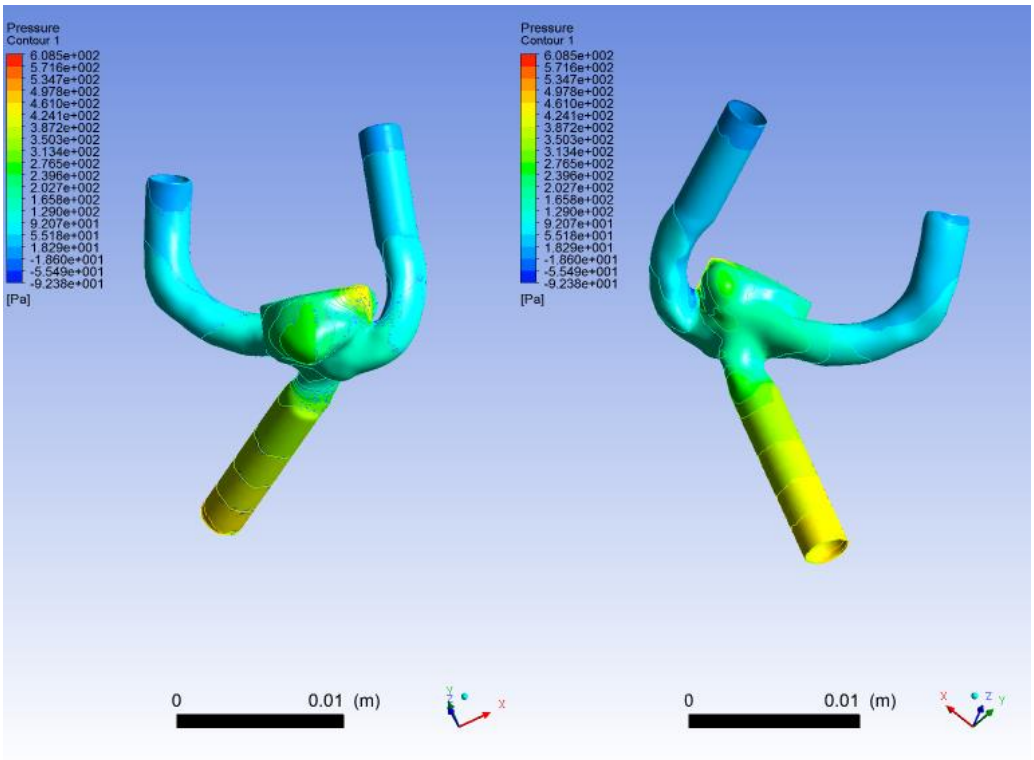

Tenth

WSS 0.6

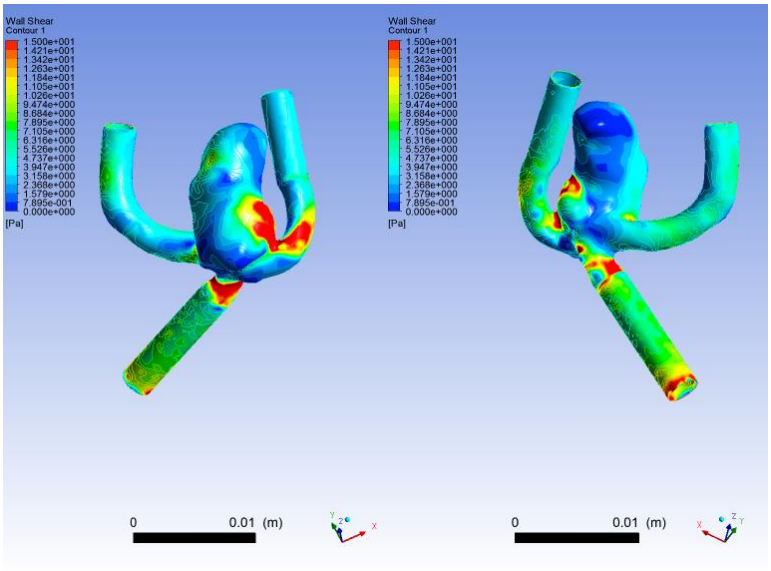

Whole

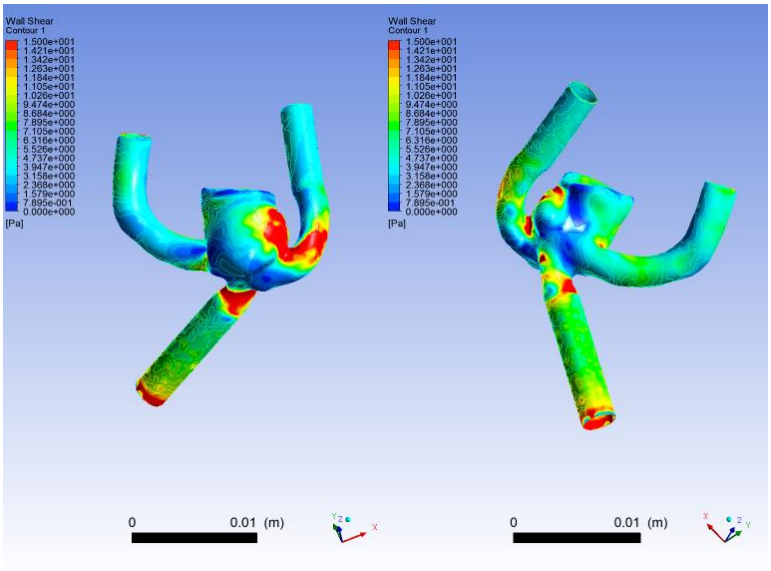

Half

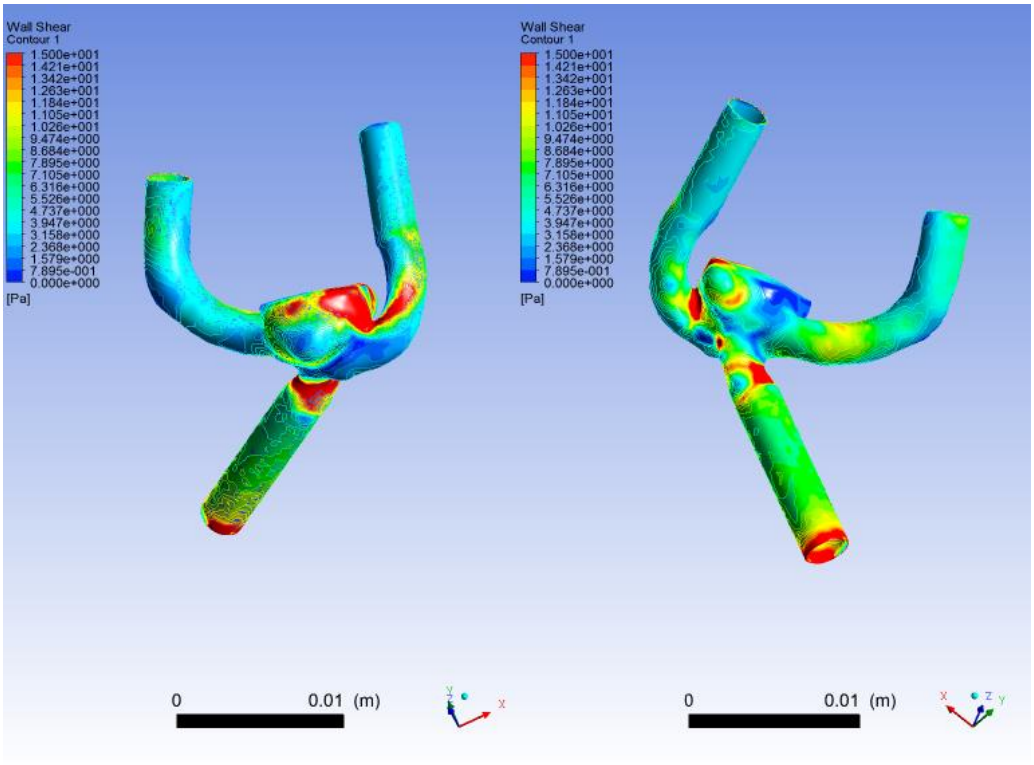

Tenth

Pathlines 0.6

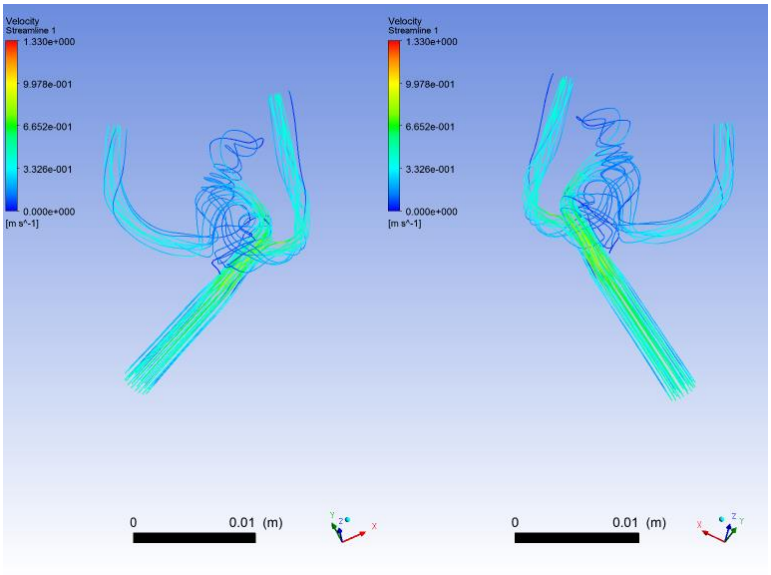

Whole

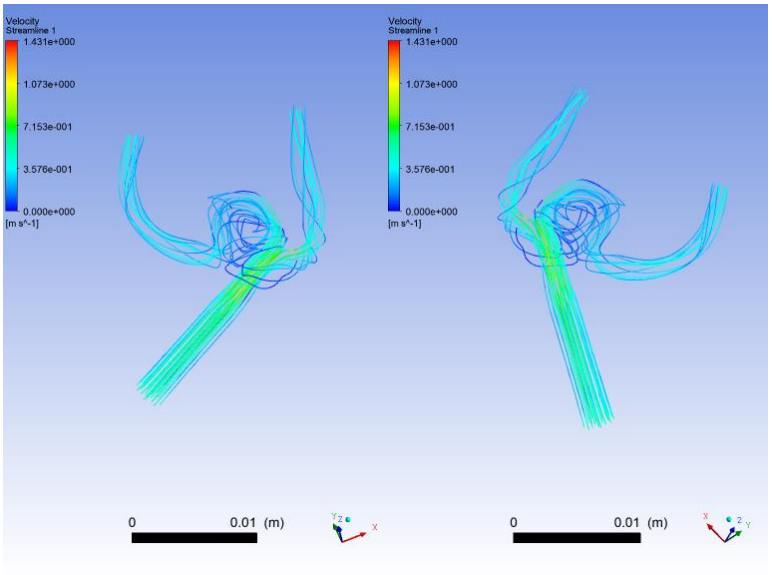

Half

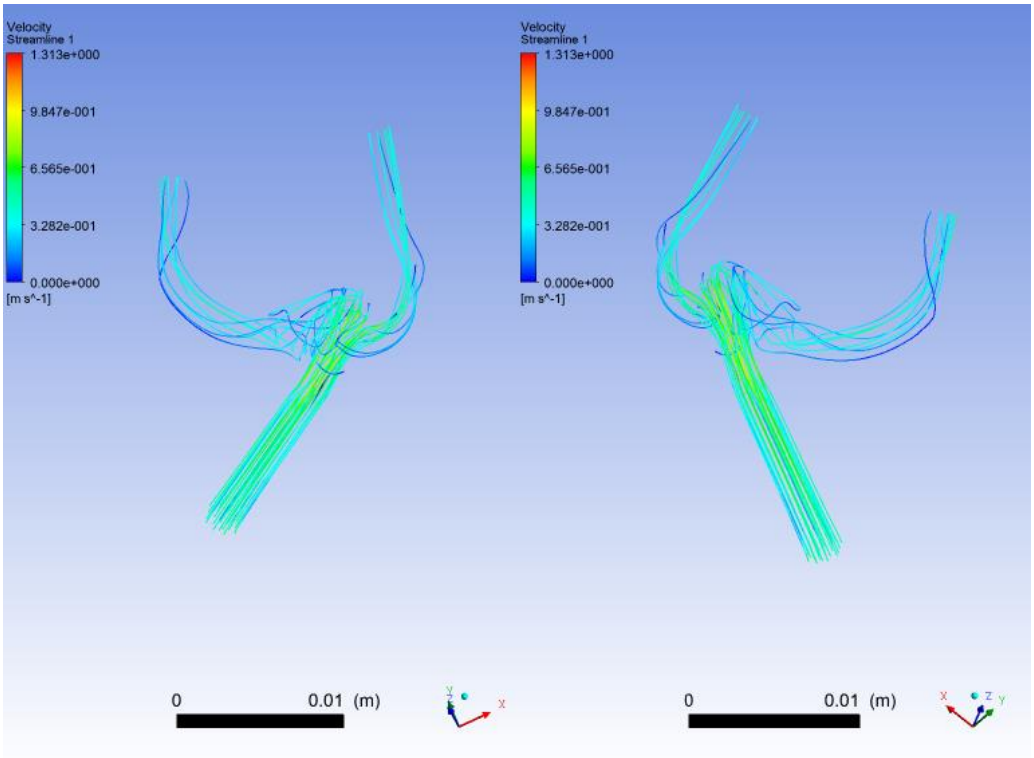

Tenth

OSI 0.8

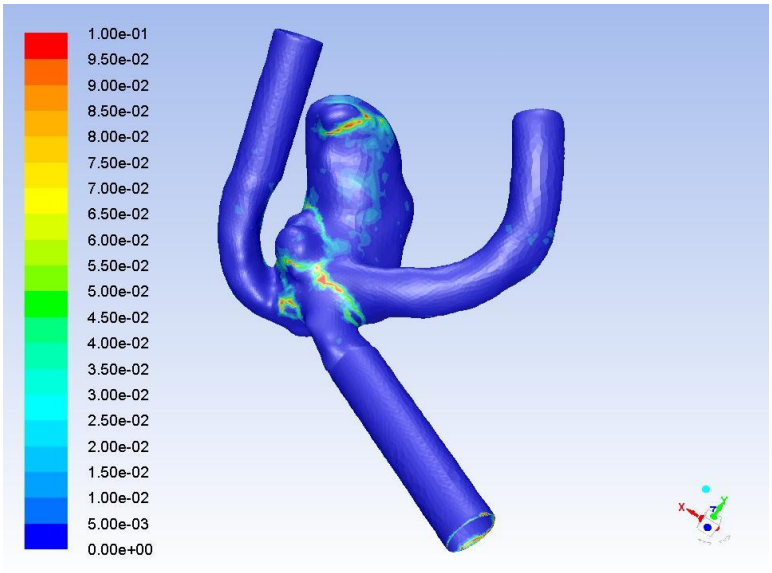

Whole front view

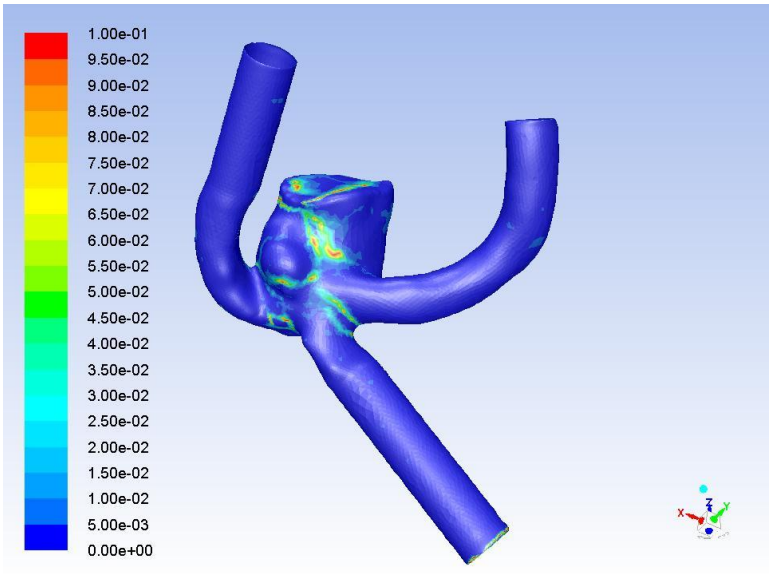

Half front view

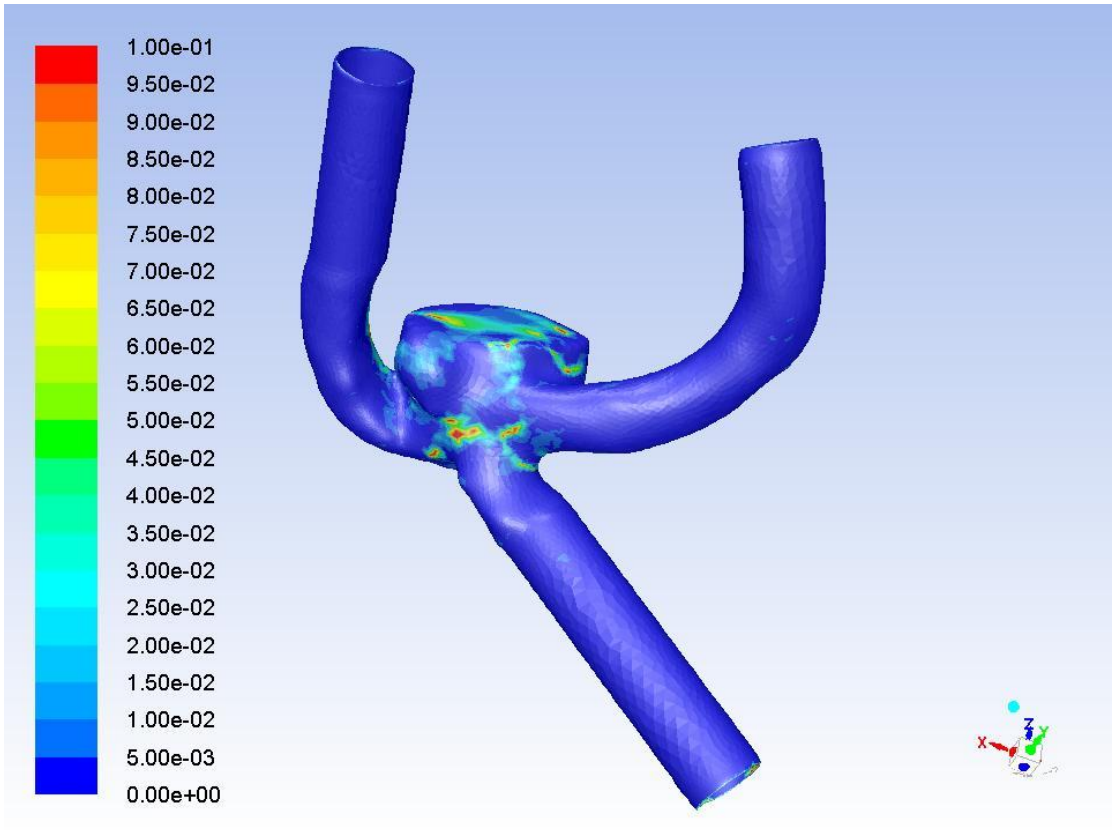

Tenth front view

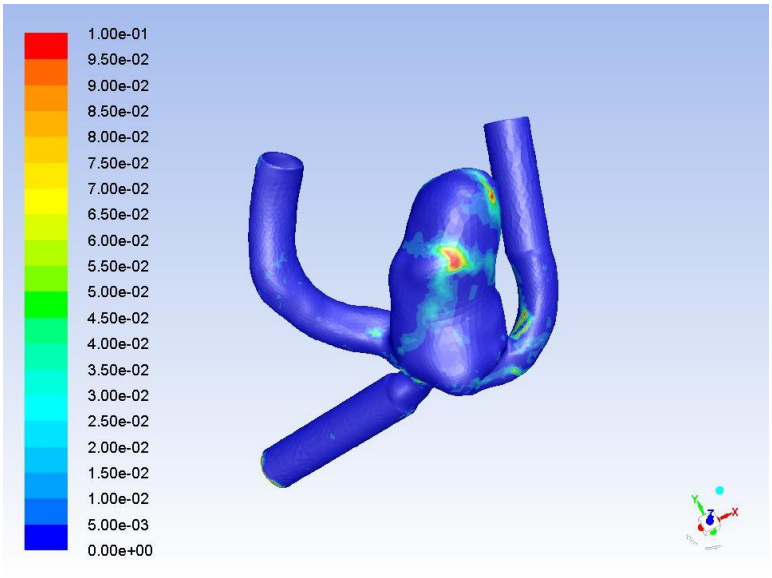

Whole front view

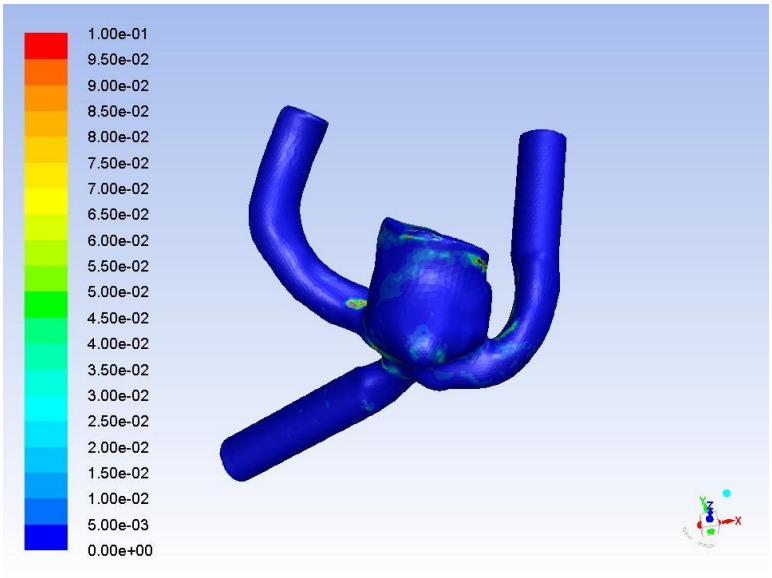

Half rear view

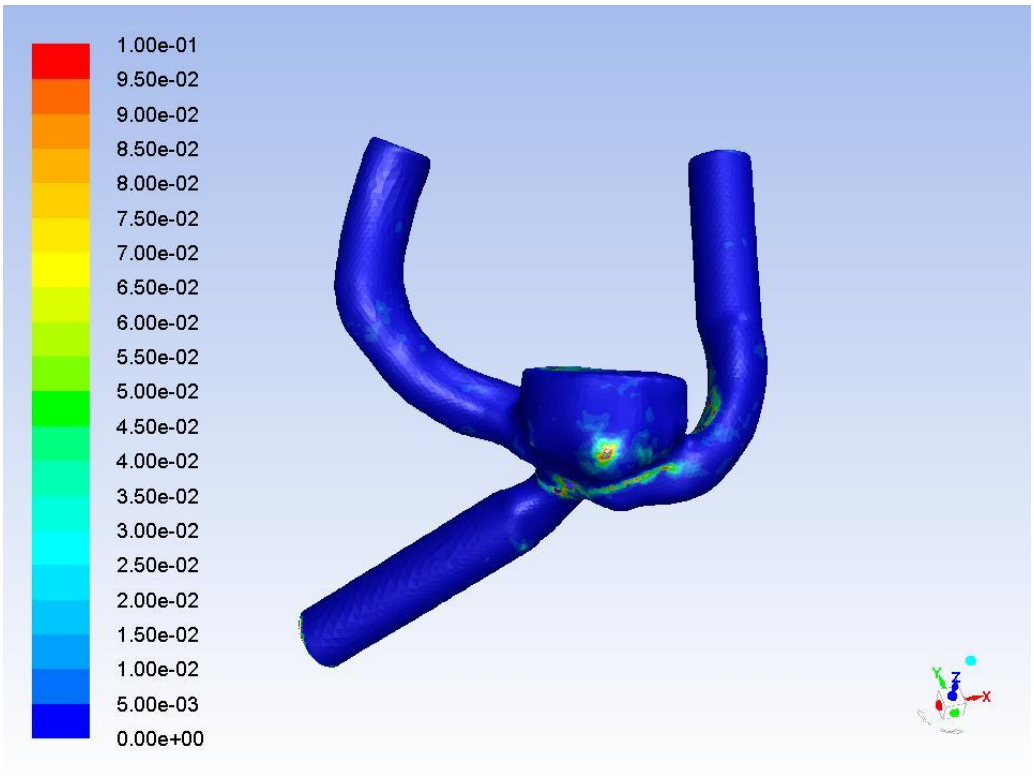

Tenth rear view

2nd patient virtual occlusion results

- The values of WSS and area averaged WSS increase as occlusion level increases.
- The regions of low WSS are less after the occlusions.
- The regions of OSI do not seem to have any significant difference

4th patient occlusions

t= 0.05 sec

	Full	Without the secondary bleb
Pressure	-2 to 545 Pa	-14 to 513 Pa
WSS	0 to 214 Pa	0 to 233 Pa
Area Aver. WSS	3.74	4.37

Pressure 0.05

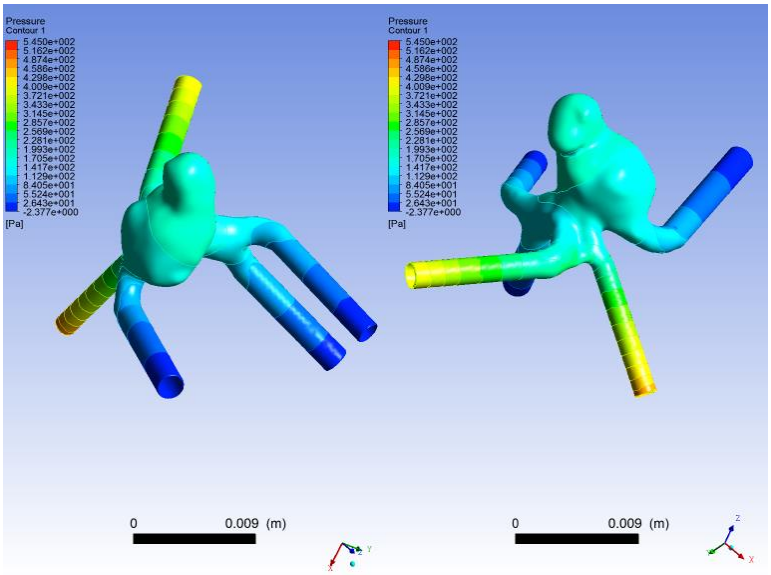

Whole

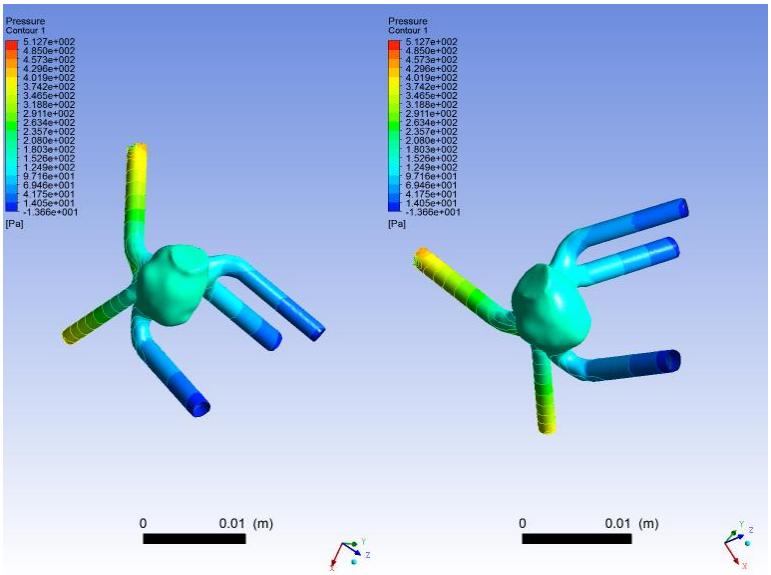

Cut

WSS 0.05

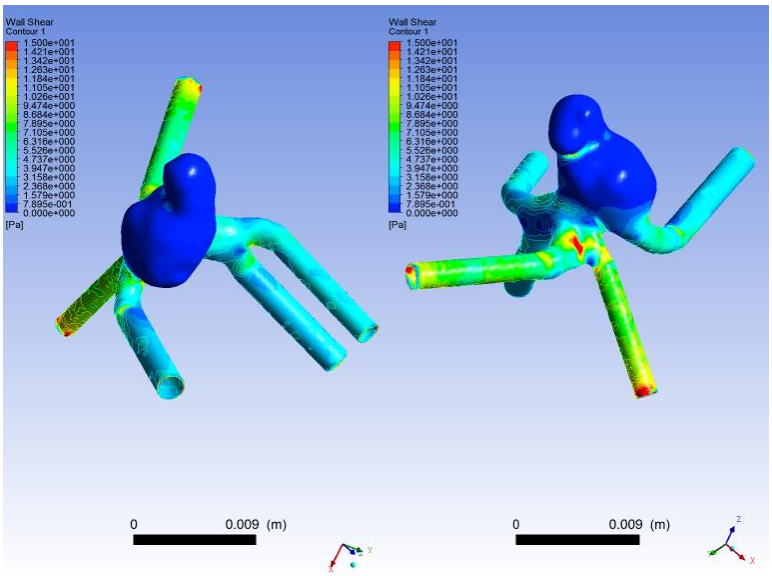

Whole

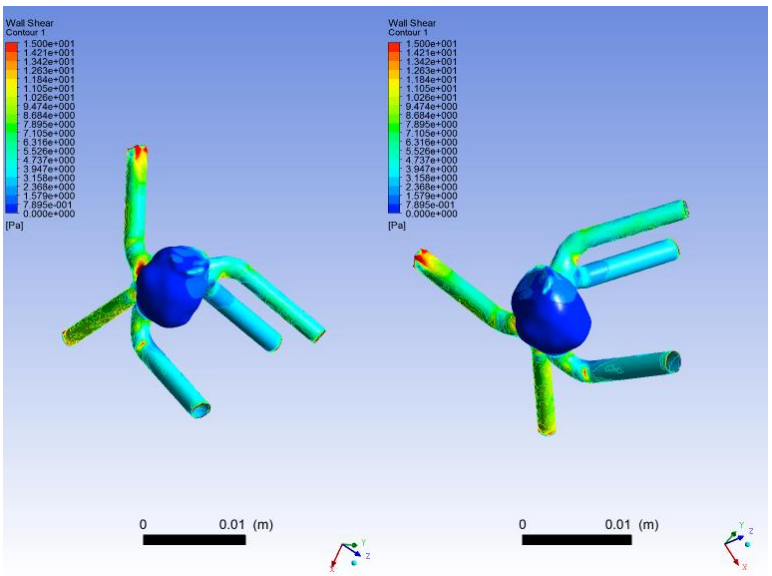

Cut

Pathlines 0.05

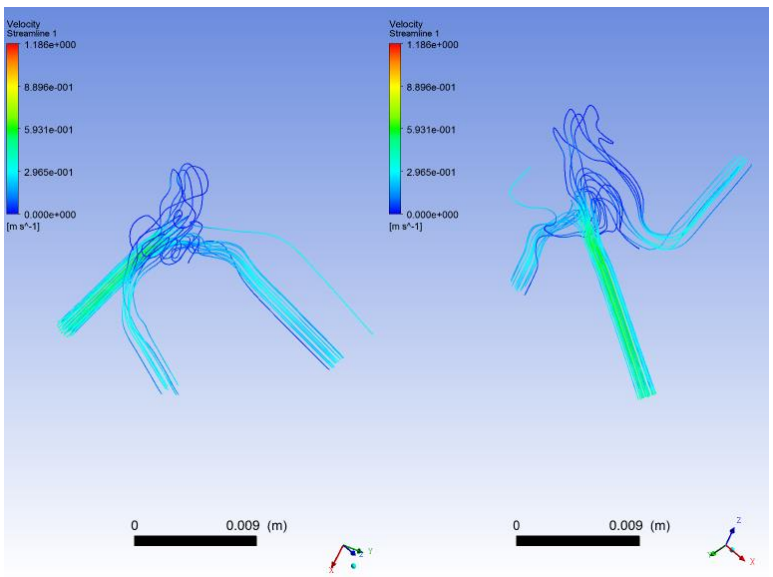

Whole

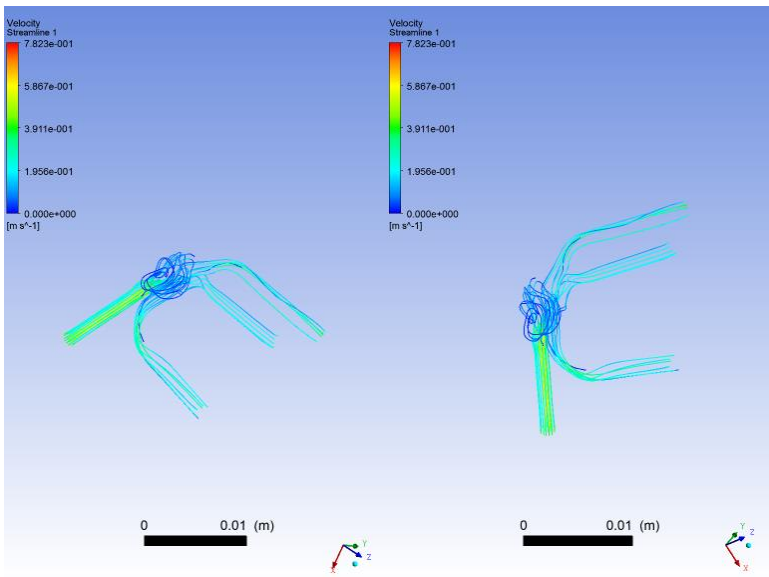

Cut

t= 0.2 sec

	Full	Without the secondary bleb
Pressure	-54 to 1002 Pa	-41 to 992 Pa
WSS	0 to 406 Pa	0 to 437 Pa
Area Aver. WSS	8.59	9.52

Pressure 0.2

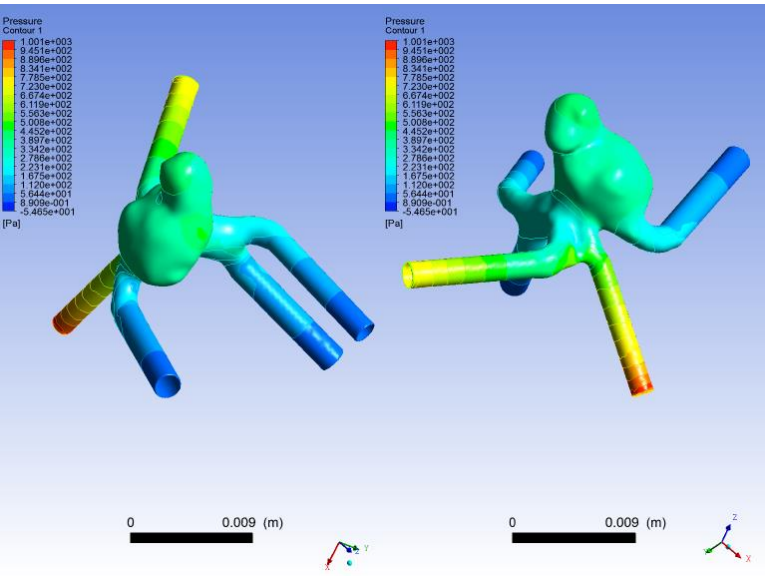

Whole

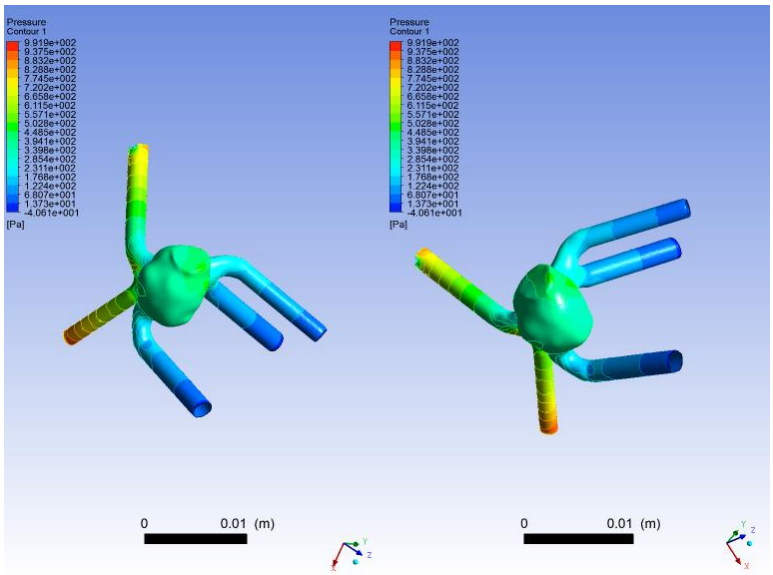

Cut

WSS 0.2

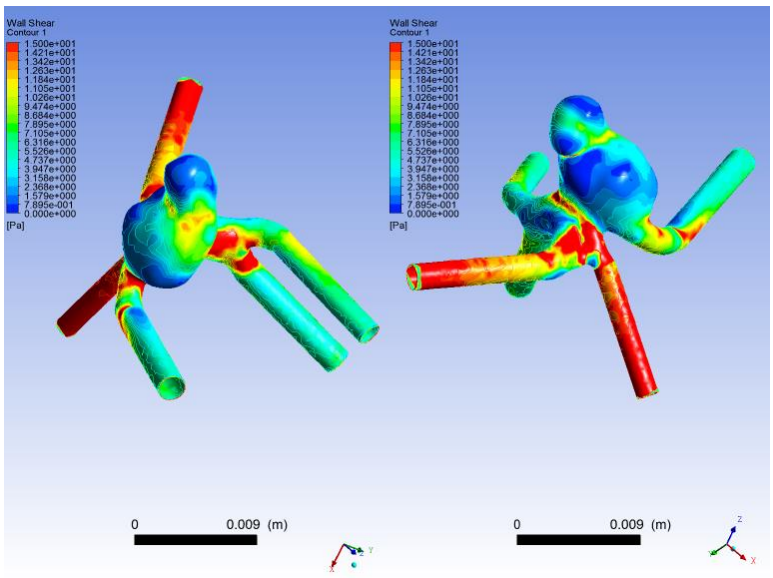

Whole

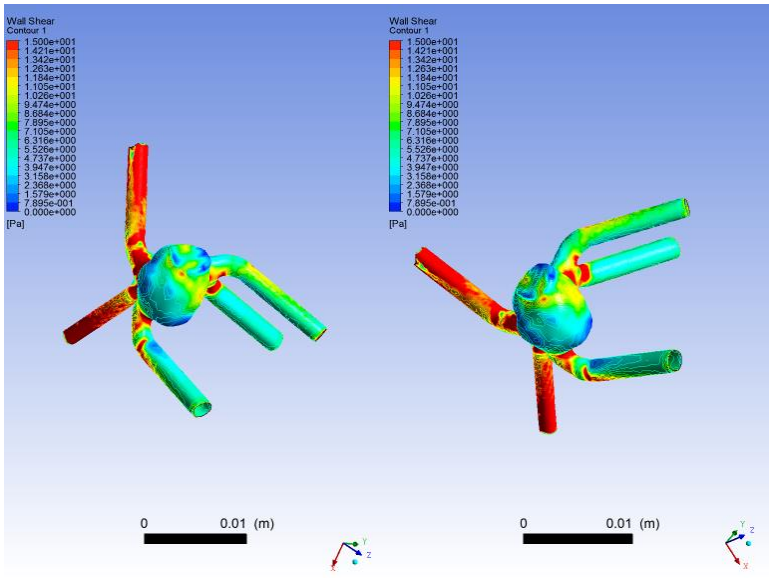

Cut

Pathlines 0.2

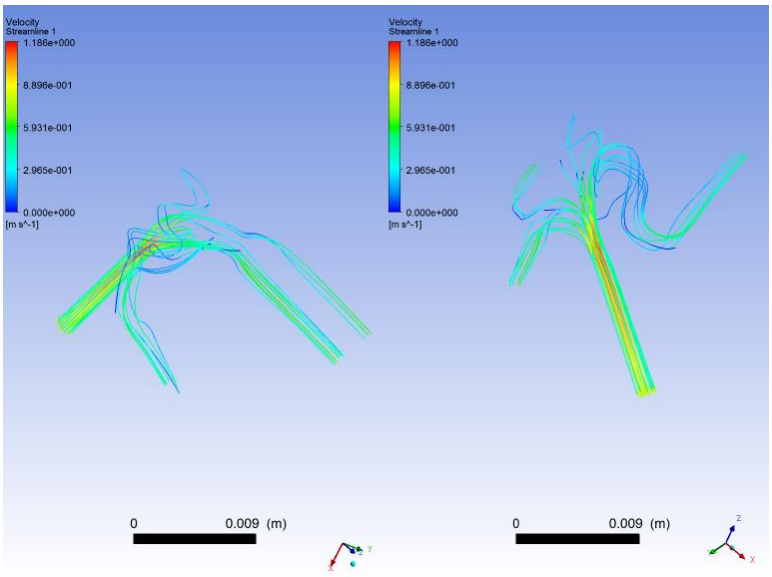

Whole

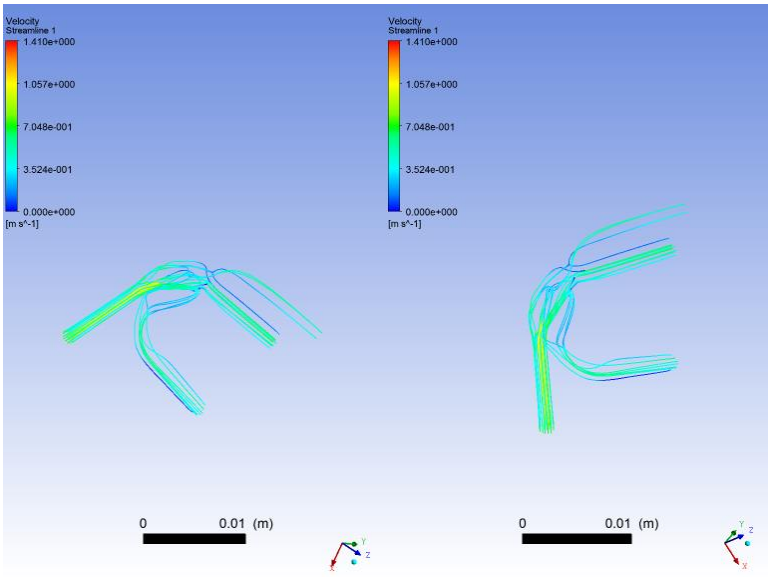

Cut

t= 0.4 sec

	Full	Without the secondary bleb
Pressure	0 to 726 Pa	0 to 738 Pa
WSS	0 to 287 Pa	0 to 310 Pa
Area Aver. WSS	5.84	6.50

Pressure 0.4

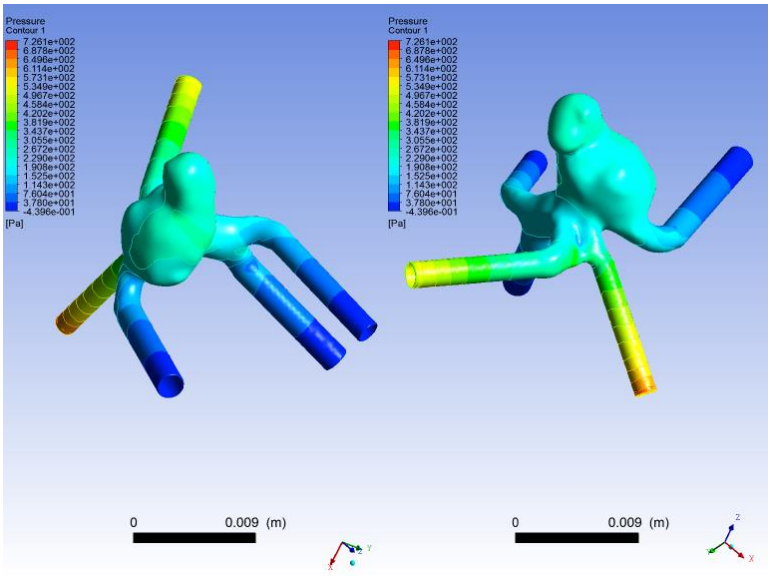

Whole

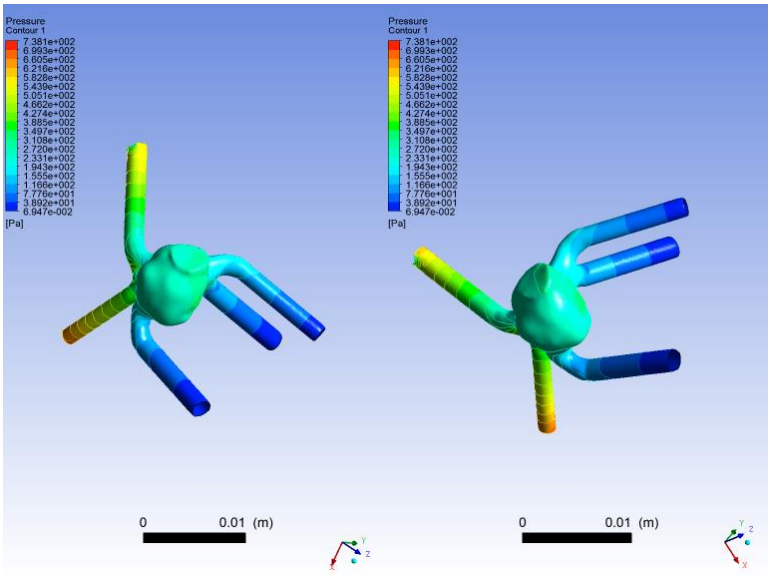

Cut

WSS 0.4

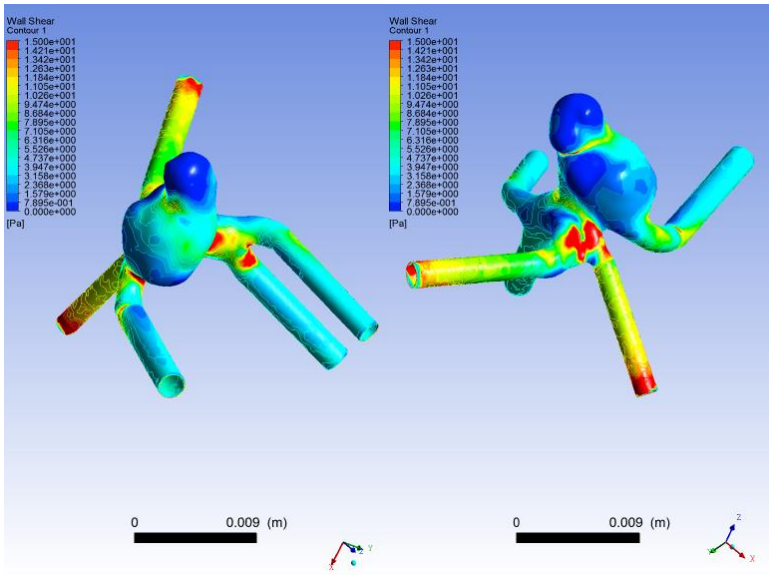

Whole

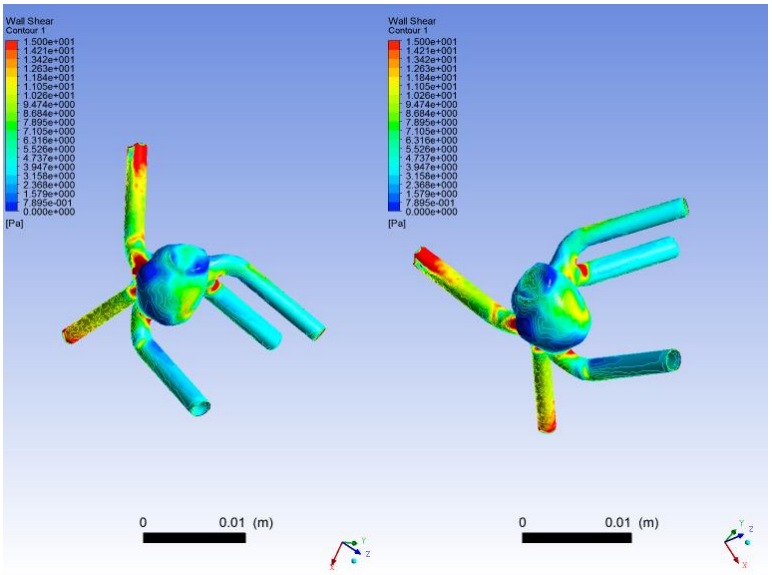

Cut

Pathlines 0.4

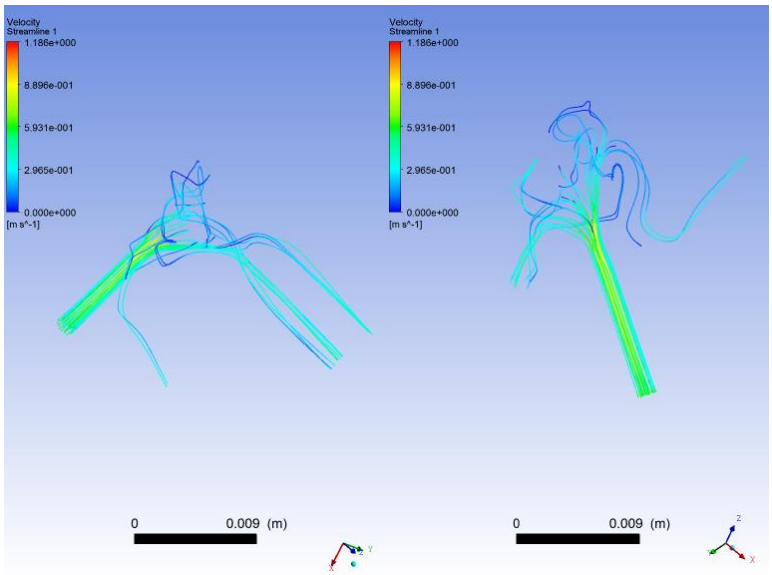

Whole

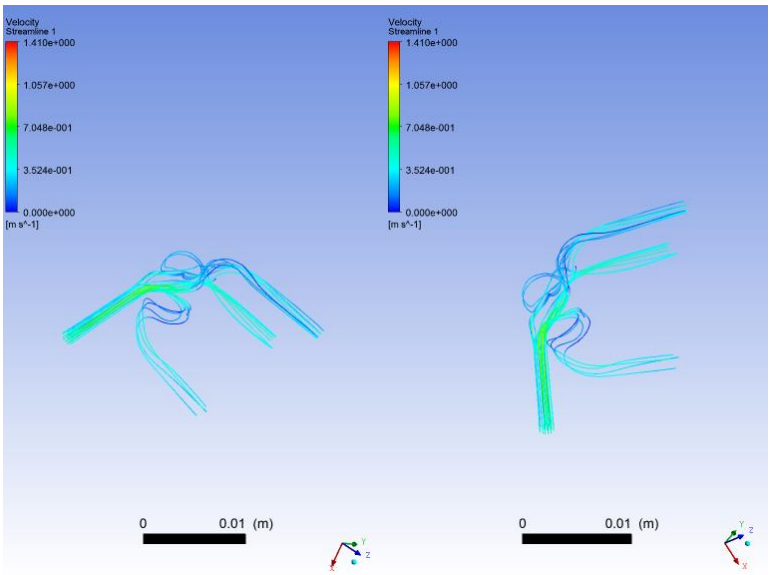

Cut

t= 0.6 sec

	Full	Without the secondary bleb
Pressure	0 to 560 Pa	0 to 554 Pa
WSS	0 to 239 Pa	0 to 260 Pa
Area Aver. WSS	4.53	5.14

Pressure 0.6

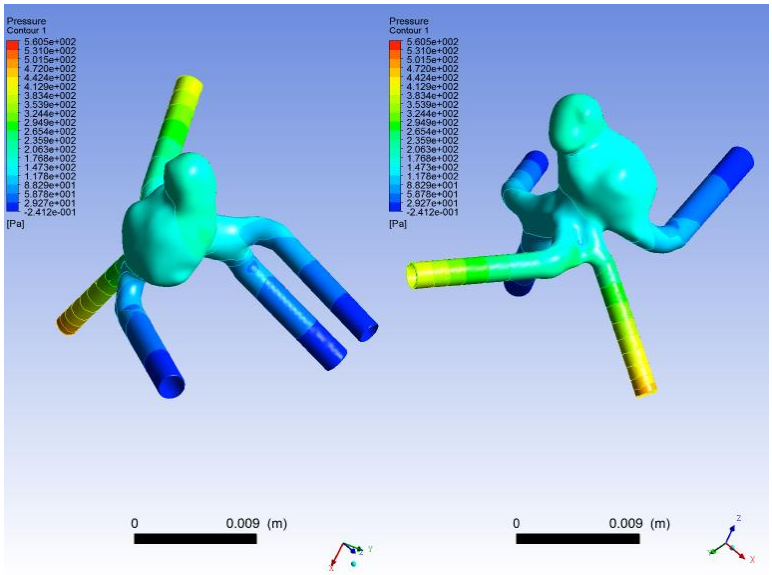

Whole

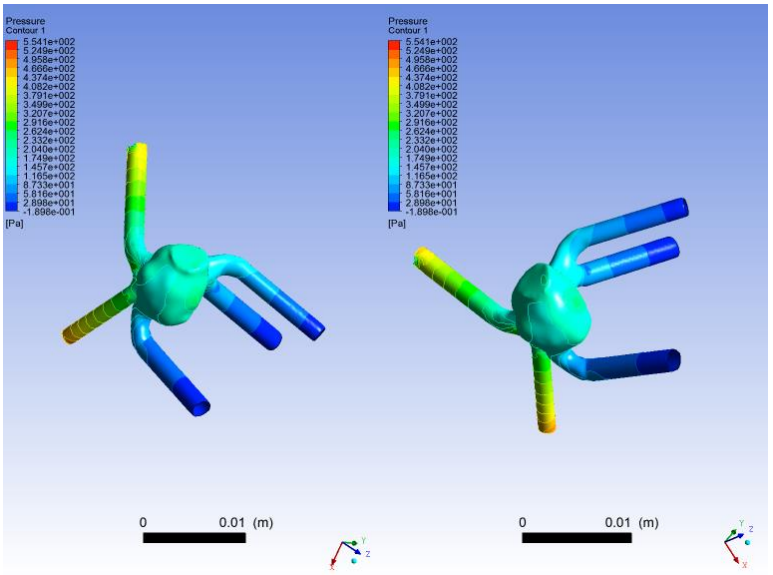

Cut

WSS 0.6

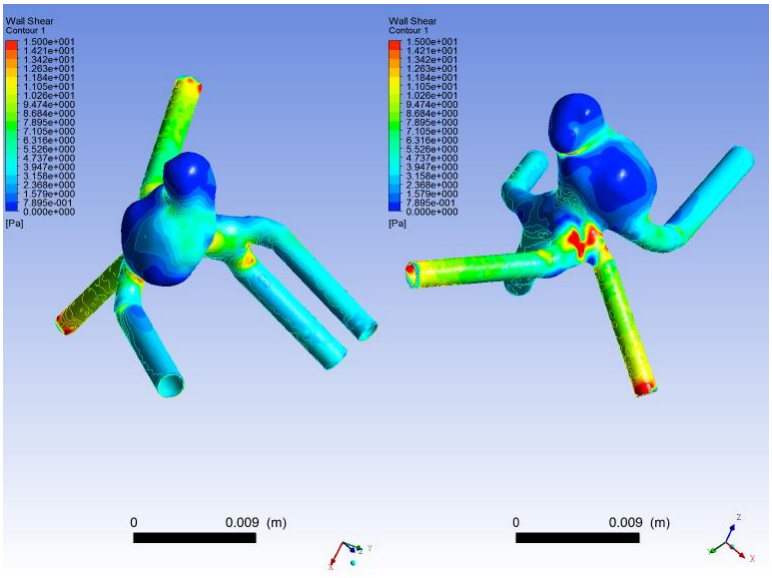

Whole

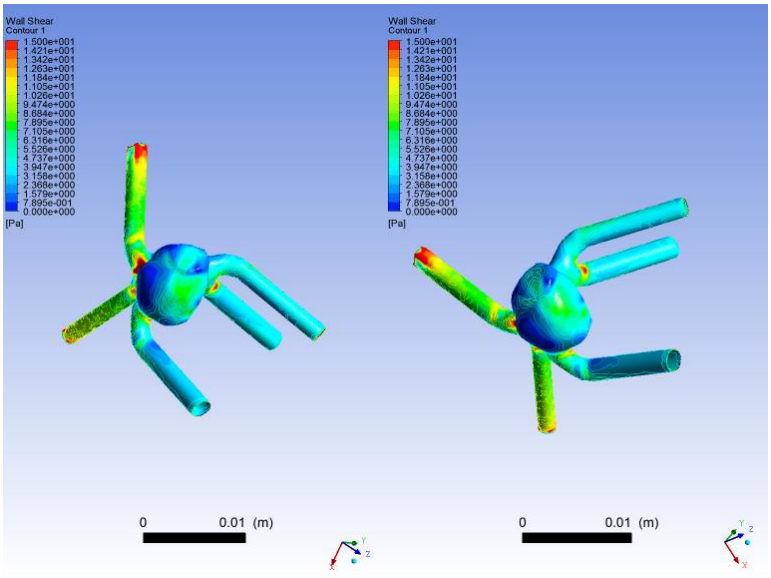

Cut

Pathlines 0.6

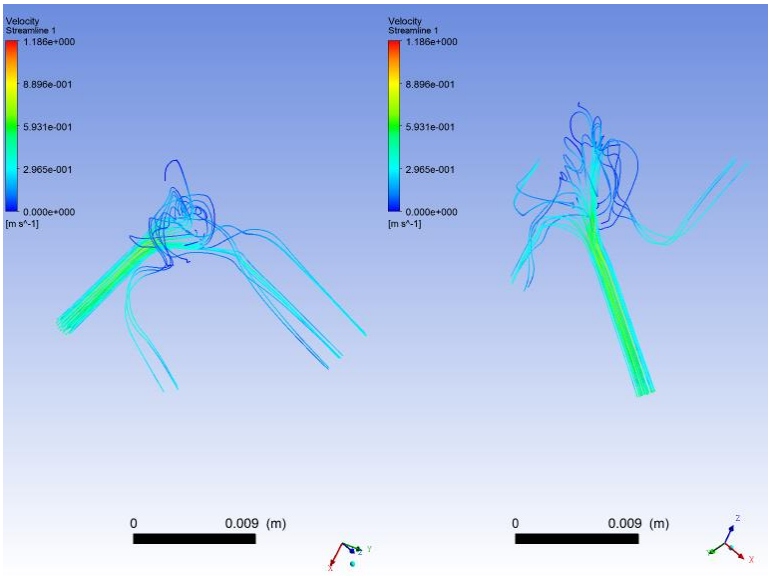

Whole

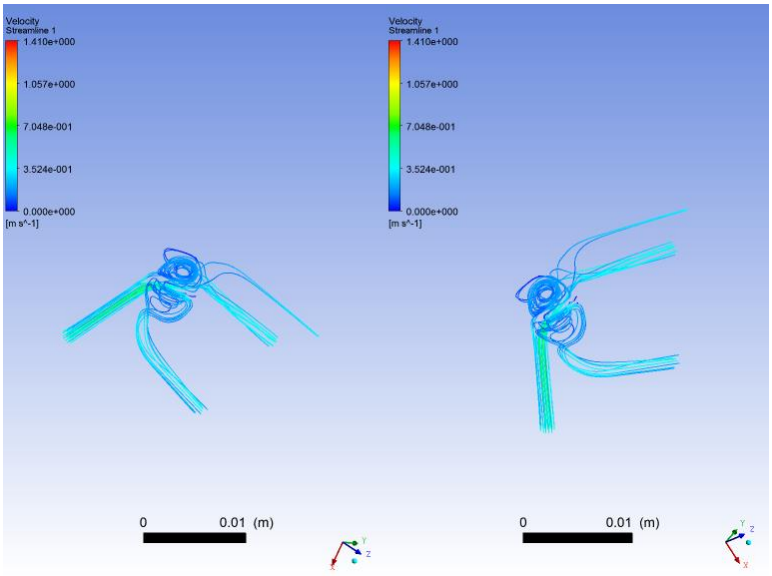

Cut

OSI 0.8

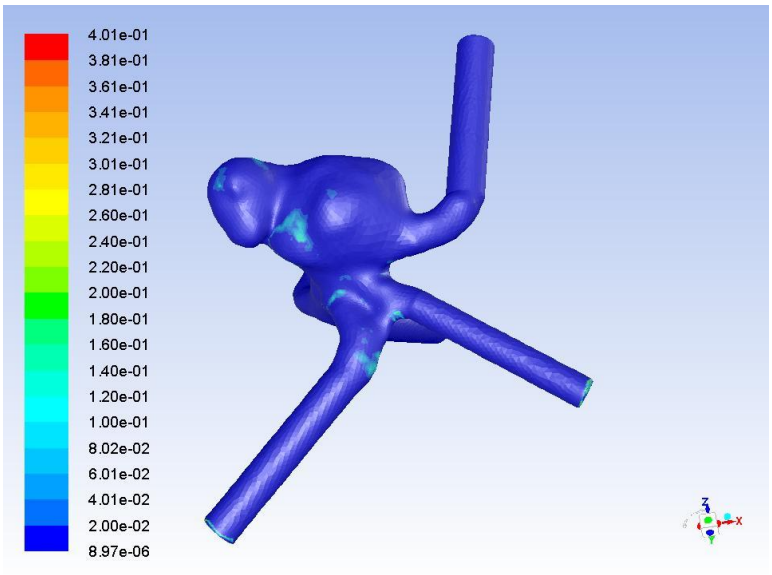

Whole

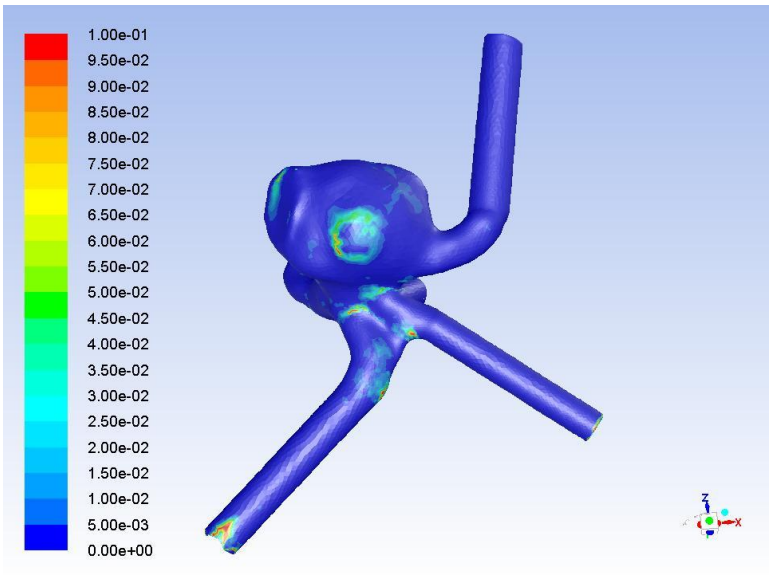

Cut

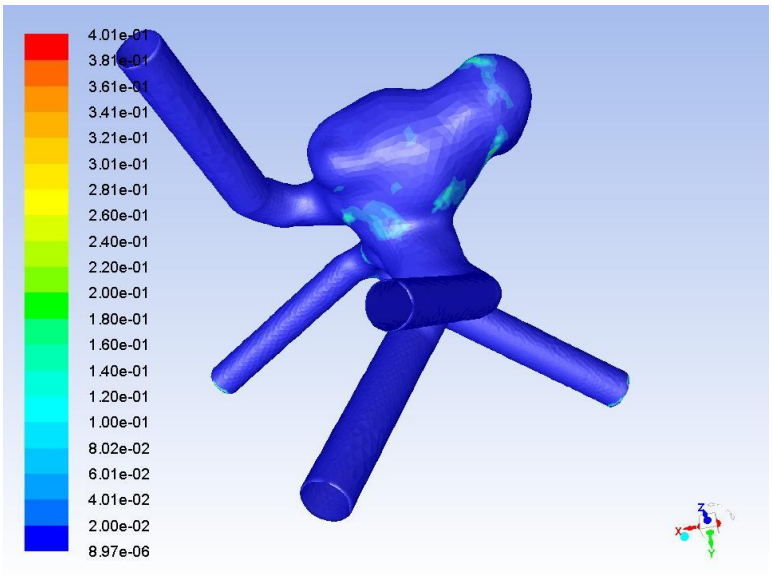

Whole Rear

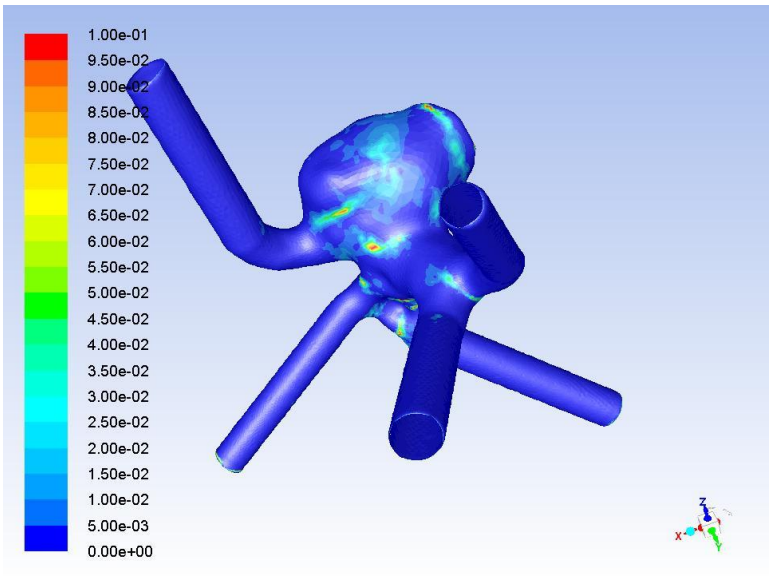

Cut rear

4th patient virtual occlusion results

- The values of WSS and area averaged WSS increase as occlusion level increases.
- The region where the bleb was formed, seems to have been a region of high WSS
- The regions of high OSI have greater extent

9. Conclusions

First and foremost, the geometry of the aneurysm as derived from the DSA and the MRA examinations, never was exactly the same. The MRA is known to have worse spatial resolution, something that can be easily noticed in the MRA images which have less edges and thus miss some details. Aside from this fact, the MRA results need to undergo an extra step of processing in order to form a 3-D object, the one performed at Mimics Medical Pro. There were cases, which obligated the virtual addition or reduction of parts on the existing geometry as it was taken from the MRA examination.

This is an inevitable fact which expectedly emerges different hemodynamic results, since the geometry ends up having some distinctive differences.

Regarding the hemodynamic parameters, it is also notable that always the maximum values of pressure, WSS, and Area Averaged WSS were lower at the DSA examinations.

The comparison of their maximum values and the blood's pathlines has shown the following results:

- Aside from the 3rd patient (57% difference), all the other comparisons of DSA and MRA revealed a difference in pressure up to 26%.
- Regarding the WSS, apart from the 1st patient (21% difference), all the other comparisons of DSA and MRA revealed a difference in WSS up to 5-10%.
- Apart from the 1st patient (40% difference), all the other comparisons of DSA and MRA revealed a difference in Area Averaged WSS up to 28%.
- The pathlines where more or less up to a certain degree of agreement, as a result of the different geometry.

The values of the hemodynamic parameters in this thesis are in part with those found in the bibliography [43], which means that the steps followed throughout the modelling and simulating process are in the right direction.

Furthermore, the virtual treatment scenarios applied revealed an overall increase in the maximum value of WSS and the Area Averaged WSS. This means that there is a smaller extent of the aneurysm's surface that has low WSS, which is known to be one of the main reasons for rupture. Of course, this a virtual treatment scenario based on a software induced occlusion, but the fact that the results indicate a decreased risk of rupture after a virtual treatment is without a doubt positive.

Computational fluid dynamics is an emerging tool that could potentially guide the management of cerebral aneurysms. However, the heterogeneity and frequent contradictions in results is holding CFD back from clinical utility. Small datasets, inconsistent parameter definitions, mechanistic complexity of aneurysm rupture, and compromises like laminar flow, rigid walls and Newtonian blood, are some of the limitations.

The results of this thesis lead to certain recommendations. First of all, the DSA examination is undoubtedly the more precise, less invasive and time-efficient one in order to perform the modelling and simulation process. On the other hand, it is worse for the patient since it uses ionizing radiation and a riskier process compared to MRA. Since the results of key hemodynamic parameters like WSS and Area Averaged WSS do not show margins greater than 30%, MRA cannot be rejected as a base for a Computational research. On the contrary, given an initial MRA examination the follow up angiography would be more beneficial if it was an MRA rather than a DSA.

Regarding our future interests, post treatment examinations right after the treatment and in a later stage where recurrence has occurred, would be cases of great importance.

About the CFD aided researches on cerebral aneurysms, it is clear that for the CFD results to be applied in clinical practice, many changes should be made. Results of various studies that have different parameter definitions and single or limited number of cases are undoubtedly helpful as they stand, but only for statistical reasons.

As long as a general protocol for the modeling and simulating process does not exist comparing the results of different studies will be akin comparing apples and oranges. Taking a look at section 7.3 of this thesis can be pretty enlightening. The whole process is simply, very user dependent and prone to produce different results. In addition, there are various software programs for the implementation of each stage, which can lead to even greater variations.

Consequently, an essential step towards a more substantial research in the field of cerebral aneurysms should be made. This includes a detailed description of the steps followed and the software programs used, so that the researchers are allowed to perform even comparisons and gradually conclude to a protocol-based research in this field.

10. Bibliography

1. Kroon M. Simulation of Cerebral Aneurysm Growth and Prediction of Evolving Rupture Risk. Vol 10.; 2011. doi:10.1155/2011/289523

2. Unruptured brain aneurysm. Mayfieldclinic.com. https://mayfieldclinic.com/PE-AneurUn.htm. Published 2015.

3. Ujiie H, Tachibana H, Hiramatsu O, et al. Effects of Size and Shape (Aspect Ratio) on the Hemodynamics of Saccular Aneurysms: A Possible Index for Surgical Treatment of Intracranial Aneurysms. Neurosurgery. 1999;45(1):119. doi:10.1227/00006123-199907000-00028

4. Hademenos GJ, Massoud T, Valentino DJ, Duckwiler G, Vinuela F. A nonlinear mathematical model for the development and rupture of intracranial saccular aneurysms. Neurological Research. 1994;16(5):376-384. doi:10.1080/01616412.1994.11740257

5. Yoon NK, McNally S, Taussky P, Park MS. Imaging of cerebral aneurysms: a clinical perspective. Neurovascular Imaging. 2016;2(1). doi:10.1186/s40809-016-0016-3

6. RSNA A. CT Angiography (CTA). Radiologyinfo.org. https://www.radiologyinfo.org/en/info.cfm?pg=angioct. Published 2019. Accessed May 12, 2019.

7. Ajiboye N, Chalouhi N, Starke RM, Zanaty M, Bell R. Unruptured Cerebral Aneurysms: Evaluation and Management. The Scientific World Journal. 2015;2015:1-10. doi:10.1155/2015/954954

8. Glick Y. Digital subtraction angiography | Radiology Reference Article | Radiopaedia.org. Radiopaedia.org. https://radiopaedia.org/articles/digital-subtraction-angiography?lang=us. Published 2019. Accessed May 12, 2019.

9. Korja M, Lehto H, Juvela S. Lifelong Rupture Risk of Intracranial Aneurysms Depends on Risk Factors. Stroke. 2014;45(7):1958-1963. doi:10.1161/strokeaha.114.005318

10. David CA, Vishteh AG, Spetzler RF, Lemole M, Lawton MT, Partovi S. Late angiographic follow-up review of surgically treated aneurysms. Journal of Neurosurgery. 1999;91(3):396-401. doi:10.3171/jns.1999.91.3.0396

11. DICKEY P. Management of Cerebral AneurysmsPeter D. Le Roux, H. Richard Winn, David Newell, eds., Philadelphia: Saunders, 2004, ISBN 0-7216-8754-7; 704 pp, 329 illus; $149.00, rating: ⋆⋆⋆, Recommended audience: Neurosurgeons, neurosurgery residents, neurologists, neuroradiologists. Surgical Neurology. 2004;62(5):473. doi:10.1016/s0090-3019(04)00556-7

12. Chason JL, Hindman WM. Berry Aneurysms of the Circle of Willis: Results of a Planned Autopsy Study. Neurology. 1958;8(1):41-41. doi:10.1212/wnl.8.1.41

13. Alderazi YJ, Shastri D, Kass-Hout T, Prestigiacomo CJ, Gandhi CD. Flow Diverters for Intracranial Aneurysms. Stroke Research and Treatment. 2014;2014:1-12. doi:10.1155/2014/415653

14. Wikipedia Contributors. Computational fluid dynamics. Wikipedia. https://en.wikipedia.org/wiki/Computational_fluid_dynamics. Published April 6, 2019. Accessed May 12, 2019.

15. Wikipedia Contributors. Newtonian fluid. Wikipedia. https://en.wikipedia.org/wiki/Newtonian_fluid. Published March 7, 2019. Accessed May 12, 2019.

16. Kirby B. Micro- and Nanoscale Fluid Mechanics. 2009. doi:10.1017/cbo9780511760723

17. Batchelor GK. An Introduction to Fluid Dynamics. 2000. doi:10.1017/cbo9780511800955

18. Laminar Flow Fluid Flow Review - Engineers Edge. Engineersedge.com. https://www.engineersedge.com/fluid_flow/laminar_flow.htm. Published 2019. Accessed May 12, 2019.

19. Wikipedia Contributors. Navier–Stokes equations. Wikipedia. https://en.wikipedia.org/wiki/Navier%E2%80%93Stokes_equations. Published April 25, 2019. Accessed May 12, 2019.

20. Liang L, Steinman DA, Brina O, Chnafa C, Cancelliere NM, Pereira VM. Towards the Clinical utility of CFD for assessment of intracranial aneurysm rupture – a systematic review and novel parameter-ranking tool. Journal of NeuroInterventional Surgery. 2018;11(2):153-158. doi:10.1136/neurintsurg-2018-014246

21. Isoda H, Ohkura Y, Kosugi T, et al. Comparison of hemodynamics of intracranial aneurysms between MR fluid dynamics using 3D cine phase-contrast MRI and MR-based computational fluid dynamics. Neuroradiology. 2009;52(10):913-920. doi:10.1007/s00234-009-0634-4

22. Wiebers DO, Whisnant JP, Huston J, et al. Unruptured intracranial aneurysms: natural history, clinical outcome, and risks of surgical and endovascular treatment. Lancet (London, England). 2003;362(9378):103-110. https://www.ncbi.nlm.nih.gov/pubmed/12867109. Accessed May 12, 2019.

23. Fan J, Wang Y, Liu J, et al. Morphological-Hemodynamic Characteristics of Intracranial Bifurcation Mirror Aneurysms. World Neurosurgery. 2015;84(1):114-120.e2. doi:10.1016/j.wneu.2015.02.038

24. Shojima M, Oshima M, Takagi K, et al. Magnitude and Role of Wall Shear Stress on Cerebral Aneurysm. Stroke. 2004;35(11):2500-2505. doi:10.1161/01.str.0000144648.89172.0f

25. Backes D, Vergouwen MDI, Velthuis BK, et al. Difference in Aneurysm Characteristics Between Ruptured and Unruptured Aneurysms in Patients With Multiple Intracranial Aneurysms. Stroke. 2014;45(5):1299-1303. doi:10.1161/strokeaha.113.004421

26. The Natural Course of Unruptured Cerebral Aneurysms in a Japanese Cohort. New England Journal of Medicine. 2012;366(26):2474-2482. doi:10.1056/nejmoa1113260

27. Rahman M, Smietana J, Hauck E, et al. Size Ratio Correlates With Intracranial Aneurysm Rupture Status. Stroke. 2010;41(5):916-920. doi:10.1161/strokeaha.109.574244

28. Meng H, Tutino VM, Xiang J, Siddiqui A. High WSS or Low WSS? Complex Interactions of Hemodynamics with Intracranial Aneurysm Initiation, Growth, and Rupture: Toward a Unifying Hypothesis. American Journal of Neuroradiology. 2013;35(7):1254-1262. doi:10.3174/ajnr.a3558

29. Cebral JR, Mut F, Weir J, Putman CM. Association of Hemodynamic Characteristics and Cerebral Aneurysm Rupture. American Journal of Neuroradiology. 2010;32(2):264-270. doi:10.3174/ajnr.a2274

30. Riccardello GJ, Changa AR, Al-Mufti F, et al. Hemodynamic impingement and the initiation of intracranial side-wall aneurysms. Interventional Neuroradiology. 2018;24(3):288-296. doi:10.1177/1591019918754380

31. Duan Z, Li Y, Guan S, et al. Morphological parameters and anatomical locations associated with rupture status of small intracranial aneurysms. Scientific Reports. 2018;8(1). doi:10.1038/s41598-018-24732-1

32. Baharoglu MI, Schirmer CM, Hoit DA, Gao B-L, Malek AM. Aneurysm Inflow-Angle as a Discriminant for Rupture in Sidewall Cerebral Aneurysms. Stroke. 2010;41(7):1423-1430. doi:10.1161/strokeaha.109.570770

33. Schirmer CM, Malek AM. Critical Influence of Framing Coil Orientation on Intra-Aneurysmal and Neck Region Hemodynamics in a Sidewall Aneurysm Model. Neurosurgery. 2010;67(6):1692-1702. doi:10.1227/neu.0b013e3181f9a93b

34. Wong GKC, Poon WS. Current status of computational fluid dynamics for cerebral aneurysms: The clinician's perspective. Journal of Clinical Neuroscience. 2011;18(10):1285-1288. doi:10.1016/j.jocn.2011.02.014

35. Cebral JR, Mut F, Raschi M, et al. Aneurysm Rupture Following Treatment with Flow-Diverting Stents: Computational Hemodynamics Analysis of Treatment. American Journal of Neuroradiology. 2010;32(1):27-33. doi:10.3174/ajnr.a2398

36. Longo M, Granata F, Racchiusa S, et al. Role of Hemodynamic Forces in Unruptured Intracranial Aneurysms: An Overview of a Complex Scenario. World Neurosurgery. 2017;105:632-642. doi:10.1016/j.wneu.2017.06.035

37. Meng H, Wang Z, Hoi Y, et al. Complex Hemodynamics at the Apex of an Arterial Bifurcation Induces Vascular Remodeling Resembling Cerebral Aneurysm Initiation. Stroke. 2007;38(6):1924-1931. doi:10.1161/strokeaha.106.481234

38. Kolega J, Gao L, Mandelbaum M, et al. Cellular and Molecular Responses of the Basilar Terminus to Hemodynamics during Intracranial Aneurysm Initiation in a Rabbit Model. Journal of Vascular Research. 2011;48(5):429-442. doi:10.1159/000324840

39. Dolan JM, Kolega J, Meng H. High Wall Shear Stress and Spatial Gradients in Vascular Pathology: A Review. Annals of Biomedical Engineering. 2012;41(7):1411-1427. doi:10.1007/s10439-012-0695-0

40. Kulcsár Z, Ugron Á, Marosfői M, Berentei Z, Paál G, Szikora I. Hemodynamics of Cerebral Aneurysm Initiation: The Role of Wall Shear Stress and Spatial Wall Shear Stress Gradient. American Journal of Neuroradiology. 2011;32(3):587-594. doi:10.3174/ajnr.a2339

41. Dolan JM, Meng H, Sim FJ, Kolega J. Differential gene expression by endothelial cells under positive and negative streamwise gradients of high wall shear stress. American Journal of Physiology-Cell Physiology. 2013;305(8):C854-C866. doi:10.1152/ajpcell.00315.2012

42. Bian C, Xu G, Wang J, Ma J, Xiang M, Chen P. Hypercholesterolaemic Serum Increases the Permeability of Endothelial Cells through Zonula Occludens-1 with Phosphatidylinositol 3-Kinase Signaling Pathway. Journal of Biomedicine and Biotechnology. 2009;2009:1-5. doi:10.1155/2009/814979

43. Zhou G, Zhu Y, Yin Y, Su M, Li M. Association of wall shear stress with intracranial aneurysm rupture: systematic review and meta-analysis. Scientific Reports. 2017;7(1). doi:10.1038/s41598-017-05886-w

44. Wang Y, Leng X, Zhou X, Li W, Siddiqui AH, Xiang J. Hemodynamics in a Middle Cerebral Artery Aneurysm Before Its Growth and Fatal Rupture: Case Study and Review of the Literature. World Neurosurgery. 2018;119:e395-e402. doi:10.1016/j.wneu.2018.07.174

45. Woodward J. Mid-side nodes: Do they really help? PADT, Inc. - The Blog. http://www.padtinc.com/blog/the-focus/mid-side-nodes-do-they-really-help. Published October 31, 2012. Accessed May 12, 2019.

46. Patch Independent Algorithm for Tetrahedrons Method Control. Sharcnet.ca. https://www.sharcnet.ca/Software/Ansys/17.0/en-us/help/wb_msh/msh_Patch_Ind_Algor.html. Published December 2, 2015. Accessed May 12, 2019.

47. Xu J, Yu Y, Wu X, et al. Morphological and Hemodynamic Analysis of Mirror Posterior Communicating Artery Aneurysms. Baron J-C, ed. PLoS ONE. 2013;8(1):e55413. doi:10.1371/journal.pone.0055413

48. Janela J, Moura A, Sequeira A. A 3D non-Newtonian fluid–structure interaction model for blood flow in arteries. Journal of Computational and Applied Mathematics. 2010;234(9):2783-2791. doi:10.1016/j.cam.2010.01.032

49. Mhd H, Alargha H. Numerical Analysis for the Hemodynamics in Unruptured Cerebral Aneurysms.; 2016. https://scholarworks.uaeu.ac.ae/cgi/viewcontent.cgi?article=1337&context=all_theses. Accessed May 12, 2019.

50. Miri M, Ghanaati H, Salamati P, et al. Coil Embolization of Intracranial Aneurysms: A Six-Month Follow-Up Study. Iranian Journal of Radiology. 2015;12(3). doi:10.5812/iranjradiol.10986v2

51. Abou-Chebl A. Cerebral aneurysms. Nih.gov. https://www.ncbi.nlm.nih.gov/books/NBK27372/. Published 2015. Accessed May 12, 2019.

52. Meshing -- CFD-Wiki, the free CFD reference. Cfd-online.com. https://www.cfd-online.com/Wiki/Meshing. Published 2012. Accessed May 12, 2019.